Photoautotrophic Production of Biomass, Laurate, and Soluble Organics by *Synechocystis* sp. PCC 6803

by

Binh Thanh Nguyen

A Dissertation Presented in Partial Fulfillment
of the Requirements for the Degree
Doctor of Philosophy

Approved August 2015 by the
Graduate Supervisory Committee:

Bruce E. Rittmann, Chair
Rosa Krajmalnik-Brown
Paul Westerhoff

ARIZONA STATE UNIVERSITY

December 2015

ABSTRACT

Photosynthesis converts sunlight to biomass at a global scale. Among the photosynthetic organisms, cyanobacteria provide an excellent model to study how photosynthesis can become a practical platform of large-scale biotechnology. One novel approach involves metabolically engineering the cyanobacterium *Synechocystis* sp. PCC 6803 to excrete laurate, which is harvested directly.

This work begins by defining a working window of light intensity (LI). Wild-type and laurate-excreting *Synechocystis* required an LI of at least 5 $\mu E/m^2$-s to sustain themselves, but are photo-inhibited by LI of 346 to 598 $\mu E/m^2$-s.

Fixing electrons into valuable organic products, e.g., biomass and excreted laurate, is critical to success. Wild-type *Synechocystis* channeled 75% to 84% of its fixed electrons to biomass; laurate-excreting *Synechocystis* fixed 64 to 69% as biomass and 6.6% to 10% as laurate. This means that 16 to 30% of the electrons were diverted to non-valuable soluble products, and the trend was accentuated with higher LI.

How the C_i concentration depended on the pH and the nitrogen source was quantified by the proton condition and experimentally validated. Nitrate increased, ammonium decreased, but ammonium nitrate stabilized alkalinity and C_i. This finding provides a mechanistically sound tool to manage C_i and pH independently.

Independent evaluation pH and C_i on the growth kinetics of *Synechocystis* showed that pH 8.5 supported the fastest maximum specific growth rate (μ_{max}): 2.4/day and 1.7/day, respectively, for the wild type and modified strains with LI of 202 $\mu E/m^2$-s. Half-maximum-rate concentrations (K_{Ci}) were less than 0.1 mM, meaning that *Synechocystis* should attain its μ_{max} with a modest C_i concentration ($\geq$1.0 mM).

Biomass grown with day-night cycles had a night endogenous decay rate of 0.05-1.0/day, with decay being faster with higher LI and the beginning of dark periods. Supplying light at a fraction of daylight reduced dark decay rate and improved overall biomass productivity.

This dissertation systematically evaluates and synthesizes fundamental growth factors of cyanobacteria: light, inorganic carbon (C_i), and pH. LI remains the most critical growth condition to promote biomass productivity and desired forms of biomass, while C_i and pH now can be managed to support optimal productivity.

DEDICATION

To Dad and Mom

ACKNOWLEDGMENTS

Getting a Ph.D is a long, memorable and incredible journey. During that journey, I am indebted to people and organizations for support, comfort, and opportunity.

The first and foremost appreciation is to my advisor, Dr. Bruce E. Rittmann. You bet on me among other great prospects. I am fortunate to receive your mentorship and supports in last five years.

And to Dr. Rosa Krajmalnik-Brown, who gives me new perspectives to communicate to general audience, data presentation, and experiment in biology.

And to Dr. Paul Westerhoff who instructed me in core courses of environmental engineering. Your straightforward approach inspires me to tackle challenge.

Together, my committees, Drs. Rittmann, Karjmalnik-Brown, and Westerhoff, provide feedbacks and critical thoughts on my study and that helps me immensely.

I must thank my colleagues who assisted during this journey among them are Dr. Raveender Vannela, Dr. Hyun Woo Kim, Dr. Robert W. Roberson, Dr. Shuquin Li, Dr. Willem F.J. Vermaas, Dr. Prathap Parameswaran, Dr. Jie Sheng, Chao Zhou, Joshua McIlwain, Swathi Sridharakrishnan, Ricardo Reyes, Alex Zevin, Matt Thompson, Megha Patel, Michelle Young, and Carole Flores. I owe a big thank to the lab manager Diane Muller Hagner, and my lab mate, Levi Straka, for the support and company.

Living afar from my family is hard and that would have been harder without helps from my friends, among them are: anh Quan Nguyen, Anh Nguyen, Dr. Anh Le, and Phien Pham.

My study and this dissertation are not possible without financial supports from Vietnam Education Foundation, Swette Center for Environmental Biotechnology, ARPA-

E project, and grant EE0006100: “Managing the Microbial Ecology of a Cyanobacteria-Based Photosynthetic Factory Direct!,” from the U.S. Department of Energy U.S Department of Energy.

TABLE OF CONTENTS

Page

LIST OF TABLES xi

LIST OF FIGURES xii

CHAPTER

1 INTRODUCTION 1

1.1 Fossil Fuels and Atmospheric Carbon Dioxide 1

1.2 Biofuels From Conventional Biomass 3

1.3 Shortcomings of Current Energy Crops 7

1.4 Microalgae as Biofuel Feedstock 8

1.4.1 Eukaryotic Microalgae 8

1.4.2 Cyanobacteria 10

1.4.3 Life Cycle Assessment and Technoeconomics of Microalgal Biofuel. 13

1.4.4 *Synechocystis* sp. PCC 6803 and Its Genetic Engineering. 16

1.5 Objectives and Dissertation Outline 21

2 LIGHT INTENSITY LIMITS OR INHIBITS PHOTOSYNTHESIS 27

2.1 Introduction 27

2.1.1 Light Intensity 27

2.1.2 General Photosynthesis 28

2.1.3 Photo-Inhibition and Photo-Limitation 31

2.1.4 Light Intensity to Growth Kinetic Model and Its Application to PBR Engineering. 34

CHAPTER Page

2.2 Materials and Methods 38
2.2.1 BG-11 Medium Preparation 38
2.2.2 Inoculum and Experiment Preparation 39
2.2.3 Experimental Conditions 40
2.2.4 Analyses 41
2.3 Results and Discussion 43
2.3.1 Photo-Inhibition Under High Light Intensity 43
2.3.2 Photo-Limitation by Low Light Intensity 49
2.3.3 Growth Kinetics Without Controlling pH 54
2.4 Synthesis and Application 58
3 EFFECT OF LIGHT INTENSITY ON DISTRIBUTION OF PARTICULATE AND SOLUBLE BIOMASS 59
3.1 Introduction 59
3.2 Materials and Methods 64
3.2.1 Experiment Setup 64
3.2.2 Analyses 65
3.3 Electron Partitioning 66
3.4 Correlation of Laurate and SMP Production to Biomass Growth Rate 67
3.5 Results and Discussion 67
3.5.1 Electron Partitioning 67

CHAPTER Page

3.5.2 Correlation of Specific Growth Rates to Laurate and Generic SMP Production 82

3.6 Synthesis and Application 85

4 EFFECT OF NITROGEN SOURCES ON ALKALINITY AND INORGANIC CARBON 86

4.1 Introduction 86

4.2 pH-Stat PBR 89

4.3 Using the Proton Condition to Model Dissolved Inorganic Carbon Trends 92

4.4 Materials and Methods 98

4.4.1 Inoculum Preparation 98

4.4.2 Modified BG-11 Growth Medium 98

4.4.3 Experimental Setup 98

4.4.4 Analysis 99

4.5 Results and Discussion 100

4.6 Synthesis and Application 107

5 INDEPENDENT EFFECTS OF PH AND INORGANIC CARBON ON GROWTH KINETICS OF *SYNECHOCYSTIS* 108

5.1 Introduction 108

5.1.1 Carbon Speciation 109

5.1.2 CO_2-Concetrating Mechanism 111

CHAPTER Page

5.1.3 Effects of pH on Growth Kinetics 114

5.1.4 Effects of C_i to Growth Kinetics 116

5.2 Methods and Materials 118

5.2.1 Experiment Setup 118

5.2.2 Growth Media 118

5.2.3 Experimental Setup 120

5.2.4 Analyses 121

5.2.5 Average Internal Light Intensity 121

5.2.6 Kinetic Modeling 126

5.3 Results and Discussion 127

5.3.1 Growth Kinetics in pHs and Nutrient-Sufficient Medium 127

5.3.2 Growth Kinetics of *Synechocystis* Based on Inorganic Carbon 132

5.4 Synthesis and Application 151

6 EFFECT OF PHOTOPERIODS TO BIOMASS PRODUCTION, DARK AND LIGHT RESPIRATION 152

6.1 Introduction 152

6.2 Methods and Materials 155

6.2.1 Experiment Setup 155

6.2.2 Medium and Inoculum Preparation 157

6.2.3 Sampling and Assaying 157

6.2.4 Kinetic Analysis 158

6.2.5 Buffer Intensity 159

CHAPTER Page

6.3 Results and Discussion 160

6.3.1 Biomass and FFA Production in Uncontrolled pH 160

6.3.2 Photoperiods with pH-Stat PBR 162

6.4 Synthesis and Application..... 179

7 SUMMARY, SIGNIFICANCE, AND FUTURE WORK..... 181

REFERENCES 187

LIST OF TABLES

Table Page

1.1: Fuel Yield of Various Crops, Including Microalgal Candidates 8

2.1: Summary of Fitted Model Parameters 57

3.1: Results of Light Microscopy for the Wild-Type and the Laurate-Excreting Strains 72

3.2: Linear Regression Equations for Newly Generated Total COD (TCOD), Biomass (PCOD), and SMP (SCOD) for the Wild-Type S*ynechocystis* 77

3.3: Linear Regression Equations for Newly Generated Total COD (TCOD), Biomass (PCOD), and SMP (SCOD) for the Wild-Type S*ynechocystis* 78

3.4: Linear-Regression Slopes (p) and Correlation Coefficients (R^2) for the Specific Production Rates of Laurate and Generic SMP Production in Figure 3.6..... 83

5.1: Summary of Key Difference Between Two Approaches to Study Growth Kinetics by C_i and pH 120

5.2: Incident LI Each Location by PAR Sensor..... 124

5.3: Summary of Inputs for the Beer-Lambert Law 124

5.4: Best-Fit Monod Parameters for Wild-Type *Synechocystis* sp. PCC 6803 With Three pH Values and a Common AILI of 202 µE/m^2-s 144

5.5: Best-Fit Monod Parameters for the Laurate-Excreting *Synechocystis* sp. PCC 6803 with Three pH Values and a Common AILI of 202 µE/m^2-s.. 145

LIST OF FIGURES

Figure Page

1.1: Energy Balance of Biofuels 5

1.2: Systematic of Microalgal Diesel Production for LCA Study 15

1.3: Transmission Electron Micrograph of *Synechocystis* sp. PCC 6803 cells 17

1.4: Scheme of an FFA-Excreting Modified Strain Achieved by Overexpressing Thioesterases and Deletion of *aas slr1609* 21

2.1: Diagram of Dark and Light Reactions in Photosynthesis 28

2.2: Generic Light-Response Curve Showing Limitation, Saturation, and Inhibition Stages (J. C. J. Goldman, 1979b) 30

2.3: A Scheme of Photo-Inhibition Due to Excessive Light 33

2.4: Biomass Dry Weight (DW- Closed Symbols) and AILI (Open Symbols) of Flasks with Different Incident LI on Wild-Type *Synechocystis* (Panel a) and the Laurate-Excreting *Synechocystis* (Panel b) for the Range of Incident LI Shown in the Top Rows ($\mu E/m^2$-s) 45

2.5: Digital Pictures of *Synechocystis* Wild-Type at day 2, 8, 16, and 18 (Left Column) and *Synechocystis* Laurate-Excreting Strain at Day 2, 8, 18, and 24 (Right Column) 47

2.6: Digital-Color and LM Images of *Synechocystis* Laurate-Excreting Strain of the Last Day (Day 21) 48

2.7: Biomass DW and AILI of Flasks with Different Incident LI on the Wild-Type (Panel a) and Laurate-Excreting Strain (Panel b) of *Synechocystis* in Low LI 50

Figure Page

2.8: Particulate COD of Wild Type (Panel a) and Laurate-Excreting *Synechocystis* (Panel b). 51

2.9: Digital Picture of Experiment Setup (Top); the Wide-Type Culture (Left-Bottom) and the Laurate-Excreting Culture (Right-Bottom) at the End of the Experiment (Day of 34)..... 52

2.10: pH Readings of Culture with Different LIs on *Synechocystis* Wild-Type Strain (Left) and Laurate-Excreting Modified Strain (Right), Black Arrow Indicates Time to Replace by Fresh BG-11 (Day 26). 53

2.11: Fits of the Specific Growth Rate to AILI for *Synechocystis* Wild Type (Panel a) and the Laurate-Excreting Strain (panel B) Based on Monod and the Substrate Self-Inhibition Models Using the Parameter Values in Table 2.1..... 55

3.1: Mass Fluxes of Active Biomass, Inert Biomass, EPS, SMP, and Substrates in Laurate-Excreting Culture in the Presence of Heterotrophic Bacteria 61

3.2: Panel a1-a3: Total COD, Calculated COD of Particulate Biomass, and Generic SMP COD of Wild-Type *Synechocystis*. Panel b1-b4: Total COD, Calculated COD of Particulate Biomass, Generic SMP COD, and COD Equivalent of Laurate for Laurate-Excreting *Synechocystis* 70

3.3: Panel a: COD Fractions of SMP and Particulate Biomass Normalized to the Total Electron Equivalents Harvested by Photosynthesis for Wild-Type *Synechocystis* sp. PCC 6803. Panel b: COD Fractions of SMP, Particulate Biomass, and Laurate Normalized to the Total Electron Equivalents Harvested by Photosynthesis by Laurate-Excreting *Synechocystis* 71

Figure Page

3.4: Newly Generated Total COD from Photosynthetic Activity (ΔTCOD), Newly Generated Biomass (ΔPCOD), Newly Produced SMP (ΔSCOD), and Newly Excreted Laurate (ΔLaurate COD), all Normalized to the Average Biomass Concentration ($PCOD_{avg}$) for Wild-Type *Synechocystis* (Panels a1 to a3) and the Laurate-Excreting Strain (Panels b1 to b4) 75

3.5: Dry Weight Biomass Equivalent (Panel a) and Laurate Concentration (Panel b) of Laurate-Excreting *Synechocystis* Grew in Fixed Incident LI from 111 $\mu E/m^2$-s to 598 $\mu E/m^2$-s. Panel c Summarizes Fixed Electron Partitioning to Laurate (LA) Relative to Biomass (BM) of Two Replicated Run 81

3.6: Correlation to the Biomass Specific Growth Rate with the Specific Rates of Laurate Production (Panel a) and SMP Production (Panel b) by the Laurate-Excreting Strain 82

4.1: Schematic Diagram of the PBR Equipped with a pH-Stat 91

4.2: Schematic Diagram of the Full Version of the pH-Stat PBR 92

4.3: Left Panel: Growth Curves of *Synechocystis* in the Standard BG-11 Medium with Different Growth pHs, Shown on the Top Row. Right Panel: C_i Concentration as S*ynechocystis* Grew in Standard BG-11 (Containing only NO_3^-), Starting with ~0.2 mM Carbonate 101

Figure Page

4.4: Left Panel: Growth Curves of *Synechocystis* in a Modified BG-11 Medium and Right Panel: C_i Trends as *Synechocystis* Grew in the Standard BG-11 Augmented with 5 mM of Bicarbonate (i.e., Making the Starting Alkalinity 5.4 meq/L (pH = 8.5), Circles with Growth pH = 7.5, 8.5 and 9.5) and BG-11 Contained 1.5 and 3.5 mM of C with Growth pH = 8.5 102

4.5: Left Panel, the Growth Curves of *Synechocystis* and Right panel, C_i Trends as *Synechocystis* Grew in BG-11 Modified by Substituted Sodium Nitrate with Ammonium Nitrate 104

4.6: Left Panel: Growth Curves and Right Panel: C_i Trends as *Synechocystis* Grew in BG-11 Modified by Substituted Sodium Nitrate with Ammonium Nitrate 105

5.1: Distribution of Carbon Species from Total DIC with pH..... 111

5.2: Plan View of PBR Includes the Main Reactor (Circle, Center), Two Squares, Light Reflector, and Fluorescent Bulbs..... 123

5.3: Local Light Intensity (Open Symbols) and Predicting Values by Beer-Lambert Law for *Synechocystis* Culture 125

5.4: Specific Growth Rates of *Synechocystis* Wild-Type (WT, Panel a) and a Comparison of the Wild-Type and the Modified Strains (MS) in BG – 11 Growth Medium (Panel b) 128

5.5: Biomass Growth of *Synechocystis* Wild-Type Strain (Panel a and b) and of the Modified Strain (Panel c and d) in Standard BG-11 with pH = 6.5 to 10.0. 129

5.6: pH Readings of Screening Experiments 131

Figure Page

5.7: Biomass Concentration (Panel a) During Growth of *Synechocystis* Wild-Type Strain in Standard BG-11 with pH = 6.5 to 10.0. 132

5.8: Biomass Growth of *Synechocystis* Wild-Type in in the BG-11 with Additional 5 mM Bicarbonate (Panel a) and Specific Growth Rate with Corresponding AILI in Different Growth pH Given by the Top Row ($\mu E/m^2$-s). 133

5.9: Biomass Growth for Wild-Type *Synechocystis* Grown at a Fixed pH of 7.5 136

5.10: Biomass Growth for Wild-Type *Synechocystis* Grown at a Fixed pH of 8.5 137

5.11: Biomass Growth for Wild-Type *Synechocystis* Grown at a Fixed pH of 9.5 138

5.12: Biomass Growth for Laurate-Excreting *Synechocystis* Grown at a Fixed pH of 7.5 139

5.13: Biomass Growth for Laurate-Excreting *Synechocystis* Grown at a Fixed pH of 8.5 140

5.14: Biomass Growth for Laurate-Excreting *Synechocystis* Grown at a Fixed pH of 9.5 141

5.15: Measured Specific Growth Rate (Symbols) and Monod Best-Fit Curves Using C_{ib} (the Sum of H_2CO_3* and HCO_3^-) for the Fixed pH of 7.5, 8.5, and 9.5 143

5.16: Measured Specific Growth Rate (Symbols) and Monod Best-Fit Curves Using Bioavailable Inorganic Carbon (C_{ib}) with pH= 7.5, 8.5, and 9.5 146

5.17: Measured Specific Growth Rate (Symbols) of Wild-Type *Synechocystis* and Monod Best-Fit Curves Using $H_2CO_3^*$ (Top Row), HCO_3^- (Middle Row), and CO_3^{2-} (Bottom Row) for the Fixed pH of 7.5, 8.5, and 9.5 148

Figure Page

5.18: Measured Specific Growth Rate (Symbols) of the Laurate-Excreting *Synechocystis* and Monod Best-Fit Curves Using $H_2CO_3^*$ (Top Row), HCO_3^- (Middle Row), and CO_3^{2-} (Bottom Row) for the Fixed pH of 7.5, 8.5, and 9.5 149

6.1: Buffer Intensity over Applicable pH Range for BG-11..... 159

6.2: Effects of Photoperiods with Light Acclimation (l.a) and Without Light Acclimation (w/o l.a) by the Laurate-Excreting Strain; Biomass Density (Open Symbols); pH (Closed Symbols) on the Left Panel, and FFA, Mainly Laurate, over Time on the Right Panel..... 160

6.3: Panels a to d: Biomass Density, Specific Growth and Decay Rate, the Culture pH and Dissolved Oxygen, and Inorganic Carbon of Experiments with a Fixed pH of 9.5 163

6.4: Correlation of Specific Growth Rate (μ_{obs}) with Absolute Value of Specific Decay Rate (μ_{dec}) 166

6.5: Biomass Production in Batch Experiments with Different Photoperiods at pH = 8.5 in the Light. Panel a: OD Values over all of the Entire Experimental Time. Panel b: OD Values Plotted for the Time of Illumination Only..... 167

6.6: Specific Growth Rate (μ_{obs}, Positive Values for Light On) and Specific Decay Rate (μ_{dec}, Negative Values for Light Off) for *Synechocystis* Experiencing Different Photoperiods 168

6.7: Correlation of Specific Decay Rate in Dark with the Preceding Specific Growth Rate in the Light..... 169

Figure Page

6.8: pH and DO Value for the *Synechocystis* Culture with Four Different Photoperiods Using the A-unit pH-Stat. The pH Patterns Were the Same with the B-unit. 172

6.9: Photosynthesis of Culture with Depleted C_i and Sufficient Light Energy 174

6.10: Comparison of Decay Rate During Dark Periods of Different Photoperiods with No Light (Open Symbols) and Illuminating Culture with 30 µE/m^2-s (Filled Symbols) 176

6.11: Net Specific Growth Rate over One Day Duration, Including Dark and Light Periods. The Open Symbols Gives Runs With Dark Periods (-NL) and the Filled Symbols Represents Runs Augmented with 30 µE/m^2-s at Night (-HL) 177

6.12: pH and DO with 30 µE/m^2-s Illuminated at Night 178

ABBREVIATIONS

AILI	Average Internal Light Intensity
AU	Absorbance Unit
CCM	CO_2-Concentrating Mechanism
COD	Chemical Oxygen Demand
DI	De-Ionized (water)
DIC	Dissolved Inorganic Carbon
DO	Dissolved Oxygen
DW	Dryweight
EPS	Extracellular Polymeric Substances
FFA	Free Fatty Acids
GC	Gas Chromatography
GHG	Greenhouse Gases
LCA	Life Cycle Assessment
LI	Light Intensity
LM	Light Microscopy
OD	Optical Density (of biomass)
PAR	Photosynthetically Active Radiation
PBR	Photobioreactor
PC	Proton Condition
SMP	Soluble Microbial Products

1 INTRODUCTION

1.1 Fossil Fuels and Atmospheric Carbon Dioxide

Today, more than 80% of the energy used by human society comes from fossil sources. However, fossil reserves can only supply humans' energy needs for a finite period. Ratios of proven reserves to current production rates indicate that oil may last about 53 years, 56 years for natural gas, and 109 years for coal (BP, 2013). Recent exploration and development of shale gas, gaseous hydrocarbons locked in rock in deep underground, may extend the longevity to about 90 years for the gas reserves (Rotman, 2009). In the U.S., 94 percent of energy use comes from fossil fuels, which are used for power generation (38%), transportation (31%), industry (14%), and residential/ commercial (10%) (US EPA, 2013). The 31% for the transportation sector equals 0.63 billion m^3 of liquid fuels (EIA, 2013).

Burning fossil fuels inevitably releases carbon dioxide (CO_2), the main greenhouse gas. In last 240 years, atmospheric CO_2 has increased from 280 ppmv (pre-Industrial Revolution) to 395 ppmv in 2013, and 40 ppmv of that increment has come in the past 20 years (1992-2013) (Leuenberger, Siegenthaler, & Langway, 1992; NOAA, 2013; Siegenthaler & Sarmiento, 1993). Approaching 450 ppmv is perilous because it is considered a tipping point for irreversible climate change (Pachauri & Reisinger, 2007). The World Economic Forum ranked failure to adapt and mitigate climate change as the fifth biggest challenges in next 10 years (Marsh & McLennan Companies et al., 2014).

For reasons of resource depletion and stemming global climate change, human society must find energy source that are renewable and able to replace most fossil sources. Harnessing solar energy through photosynthesis is one promising option.

Photosynthesis, one of oldest biochemical processes on Earth, produced our oxygen-abundant planet. Each year, about 0.1% of incident solar energy is captured by photosynthesis. This leads to about 4500 EJ (1 EJ = 10^{18}J) of solar energy being embodied into living biomass annually; this is roughly 10 times more than the 2007 global energy consumption by human society (World Energy Council, 2013).

In the United States, about 214 billion dry tons of biomass, including firewood, residual, and biofuel feedstock, are being used by human society for various energy purposes (Perlack & Stokes, 2011). Liquid bio-fuels, such as bioethanol and biodiesel, can be produced from a wide range of feedstock, such as corn, soybeans, residual fats, and other oily nuts, cellulosic biomass, and microorganisms (Bruce E Rittmann, 2008). However, a only small portion of U.S. energy, about 22 EJ, is provided from terrestrial energy crops (Chynoweth, Owens, & Legrand, 2000; Bruce E Rittmann, Torres, & Marcus, 2008). Even more importantly, these terrestrial plant sources cannot generate enough renewable feedstock to come close to meeting the demand. For example, palm trees, the most commercially productive biodiesel crop, would need to be planted on about 50% of U.S. arable land to meet the 2005 transportation demand of the U.S. (Chisti, 2007).

Microalgae, the collective name for eukaryotic microalgae and cyanobacteria, represent a new area for biofuel research and development. Unlike higher plants, microalgae have simple cell structures and genetic systems that make them robust, more

efficient at photosynthesis, and amenable to genomic modification. One form of microalgae – cyanobacteria – is the focus of my proposed research.

In next sections, I review biofuels production, including their environment benefits and drawbacks. Key topics are key biological characteristics, energy yields, and the technical *status quo* for microalgae. Lastly, this dissertation presents research topics on environmental conditions of cultivation and how success with them can advance microalgae technology for producing biofuel feedstock.

1.2 Biofuels from Conventional Biomass

Conventional biofuels, such as ethanol and biodiesel, were dominant liquid fuels from the 18th century until 1925, when the price of petroleum dropped and was able to out-compete biofuels (Balat & Balat, 2009). Petroleum price hikes during the Arab oil embargo in 1970s and the geopolitical conflicts in the early 2000s drove many countries to start renewable-energy programs and to secure liquid fuels from other sources than petroleum. Brazil has run its National Alcohol Fuel Program (ProAlcool) since the 1970s, making it the largest ethanol producer up to 2006, thanks to cheap and abundant sugar cane (Rosillo-Calle & Cortez, 1998). In the U.S, a government-funded program called Aquatic Species Program (APS) ran from 1979-1996 and screened over 3000 strains of microalgae for lipid production. The U.S. enacted the Energy Policy Act and the Energy Independence and Security Act in 2007 to promote biofuel production, targeting 36 billion gallons of ethanol produced by 2022, mostly from cellulosic feedstock. By 2011, the U.S. produced 8.3 billion gallons of bioethanol, doubling Brazil's production and accounting for 60% of the global output.

Producing biofuels from a conventional feedstock like corn, wheat, cassava, and soybeans is technically robust thank to conversion technology in place; however, increasing biofuel production reduces food supply for humans and livestock (Boddiger, 2007; Escobar et al., 2009; Fischer, 2009). Starting in 2005-2006, grains were diverted significantly towards the bioethanol industry: for example, in the U.S., about 37% of the corn crop went for ethanol in 2007 (USDA, 2013), leading to a global hike in food prices. DiPardo (2000) and Tokgöz and Elobeid (2006) found a strong correlation in price of corn and other alternative grains to ethanol production. Cost of cereals and animal products increased dramatically, by 12 to 200% across the globe in 2007 (Brown, 2008). Mobilizing food grains to fuels exacerbate global food supplies, in which 60% of the world's population is malnourished (Pimentel, 2008).

Corn and soybeans also have inherent drawbacks of intensive agrochemicals and energy uses during cultivation and conversion. Corn ethanol, for example, saves only 13% of greenhouse gases (GHGs) over fossil fuel and yields only 25% more energy than its inputs, as shown in **Figure 1.1**. Soybean diesel is better when credits for co-products reduce GHGs up to 60% and provide a net energy yield 93% of invested energy (Hill, Nelson, Tilman, Polasky, & Tiffany, 2006); however, soybean crops have low aerial yields that are impractical for large-scale production for fuel (Timilsina & Shrestha, 2011).

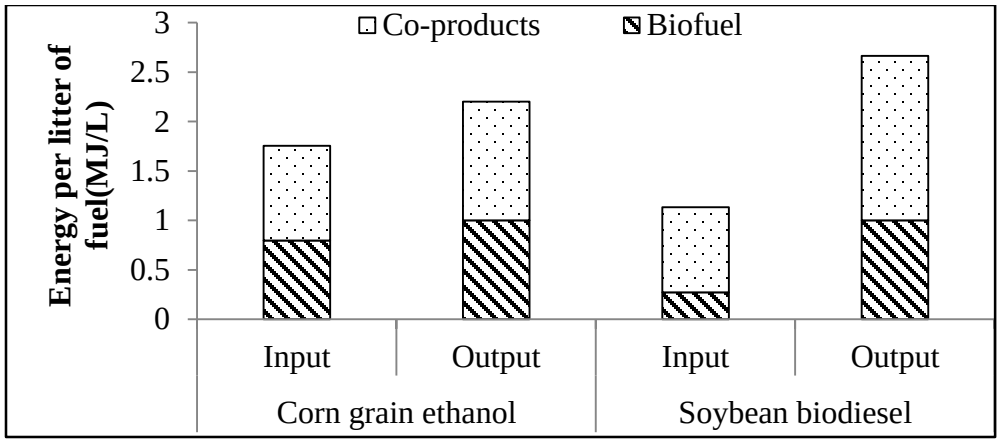

Figure 1.1: Energy Balance of Biofuels
Data extracted from Hill et al. (2006)

Intensive use of fertilizers to grow corn and soybean indirectly deteriorates the quality of nearby and distant waters by spurring eutrophication and hypoxia. Run-off from the Corn Belt into Mississippi River Basin is believed to cause dead zones in Mexico Gulf (Walsh, 2013). Nitrogen and phosphate promote blooming of algae. When the microalgae die, their biomass decay depletes dissolved oxygen (hypoxia) that leads to a deterioration of the aquatic habitat ecosystem (ScienceDaily, 2013).

Displacing native biomass (e.g., forest, peat, and grass land) by energy crops also changes the carbon balance: The lost amount of C fixed by photosynthesis plus the extra C emitted by land clearance and cultivation are normally referred to as carbon debts. Depending on types of biofuel crops and pre-existing ecology, the payback time to reverse the carbon debt due to land change could take 10 to 400 years (Danielsen et al., 2009; Fargione, Hill, Tilman, Polasky, & Hawthorne, 2008; Searchinger et al., 2008).

Alternatively, biofuel can be produced from biomass residuals. Cellulosic feedstock has a great potential because it exists in massive quantities from waste biomass. Biomass residuals, such as corn stover, consist of leaves, stalk, cob, and husk; they are

the largest agricultural residues today in the U.S. Annually, corn crops generate about 200-250 million metric tons dry weight of corn stover, of which 70% is cellulose and hemicellulose and 15-20% is lignin (Atchison & Hettenhaus, 2004; Glassner, Hettenhaus, & Schechinger, 1998). Larson et al. (1978) and Lindstrom et al. (1979) estimated that corn stover could produce 200 million tons of ethanol, or 30% of U.S. current use of fuel for transportation.

Another important source of cellulose is switch grass. *Panicum virgatum* and *Miscanthus* are perennial grasses that grow rapidly on marginal lands. *Miscanthus* can capture 1.0% of sunlight energy, or 10-times higher than the average plant, and it yields up to 30-ton dry biomass per hectare (Khanna, Dhungana, & Clifton-Brown, 2008). To generate biomass for 36 billion gallon bioethanol production required by EISA (2007), only 9.3% (12 million hectares) of current cropland in U.S. would be needed (Heaton, Dohleman, & Long, 2008; Melis, 2009). That yield of *Miscanthus* is 2.7-time higher than corn and avoids substantial use of agrochemicals.

However, cellulose-based ethanol encounters a great challenge: converting cellulose and hemi-cellulose to simple sugar by hydrolysis. While true hydrolysis is carried with enzymes, options for pre-treatment are diverse. Key functions of pretreatment are to remove lignin and hemicellulose, to crush cellulose crystallinity, and to increase porosity (Sun & Cheng, 2002). Cellulosics to ethanol still requires major breakthroughs to improve hydrolysis efficiency and lower the cost of enzymes (Kazi et al., 2010).

1.3 Shortcomings of Current Energy Crops

Biofuels are not without problems. For example, ethanol contains only 64% of the energy value per volume compared to gasoline (Chisti, 2008). This translates to lower mileage and larger fuel tanks with more frequent refills. Ethanol also is considerably toxic and volatile in an open environment, which leads to extra costs for storage and handling. The most critical problem with current biofuel feedstock is low aerial yield (**Table 1.1**). Current commercial feedstock only produces 1% of the current demand for liquid fuels while requiring 1% of arable land (15 million hectares) worldwide (Brennan & Owende, 2010). As emerging economies become wealthier and demand more fuels, arable land may shrink and not be replaceable with urban, forest, and non-arable land (FAOSTAT, 2013; Pimentel, 2008).

Interest in finding higher-yielding crops dovetails with research on microalgae. A comparison of the fuel yield of different energy crops is in **Table 1.1**. The statistics indicates a great potential of microalgae to produce fuel with superior productivity. In the next sections, I review key characteristics of eukaryotic microalgae and cyanobacteria in their roles as biofuel sources.

Table 1.1: Fuel Yield of Various Crops, Including Microalgal Candidates

Crop	Oil content per dry weight	Fuel yield		Reference
		L/ha.yr	T/ha.yr	
Sugar cane	For ethanol	7,500	5.9	Chisti, 2008
Corn	For ethanol	3,632	3.1	Hill et al., 2006
Corn	44% (of seed)	172	0.152	Mata et al., 2010
Soybean	18-20% (of seed)	544-636	0.48-0.60	Scott et al., 2010
Sunflower	40% (of seed)	1070	946	Mata et al., 2010
Oilseed rape	40-44% (of seed)	1560	1.4	Scott et al., 2010
Jatropha	30% (of seed)	2700	2.4	
Palm oil	36% (of kernel)	5,366	4.72	
Chlorella vulgaris	up to 46%	8200	7.2	Mata et al., 2010
Nannochloropsis	up to 50%	23,000-34,000	20-30	
Microalgae	30%	58,700	51.7	Chisti, 2007
Microalgae	70%	136,900	120.5	

1.4 Microalgae as Biofuel Feedstock

1.4.1 Eukaryotic microalgae

Algae have been cultivated for food since ancient times, and modern mass culturing of microalgae began in Germany during World War II as a means to produce protein-rich biomass for food (A. E. Richmond & Soeder, 1986). In the U.S., research on engineering conditions for large-scale production began at the Stanford Research Institute

in 1948, and a small pilot plant to grow *Chlorella* at the Carnegie Institute started in 1951. These works provided the conceptual basis for growing microalgae in raceway ponds. The effort was continued by the APS during 1978-1996 and funded with $25 million from the Department of Energy (Qiang Hu et al., 2008; Sheehan, Dunahay, Benemann, & Roessler, 1998).

Under the APS, over 3000 algal strains were screened for their growth conditions (e.g., pH, salinity, and temperature). Of high importance to biofuels is that lipid accumulates in eukaryotic microalgae based on different conditions of nutrients, temperature, light intensity, and growth phase. Green algae, diatoms, and non-green microalgae can accumulate lipid up to 46% of total dry weight in stressed conditions. In normal conditions, the lipid content ranges from 23-27% of total dry weight for the same microalgae (Qiang Hu et al., 2008).

Nitrogen deprivation is the primary trigger of lipid accumulation in eukaryotic microalgae (Qiang Hu et al., 2008; Spoehr & Milner, 1949). Likewise, algal cells in stationary phase accumulate 2 to 4 times more lipid than cell in exponential phase (Qiang Hu et al., 2008). Temperature and light intensity also influence lipid composition. Lower temperature or light intensity (LI) induces more unsaturated fatty acids, which could be a thermal response to change of membrane properties (Patterson, 1970), while higher light or temperature promotes neutral and saturated fatty acids.

Biomass production and lipid content are the two dominant factors to commercialize algal biofuel (Davis, Aden, & Pienkos, 2011; Scott et al., 2010). Because lipid content varies among species, strain selection is of great importance. Green microalgae like *Scenedesmus* sp, *Chlomydomonas reinhardtii*, *Dunaliella* sp, *Chlorella*

sp, and *Botryococccus* and diatoms like *Phaeodactylum tricornutum* and *Thalassiosira pseudnana* are promising strains that can accumulate up to 46-50% lipid to dry mass (Mata et al., 2010; Sheehan et al., 1998).

Potential benefits of microalgae as a "next-generation biofuel" are higher photon efficiency than plants, high triacylglycerol (TAG) content, and, thus, lower land demand. The critical drawback with eukaryotic microalgae is the trade-off between rapid growth and high lipid content. Algal cells only accumulate high lipid in stress conditions (e.g., nutrient deprivation), in which growth rate is hampered. Therefore, it is unrealistic to grow eukaryotic fast and at the same time accumulate high lipid content.

1.4.2 Cyanobacteria

Another class of photosynthesis microorganisms is cyanobacteria, sometimes called "blue-green algae." Their cell structure is different from eukaryotic algae, because they are prokaryotes. They do not have a membrane-bounded nucleus, a chloroplast (a special organelle that houses photosynthetic systems), or vesicles to store lipids. Instead, the photosynthetic apparatus is situated in thylakoid membranes contained in the cell's cytoplasm. Cyanobacteria have drawn interest for their ability to produce valuable organic products, including fuel feedstock (Angermayr, Hellingwerf, Lindblad, & de Mattos, 2009; Ducat, Way, & Silver, 2011; David O. Hall, Markov, Watanabe, & Krishna Rao, 1995; W. Vermaas, 2013).

Long evolution has provided cyanobacteria a full apparatus for photosynthesis: a water-splitting center (in photosystem (PS) II) and an energy-elevating center (PS I). With PS II and PS I, the electron-transport-chain in cyanobacteria can reduce oxidant

$NADP^+$ to reductant NADPH and store energy chemically in ATP. The reducing power and ATP then fuel the Calvin-Benson-Bassham cycle to reduce carbon dioxide (CO_2) to polysaccharide $(CH_2O)_n$ (R. E. Blankenship, 2010). Having the full set of *chlorophylls* (*a*-*d*) enables cyanobacteria to collect the full spectra of visible sunlight (R. Blankenship, 2008), which can lead to high photo efficiency (3-9%). With incident sunlight on US land of about 2,300 TW, cyanobacteria might be able to convert sunlight to energy feedstock in excess of 3.2 TW, the US's energy use rate in 2009 (Ducat et al., 2011).

Cyanobacteria can grow in diverse and marginal environments, including high pH, brackish and saline water, a wide range of temperatures, and only with simple nutrients. For example, species like *Spirulina maxima* thrives in pH~11 and salinity up to 7 times higher than seawater (Belkin & Boussiba, 1991). These abilities, in part, are inherited from long evolution that equipped cyanobacteria with mechanisms to cope with stress and scarcity.

A key difference between cyanobacteria and eukaryotic microalgae is how they react to nutrient deficiency. Nitrogen deprivation can induce lower lipid content, not higher, in cyanobacteria. They also tend to synthesize more saturated and mono-unsaturated fatty acids and decrease fatty acids with nutrient limitation (Olson & Ingram, 1975; Saha, Uma, & Subramanian, 2003). With sufficient nitrogen, the lipid content typically is 15-17% of the dry weight. Lower or higher temperature than optimal range (~30^{o}C) also may reduce lipids in *Synechocystis* sp. PCC 6803 biomass (Sheng, Vannela, & Rittmann, 2011).

Thus, a key advantage of cyanobacteria is that they can grow fast and continuously synthesis lipids at the same time. For example, a marine eustigmatophyte

called *Nannochloropsis* can increase lipid productivity by 17% while only reducing 16.7% its biomass productivity when switching from nutrient-sufficient to nitrogen-deprived growth media (Rodolfi et al., 2009). This ability makes *Nannochloropsis* even more productive than *Chlorella vulgaris* (about 1.8 times more) (Scott et al., 2010).

Concern about water use favors microalgae over terrestrial crops, particularly corn (NAP, 2008). Recycling water within a closed growth vessel reduces water usage by about 5 times compared open ponds and 3 times than corn and soybean biofuels (Harto, Meyers, & Williams, 2010). Recycling culture medium also allows nutrient recovery, an important feature to reduce energy inputs and to avoid competition with agriculture for nutrients (Larsen, Udert, & Lienert, 2013).

Deploying cyanobacteria at commercial scale requires that several major challenges be resolved. Light distribution and attenuation are prominent challenges for autotrophic microorganisms (Chisti, 2007). Chlorophylls only absorb certain spectra in the visible region. With excessive light intensity (LI), only a small portion of that energy is transferred in useful forms (NADPH, ATP), and the surplus energy is dissipated as heat that can raise water temperatures to undesired levels (Cheng & Fleming, 2009; Li, Wakao, Fischer, & Niyogi, 2009). Too low irradiance limits photosynthesis that makes the culture unproductive (Grima, Sevilla, Pérez, & Camacho, 1996). Designing a very thin photobioreactor could ameliorate the latter obstacle, but is not cost-effective (Brenner, Bildsten, Dyson, & Fortson, 2006).

1.4.3 Life Cycle Assessment and Technoeconomics of microalgal biofuel

Life Cycle Assessment (LCA) is a tool used to assess environmental impacts of a product starting from raw material extraction and extending through manufacture, use, and disposal. LCA is a useful tool to evaluate environmental aspects of microalgae fuel and to diagnose key inputs and processes to improve sustainability.

A basic inventory for microalgae technology is listed in **Figure 1.2**. Energy and associated GHGs emissions of inputs materials can be extracted from databases such as EIO-CLA, GREET, and ECOINVENT[1], which include almost any manufacturing processes. The net energy yield is critical for biofuels. Lardon et al. (2009) reported that microalgal fuel could generate net energy if lipids are obtained by wet extraction on high lipid algal paste (Lee, Yoo, Jun, Ahn, & Oh, 2010). Lardon et al. (2009) used *Chlorella vulgaris* and "cradle to combustion" to delineate an LCA model. Assumptions of mass flux and energy allocation were presented elsewhere (Benemann, Woertz, & Lundquist, 2012; Campbell, Beer, & Batten, 2011; Lardon et al., 2009; Sander & Murthy, 2010). The major energy expenditures associated with fertilizer production, microalgae cake drying, and oil extraction. Drying microalgae cake alone accounted for 60-70% of the energy input (Sander & Murthy, 2010). Alternatively, lipid can be extracted from algal sludge (20 g biomass/L), wet extraction, with reported recovery up to 70% (Lee et al., 2010).

[1] www.eiolca.net; http://greet.es.anl.gov/; http://www.ecoinvent.ch/

A novel approach is to engineer microbes to excrete actively desired products into growth medium and then harvest the products directly; this avoids biomass harvesting, drying, and lipid extraction. The next section introduces this approach for *Synechocystis*.

Besides environmental sustainability, economic viability is essential to commercial success. Productivity of at least 10-15 g biomass/m^2-day with open ponds is necessary (Sheehan et al., 1998). Doubling productivity over that level makes the economic analysis favorable for microalgal fuels (Davis et al., 2011; Huntley & Redalje, 2006).

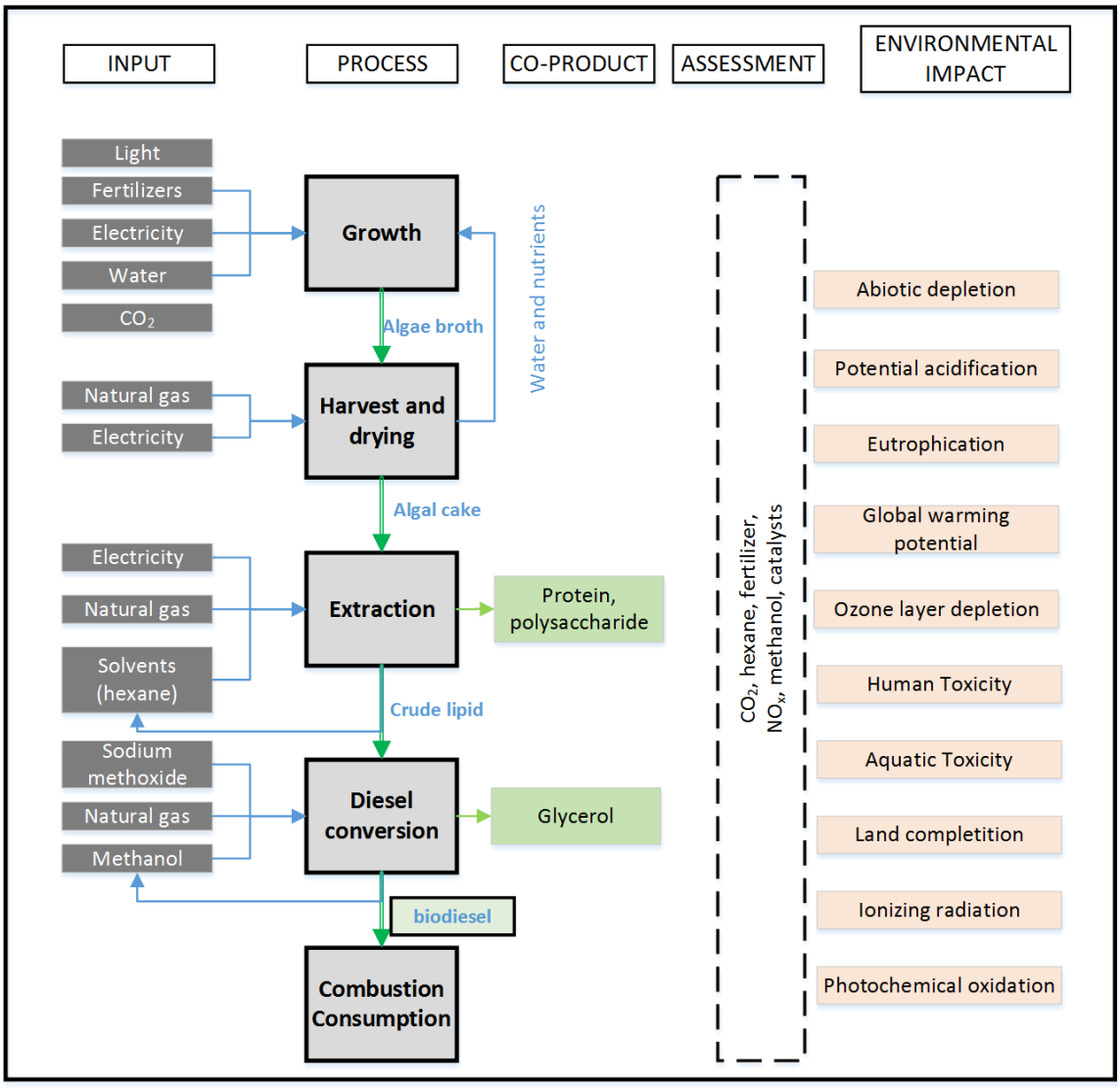

Figure 1.2: Systematic of Microalgal Diesel Production for LCA Study
Constructed based on Lardon et al. (2009 and Sander and Murthy (2010)

In the next section, I present a strain of cyanobacteria – *Synechocystis* sp. PCC 6803 – as the model photoautotrophic organism in my research. That section also includes a novel application of biotechnology to excrete fatty acid, mostly lauric acid, by a *Synechocystis* modified strain to reduce downstream processing costs.

1.4.4 *Synechocystis* sp. PCC 6803 and its genetic engineering

Synechocystis sp. PCC 6083 (hereafter called *Synechocystis*), pictured in **Figure 1.3**, is a spherical, unicellular cyanobacterium with a cell diameter of about 2 µm and no gas vesicles. While *Synechocystis* normally grows autotrophically, it also is capable of heterotrophic or mixotrophic growth (W. Vermaas, 1996). Its doubling time is relatively short, 12-14 hours with inorganic carbon as the carbon (C) source (W. Vermaas, 1996). Growth is robust in wide ranges of temperature, salinity, and pH (Kim, Vannela, Zhou, Harto, & Rittmann, 2010). *Synechocystis* may be the oldest oxygenic phototroph (about 2.5 to 3.8 billion years) and the primary producer of oxygen on the Earth (R. E. Blankenship, 2010; Schopf & Walter, 1982). Widely accepted is the hypothesis proposed in 1910 by a botany professor, Mereschowsky, that eukaryotic microalgae and plant photosynthesis acquired chloroplast from cyanobacteria such as *Synechocystis* via endosymbiosis (Ikeuchi & Tabata, 2001; Raven & Giordano, 2014). For example, gene *slr0473*, coding for light-regulated trans-membrane protein, is the same in *Synechocystis* and in the phytochrome of plants (Lamparter et al., 1997). Likewise, a large amount of tRNA is similar to between the two groups.

Distinctive benefits of studying and using a cyanobacterium like *Synechocystis* are that it (1) has a fully sequenced genome, available at Cyanobase website (http://genome.microbedb.jp/cyanobase/); (2) readily accepts foreign genomes, facilitating genetic modification; and (3) has known multiple antibiotic makers to select mutant (W. Vermaas, 1996). Besides being amenable to genetic engineering, *Synechocystis* can produce lipids without being exposed to stress conditions that hamper

its growth. This makes it different from eukaryotic algae, for which high lipid content normally is obtained only with nutrient deprivation, when growth is hampered.

Synechocystis is widely exploited as a biological model. The first published study on transformation of *Synechocystis*, using erythromycin or ethionine selection, was in 1981 (Grigorieva, Grigorieva, & Shestakov, 1981). *Synechocystis* was the first photosynthetic organism to have its genome sequenced in 1996 (Kaneko et al., 1996; Nakamura, Kaneko, Hirosawa, Miyajima, & Tabata, 1998). Since then, *Synechocystis* has been a model to evaluate photosynthetic mechanisms.

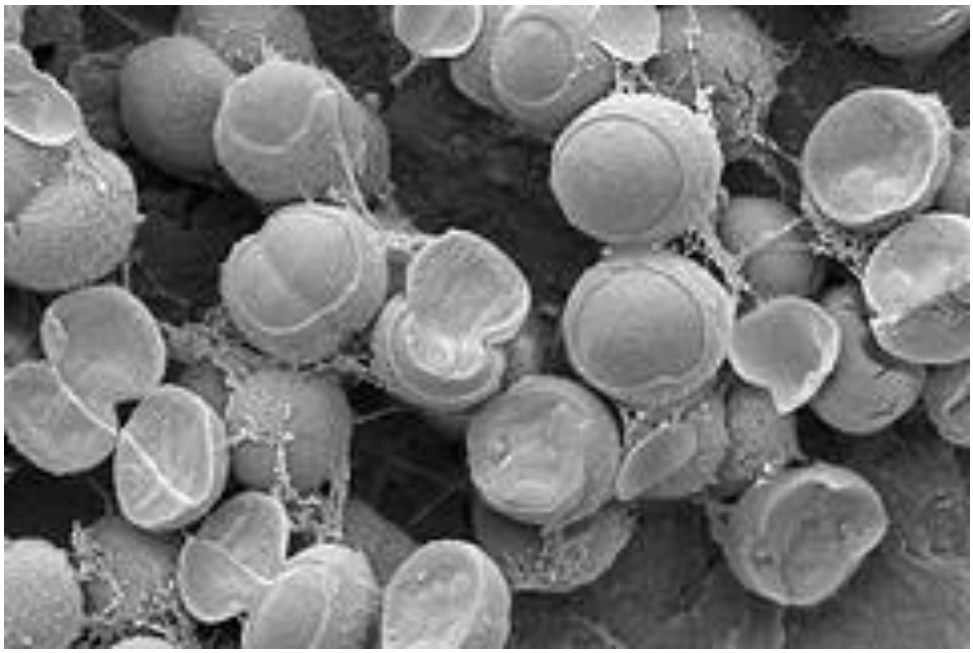

Figure 1.3: Transmission Electron Micrograph of *Synechocystis* sp. PCC 6803 cells Source: biodesign.asu.edu

Synechocystis, like other cyanobacteria, does not accumulate lipid inclusions, although it can have extensive thylakoid membranes; the former leads to a relatively modest lipid content, e.g., 15-17% crude lipid (Sheng, Vannela, et al., 2011). Furthermore, cyanobacteria produce lipids in form of diacylglycerides (DAG) that are

distributed throughout the thylakoid membranes. DAG contains two acyl groups and one functional group, and it is associated with proteins in the membrane. These characteristics of DAG are different from TAG that is produced by eukaryotic algae. TAG, composed of three acyl groups, is lipophilic and is stored in dense inclusions. DAG, being amphiphilic and more polar that TAG, is less readily extracted by solvents.

A shared disadvantage of cyanobacteria and eukaryotic microalgae is that current techniques to harvest the biomass and extract the lipid feedstock are major energy expenditures, up to 80% of total energy uses, and cost factors, 70-80% biofuel production cost (Molina Grima, Belarbi, Acién Fernández, Robles Medina, & Chisti, 2003; Sander & Murthy, 2010).

In a recent effort to reduce downstream processing costs for biofuels, Dr. Willem F.J. Vermaas and his group in the School of Life Sciences, Arizona State University produced a genetically modified laurate-excreting strain, *Synechocystis* sp. PCC 6803 **Δ** *slr1609*/TE *KatB-SodG*, that is capable of directly excreting fatty acids (FFA, mostly lauric acid, C12:0) into the growth medium. FFAs can be adsorbed to ion exchange resin and then recovered for downstream processing. Recovered FFAs are decarboxylated and then cracked to form a mixture of alkanes that resemble jet fuel (C5-C7). By avoiding biomass drying and extraction, this excretion-based method should significantly reduce energy consumption. I call this modified strain the "laurate-excreting *Synechocystis* strain," because lauric acid exists in laurate form in the growth BG-11 and is the dominant excreted fatty acids.

Liu et al. (2011) and Ducat et al. (2011) presented systematic means to engineer the biochemical pathways of *Synechocysistis* to produce alkanes, isobutyraldehyde,

ethanol, lactate, isoprene, glucose/ fructose, or hydrogen gas. To produce fatty acids, deletion (or inactivation) of gene(s) responsible fatty acids synthesis (FAS) is vital. A gene called *FadD* is responsible for incorporating exogenous long chain fatty acids into *acyl-CoAs*. Studies done in a nitrogen-fixing bacterium *Sinorhizobium meliloti* revealed that a *fadD*-deficient strain accumulated a mixture of fatty acids. Likewise, *Escherichia coli* mutants deficient in *fadD* accumulated fatty acids and released them across their phospholipid membrane (Pech-Canul et al., 2011).

In cyanobacteria, a long-chain fatty acid *CoA ligase,* or the *fadD* gene, is annotated in Cyanobase for open reading frame *slr1609* as an enzyme for fatty acid activation. *Slr1609* is referred to an acyl-ACP synthetase (*aas*) in another study (Gao, Wang, Zhao, & Lu, 2012). Cyanobacteria have the ability to incorporate exogenous fatty acids via *de novo* synthesis. Knocking out this gene results renders them unable to use exogenous fatty acids, which then are excreted into the growth medium in *Synechocystis* and *Synechococcus elongatus* PCC 7942 (Kaczmarzyk & Fulda, 2010). In addition, engineering overproduction of FFA in cyanobacteria takes advantage of a direct feed of acetyl – CoA (the precursor of FFA) that is a part of Calvin-Benson-Bassham cycle, thus increasing solar energy conversion. This is different from heterotrophic microorganisms, because they produce acetyl – CoA by sugar metabolism via the tricarboxylic acid "Krebs" cycle (Liu et al., 2011).

Liu et al. (2011) employed *Escherichia coli*'s FAS to overproduce and excrete free fatty acids (FFA) to the growth medium. In their work, modified strains were constructed with deactivated FAS by over-producing thioesterase (TE) I, which is an

enzyme that cleaves bonds acyl-CoA and intermediates of FFA. Over-producing TE resulted in accumulation of FFA in *E.coli* (Cho & Cronan, 1995).

Over-producing TE also reduces activity of *acyl-acyl* carrier proteins (ACP) – the inhibitor feedback of FAS type II – thus stimulating FAS type II flow. TE from different organisms seemed to promote the production of certain FFA. For example, TE from *Cinnamonmum camphorum* promoted excretion of myristate (C14:0); TE from *Umbellularia California* promoted laurate (C12:0); and TE from *Cuphea hookeriana* promoted decanoate (C10:0) and octanoate (C8:0) (Liu et al., 2011). **Figure 1.4** illustrates how overproduction of FFA results in natural excretion to the growth medium. Liu et al. (2011) reported that excreting FFAs were 200mg/L of culture and accounted for 13% of fixed C in biomass – a very key achievement. However, another study reported that over-expression of TE from *Cinnamonum camphora* and *E. coli* altered the fatty acid structure (Howard et al., 2013).

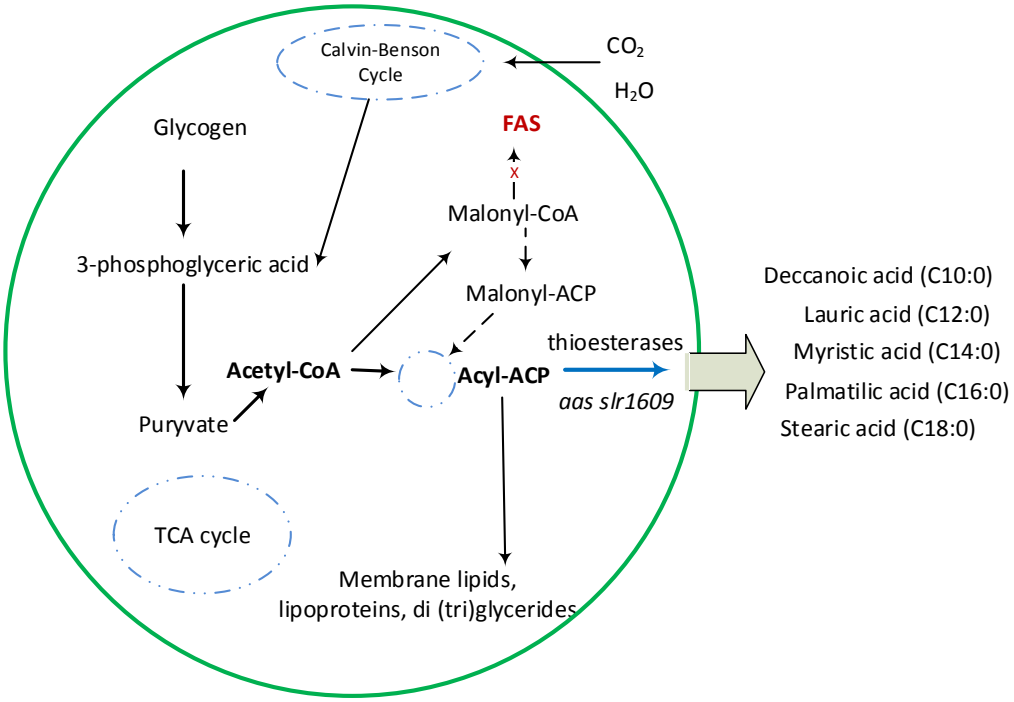

Figure 1.4: Scheme of an FFA-Excreting Modified Strain Achieved by Overexpressing Thioesterases and Deletion of *aas slr1609*
Constructed based on Liu et al. (2011)

Not all fatty acids are excreted through the membrane equally. Theoretically, unsaturated FFAs or those having a longer carbon chain are excreted less rapidly. FFA profiles of the modified strain in Liu et al. (2011) indicted that medium-length C chains were excreted the best. Palmitic acid (C16:0) was the dominant secreted FFAs, followed by stearic acid (C18:0), myristic acid (C14:0), and lauric acid (C12:0).

1.5 Objectives and Dissertation Outline

Managing environmental conditions to support photosynthesis of microalgae at a maximal rate is my ultimate goal. This works focus on inorganic carbon (C_i), Light Intensity (LI), and pH. These three parameters are connected. Light fuels the

photochemical reaction, while C_i is reduced and stores most photosynthetically fixed electrons. In microalgal biomass, carbon comprises ~50% of the biomass dry weight and 70% of fixed electrons. The growth pH affects functional groups in the cell membrane, the bioavailability of nutrients (especially C_i), and microbial products. Robust measuring of pH expedites monitoring and controlling to ensure the performance of microalgae in closed growth vessels, i.e., Photobioreactors (PBRs).

Managing LI is vital for making photosynthesis practical and productive. While about 70 years of research on mass cultivation of microalgae gives important understanding about the impacts of LI, most is relevant only to small-scale laboratory experiments, not realistic outdoor settings. While light is the phototrophs' light source, undesirable consequences can occur when the rate of supply is out of balance. For example, supplying light at a rate faster than it the flow of photoactivated electrons can be used to fix CO_2 and lead to inhibition of photosynthesis. In contrast, a too-low rate of light supply limits photosynthesis. Both cases needed to be quantitatively understood to define a favorable light regime for high productivity of microalgal biomass. This is part of my task.

Microalgae growth results in release of generic soluble microbial products (SMP). Generic SMP present a fixed carbon and electron pool without commercial value. SMP also support the growth of heterotrophic bacteria in chemoautotrophic systems; a photoautotrophic culture is prone to invasive heterotrophs that live on SMP. Maintaining environmental conditions that support biomass growth and production of a high-valued product (with a modified strain) demand that SMP production be minimized. Another of my tasks is to understand what controls the production of SMP by *Synechocystis*.

The influence of C_i on microalgae growth is obvious, as it is the cells' carbon source, and more than 50% of biomass dry weight is C. Previous work found that cyanobacteria possess constitutive (with a high exogenous C_i concentration) and inducible (with a low exogenous C_i) uptake systems that evolved along with a CO_2-Concentrating Mechanism (CCM). Because the CCM requires energy, maintaining proper C_i concentration and speciation of C_i should reduce the energy demand and improve growth rate and biomass production. This requires a systematic approach to separate effects of C_i and growth pH on photosynthesis, one more of my tasks.

To achieve the research goals, I laid out specific tasks to understand effect of LI and the nexus of pH – C_i.

1. I quantify LI thresholds that limit or inhibit photosynthesis of *Synechocystis* culture; thus, I establish a range of LI that supports photosynthesis of the wild type and laurate-excreting strains, and I evaluate growth kinetics.

2. I characterize the distribution of fixed electrons in soluble and particulate biomass of *Synechocystis* for different LI. This includes the distribution of laurate by the laurate-excreting strain.

3. I define the effects of different nitrogen sources on the alkalinity of the culture and the trend of C_i concentration. This task includes mathematical prediction using the Proton Condition (PC) and experimentally validating the predictions for *Synechocystis* wild type in a pH-stat PBR.

4. I experimentally determine how the growth kinetics of wild-type and laurate-excreting *Synechocystis* are affected independently by C_i and growth pH. The outcome directly relates to the arching goal – providing growth conditions to support maximal

photosynthesis. This task includes identifying an optimal growth pH and a minimal C_i concentration to support maximum growth rate.

5. I evaluate biomass growth and decay in simulated diurnal cycles (day and light periods). This task focuses on the decay rate in the dark periods and possible means to reduce the decay rates. In addition, I confirm that this laurate-excreting *Synechocystis* does not re-uptake exogenous laurate.

I organize this dissertation into the seven chapters that follow:

Chapter 2 introduces LI effects on *Synechocystis* growth, particularly photo-limitation and photo-inhibition. The main part of Chapter 2 presents experiments with different incident LI to evaluate values that either inhibit or limit photosynthesis. The lower limit of LI is defined by net zero biomass production, in which new biomass synthesis is equal to biomass decay. The upper limit is defined as an LI that causes damage to the photosynthetic apparatus and biomass healthiness; photo-inhibition is evidenced by light microscopy (LM) images with auto-florescent to confirm if the culture was photosynthesis inactive. Chapter 2 also includes initial growth kinetics by fitting data with Monod and "substrate self-inhibition" models. I show that *Synechocystis* wild type grew faster than the modified strain and was less susceptible to photo-inhibition. Part of these results was presented at the 1st UA/ASU Student Conference on Renewable Energy Science (Tempe, AZ, 2013).

Chapter 3 introduces SMP – its composition and function – and experimentally documents how *Synechocystis* wild-type and modified strains partition electrons photosynthetically fixed when exposed to incident LI from 111 to 598 $\mu E/m^2$-s. Fixed electrons in biomass, SMP, and excreted laurate (for a modified strain) were quantified

using Chemical Oxygen Demand (COD. The work has been submitted to *Biomass and Bioenergy*.

Chapter 4 presents the effects of growth pH, C_i, and the CCM of *Synechocystis* during photoautotrophic growth. I employ the PC to mathematically predict how the N source affects the culture's alkalinity and C_i concentration, and I verify the effects experimentally in a pH-Stat. With pH controlled at a fixed level by CO_2 addition, using nitrate as the N source increases the alkalinity and C_i concentrations, but ammonium lowers alkalinity and C_i. These trends provide a mechanistic basis for managing the C_i for photoautotrophic cultures through the N source. In particular, using ammonium nitrate makes it possible to control C_i and pH independently in a pH-Stat. The results were presented orally at the 249th ACS National Meeting and Exposition (Denver, CO, 2015) and is accepted for publication by *Environmental Science and Technology*.

Chapter 5 presents growth kinetics of *Synechocystis* wild-type and laurate-excreting strains; this work extends research that was started in Chapter 2 and takes advantages of Chapter 4 so that I can independently study the effects of growth pH and C_i on growth kinetics of *Synechocystis*. I grew *Synechocystis* at pH values of 6.5, 7.5, 8.5, 9.5, and 10.0 with a constant C_i concentration ranging from 0.05 to 3.3 mM, and at an average internal light intensity of ~202 $\mu E/m^2$-s. Among the pH values tested, pH = 8.5 supported the highest maximum specific growth rate (μ_{max}), 2.4/day and 1.7/day, respectively, for wild-type and modified strains. I fit the data using the Monod model and estimated half-maximum-rate concentrations (K_C) 0.084 mM to 0.130 mM of bioavailable C_i, or C_{ib}. This range of K_C indicating that *Synechocystis* has a high affinity for inorganic carbon, and maintaining ~1 mM (12 mgC/L) supports wild-type grow at its

μ_{max} and ~90% of μ_{max} for the laurate-excreting strain. Part of the results was presented at the 5th International Conference on Algal Biomass, Biofuels and Byproducts (San Diego, CA, 2015). The results have submitted to *Algal Research*.

Chapter 6 presents how diurnal photoperiods affect biomass production and decay. The work addresses biomass production in the light, biomass loss in the dark (dark respiration/decay), and biomass loss during the day (light respiration/decay). The work focuses on respiration/decay rates in dark periods and means to reduce the negative effects of dark decay. The results are in preparation for a peer-reviewed journal.

Key achievements are summarized in Chapter 7, along with the significance and three areas of future work.

2 LIGHT INTENSITY LIMITS OR INHIBITS PHOTOSYNTHESIS

2.1 Introduction

2.1.1 Light intensity

Light, essential for photosynthetic organisms, is electromagnetic radiation that can be quantified as a pseudo-particle, or a photon. Sunlight consists of wide spectrum of wavelengths, including ultra-violet (UV), visible, and infrared irradiance (Burger & Edwards, 1996; Powles, 1984). The energy of each photon depends on its wavelength: A shorter wavelength carries more energy than a longer one, but only photons in the visible spectra (violet – 400 nm to red – 700 nm) can be utilized in photosynthesis. Called photosynthetically active radiation (PAR), these wave lengths account for 40% - 47% of the energy in full spectrum sunlight (Melis, 2009; Giuseppe Torzillo, 2004). Shorter wavelengths, like UV radiation, damages the photosynthetic apparatus and inhibits repair of essential proteins, while those longer than 700 nm carries inadequate energy to drive photosynthesis in most organism.

Light Intensity (LI) can be expressed as radiant energy flux in W/m^2 or as photo density in $\mu E/m^2$-s, where W stands for Watts and E stands for Einsteins. One Einstein equals one mole of photons, and two terms are used interchangeably. Energy flux can be converted to photo density with conversion factors appropriate to the light source. For fluorescent bulbs, the conversion factor is 4.6 $\mu E/m^2$-s per W/m^2. The conversion factor is lower with sunlight (between 4.2-4.5 $\mu E/m^2$-s per W/m^2), but is higher for a quartz-iodize bulb (5.0 $\mu E/m^2$-s per W/m^2) (McCree, 1972).

2.1.2 General photosynthesis

Photosynthesis involves two stages, called the light-dependent reaction (requires photon energy) and the light-independent reaction (does not requi photon energy) (Hall at el., 1999). **Figure 2.1** illustrates the two stages of photosynthesis. The example here represents the stoichiometric requirement of energy (ATP) and of reducing power (NADPH) to produce glucose from carbon dioxide:

$$6\ CO_2 + 12\ NADPH + 18\ ATP + 6\ H_2O \rightarrow (C_6H_{12}O_6) + 6\ O_2 + 18\ ADP + 18\ P_i + 12\ NADP$$

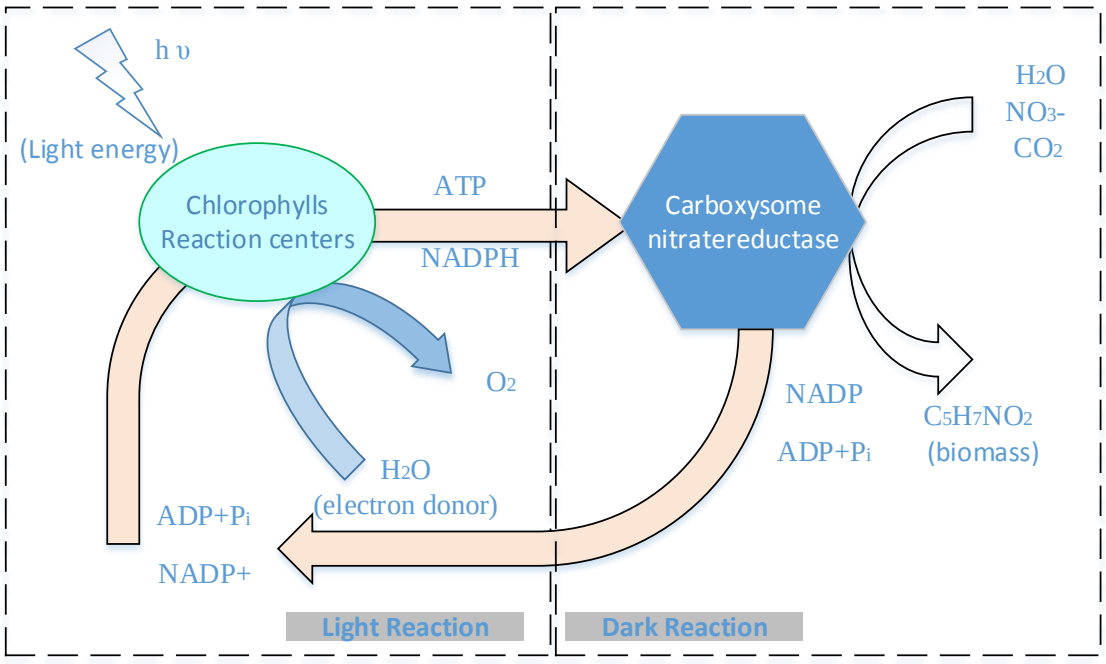

Figure 2.1: Diagram of Dark and Light Reactions in Photosynthesis

Experimentally, the photosynthesis rate usually is measured by the rate of oxygen evolution in response to the LI, called a light-response curve. Increasing LI when the light irradiance is low usually gives a linear increase in the oxygen-evolution rate. Increasing LI to a medium range does not yield a proportional increase in the O_2-

evolution evaluation rate, and this is called the saturation stage, ~ 400 μE/m^2-s in most wild-type microalgae (Melis, 2009). When irradiance is high enough, light inhibits photosynthesis because excessive energy produces free radicals that consequently break down chlorophylls and electron-transport molecules; this is the photo-inhibition stage.

Figure 2.2 illustrates the three stages. For example, experiments carried out with plant leaves show that, for LI < 100 μE/m^2-s, nearly 80% of incident energy is utilized. With LI > 300 μE/m^2-s, increasing incident LI does not improve the utilization rate. With high enough sunlight intensity (1000 μE/m^2-s), the utilization efficiency is roughly 25% at 25°C (Robt Emerson, 1958).

With microalgae like *Chlorella*, saturation was reached around 500 μE/m^2-s (D O Hall et al., 1999). Sorokin & Krauss (1958) grew *Chlorella*, *Scenedesmus,* and *Chlamydomonas* in an inorganic medium at 25°C and found that all three strains reached photon-saturation around 160 μE/m^2-s and photon-inhibition with 350-650 μE/m^2-s in PAR[2]. All of these levels are far less than full sunlight at noon in summer Phoenix, which reaches up to 1800 μE/m^2-s as PAR (NREL, 2010). Furthermore, high temperature induced photo-saturation and photo-inhibition at lower photon fluxes (Robt Emerson, 1958). Therefore, managing high intensity of light in outdoor cultivation of microalgae is an important research arena.

For many reasons, outdoor mass culturing gives far less productivity than what has been observed in laboratory experiments. The diurnal light cycle and its parabolic

---

[2] The conversion to PAR is assumed with the use of Plant Growth Fluorescent bulbs, and conversion factors from this website http://www.egc.com/useful_info_lighting.php. For reference, 0.071 W/m^2 per 1 ft. candle, 0.327 μE/m^2-s per 1 ft. candle

pattern of irradiance during the day lead to sub-optimal quantum yield. LI is low near sunrise and sunset, but intense LI -- over 1000 μE/m^2-s in an typical 8 AM to 4 PM period – can lead to photo-inhibition for most microalgae (Robt Emerson, 1958; Melis, 2009). In addition, mutual shading by cells in a dense culture precludes light penetration and limits LI to cells located in deeper culture (Tredici & Zlttelli, 1998).

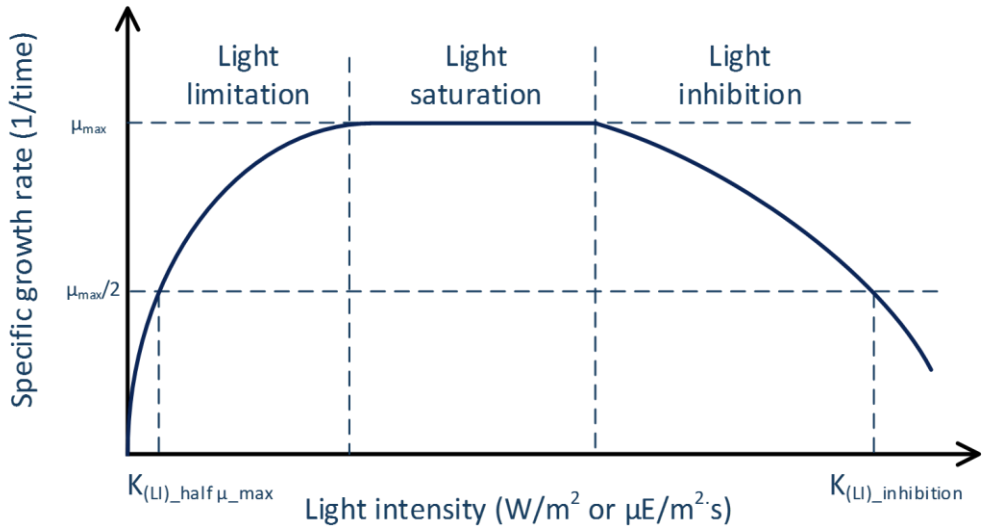

Figure 2.2: Generic Light-Response Curve Showing Limitation, Saturation, and Inhibition Stages (J. C. J. Goldman, 1979b)
The curve depicts the dual property of LI to photosynthesis: a "substrate" at low density, but an inhibitor at high density

Quantum yield is a key parameter to assess photosynthesis efficiency of different organisms and is calculated as the ratio of energy stored in products to energy carried by photons (Robt Emerson, 1958). Theoretically, the quantum yield of photosynthesis for PAR is 12% with the model based on the energy released per one mole glucose and the energy required to fix C_i (Radmer & Kok, 1977; Walker, 2009). Experimentally, green microalgae like *Chlorella* can obtain a maximum 9-12% quantum yield with selected

irradiance, e.g. those in 400-480 nm and 640 – 680 nm (Barbosa & Wijffels, 2013; Robert Emerson & Lewis, 1943; Evans, 1987). Pilot studies with microalgae grown in open ponds and PBRs reported a 4.5-7% quantum yield, which translates to 30-40 g biomass/m^2-d (Amaro, Guedes, & Malcata, 2011; Scragg, Illman, Carden, & Shales, 2002). Data collected over two years for *Scenedesmus* grown in a 3-m^3 tubular PBR indicated that it could produce 3.8 metric tons biomass annually, which converts to 20 g biomass/m^2-d and a 3.6% quantum yield (Acién, Fernández, Magán, & Molina, 2012). A rate of 15 g/m^2-d biomass is considered as a baseline productivity of algae, and doubling that rate is considered a high-productivity scenario (Campbell et al., 2011; Davis et al., 2011). While these actual productivities are less than possible peak productivity, 120-130 g/m^2-d (A. Richmond, 2000), the superior yields of microalgae and cyanobacteria, compared to plants, merit their consideration as energy crops.

2.1.3 Photo-inhibition and photo-limitation

One way to improve biomass productivity is to increase incident LI. However, this approach may provide excessive photons to layers of cells near the light inlet, resulting in photo-inhibition, which can be classified as "dynamic" or "chronic." Dynamic photo-inhibition occurs when photosynthetic organisms begin to dissipate light energy as heat (Adir, Zer, Shochat, & Ohad, 2003; Xu & Shen, 1999). Extra heat exacerbates protein deactivation locally and increases the culture's temperature in other ways that reduce culture productivity. Chronic photo-inhibition occurs later through free-radical attack on and damage to the photosynthetic enzymes, reaction centers, and electron-transport chain (Xu & Shen, 1999).

Photo-inhibition was recognized as early as 1900 and was studied first by Kok (1956), who exposed *Chlorella* to different fractions of full light (33%, 59%, and 100%) and measured the oxygen-evolution rate. The cells initially produced oxygen constantly for 7 minutes, but the rate gradually dropped to zero due to the sustained impact of photo-inhibition and destruction of photochemical reaction centers. Photo-inhibition increased with longer exposure, which lead to leaching of oxygen-depended pigments (Belay, 1981; Samuelsson, Lönneborg, Gustafsson, & Oquist, 1987). Understanding photo-inhibition and repair mechanism has been an active research topic beginning in the late 20^{th} century (Adir et al., 2003; Nixon, Michoux, Yu, Boehm, & Komenda, 2010; Silva, Thompson, & Bailey, 2003).

Photo-inhibition can occur at either the light-harvesting complex (LHC) or the reaction centers (RC), as illustrated in **Figure 2.3**. The product of excessive photon energy is usually a radical oxygen species (ROS), in which singlet oxygen ($^1O_2$) is one powerful oxidant (Mittler, 2002) that can oxidize the D1 protein, chlorophylls, and carotenoids (Xu & Shen, 1999). D1 proteins, encoded by the *psbA* gene and vital for photosynthesis, are reaction centers in PSII that are particularly prone to damage (Adir et al., 2003).

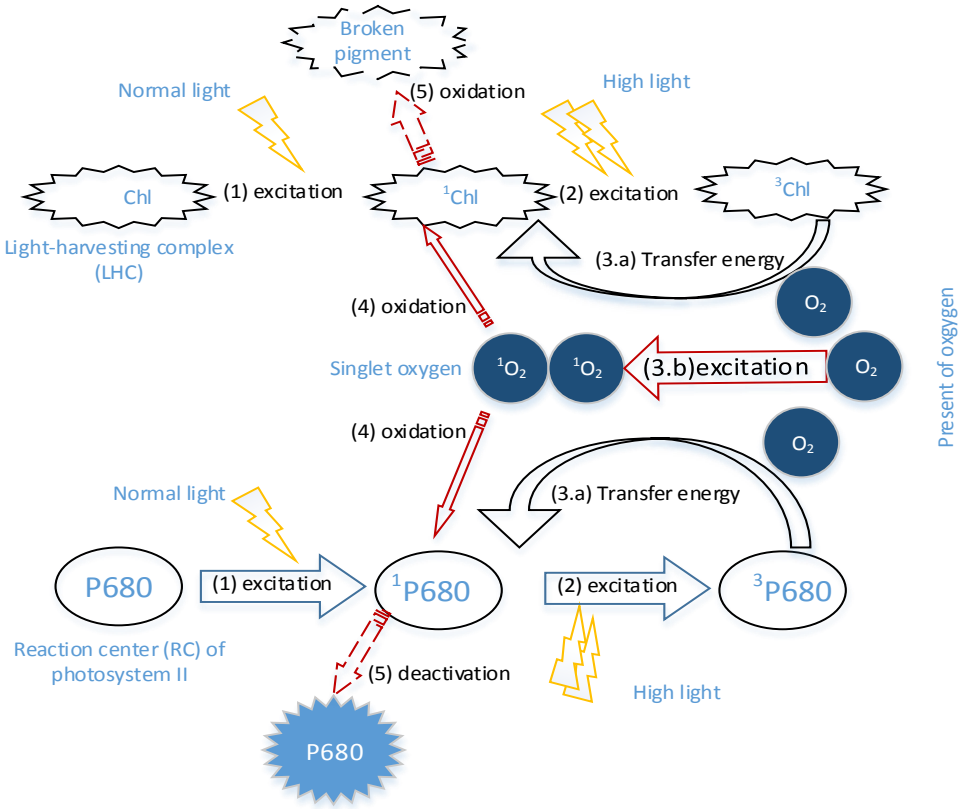

Figure 2.3: A Scheme of Photo-Inhibition Due to Excessive Light

When a photosynthetic organism is exposed to excessive LI, its light-harvesting complex (LHC) and reaction center (RC) in PS II create triplet states of chlorophyll and energized P680 (^{3}Chl and ^{3}P680). The triplets are longer-lived than are their singlet states, and they transfer energy to oxygen and form singlet oxygen ($^1O_2$). Singlet oxygen is a powerful oxidant and unselectively oxidizes proteins nearby, which causes deactivation of RC and broken pigments from LHC. Numbers with each process shows the sequence of events.

Exposure duration and temperature affect photo-inhibition, but in different ways. Experiments with *Spirulina* indicated that photosynthesis was reduced 50% when the illumination flux was 1800 µE/m^2-s for 30 minutes at 25^{o}C and 60 minutes at 30^{o}C (Jensen & Knutsen, 1993). With a lower LI shock (800 µE/m^2-s), no significant photo-inhibition was observed during a 160-minute exposure. Temperature affects the rate of

repair after photo-inhibition as well. During a 60-minutes incubation at 110 μE/m^2-s, cells at 35 – 40^{o}C showed complete recovery, but recoveries were only 93% at 30^{o}C and 17% at 20^{o}C (Jensen & Knutsen, 1993).

Acclimation to a high-light condition can reduce the damage from photo-inhibition. *Synechococcus* 6301, a cyanobacterium, was grown in low light (10 μE/m^2-s) or high light (120 μE/m^2-s) prior to exposing the cells to a high-light experiment. Previous to the high-light exposure, the cells were acclimated to 130 μE/m^2-s or to 450 μE/m^2-s for 90 minutes and at 38^{o}C (Samuelsson et al., 1987). Cells grown in higher light were three times more resistant to photo-inhibition and had 2.6-times faster of repair than cells grown in lower light.

2.1.4 Light intensity to growth kinetic model and its application to PBR engineering.

Earlier studies used incident LI near the interface of the culture vessel to modulate the photon flux to the whole culture. This approach works well with small and thin setups (Robt Emerson, 1958; Kok, 1956), but incident LI does not represent well the average intensity with a large reactor having a long light path (J. C. J. Goldman, 1979a). Thus, one can use a light-absorption model to estimate the local LI at certain depths in a culture. The common means to estimate local LI is with the Beer-Lambert law (Kim et al., 2010; Suh & Lee, 2003), which assumes isotropic adsorption of monochromatic light (F. G. Fernández, Camacho, Pérez, Sevilla, & Grima, 1997):

$$\mathrm{LI}(\lambda) = \mathrm{LI}_0(\lambda).\exp[\varepsilon(\lambda).\mathrm{X}.\mathrm{w}] \qquad (2.1)$$

where w: distance to light source [length];

$LI_0(\lambda)$: LI at the surface entering the reactor ($\mu E/m^2$-s)

$LI(\lambda)$: local LI at depth w ($\mu E/m^2$-s).

$\varepsilon(\lambda)$: absorptivity coefficient for the adsorbent (cell) and wavelength λ [$length^2/mass$]

X: adsorbent (cell) concentration [$mass/length^3$]

Growth kinetics as a function of local LI has been based on many empirical approaches. A recent article reviewed in detail the published light models for phototrophic growth kinetics (Béchet at el., 2013). To model three-stage photosynthesis, the most relevant model for my work is the "light self-inhibition" model (Eqn. (2.2)):

$$\mu = \mu_{max} \frac{LI}{K_{LI} + LI + LI^2/K'_{LI}} \tag{2.2}$$

where: K_{LI}: light intensity giving one-half the maximum growth rate if photo-inhibition is not active; K_{LI}': light intensity causing a 50% reduction if μ_{max} due to photo-inhibition; and LI is a local or volume-averaged light intensity calculated using the Beer-Lambert Law. This model is similar to the Haldane substrate-self-inhibition model for cells or enzymes (Waley, 1964).

Much previous research has related incident LI (or photon density) to the biomass growth rate (Robt Emerson, 1958; J. C. J. Goldman, 1979b; Kok, 1956). A major complication for kinetic modeling is that the LI inside the growth medium usually is lower than the incident LI due to light attenuation. Growth-rate experiments carried out in very small reactors, e.g., in 16 × 150-mm test tubes (Sorokin and Krauss, 1958) or micro-vessels (2 – 5 µl per irradiated cm^2) (Kok, 1956), may allow the incident LI to approximate to average LI inside the reactor. However, using very small vessels usually

is impractical for kinetic experimentation, and it is totally infeasible for engineering scale.

Incident LI varies with diurnal and seasonal cycles that lower biomass yield. For outdoor cultivation, an engineer has some leeway to alter the incident LI based on PBR orientation and shading. Always of importance is the LI decline inside PBR due to cell self-shading.

The photochemical reactions -- light and dark reactions -- in photosynthetic organism occur nearly instantly. (Robert Emerson & Arnold, 1932) experimented with flask lighting with *Chlorella* and reported that the light reaction is complete within 10 μs, while the dark reaction is 2000 times slower. Molecular work later revealed that energy transfer in the light reaction occurred in ~100 μs (Feher, Allen, Okamura, & Rees, 1989). Using flashing light to a tomato leaf revealed that 1.5-μs pulsing at 5000 $\mu E/m^2$-s had the same quantum yield as a 50 $\mu E/m^2$-s equivalent to a continuous illumination (Tennessen, Bula, & Sharkey, 1995). Longer flashing (200 μs) yielded half the efficiency than the equivalent continuous illumination (Tennessen et al., 1995). Because the photochemical reactions happen so quickly, PBR mixing may affect photo-inhibition related to the local LI. Therefore, creating a uniform condition (e.g., through mixing) so cells are exposed to variations in LI, even in very short periods (~0.02s), may improve biomass productivity.

For applications, using either incident LI or average internal LI (AILI) as a performing indicator bears consideration. Incident LI is far easier to monitor, simply by measuring photon density onto a reactor surface. However, incident LI does not represent the light intensity inside the reactor, but is the highest possible LI to which the phototrophs can be exposed. Incident LI also is not a suitable pseudo-concentration to fit

in growth model such as the Monod's. The use of AILI is preferable in this case. The problem with AILI is that it must be calculated by a model, such as the Beer-Lambert law. The use of AILI is subject to incident LI and attenuation that depends on factors specific to the culture and the reactor configuration.

In my study, I used incident LI and AILI to represent light energy. The incident LI is used to make an initial assessment of different exposure modes, such as in **Figure 2.2**. The incident LI is suitable to study acute photo-inhibition effects because of high dosage exposure. That high incident LI inhibits photosynthesis may imply that high AILI also causes photo-inhibition, but the relationship is not yet clear. AILI is better suited to study volumetric productivity of photosynthesis biomass, particularly when photo-inhibition is not an issue. The difference between incident LI and AILI can be overcome either by shortening light path (very thin reactor) or by mixing vigorously; therefore cells have the same opportunity to be exposed to the incident LI.

The challenge of using incident LI or AILI to model photosynthesis in large volume is not unique. Adsorption, in which Langmuir isotherm treats adsorbent as mono-layer and Freundlich equation as multiple layers, shares the challenge. Nevertheless, photosynthesis introduces the complexity of an optimal LI range that saturates photosynthesis. Therefore, any model to represent the relationship between LI and photosynthesis has to incorporate two phenomena: photo-inhibition in high LI and photo-limitation in low LI. In the next section, I use incident LI to study the inhibitory effect of light and AILI to present the volumetric potential of light for photosynthesis.

To determine values of LI that limit or inhibit photosynthesis of *Synechocystis*, I designed and implemented batch experiments with a wide range of incident LI. This

allowed me to define the photo-limitation and photo-inhibition thresholds, and it enabled me to characterize growth kinetics of *Synechocystis* in the next chapters.

2.2 Materials and Methods

2.2.1 BG-11 medium preparation

Standard BG-11 medium (Rippka, Deruelles, Waterbury, Herdman, & Stanier, 1979; UTEX, 2009) is a typical growth medium for cyanobacteria. Each liter of BG-11 consists of: 17.6 mM $NaNO_3$, 0.22 mM K_2HPO_4, 0.03 mM $MgSO_4.7H_2O$, 0.2 mM $CaCl_2.2H_2O$, 0.02 mM Ammonium Ferric Citrate (AFC-brown); 0.002 mM $Na_2EDTA.2H_2O$, 0.18 mM Na_2CO_3, and trace minerals of 46 μM H_3BO_4; 9 μM $MnCl_2.7H_2O$; 0.77 μM $ZnSO_4.7H_2O$; 1.6 μM $Na_2MoO_4.2H_2O$; 0.3 μM $CuSO_4.5H_2O$; and 0.17 $Co(NO_3)_2.6H_2O$. Chemicals were purchased from Acros Organic, EMD, J.T. Baker, Alfa Aesar, VWR, Sigma-Aldrich, all with A.C.S analytical grade. I prepared the medium in four solution stocks: (1) 100 X of $NaNO_3$ and trace minerals, (2) 1000X of K_2HPO_4, (3) 1000X of AFC, and (4) 1000X of Na_2CO_3. Aluminum foil was wrapped around the stock (3) bottle to prevent photo degradation of AFC. Stocks (1) and (3) were kept in 4^{o}C and stocks (2) and (4) were kept in an air-conditioned room (~ 25°C).

Growth medium was prepared and autoclaved in a 2-L glass bottle (VWR, U.S.). To prepare 2 L of standard growth medium, I first added 1.5 L DI water, followed by the ingredient stocks: 20.0 mL of stock (1) and 2.0 mL each stock (2), (3) and (4). Additional DI water was added later to bring the water to a liquid volume of 2.0 L. The solution was then autoclaved with liquid cycle (121^{o}C and 15 minutes) in a Tabletop

Sterilizers (SterileMax, Thermo Scientific, IA). Although sterilization caused the formation of mineral precipitates, shaking the autoclaved medium caused them to dissolve.

2.2.2 Inoculum and experiment preparation

Synechocystis sp. PCC 6803 wild-type and laurate-excreting strains were provided on agar plates by the laboratory Dr. Vermaas, School of Life Sciences, ASU. Pure colonies were transferred and suspended into a 250-ml Erlenmeyer glass flask containing ~150 ml of the standard BG – 11 medium. The liquid inoculum was then incubated in a biological incubator (Percival Scientific, Inc. IA) in 4-5 days at 30^{o}C and LI ~ 80 μE/m^{2}-s. Carbon dioxide was supplied to the culture by aerating filtered atmospheric air.

Experiments were first carried in 1-L Erlenmeyer flasks with a high range of incident LI (111 to 598 μE/m^{2}-s). CO_2 supply and mixing were provided via a glass pipet connected to silicon tubing and 1-μm bacterial filter (Pall® Life Sciences) to an air pump. Closed growth environment was maintained by capped cheesecloth. Before transferring the autoclaved BG – 11 into the growth vessel, entire growth apparatus was steam-autoclaved with unwrap cycle (135^{o}C for 3 minutes, followed by 15-minute drying).

In addition to Erlenmeyer flasks, I used Corning flasks with 0.4-L working volume (VWR, US) to study a lower range of incident LI (40 to 150 μE/m^{2}-s). A Corning flask has a flat surface and is made of polystyrene (PS), which allows better light transport than glass (Engineering ToolBox, 2015). The thin depth (4.25 cm) made it easier for me to use AILI to investigate photo-limitation. However, the Corning flask cannot be sterilized by steam; instead, I soaked the inside surface with 70% isopropanol,

dried the flask, and then exposed the flask to a 253.7-nm germicidal lamps (T8, Philips, Holland) in 15 minutes before inoculating.

2.2.3 Experimental conditions

Fresh inoculum removed from the biological incubator was inoculated into 500 mL of sterilized BG-11 medium in a sterilized flask. The transfer was carried out in a laminar-flow biosafety hood (Thermo Fisher Scientific) to reduce the risk of biological contamination. The starting optical biomass density of experimental culture was in the range of 0.1 - 0.15 Absorbance Unit (AU), which allowed me to explore growth from the beginning and reduce effects of aging culture and endogenous decay. One unit of AU is equivalent to 90% of the incident light be absorbed or reflected by the sample.

The flask reactor was then situated a specified distance from the fluorescent bulb panel so that each reactor had a particular incident LI. I used a light meter (details below) to check the actual LI and decide if further adjustment was needed. All experiments were carried out at room temperature (~25^{o}C) and with continuous illumination, and the temperature of the cultures was 26, 27, 28, and 33^{o}C for the lowest to the highest LI measured from 111 to 598 $\mu E/m^2$-s. Atmospheric CO_2 (~ 395 ppm CO_2) was supplied through a glass pipette tip and pumped by Top Fin® Air Pump filtered by the 1.0- pipette tip and pumped by Top Fine fluorescent bulb e air-supply rate was ~1.5 L air/L liquid-minute to ensure a well-mixed culture.

2.2.4 Analyses

Samples were taken regularly, daily or every-two days inside a laminar-flow biosafety hood by a sterilized pipet into 15-ml screw-cap Falcon Polypropylene centrifuge tubes (VWR, U.S.). Samples were immediately measured for optical density (OD) by a UV-Vis BioSpec-mini spectrometer at wavelength of 730 nm (Shimadzu Corp., Japan). To ensure reliable measurement, I diluted a sample with deionized ion (DI) water to obtain an OD less than 0.7. The spectrometer was auto-zeroed with DI water before measuring each batch of samples. The OD reading then was converted to biomass dry weight using an empirical conversion factor of 254 mg biomass/L per of unit of OD (Kim, Vannela, & Rittmann, 2013). The remaining was then stored in a 4^{o}C refrigerator for further analyses.

LI was measured by a LI-190 quantum sensor (LI-COR®, NE) integrated with an U1252 micro-ammeter (Agilent, CA). The unit displays an output in microamperes (μA) that are converted to μE/m^2-s by a conversion factor provided by LICOR. The incident LI was measured on the front side of each flask and represents the incident and the highest LI for each reactor.

AILI, the volumetric representation of LI, was calculated based on the Beer-Lambert law (Eqn.(2.1), with an absorptivity coefficient representative of *Synechocystis* biomass. The AILI, expressed in μE/m^2-s, equals the average of the local LI values for the entire light path inside the reactor (Eqn. (2.3)). Incident LI (LI_0),) ranged from 111 to 598 μE/m^2-s, and the absorptivity coefficient (ε), shown in **Table 5.3**, was 0.255 (m^3/g-m). X is the biomass concentration (g/m^3) and dw is the integrand for depth of light path

(m). I present step-by-step calculation in the Average Internal Light Intensity section of Chapter 6.

$$\mathrm{AILI} = \frac{\mathrm{LI}_0 \int_0^{\mathrm{d}} \mathrm{e}^{-\varepsilon \mathrm{X} \mathrm{w}} \mathrm{dw}}{\mathrm{d}} \tag{2.3}$$

I inspected the cultures using Light Microscopy (LM) to check the status of *Synechocystis* cells, as well as look for the presence of other microorganisms. Cells were immediately fixed using freshly prepared 4% (v/v) formaldehyde in phosphate buffer (0.1M, pH 7.0) for two hours, followed by washing in phosphate buffer and stored at 4°C until imaged. Fixed samples were examined with an Axioskop light microscope (Carl Zeiss, Inc., Thornwood, NY) with appropriate optics, recorded with a Roper Cool SNAP ES digital camera (Roper Scientific, Inc., Tucson, AZ), and processed using MetaMorph 6.0/6.1 software (Universal Imaging Corporation, Downingtown, PA). Imaging was carried out in the laboratory of Dr. Robert W. Roberson Laboratory, School of Life Sciences, ASU.

Auto-florescence uses a laser with < 598 nm to excite chlorophylls and detect florescence (Zhang, Gase, & Baldwin, 2010). Healthy and photosynthesis-active cells absorb certain exciting laser wavelengths and florescence with lower wavelengths. Those cells appear greenish on LM image; in contrast, a deactivated cell does not react to excited light and appears grayish in LM.

2.3 Results and Discussion

2.3.1 Photo-inhibition under high light intensity

To evaluate the LI level that inhibits photosynthesis, I illuminated continuously wild-type and laurate-excreting strains of *Synechocystis* with LI from 111 to 598 μE/m^2-s. I first present quantitative comparisons of incident LI and AILI to biomass concentration based OD. Later, I provide colored-digital and LM images to collaborate pigment color of photo-inhibition and healthy photosynthetic culture.

Figure 2.4 shows that the biomass for wild-type and modified strains grew well for the first two weeks. Wild type grew faster and attained 1200 mg/L dry weight with 598 μE/m^2-s, nearly double the dry weight produced by the modified strain with the same LI. The intensity of incident light corresponded to biomass density with both strains.

From day 12, the biomass density of wild type leveled off, and the culture exposed to 598 μE/m^2-s had declining biomass density. This change is consistent with the change of biomass color (**Figure 2.5**). The biomass density of the laurate-excreting strain did not a drop like the wild-type strain with 598 μE/m^2-s, but a similar color change occurred from day 8.

The wild-type strain showed more resistance to high LI than the laurate-excreting strain. For example, it maintained a healthy green color longer than the laurate-excreting strain with the same experimental conditions (**Figure 2.5**). The laurate-excreting strain showed the onset of photo-inhibition with a lower LI, 346 μE/m^2-s.

While the incident LIs were constant, the corresponding AILI ranged from 10 to 598 μE/m^2-s in the Erlenmeyer triangular flasks. Panel a of **Figure 2.4** correlates biomass density to AILI for the wild-type strain. As biomass grew, AILI declined significantly, and the LI stabilized between 10 and 20 μE/m^2-s from day 6 onward. The flask illuminated by 598 μE/m^2-s had its biomass concentration plummet around day 14, and this correlated with the biomass color clearly turning brownish with loss of green pigments (**Figure 2.5**). The AILI at day 14 was about 20 μE/m^2-s, which should not have been high enough to cause direct inhibition; however, a combination of previous exposure to high AILI (up to 598 μE/m^2-s near the start of the experiment) and high local LI (i.e., at the face of the flask) could have accumulated inhibition effects that later resulted in low observable effects of photo-inhibition.

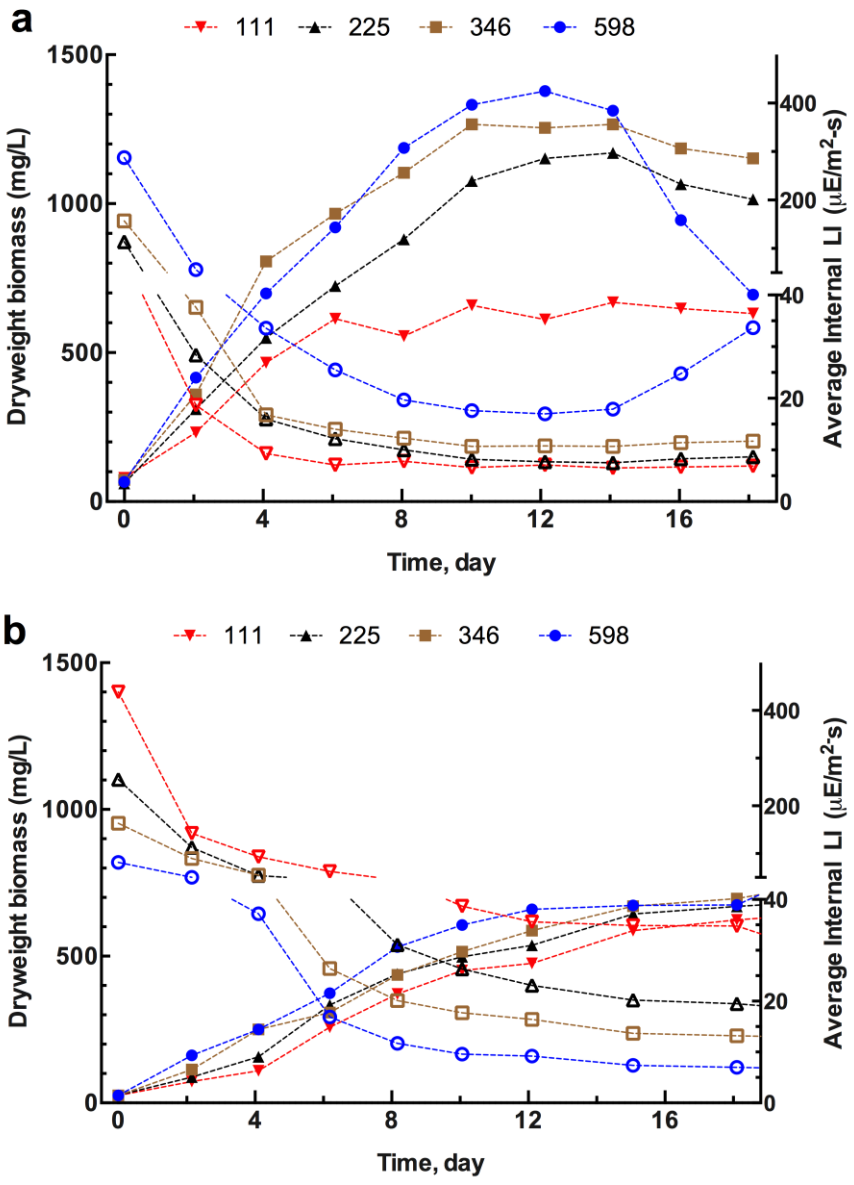

Figure 2.4: Biomass Dry Weight (DW- Closed Symbols) and AILI (Open Symbols) of Flasks with Different Incident LI on Wild-Type *Synechocystis* (Panel a) and the Laurate-Excreting *Synechocystis* (Panel b) for the Range of Incident LI Shown in the Top Rows ($\mu E/m^2$-s)

The same type of representation is in panel b of **Figure 2.4** for the laurate-excreting strain. Similar to the wild-type culture, the AILI declined to less than 20

$\mu E/m^2$-s in all flasks by day 15. Compared to wild type, the laurate-excreting strain had a significantly slower growth rate for 346 and 598 $\mu E/m^2$-s. An early onset of photo-inhibition, presumably caused by high LI, can be seen around day 8 (pictured, **Figure 2.5**), when the corresponding AILI was ~70 $\mu E/m^2$-s. The culture continued to grow, but its color was light green to yellowish and brownish from that day until the end of the experiment.

Figure 2.5 presents digital pictures of wild-type and laurate-excreting *Synechocystis* at different times in the experiments. The wild-type strain grew normally in all flasks during the first week. In the second week, the culture with an LI of 598 $\mu E/m^2$-s changed to slightly light green and then turned to slightly yellowish a week after that. The milky, yellowish culture was associated with photo-inhibition with a 2-week exposure. The change in pigment colors in **Figure 2.5** connects well with a biomass concentration dropping on day 14 for the wild type in **Figure 2.4**.

The lightening of the green color for the cultures in the top row is less obvious with just a few days exposure to incident LI of 598 $\mu E/m^2$-s (AILI $\geq$ 70 $\mu E/m^2$-s), although the laurate-excreting strain growing more slowly than the wild-type strain. The color photographs affirm that photo-inhibition resulted from a long-term exposure to high LI and may have correlated more to local LI near the light inlet than to AILI.

The laurate-excreting strain was susceptible to photo-inhibition at a lower LI than was the wild type. Although LI of 346 $\mu E/m^2$-s (AILI $\geq$ 10 $\mu E/m^2$-s) caused a less severe impact that 598 $\mu E/m^2$-s, the laurate-excreting culture became a milky light green by the end of the 3-week experiment.

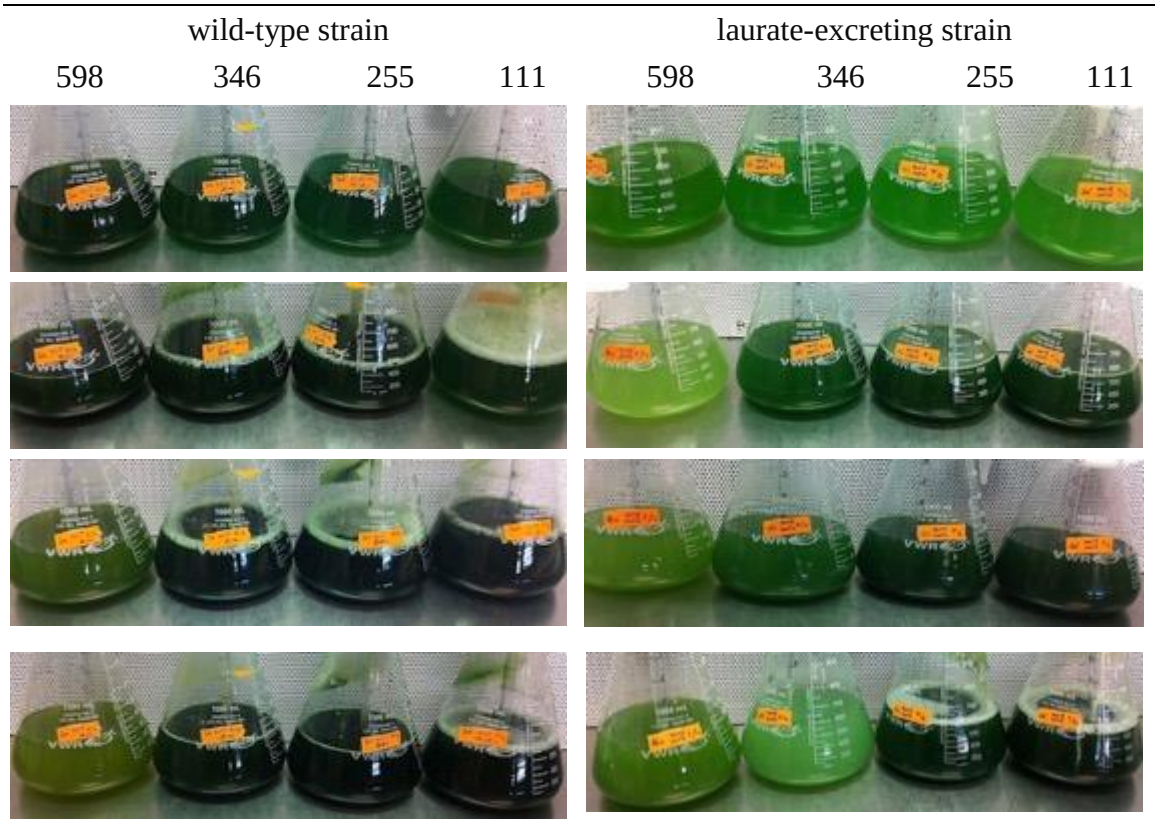

Figure 2.5: Digital Pictures of *Synechocystis* Wild-Type at day 2, 8, 16, and 18 (Left Column) and *Synechocystis* Laurate-Excreting Strain at Day 2, 8, 18, and 24 (Right Column)

A dark green color signifies a healthy culture; in contrast, a light, milky green color signifies stress from photo-inhibition. The numbers in the first row represent incident LIs in $\mu E/m^2$-s for each flask in the column

Photo-inhibition of the laurate-excreting strain due to high LI was confirmed by a second run with similar conditions. Photographs in **Figure 2.6** confirm the same phenomenon - a milky, yellow and light green color. The literature reveals that a yellowish color may be attributable to xanthophylls – a group of pigments that sequester radical oxygen species and are expressed with photo-inhibition conditions (Robt Emerson, 1958; Huner et al., 1993).

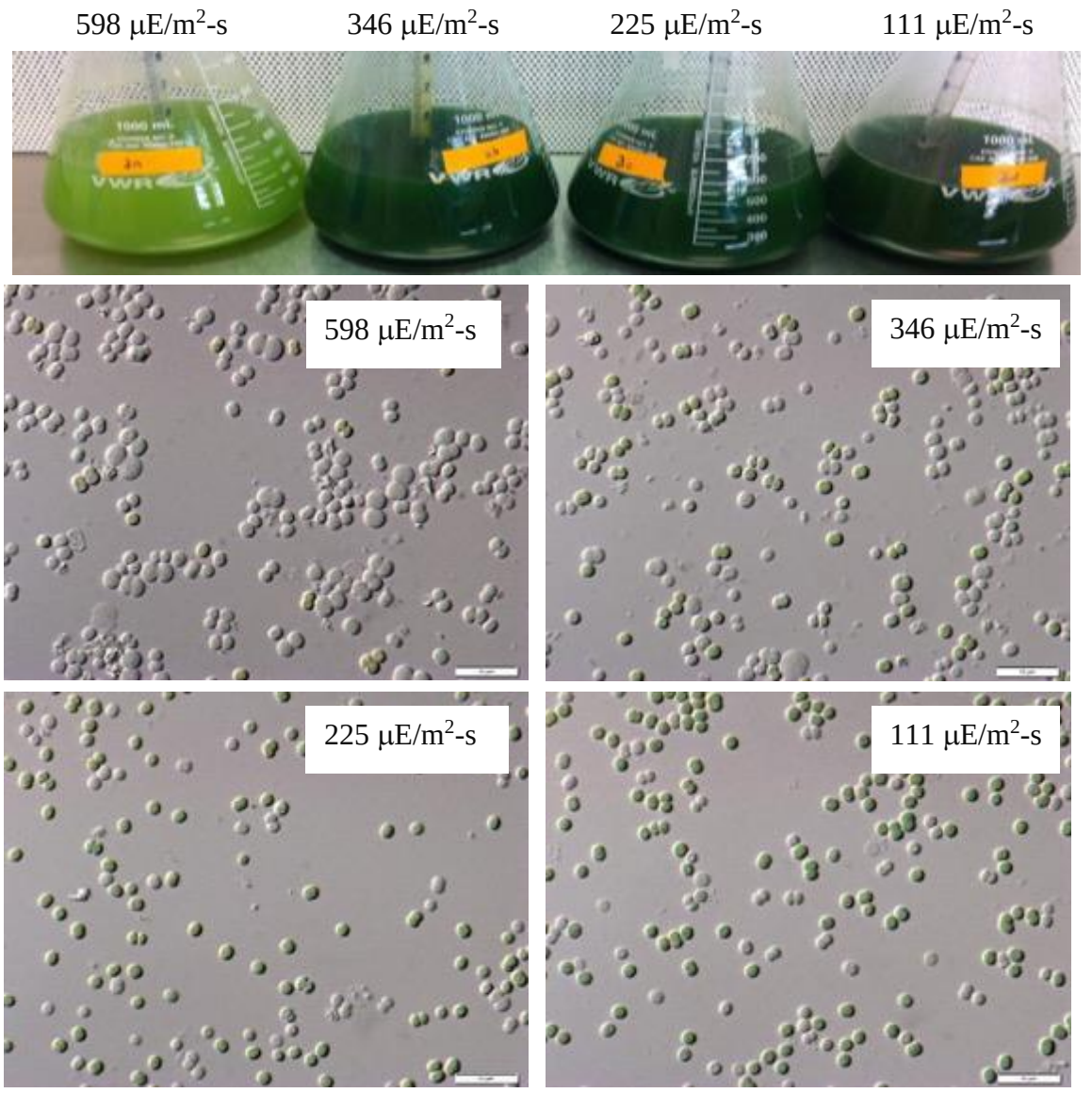

Figure 2.6: Digital-Color and LM Images of *Synechocystis* Laurate-Excreting Strain of the Last Day (Day 21)

The top row shows incident LIs to each reactor; the greenish cells indicate photosynthetic viability; brownish cells indicate inactive photosynthesis. An axenic *Synechocystis* culture was maintained throughout experiment. The small at the bottoms of each LM image is the 10-μm bar

LM images in **Figure 2.6** indicate that the culture illuminated by 598 μE/m^2-s had very few greenish cells (carrying out photosynthesis) and a large portion of grayish cells

(inactivated). This is direct evidence of cell having photosynthesis deactivated by long-term exposure to 598 $\mu E/m^2$-s.

In summary, the experiments successfully identified a limit of LI, 598 $\mu E/m^2$-s, inhibiting photosynthesis. Photo-inhibition affected the photosynthetic apparatus, culture pigment, and biomass production. Long duration of exposure and high local LI amplified photo-inhibition effects. These trends suggest that a modest and homogeneous LI may ameliorate photo-inhibition effects.

2.3.2 Photo-limitation by low light intensity

As mentioned in the Materials and Methods section, the main difference in the experiments on photo-limitation was the use of Corning flasks having flat interfaces. This setup gave better light transport through polystyrene and a shorter light path. I selected biomass stationary phase as the indicator of photo-limitation in low LI.

Figure 2.7 presents biomass DW and AILI for *Synechocystis* wild-type (panel a) and laurate-excreting cultures (panel b). Biomass grew at virtually the same rate for all of incident LIs. All AILIs were in a close range (5 – 20 $\mu E/m^2$-s), which may explain why growth curves were not much different. Most importantly, the biomass concentration reached a stationary phase that should have been caused by photo-limitation.

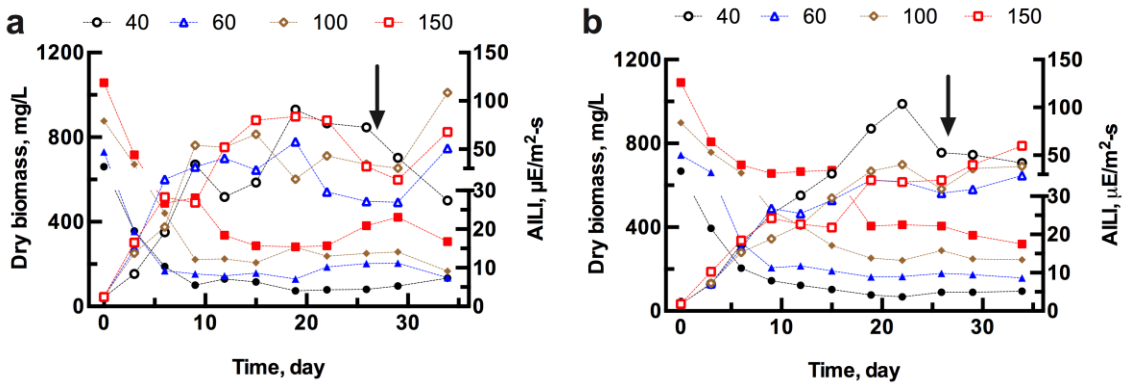

Figure 2.7: Biomass DW and AILI of Flasks with Different Incident LI on the Wild-Type (Panel a) and Laurate-Excreting Strain (Panel b) of *Synechocystis* in Low LI Numbers on top gives the incident LI ($\mu E/m^2$-s). The arrows showed when the growth medium was replaced by fresh BG-11.

During the experiment, I observed that the cultures illuminated with 40 $\mu E/m^2$-s and 60 $\mu E/m^2$-s had a darker green color, and I was concerned that OD might not be sufficient to characterize biomass density; therefore, I included chemical oxygen demand (COD) as the additional gauge. The data in **Figure 2.8** provide particulate COD from day 11 onward for wild-type and modified strains. COD data are consistent with the stationary trends in **Figure 2.7**, which supports that the OD measurements for DW were adequate.

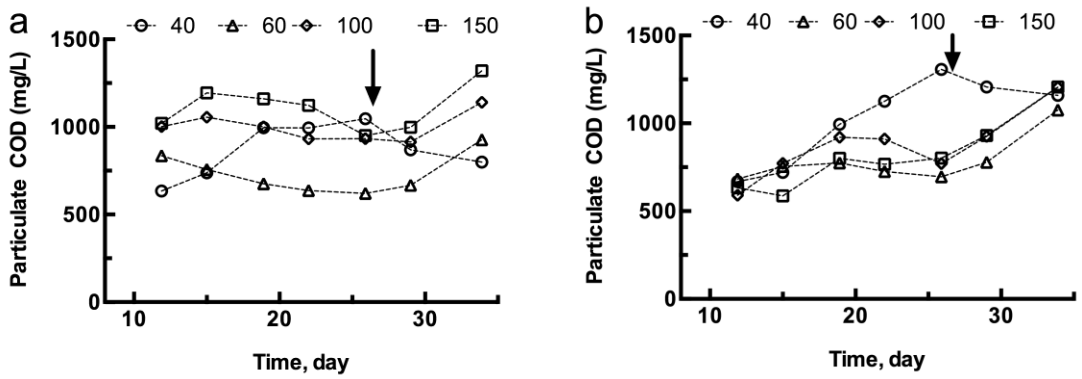

Figure 2.8: Particulate COD of Wild Type (Panel a) and Laurate-Excreting *Synechocystis* (Panel b).

Figure 2.9 shows the culture's condition on the last experimental day. As expected, all cultures had a dark-green color, meaning that photo-inhibition did not occur for incident LI from 40 to 150 $\mu E/m^2$-s (the corresponding AILI values were 5 to 150 $\mu E/m^2$-s).

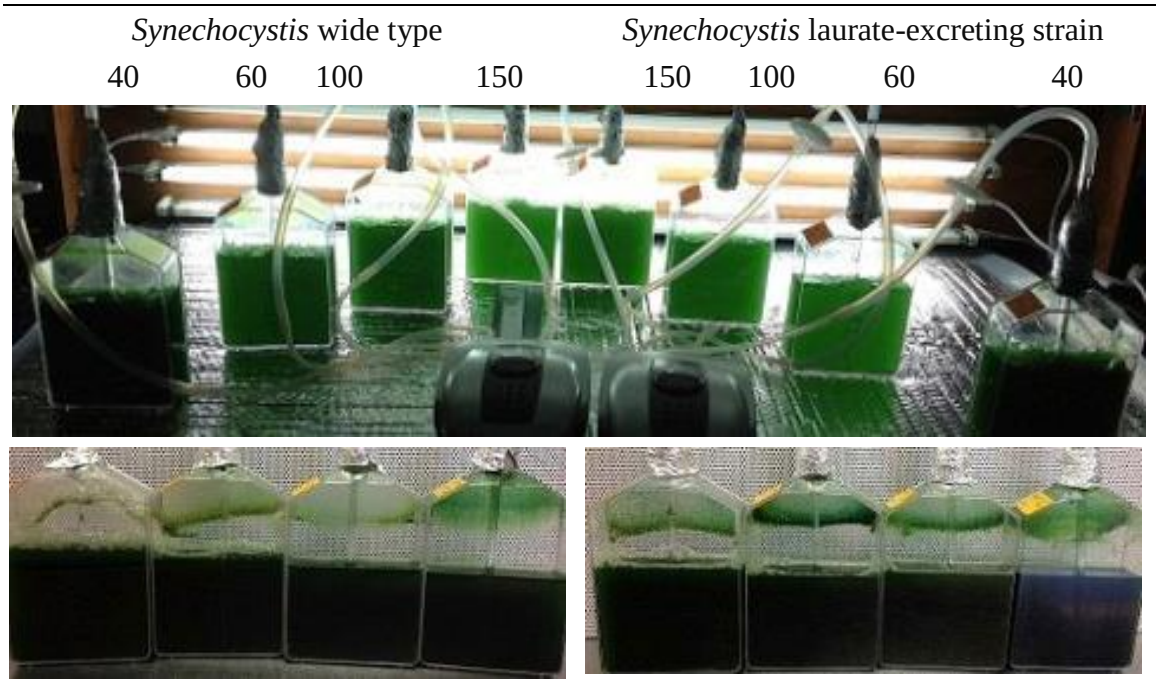

Figure 2.9: Digital Picture of Experiment Setup (Top); the Wide-Type Culture (Left-Bottom) and the Laurate-Excreting Culture (Right-Bottom) at the End of the Experiment (Day of 34)

The second row gives incident LI to each flask, in $\mu E/m^2$-s. Cultures in all flasks show dark-green color, indicative of active photosynthesis.

To diagnose other possibilities for attaining stationary phase, I monitored inorganic carbon. Photosynthesis increases the pH because cells fix inorganic carbon (C_i, mainly HCO_3^- + dissolved CO_2) and produce base (OH^-). If the pH remains constant, then the C_i supply was sufficient to match the C_i taken up by photosynthesis; insufficient CO_2 supply would cause a large rise in pH. Data shown in **Figure 2.10** indicate that the growth pH of all flasks correlated well with incident LI: Higher pH reflected higher uptake of C_i for biomass production by photosynthesis than the CO_2 supply rate. With CO_2 supplied from atmospheric air, a pH of 9.0-9.5 means that at least ~0.2 mM/L C_i was available by the alkalinity supplied in BG-11 in cell-free medium for photosynthesis for

lower LI (40, 60 μE/m^2-s, both strains). In Chapter 4, I demonstrate that the alkalinity increases as biomass grows using NO_3^- as the N source; with a pH stable, denser biomass means that alkalinity and C_i are higher. For example, 700 mg DW led to an equivalent additional of 6.0 mM C_i. This concentration of C_i was greater than that needed for photosynthesis.

Except for one abnormal point with wild type around day 17, both flasks with 40 μE/m^2-s incident LI had the lowest pH throughout the experiment. AILI values inside those reactors were around 5 μE/m^2-s (**Figure 2.7**).

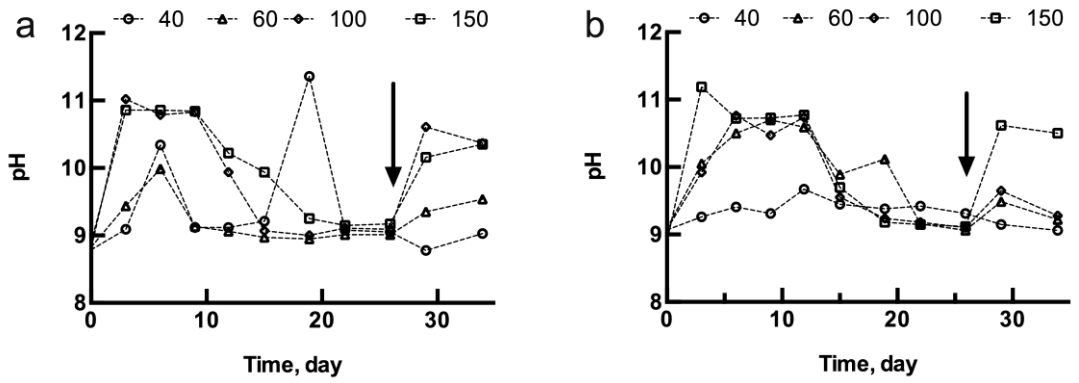

Figure 2.10: pH Readings of Culture with Different LIs on *Synechocystis* Wild-Type Strain (Left) and Laurate-Excreting Modified Strain (Right), Black Arrow Indicates Time to Replace by Fresh BG-11 (Day 26).

To eliminate any impact of N or P limitation for causing stationary growth, old medium was replaced by fresh BG-11 in all flasks at day 26. All flasks having AILI > 5 μE/m^2-s showed a small rebound in pH; on the other hand, pH remained constant with AILI = ~5 μE/m^2-s, and this indicates insufficient photon density to generate net photosynthesis.

Photo-limitation at ~5 μE/m^2-s is a significantly lower value than what was reported previously by Kim et al. (2010), who saw the specific growth rate of the wild-type *Synechocystis* sp. PCC 6803 significantly reduced when AILI < 40 μE/m^2-s, although C_i > 10 mM. A lower AILI for photo-limitation benefits microalgal production by expanding the lower end of the operational LI range.

2.3.3 Growth kinetics without controlling pH

To compare growth rates between *Synechocystis* wild-type and the laurate-excreting strains, I fit the empirical data from photo-inhibition and photo-limitation experiments using Monod and "substrate self-inhibition" models, in which light energy is treated as a conventional "substrate." The Monod model assumes AILI causes no inhibition; the substrate self-inhibition model lets AILI be a "substrate" at low AILI and an "inhibitor" at high AILI.

I fit parameters using the Graphpad Prism program. In particular, I selected specific growth rates for all runs in the first three days, which eliminated any impacts of nutrient limitation and prolonged photo-inhibition. I selected a half-maximum-rate intensity of 598 μE/m^2-s for photo-inhibition, because this level inhibited photosynthesis after 3-week exposure (**Figure 2.4**). Results of fitting both models for the wild-type and the modified strains are shown in **Figure 2.11** using the parameter values in **Figure 2.1**.

Regardless of the model used, *Synechocystis* wild type showed robust growth and no light saturation up to AILI of ~100 μE/m^2-s. The laurate-excreting strain showed a tendency to reach light saturation around AILI of 300 μE/m^2-s. This comparison is an

initial assessment, because fluorescent bulbs did not allow me to test *Synechocystis* with higher LI.

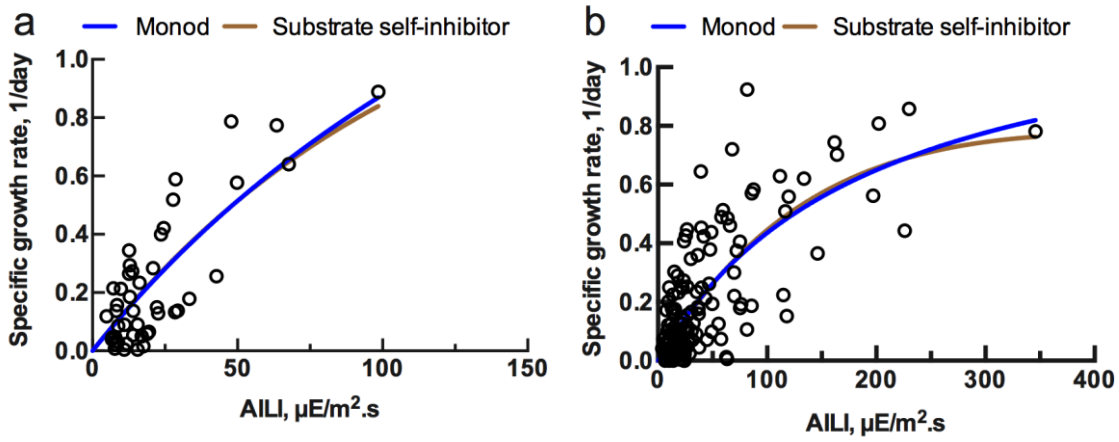

Figure 2.11: Fits of the Specific Growth Rate to AILI for *Synechocystis* Wild Type (Panel a) and the Laurate-Excreting Strain (panel B) Based on Monod and the Substrate Self-Inhibition Models Using the Parameter Values in **Table 2.1**.

Based on the maximum specific growth rate (μ_{max}) values in **Table 2.1**, *Synechocystis* wild type had a significantly faster μ_{max} than the laurate-excreting strain. However, the parameter estimates for μ_{max} are based on a constrained range of AILI, and the highest specific growth rate observed was less than 1/day for wild type, a value lower than 1.25/day reported by Bouterfas et al. (2002).

The K_{LI} values, ~187 µE/m^2-s for the wild type and ~217 µE/m^2-s for the laurate-excreting strain, are for about 10% of peak sunlight PAR. Other studies have tried to model LI on growth kinetics. For example, Wang et al. (2007) used five colors of light emitting diodes (LEDs) and Monod kinetics with incident LI as the representation of light input with the cyanbacterium *Spirulina*. They found K_{LI} values ranging from 461 µE/m^2-s to 1460 µE/m^2-s, depending on the color of the LED. Yun and Park (2003) also used

Monod kinetics and quantified K_{LI} values based on four models taking LI as the local, average photon fluxes and local, average absorption rates with *Chlorella*. K_{LI} varied significantly depending on LI quantification. K_{LI} of photon-flux (or "supply") models are from 16 μE/m^2-s to 49 μE/m^2-s and of absorption-rate (or "consumption") models are from 3,000 to 12,600 μE/m^2-s. Lower numbers indicate a higher affinity of biomass to the input, which is LI. Clearly, modeling growth kinetic on LI as the limiting input is challenging. Nevertheless, a K_{LI} of ~200 μE/m^2-s is about a half of LI to saturate photosynthetic activity found in different microalgae (Robt Emerson, 1958; David O. Hall et al., 1995; Melis, 2009) and my results are logical.

Modifying *Synechocystis* to produce and excrete of free fatty acids should divert energy, electrons, and C away from cell synthesis. Thus, a lower specific growth rate for the laurate-excreting strain is expected. Mine is the first quantification of the difference, and the results in **Figure 2.11** and **Table 2.1** show that the difference is quite large. Perhaps part of the difference is explained also by the higher output of generic soluble microbial products (SMP) and extracellular polymeric substances (EPS) by the laurate-excreting strain. I explore the difference in fixed electron partitioning wild-type and modified strain in Chapter 3.

Table 2.1: Summary of Fitted Model Parameters

I selected μ_{max} for the wild-type strain and K'_{LI} values for both strains *a priori* based on Vermaas, (1996). LI is represented by the AILI

Fitting model	Fitting parameter	Wild-type strain	Modified strain
Monod model	μ_{max} (1/day)	2.90	1.29±0.27
$\mu = \mu_{max}\frac{LI}{LI + K_{LI}}$	K_{LI} ($\mu E/m^2$-s)	217±210	187±61
Substrate self-inhibition	μ_{max} (1/day)	2.90	1.92±1.91
model	K_{LI} ($\mu E/m^2$-s)	212±880	303±354
$\mu = \mu_{max}\frac{LI}{LI + K_{LI} + \frac{LI^2}{KI_{LI}}}$	K'_{LI} ($\mu E/m^2$-s)	598	598

My first attempt to model growth kinetics with AILI as the rate-limiting input showed some uncertainty for μ_{max} and K_{LI} values (standard deviations in **Table 2.1**). The uncertainty indicates that the experimental design was not sufficient. In particular, the simple flask setup did not create a consistent environment in terms of pH and C_i. To overcome these limitations, I build a pH-Stat PBR to automatically controlling pH, C_i, and AILI. Results from the pH-Stat are presented in Chapters 4, 5, and 6.

The Monod and "substrate self-inhibition" models represented my experimental results about equally well. In practice, an equally good fit by these two models suggests the tested range of LI did not induce a significant inhibitory mechanism up to AILI of 250 $\mu E/m^2$-s. Therefore, using Monod-kinetics could fit the empirical data up to 250 $\mu E/m^2$-s.

2.4 Synthesis and Application

Synechocystis wild type grew faster than the laurate-excreting strain and was less susceptible to light inhibition. The preliminary μ_{max} values obtained by model fitting indicate that *Synechocystis* wild type grew significant faster than the laurate-excreting strain, while the AILIs for half μ_{max} (K_{LI}) were not significantly different for Monod kinetics. *Synechocystis* wild type was more tolerant to high LI than the laurate-excreting strain. The wild-type strains was photo-inhibited by incident LI of ~598 $\mu E/m^2$-s, while the laurate-excreting strain was photo-inhibited by an incident LI of ~346 $\mu E/m^2$-s. The corresponding AILI values were ~20 and ~10 $\mu E/m^2$-s, and this suggests that localized high LI or cumulative effects of high incident LI when the biomass concentration was low may have caused photo-inhibition more than the AILI.

Net zero biomass production with AILI of 5 $\mu E/m^2$-s indicates insufficient energy capture to synthesize net new biomass. The value was about the same for wild type and laurate-excreting strains. Having medium replete with nutrients confirms that LI caused the limitation.

The results in this chapter define the lower (~5 $\mu E/m^2$-s) and upper (~598 $\mu E/m^2$-s) limits for a working window of LI for *Synechocystis*. This window defines a practical range to produce biomass. More immediately relevant is that it allowed me to define a workable LI range for the experiments in the following chapters.

3 EFFECT OF LIGHT INTENSITY ON DISTRIBUTION OF PARTICULATE AND SOLUBLE BIOMASS*

3.1 Introduction

Photoautotroph like *Synechocystis* harvest sunlight and fix that energy mainly in carbon. Reduction of inorganic carbon (C_i) to organic carbon requires energy and, thankfully, cyanobacteria have been carrying out this redox reaction via photosynthesis for the last 3 billion years (R. E. Blankenship, 2010). While photosynthesis is sustainable, it is not very efficient. Previous chapters listed the quantum yields, the ratio of chemical-bond energy embodied in biomass to incident light energy, and it is only 3-6% of PAR by microalgae and much lower by terrestrial plants (I. Fernández et al., 2012; Scragg et al., 2002).

Means to improve the efficiency of photosynthesis can be through increasing quantum yield and/or channeling fixed electron to the desired products. For the latter approach, however, not all photosynthetically fixed electrons and carbons are embodied in the right form: in the case of *Synechocystis* culture, particulate biomass by the wild type and lauric acid and other fatty acids (C10 to C18) by the laurate-excreting strain.

Not all microbial products originating from photosynthesis are useful to humans. For example, generic soluble microbial products (SMP) are ubiquitously produced

---

* Results in this chapter were submitted to *Biomass and Bioenergy* as Nguyen, B.T. and Rittmann, B.E. (2015). Electron partitioning in soluble organic products by wild-type and modified *Synechocystis* sp. PCC 6803**.**

mixtures of polysaccharides, proteins, nucleic acids, and humic acids that are formed either by the hydrolysis of extracellular polymeric substances (EPS) or are released directly by microorganisms as part of their metabolism (Laspidou, 2002; Namkung & Rittmann, 1986; B E Rittmann, Bae, Namkung, & Lu, 1987). SMP contain carbon-embodied electrons and energy, but they are distinct from valuable products that can be excreted by modified phototrophs.

A main source of SMP is the hydrolysis of EPS (Laspidou, 2002), which are essential to aggregation, such as with flocs and biofilms, and EPS also protects cells from desiccation, predation, and biocides (Geesey, 1982). EPS is a solid-phase microbial product, and it can be a large fraction of total biomass in well-aggregated systems (Merkey, Rittmann, & Chopp, 2009; Ni et al., 2011). EPS is composed mainly of carbohydrates, proteins, and uronic acids and can represent 10% to 70% of biomass dry weight for phototrophs, depending on strain and growth condition (Ge, Zhang, Zhou, Xia, & Hu, 2014; Klock, Wieland, Seifert, & Michaelis, 2007; Otero & Vincenzini, 2003). EPS can be produced by active secretion, spontaneous liberation of internal cellular components, cell lysis, and adsorption of foreign materials (Wingender, Neu, & Flemming, 1999).

Historically, SMP form a class of organic products normally considered undesirable in wastewater treatment (B E Rittmann et al., 1987). For example, microorganisms in activated sludge release SMP that count towards biochemical oxygen demand (BOD) and chemical oxygen demand (COD) in the effluent. Although EPS and SMP were originally named by those with different interests (biologists vs. wastewater engineers), they are inter-related (Laspidou, 2002), as described by the unified theory

shown in **Figure 3.1**. SMP consists of biomass-associated products (BAP) and utilization associated products (UAP). While the UAP are released by cells directly as part of their catabolism, BAP are produced by hydrolysis of EPS (Laspidou, 2002). SMP are substrates that can be directly utilized by heterotrophs in the microbial community, but a substantial portion of the SMP originates as EPS.

EPS and SMPs are important electron and carbon sinks. The formation of EPS and SMP represents a diversion of C and electron flow away from the desired products. Likewise, SMP also are electron-donor substrates for heterotrophic bacteria. When SMP stimulates the growth of heterotrophic bacteria that consume an excreted product, the formation of SMP becomes a double challenge.

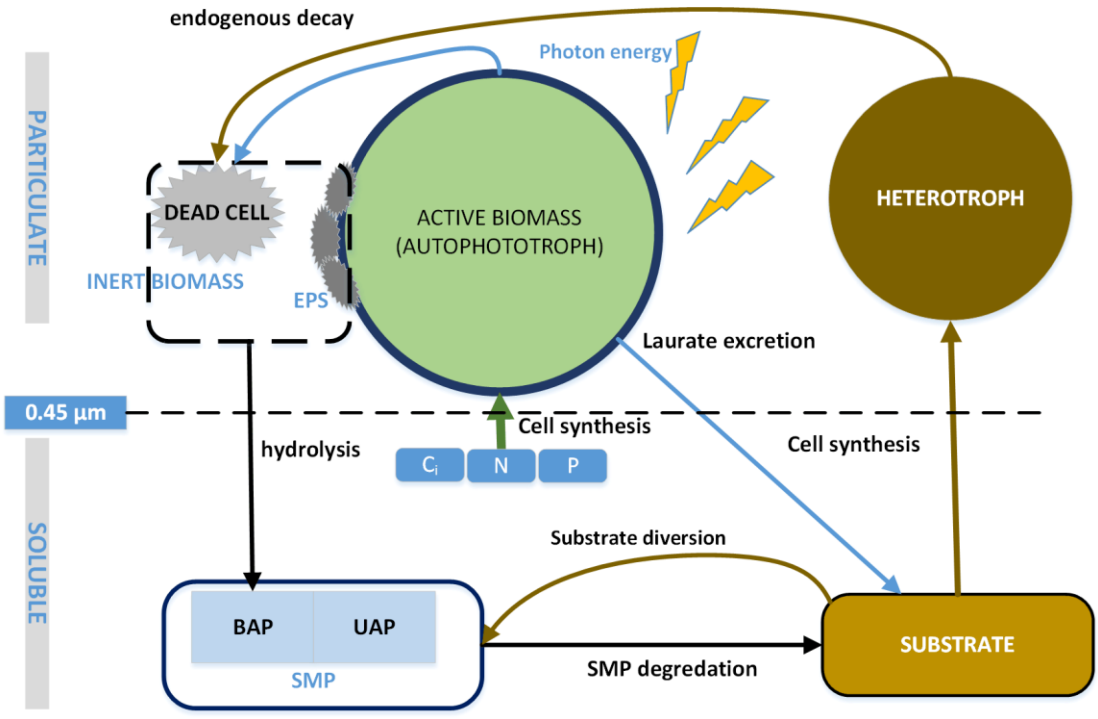

Figure 3.1: Mass Fluxes of Active Biomass, Inert Biomass, EPS, SMP, and Substrates in Laurate-Excreting Culture in the Presence of Heterotrophic Bacteria
The 0.45 µm is a typical pore size to separate particulate and soluble components

Environmental factors (pH, LI, nutrients) should influence the production of EPS and SMP. Quantifying the release of EPS and SMP by wild-type and laurate-excreting *Synechocystis* is an important need for using *Synechocystis* for large-scale production of fuel feedstock.

For phototrophs, LI was reported to affect EPS production and more general excretion of organic carbon (Dubinsky & Berman-Frank, 2001). Wolfstein and Stal (2002) studied a diatom, *Cylindrotheca*, and reported an upward increment of "colloidal EPS" from an LI of 84 to 571 $\mu E/m^2$-s. Colloidal EPS is a term sometimes used to mean SMP. A study on EPS production of a cyanobacterium, *Anabaena* sp. ATCC 33037, found a distinct increment of EPS between those culture illuminated by 115 to 345 $\mu E/m^2$-s and those illuminated by 460 to 1840 $\mu E/m^2$-s (Moreno, Vargas, Olivares, Rivas, & Guerrero, 1998). Again, EPS is a major source of SMP.

Equally important to the overall efficiency of energy capture into reduced carbon is the fraction of electrons embodied in harvestable and desirable products. Separation techniques mainly harvest particulate biomass and its valuable intracellular products, such as lipids, glycogen, and poly-beta-hydroxybutyrate (PHB) (Wu, Shen, & Wu, 2002), which the microorganisms typically produce when they experience nutrient stress (Philippis, 1992). For example, nutrient stress leads to the accumulation of triacylglycerides by eukaryotic microalgae when nitrogen is depleted (Qiang Hu et al., 2008). Genetic engineering can enhance the accumulation of internal storage products. Wu et al. (2002) engineered *Synechocystis* sp. PCC 6803 to enhance production of PHB, and the engineered strain produced 20 to 25% more PHB than the wild-type strain, making PHB about15% of the cells' dry weight.

Other valuable products can be excreted, such as aldehydes, fatty acids, or alcohols (Liu et al., 2011; Woods, Legere, Moll, Unamunzaga, & Mantecon, 2010). Engineered cyanobacteria excreted isobutyraldehyde at a rate equal to 5 – 6% of biomass production, which is equivalent to ~10 % electron partitioning (Ducat et al., 2011). Liu et al. (2011) modified *Synechocystis* to excrete free fatty acids (mostly laurate). Excreted laurate accounted for ~13% of the C fixed in biomass or ~26% electron equivalents. Algenol Biofuels claims that its Direct to Ethanol® technology can produce annually 8,000 gallons per acre of ethanol (Algenol, 2011), which is roughly 20 times higher productivity than corn-to-ethanol.

Cyanobacteria also are known to protect themselves against photochemical damage by producing chemicals that absorb UV to violet light. Some of these "sunscreens" are lipophilic, such as scytonemin and mycosporine-liked amino acids (MAA) found in the sheaths of cyanobacteria (Garcia-Pichel, Wingard, & Castenholz, 1993; Proteau, Gerwick, Garcia-Pichel, & Castenholz, 1993). Others are hydrophilic and soluble, such as glutathione, ascorbate, and urate (Dunlap & Shick, 1998). The lipophilic materials may be considered part of the EPS, while the hydrophilics may be part of the SMP.

In following section, I revisit the experiments in Chapter 2 and analyzed the partitioning of fixed electrons in soluble and particulate biomass based COD assay and Gas Chromatography (GC). I carried out other runs to evaluate the partitioning of fixed C in biomass particulate matter measured directly by OD and laurate by GC. Laurate is analyzed as part of the soluble organics produced by modified *Synechocystis*.

The partitioning of electrons in fixed carbon soluble and particulate biomass can be assayed directly by measurements of COD (Walter, 1999). I investigated the partitioning of COD by the cyanobacterium *Synechocystis* sp. PCC 6803, including how it was affected by the incident LI and strain modification to release laurate (12-C carboxylate) to the medium. Wild-type and laurate-excreting strains were grown in inorganic BG-11 growth medium and continuously exposed to irradiance by fluorescent bulbs with incident LI from 111 to 598 $\mu E/m^2$-s over 3 weeks. The results show that *Synechocystis* partitioned up to 30% of the electrons it fixed into generic SMP (not laurate), and the greatest electron partitioning into SMP occurred with the laurate-excreting strain and with the highest irradiance I tested.

3.2 Materials and Methods

3.2.1 Experiment setup

Inocula of wild-type and modified strain of *Synechocystis*, growth medium preparation, and flask setup were as described in section 2.2.1.

As mentioned in Chapter 1, the modified strain was designed to excrete mainly lauric acid to the medium (W. F. J. Vermaas, 2014; W. Vermaas et al., 2011). The laurate-excreting *Synechocystis* sp. PCC 6803 was created by inserting an acyl-ACP thioesterase that diverts part of the metabolic flux from lipid production to fatty acid synthesis (Liu et al., 2011; Roessler, Chen, Liu, & Dodge, 2008). The laurate-excreting strain also has a deletion of acyl-ACP synthetase (*srl 1609*) to prevent re-uptake up of fatty acids. Lauric acid is passively excreted to the medium due to diffusion through the

cell's membrane. Because a thick peptidoglycan layer could reduce lauric acid excretion by the modified strain (Liu et al., 2011), genes encoding that layer were deleted to promote excretion of lauric acid (Liu et al., 2011).

Although all experiments were carried out in 25^{o}C air-conditioned room, heat accumulated from fluorescent light that raised the temperature of the liquid in the flasks. The heating effect was monitored using flasks filled with water and located at the same distances as the culture-containing flasks and doubled checked by measuring directly the culture. The final temperature of the culture was 33, 29, 27, and 26^{o}C for the highest to the lowest LI.

3.2.2 Analyses

Culture samples were taken with a sterile pipette (Fisher Scientific) regularly, either one- or two-day interval, inside a laminar biosafety hood. Samples were transferred into 15-ml screw-cap Falcon polypropylene tubes (VWR) and stored in a 4^{o}C refrigerator for later assay.

COD was measured by thermal digestion and colorimetry using a HACH Kit 822, HACH DRB200 digester, and HACH DR2800 spectrophotometer according Hach method 8000 (Hach, 2014). After being removed from storage, a sample was vortexed vigorously for 30 seconds, and a 2-mL aliquot was added to one vial to measure total COD (TCOD). Soluble COD (SCOD) was obtained by filtering a sample through a 0.45-μm-pore PVDF GD/X syringes filter (Whatman). Then, 2 mL of sample was added to a HACH kit vial, mixed, and oxidized at 150^{o}C for 120 minutes in the HACH DRB200 digester. Particulate COD (PCOD) was computed by the difference between TCOD and

SCOD. I verified the kit performance by Potassium Hydrogen Phthalate (KPH) with known amount.

Laurate (for the modified strain) was measured by gas chromatography (GC) using a polar Supelco Nukol column specifically coated for long-chained FFAs (Sheng at el,, 2011). First, 20 μL of 1-M EDTA was added to a 1.0-mL of culture sample, and the mixture was centrifuged for 5 minutes at 11,000 rpm with a Microfuge® 22R Centrifuge (Beckman Coulter). Then, 1.0-mL supernatant aliquot was mixed with 80 μL sulfuric acid (50%) to lower the pH to ≤ 1.0, followed by adding 2.0 mL hexane (>99%), and the mixture was vortexed for at least 2 hours to achieve an optimal extraction. Lastly, 150 μL of liquid in hexane was analyzed by GC, and the laurate concentration was computed using a calibration curve prepared with pure lauric acid. The laurate concentration was converted to laurate COD using the stoichiometric factor 2.72 g COD/g laurate based on its molecular formula for lauric acid ($C_{12}H_{24}O_2$) and the methods in Rittmann & McCarty (2001). When laurate was present, I computed the COD of SMP as the difference between the measured SCOD and COD of the laurate. Small concentrations of other fatty acids (Capric acid, Myristic acid and Palmitic acid) were detected in a few samples, but their CODs were insignificant compared to laurate.

3.3 Electron Partitioning

To evaluate electron partitioning, I normalized the non-laurate SCOD (representing generic SMP), the COD equivalents from laurate, and the PCOD (representing particulate biomass) to TCOD (representing all COD generated by photosynthetic activity). From the 18th day onward, the modified culture illuminated by

incident LI of 111 μE/m^2-s and 225 μE/m^2-s showed rod-shaped bacteria indicative of heterotrophic bacteria. Because heterotrophic bacteria could have consumed SMP and laurate, I excluded all data beginning with day 18 for these experiments. For each LI, I calculated COD ratios for each set of samples (N = 7 to 10), averaged the ratios, and report the average value and its 95% confidence level.

3.4 Correlation of Laurate and SMP Production to Biomass Growth Rate

The sources or mechanisms of laurate or generic SMP production are important to understand in order to improve productivity of valued products, e.g., laurate, and to reduce SMP production by the modified strain. I hypothesize that this correlation is linear (eqn. (3.1)):

$$P \sim p^{*}\mu \tag{3.1}$$

where μ is specific growth rate of biomass (1/day), P is the specific production rate of laurate or generic SMP, and p is a correlating coefficient with units that depend on P (mg $COD_{(LA\ or\ SMP)}$/mg $COD_{biomass}$). Eqn. (3.2) shows the calculations for laurate (LA).

$$P = \frac{LA_{t2} - LA_{t1}}{PCOD_{t2} - PCODt_1}\frac{1}{t_2 - t_1} \tag{3.2}$$

3.5 Results and Discussion

3.5.1 Electron partitioning

The electron-partitioning experiments were carried out for up to 18 days with the wild-type strain and 24 days with the laurate-excreting strain, and the biomass-growth

curves were presented previously in **Figure 2.4**. Wild-type *Synechocystis* (panel a) reached as much as 1350 mg/L dry weight after 12 days. The biomass grown with lower incident light intensities (111 and 225 μE/m^2-s) produced less biomass density than the higher ones (346 and 598 μE/m^2-s). The modified strain (panel b) grew considerably slower than the wild type, and the highest dry weight was 650 mg/L after 12 days with the highest LI. The wild-type biomass reached stationary phase by days 6-10, and the modified strain reached stationary phase later, around day 16.

AILI also is shown in **Figure 2.4**. As biomass grew, the AILI declined quickly and then stabilized in the range of 6.5-20 μE/m^2-s, with the lowest AILI values associated with the lowest incident LI. Loss of biomass density at the end of the experiments with 598 μE/m^2-s caused the AILI to increase to > 30 μE/m^2-s.

Figure 3.2 presents results for TCOD, PCOD, and soluble components of COD (generic SMP and laurate for the modified strain) produced by *Synechocystis* wild-type (panels a1 – a3) and the laurate-excreting strain (panels b1 – b4). TCOD is the direct measure of total electron equivalents fixed into organic C by photosynthesis. For both strains, higher incident LI led to more electron fixation (panels a1 and b1), but the differences were more dramatic for wild-type *Synechocystis.* Also, photosynthetic electron capture leveled off by 12 days for the wild type, while it continued almost linearly for the modified strain out to 15 to 18 days. This difference in the generation of TCOD was driven in large part by the much faster growth of biomass, shown as PCOD in panels a2 and b2. Higher biomass concentrations for the wild type increased the overall rate of photosynthesis to TCOD.

The COD in SMP (panels a3 and b3) rose continually during the experiments, roughly in proportion to the PCOD. Except for the highest incident LI, SMP-COD concentrations for wild-type *Synechocystis* were similar to or smaller than SMP-COD concentrations for the modified strain, despite the higher production rate of PCOD by the wild-type strain. Laurate COD produced by the modified strain (panel b4) increased in parallel with biomass growth and SMP-COD, but it was produced in considerably smaller concentration than SMP-COD and PCOD.

Panels a3, b3, and b4 identify SMP-COD and laurate-COD samples for which LM detected heterotrophic bacterial rods. **Table 3.1** reports the LM results. These samples in b3 and b4 showed loss of SMP-COD and laurate COD. All samples showing evidence of heterotrophs were excluded from the analyses of electron partitioning.

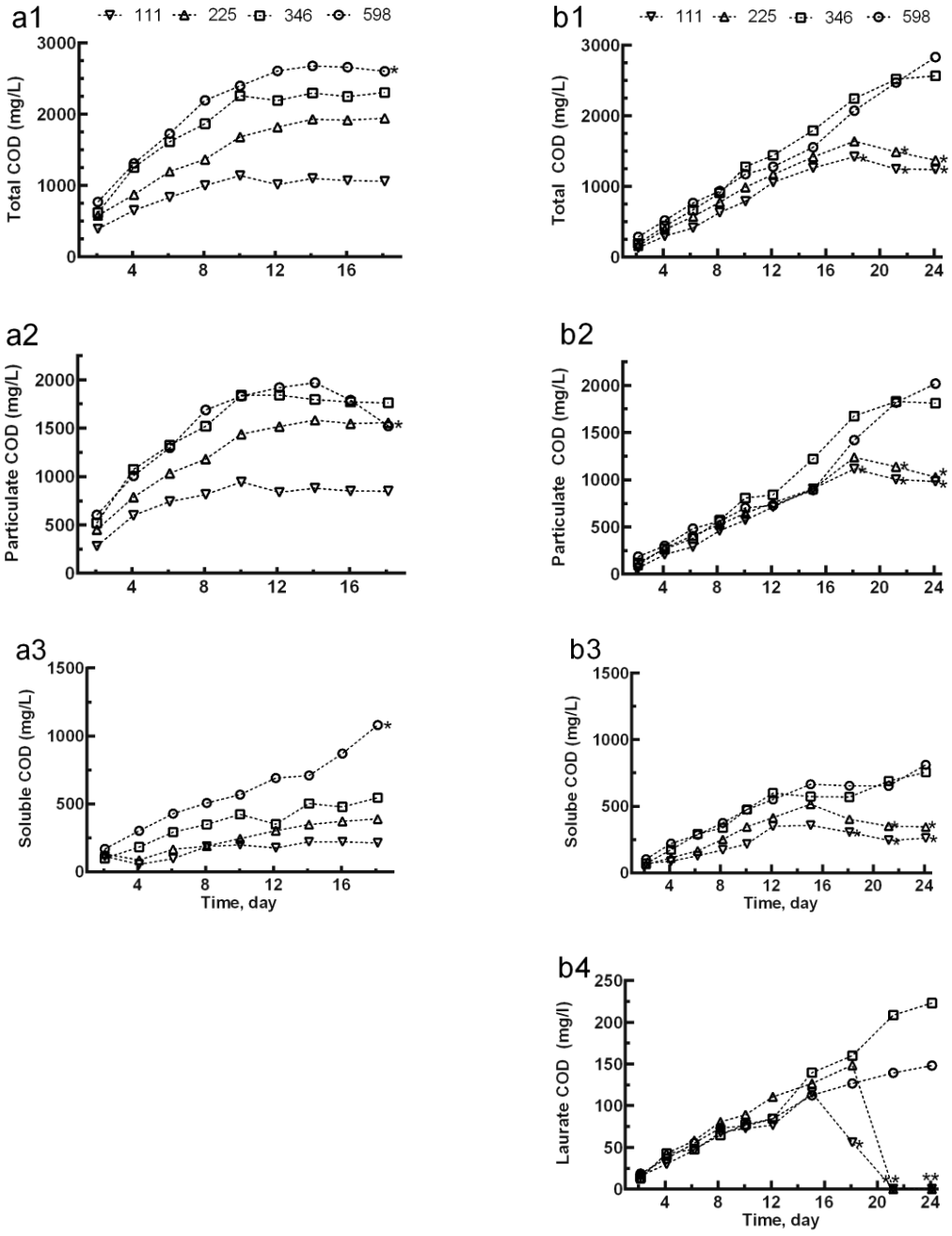

Figure 3.2: Panel a1-a3: Total COD, Calculated COD of Particulate Biomass, and Generic SMP COD of Wild-Type *Synechocystis*. Panel b1-b4: Total COD, Calculated COD of Particulate Biomass, Generic SMP COD, and COD Equivalent of Laurate for Laurate-Excreting *Synechocystis*

The open symbols with an asterisk (*) show data that had heterotrophic rods identified by LM. Numbers in the top give the incident light intensity ($\mu E/m^2$-s)

The average COD partitionings over the duration of experiments without signs of heterotrophic bacteria (N = 7 to 10) are presented in **Figure 3.3**. Electron equivalents embodied in SMP by the wild type ranged from 16% to 25% of TCOD, while PCOD was 75% to 84% (panel a). Thus, wild-type *Synechocystis* released a substantial portion of the electrons it fixed into C as SMP. For modified *Synechocystis* (panel b), laurate comprised 6.6% to 10% of the TCOD, while non-laurate SMP comprised 21% to 30% of the TCOD, leaving PCOD as 64% to 69% of TCOD. The lower partitioning of TCOD into PCOD explains part of the slower specific growth rate of modified *Synechocystis*.

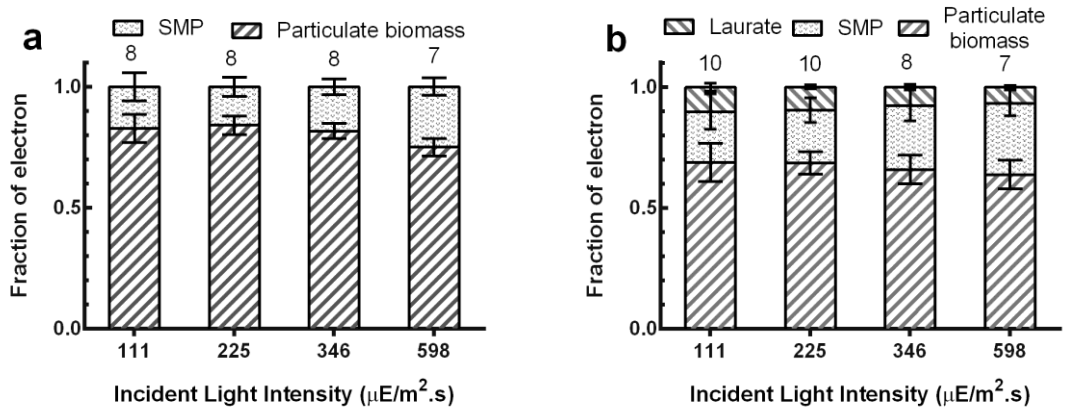

Wild-type *Synechocystis* Laurate-excreting *Synechocystis*

Figure 3.3: Panel a: COD Fractions of SMP and Particulate Biomass Normalized to the Total Electron Equivalents Harvested by Photosynthesis for Wild-Type *Synechocystis* sp. PCC 6803. Panel b: COD Fractions of SMP, Particulate Biomass, and Laurate Normalized to the Total Electron Equivalents Harvested by Photosynthesis by Laurate-Excreting *Synechocystis*

The bars represent two standard deviations, or the 95% confidence level for each component. Numbers on the top of columns give the number of samples used for each incident LI; values less than 8 for wild type and less than 10 for the modified strain indicate the exclusion of samples due to the presence of heterotrophic bacteria shown in **Table 3.1**

Table 3.1: Results of Light Microscopy for the Wild-Type and the Laurate-Excreting Strains

The numbers in percentages give the proportion of rod-shaped bacteria in the total number of cells. The number in the second-top row gives the incident Light Intensity ($\mu E/m^2$-s)

	Wild-type *Synechocystis*					Laurate-excreting *Synechocystis*			
Time, day	111	225	346	598	Time, day	111	225	346	598
0	ND	ND	ND	ND	0	ND	ND	ND	ND
4	ND	ND	ND	ND	6	ND	ND	ND	ND
8	ND	ND	ND	ND	15	ND	ND	ND	ND
14	ND	ND	ND	ND	18	<1%	ND	ND	ND
18	ND	ND	ND	7%	24	47%	50%	ND	ND

ND: no detectable rod-shaped bacteria.

From the point of view that the valuable products are in harvestable biomass and laurate, partitioning 16% to 30% of TCOD into SMP means that *Synechocystis* was significantly "wasteful." For the laurate-excreting strain, SMP-COD was two-fold to four-fold more than the COD invested in the desired soluble product, laurate. Furthermore, the fraction in SMP-COD was 25% to 30% higher for the laurate-excreting strain than for *Synechocystis* wild type. Perhaps SMP release was exacerbated as an unwanted side effect of modification to enhance the excretion of lauric acid by weakening the peptidoglycan layer (Liu et al., 2011). Alternately, the laurate-excreting strain produced more EPS that was hydrolyzed partly to SMP.

Another clear trend for both strains is that they partitioned significantly more electrons to SMP when exposed to the highest incident light. For instance, 598 $\mu E/m^2$-s generated about 1.4-fold more SMP-COD than did 111 $\mu E/m^2$-s for the wild-type strain.

The laurate-excreting strain showed a sharp increment in SMP-COD at 346 μE/m^2-s. A few studies reported that light intensity affects carbohydrate production, a main component of EPS and, consequently, SMP (Ge, Xia, Zhou, Zhang, & Hu, 2014; Moreno et al., 1998; Otero & Vincenzini, 2003). For example, the cyanobacterium *Microcoleus vaginatus* exposed to 40 and 80 μE/m^2-s produced SMP at 8.0% and 14.0% of cell dry weight, respectively (Ge, Zhang, et al., 2014). The nitrogen-fixing microalgae *Anabaena* sp. exhibited a 4-fold increment of EPS when its incident light intensity increased from 345 to 460 μE/m^2-s (Moreno et al., 1998). The flasks with the highest incident LI had higher temperatures (increasing from 26°C to 33°C). Although 44ºC increased unsaturation of fatty acids in wild-type *Synechocystis* sp. PCC 6803, the range of 25 to 33ºC showed almost no effect on the fraction of total lipids to biomass, indicating that this modest temperature range caused no profound impact on the physiology of *Synechocystis* (Sheng, Kim, et al., 2011). In addition, Wolfstein and Stal (2002) reported no change in the production of an SMP-liked pool by a diatom grown at 25 and 35˚C. Thus, the small temperature increase likely was not the cause of increases in SMP production for the highest incident LI.

I also calculated the production rates of biomass PCOD, SMP-COD, and laurate-COD per unit of PCOD, and the results are presented in **Figure 3.4**. The biomass-normalized production rates of PCOD, SMP-COD, and laurate-COD correlated to AILI. Consistent with **Figure 3.3**, the rate analyses show that the laurate-excreting strain produced less PCOD, but more SMP-COD than did the wild-type strain. Both strains, grown under a high incident LI (598 μE/ m^2-s), had reduced productivity of biomass and laurate (for the modified strain), but increased SMP production. Comparing the slopes of the overall fits reveals that about 0.2 mg SMP-COD and 0.8 mg PCOD were produced per mg of TCOD by wild-type *Synechocystis*. For the modified strain, for every mg of TCOD generated, 24.5% was embodied in SMP, 67% in particulate biomass, and 8.3% in laurate, all proportions that are consistent with **Figure 3.3**.

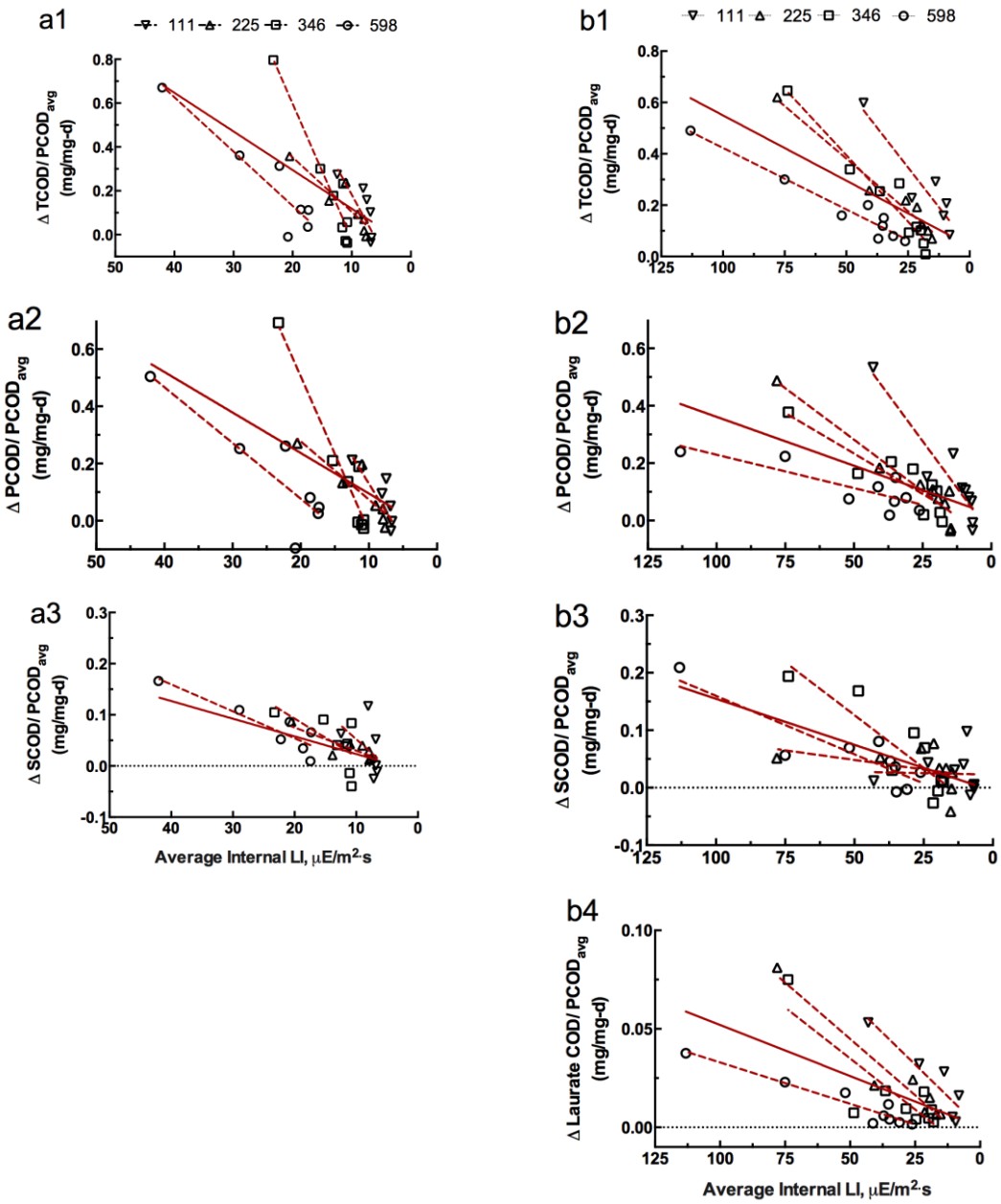

Figure 3.4: Newly Generated Total COD from Photosynthetic Activity (ΔTCOD), Newly Generated Biomass (ΔPCOD), Newly Produced SMP (ΔSCOD), and Newly Excreted Laurate (ΔLaurate COD), all Normalized to the Average Biomass Concentration ($PCOD_{avg}$) for Wild-Type *Synechocystis* (Panels a1 to a3) and the Laurate-Excreting Strain (Panels b1 to b4)

AILI was calculated using the average biomass density and the incident LI (shown on top in μE/m^2-s)). Dashed lines represent regression fitting of each flask, and solid lines represent regression fitting of the data from all flasks. Regression equations are in **Table 3.2** and **Table 3.3**.

The calculation method for the normalized rates is illustrated here for SMP-COD.

$$\frac{\Delta \mathrm{SCOD}}{\mathrm{PCOD_{avg}}} = \frac{\mathrm{SCOD_{t2}} - \mathrm{SCOD_{t1}}}{{}^{1}/_{2}\,(\mathrm{PCOD_{t2}} + \mathrm{PCOD_{t1}})} \frac{1}{\mathrm{t_2} - \mathrm{t_1}} \left[\frac{\mathrm{mg\ COD}}{\mathrm{mg\ COD}} \frac{1}{\mathrm{day}}\right] \tag{3.3}$$

where $SCOD_{t1}$ and $SCOD_{t2}$ are COD of SMP at day t_1 and t_2; $PCOD_{t1}$ and $PCOD_{t2}$ are particulate COD at day t_1 and t_2; and t_1 and t_2 are two sequential sampling times. Normalized productivity of biomass and laurate followed the same approach. The linear regressions (**Table 3.2** and **Table 3.3** and lines in **Figure 3.4**) are for data that had no rod-shaped bacteria by LM (**Table 3.1**).

The regressions illustrate that; in general, all normalized production rates decreased with lower AILI (from left to right in Fig. 3.4), which corresponds to higher OD over time. For individual flasks, the culture illuminated by the incident LI of 598 $\mu E/m^2$-s produced less biomass and laurate (for the modified strain only), along with more SMP, than flasks with lower incident LI.

Similar to wild-type *Synechocystis* (**Table 3.2**), higher AILI supported faster production all types of COD (**Table 3.3**), and the highest incident LIs produced less biomass and more SMP per PCOD than did the lower LIs. The ratios among all the slopes – 0.67 mg PCOD/ mg TCOD, 0.31 mg SMP-COD/ mg TCOD, and 0.10 mg laurate-COD/ TCOD – are consistent with the electron partitioning presented in panel b, **Figure 3.4**.

Table 3.2: Linear Regression Equations for Newly Generated Total COD (TCOD), Biomass (PCOD), and SMP (SCOD) for the Wild-Type S*ynechocystis*
For each fitting, y stands for the production rate in mg COD/mg PCOD-d, and x is AILI in $\mu E/m^2$-s

Data set identified by the incident LI and the type of COD	Regression equation	R^2
111-TCOD	$y = 4.94\times10^{-2}x - 3.12\times10^{-1}$	0.46
225-TCOD	$y = 2.48\times10^{-2}x - 1.44\times10^{-1}$	0.81
346-TCOD	$y = 6.17\times10^{-2}x - 6.36\times10^{-1}$	0.92
598-TCOD	$y = 2.48\times10^{-2}x - 3.64\times10^{-1}$	0.87
All-TCOD	$y = 1.76\times10^{-2}x - 5.74\times10^{-2}$	0.40
111-PCOD	$y = 3.87\times10^{-2}x - 2.57\times10^{-1}$	0.50
225-PCOD	$y = 2.03\times10^{-2}x - 1.29\times10^{-1}$	0.79
346-PCOD	$y = 5.42\times10^{-2}x - 5.79\times10^{-1}$	0.93
598-PCOD	$y = 1.95\times10^{-2}x - 3.13\times10^{-1}$	0.76
All-PCOD	$y = 1.42\times10^{-2}x - 4.63\times10^{-2}$	0.27
111-SCOD	$y = 1.08\times10^{-2}x - 5.54\times10^{-2}$	0.20
225-SCOD	$y = 4.52\times10^{-3}x - 1.52\times10^{-2}$	0.69
346-SCOD	$y = 7.45\times10^{-3}x - 5.64\times10^{-2}$	0.40
598-SCOD	$y = 5.26\times10^{-3}x - 5.11\times10^{-2}$	0.82
All-SCOD	$y = 3.45\times10^{-3}x - 1.11\times10^{-2}$	0.25

Table 3.3: Linear Regression Equations for Newly Generated Total COD (TCOD), Biomass (PCOD), and SMP (SCOD) for the Wild-Type S*ynechocystis*
Fitting equations are similar to the wild-type in **Table 3.2**, with addition of production rate of laurate in COD per average PCOD between two points for sampling

Data set identified by the incident LI and the type of COD	Regression Equation	R^2
111-TCOD	$y = 1.24\times10^{-2}x + 3.82\times10^{-2}$	0.85
225-TCOD	$y = 8.19\times10^{-3}x - 2.81\times10^{-2}$	0.95
346-TCOD	$y = 1.04\times10^{-2}x - 1.23\times10^{-1}$	0.94
598-TCOD	$y = 4.79\times10^{-3}x - 5.60\times10^{-2}$	0.94
All-TCOD	$y = 5.08\times10^{-3}x + 4.14\times10^{-2}$	0.50
111-PCOD	$y = 1.30\times10^{-2}x - 4.85\times10^{-2}$	0.86
225-PCOD	$y = 7.17\times10^{-3}x - 7.65\times10^{-2}$	0.92
346-PCOD	$y = 5.65\times10^{-3}x - 4.87\times10^{-2}$	0.79
598-PCOD	$y = 2.32\times10^{-3}x - 2.82\times10^{-3}$	0.68
All-PCOD	$y = 3.41\times10^{-3}x + 2.09\times10^{-2}$	0.38
111-SCOD	$y = 9.84\times10^{-5}x + 2.29\times10^{-2}$	0.02
225-SCOD	$y = 6.66\times10^{-4}x + 1.51\times10^{-2}$	0.14
346-SCOD	$y = 3.68\times10^{-3}x - 5.76\times10^{-2}$	0.77
598-SCOD	$y = 2.03\times10^{-3}x - 4.34\times10^{-2}$	0.78
All-SCOD	$y = 1.60\times10^{-3}x - 5.55\times10^{-3}$	0.45
111-LA	$y = 1.29\times10^{-3}x - 2.82\times10^{-4}$	0.83
225-LA	$y = 1.14\times10^{-3}x - 1.22\times10^{-2}$	0.93
346-LA	$y = 1.04\times10^{-3}x - 1.68\times10^{-2}$	0.72
598-LA	$y = 4.20\times10^{-4}x - 9.00\times10^{-3}$	0.91
All-LA	$y = 5.18\times10^{-4}x - 2.04\times10^{-4}$	0.37

The positive slopes for all type of COD (TCOD, PCOD, and SCOD) in **Table 3.2** indicate that higher AILI supported faster photosynthetic production per unit of wild-type biomass. For PCOD, the culture illuminated by an incident light of 598 $\mu E/m^2$-s produced less PCOD and more SMP than the others. The ratios among the slopes agree with the trends of **Figure 3.3**, panel a. Those ratios are 0.20 mg SMP-COD/ mg TCOD and 0.80 mg PCOD/ mg TCOD.

A serious consequence of exposing *Synechocystis* to LI higher than about 400 $\mu E/m^2$-s is photo-inhibition (Radakovits, Jinkerson, Darzins, & Posewitz, 2010), in which phycobilisome is degraded, turning the culture color from dark green to yellowish green (Schwarz & Grossman, 1998). Exposure to inhibitory LI leads to deactivation of the electron carrier system and, in extreme case, damage to the integrity of the cell membrane (Krause, 1988). I took regular color photographs of the cultures, and **Figure 2.5** shows a yellowish color in the culture exposed to 598 $\mu E/m^2$-s, indicating pigment degradation due to photo-inhibition.

I successful maintained axenic conditions for the run presented in **Figure 3.2** (Run #1). In addition, I replicated experimental conditions in another try (Run #2). In run #2, I sampled every day for laurate and optical density. One critical success of this run is that all reactors were free of heterotrophs during the 3-week experiment. The microbial community was checked by regular light microscopy, as shown in **Figure 2.6** in Chapter 2 for last day in experiment.

In general, **Figure 3.5** shows that the laurate fraction correlated well with biomass for all four flasks. Calculating cumulative laurate concentrations yielded average laurate productivities of 3.4, 5.0, 5.8 and 4.5 mg/L.day for incident LIs of 111, 225, 346, and 598

$\mu E/m^2$-s, respectively. During extraction, three samples (days 18-20) of culture with incident LI of 598 $\mu E/m^2$-s developed a gel-like form in hexane and yielded no laurate by GC. Those 3 points were excluded for electron partitioning calculation shown in **Figure 3.5**.

Another approach to evaluate electron partitioning is calculating relative electron partitioning to laurate and to particulate biomass. The third panel of **Figure 3.5** presents the fractions of laurate/biomass, both after being converted as COD. The average ratios were 13.2%, 14.6%, 13.7%, and 11.5% for the lowest to highest incident LI, a trend consistent with Run #1 shown in **Figure 3.2**. The consistent outcome for laurate-to-biomass indicates that the production of laurate was proportional to biomass and was influenced by incident LI in that way. This trend suggests that maximizing biomass production is a way to maximize laurate production.

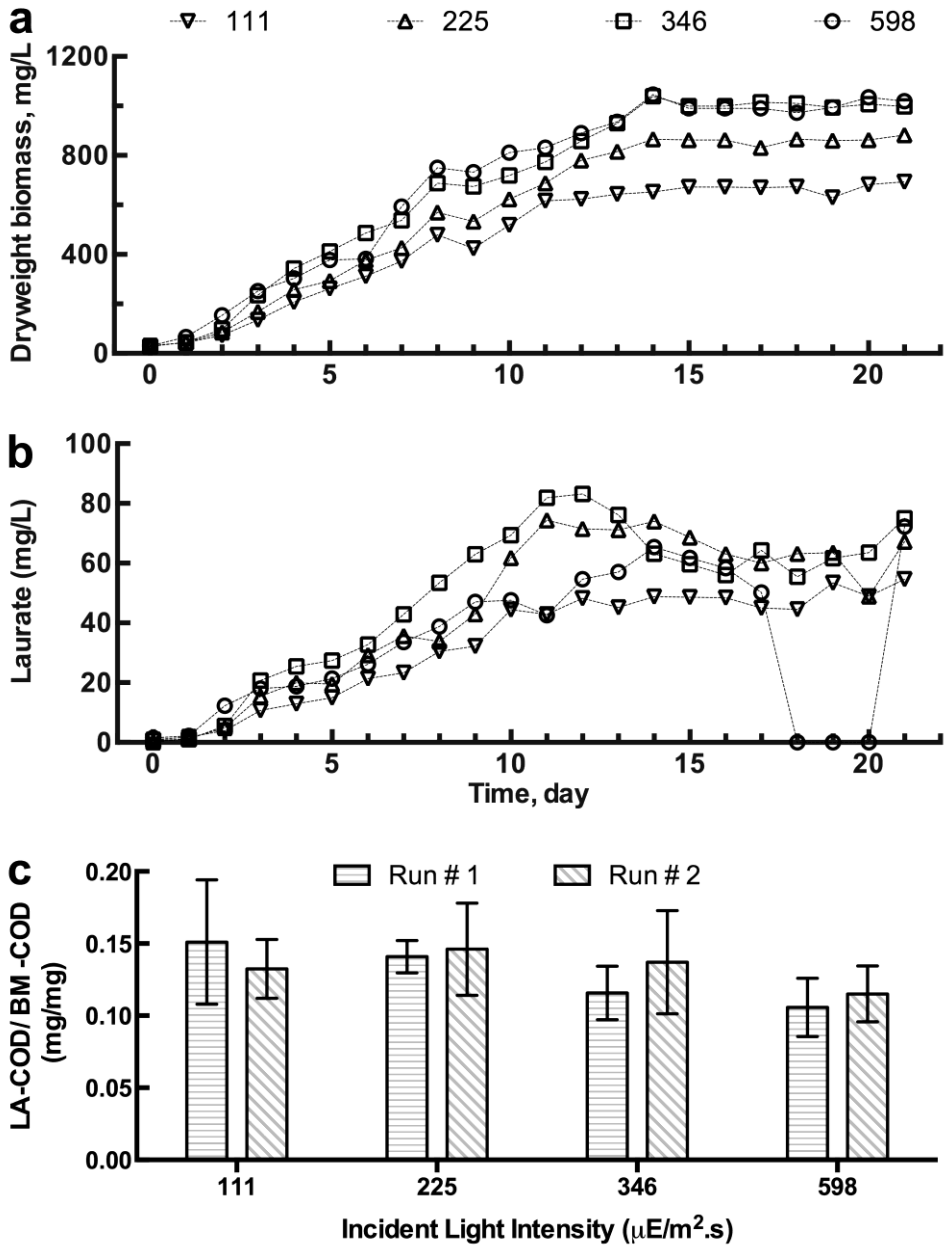

Figure 3.5: Dry Weight Biomass Equivalent (Panel a) and Laurate Concentration (Panel b) of Laurate-Excreting *Synechocystis* Grew in Fixed Incident LI from 111 μE/m^2-s to 598 μE/m^2-s. Panel c Summarizes Fixed Electron Partitioning to Laurate (LA) Relative to Biomass (BM) of Two Replicated Run

Bars represent the 95% confidence level. Only data of axenic culture is included to calculate electron partitioning

The higher proportion of electrons partitioned into SMP with exposure to the highest LI also might have led to a sunscreen response to photo-inhibition. Compounds such as scytonemin and mycosporine-liked amino acids (MAA) are found in the outer membrane and S-layer of cyanobacteria. Previous research found only a small portion of those sunscreen compounds within the total EPS extracted from cells (Garcia-Pichel et al., 1993; Proteau et al., 1993). Nevertheless, increased production of those compounds in the EPS could ultimately lead to their hydrolysis and release to the medium as SMP (Balskus & Walsh, 2010).

3.5.2 Correlation of specific growth rates to laurate and generic SMP production

The important connections of biomass specific growth rate and the specific production rate of laurate and SMP are presented in **Figure 3.6**. The results of linear regression of the rates are tabulated in **Table 3.4.**

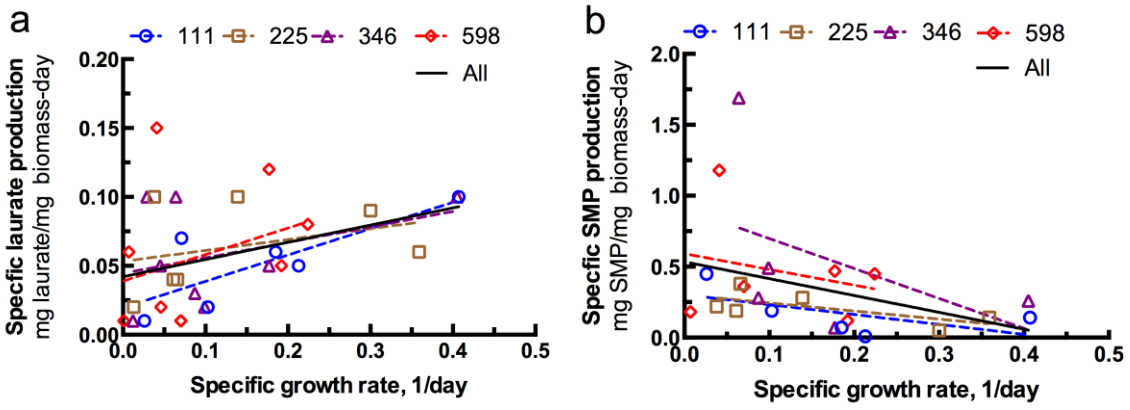

Figure 3.6: Correlation to the Biomass Specific Growth Rate with the Specific Rates of Laurate Production (Panel a) and SMP Production (Panel b) by the Laurate-Excreting Strain

Table 3.4: Linear-Regression Slopes (p) and Correlation Coefficients (R^2) for the Specific Production Rates of Laurate and Generic SMP Production in **Figure 3.6**

Dependent Parameter	Data set by incident LI in $\mu E/m^2$-s	Linear-regression slope (p), mg laurate or SMP COD/ mg biomass COD (± gives the 95% confident level of p)	R^2
Specific laurate production rate per biomass to μ	111 $\mu E/m^2$-s	0.19 ± 0.02	0.62
	225 $\mu E/m^2$-s	0.08 ± 0.03	0.11
	346 $\mu E/m^2$-s	0.11 ± 0. 04	0.14
	598 $\mu E/m^2$-s	0.19 ± 0.05	0.10
	All	0.13 ± 0.04	0.14
Specific SMP production rateper biomass to μ	111 $\mu E/m^2$-s	-0.70 ± 0.35	0.35
	225 $\mu E/m^2$-s	-0.57 ± 0.09	0.47
	346 $\mu E/m^2$-s	-2.11 ± 0.67	0.21
	598 $\mu E/m^2$-s	-1.11 ± 0.07	0.07
	All	-1.19 ± 0.37	0.14

One important and clear trend from **Figure 3.6a** and **Table 3.4** is that the specific rate of laurate production was positively correlated to the biomass specific growth rate, especially for the lower AILI values. For all the laurate results and without forcing the regression through the origin, the linear proportionality (p) was 0.13 mg (laurate-COD)/mg (biomass COD), with a correlation R^2 of 0.14. The other important trend is

that the slope was the opposite for SMP (**Figure 3.6b** and **Table 3.4**): a linear proportionality of -1.19 mg (SMP-COD)/mg (biomass COD), with R^2 of 0.14.

The distinctly different patterns can be explained by the different sources and mechanisms of laurate and SMP production. Laurate is diverted from the lipid-production pathway and excreted through the cell membrane (Ducat et al., 2011; Liu et al., 2011; Radakovits et al., 2010). Precursors include acetyl-CoA, pyruvate, and acyl-ACP, which are more available when cells grow rapidly in light- and C-sufficient conditions (as discussed in Chapter 2). The optimal growth condition that supports biomass μ near μ_{max} also supports more availability of the precursors of laurate.

In contrast, generic SMP are products of hydrolysis of EPS (Laspidou and Rittmann, 2002). It is true that high light intensity promoted higher EPS production via metabolism of simple sugars (Donot, Fontana, Baccou, & Schorr-Galindo, 2012), perhaps as a means to dump excess electrons. However, hydrolysis of EPS to generate SMP depends on environmental and cell conditions. In this case, higher SMP production with low μ suggests that cell "age" could have been a factor. The denser biomass associated with longer batch-culture time and lower μ means that more EPS was available for hydrolysis, and this may have been the main factor leading to a higher SMP production.

The opposite trends of laurate and SMP productions promise a practical means to improve in net generation of laurate by the modified strain, while minimizing undesired SMP generation: grow the modified *Synechocystis* at the highest practicable specific growth rate.

3.6 Synthesis and Application

In summary, a significant portion of energy embedded in organic carbon was fixed into SMP, and the ratio was higher in laurate-excreting *Synechocystis* than in the wild type and with higher light intensity. The latter finding identifies a need to moderate light intensity in the photobioreactor. The former finding suggests that profitable modifications to *Synechocystis* in the future would be to find ways to minimize its release of SMP, probably indirectly via EPS. In addition, laurate production was proportional to biomass production, which leads to the conclusion that the maximum rate of laurate production will correspond to the maximum rate of biomass synthesis.

4 EFFECT OF NITROGEN SOURCES ON ALKALINITY AND INORGANIC CARBON[*]

4.1 Introduction

Microalgae can capture sunlight energy and fix carbon dioxide at a rate 5 to 20 times higher than terrestrial plant, do not require arable land, and are amenable to genetic modification (Chisti, 2008; Posten & Schaub, 2009; W. Vermaas, 1996). Thus, microalgae have promise to become a major source of renewable energy and chemical feedstock (Chisti, 2007, 2008). Microalgae take up d inorganic carbon (C_i) for synthesis, and carbon makes up around 50% of the dry weight of microalgae (Kim et al., 2010).

Research interest on C_i to microalgae growth is, nevertheless, not as intense and thorough as its role. In part, microalgae possess the CO_2 concentrating mechanism (CCM), a special mechanism to elevate CO_2 concentration internally. The CCM benefits microalgae to grow in wide range of C_i concentration. Earlier studies referred to this increment of buffering capacity of microalgal broth due to formation of bicarbonate (Krauss, 1953) and hydroxyl ion (J. C. Goldman, Porcella, Joe Middlebrooks, & Toerien, 1972). Most of experiments sparged the culture with enriched CO_2 (0.1-0.5%) (Robert Emerson & Green, 1938) or 1% (J. Goldman, Azov, Riley, & Dennett, 1982)) to maintain sufficient inorganic carbon supply. No enhancement in productivity was observed with

[*] Results in this chapter were published in *Environmental Science and Technology* as Nguyen, B. T., & Rittmann, B. E. (2015). Predicting Dissolved Inorganic Carbon in Photoautotrophic Microalgae Culture via the Nitrogen Source. Vol. 49(16), 9826–9831.

CO_2-enriched aeration in 1%-99% volume (J. C. Goldman, Dennett, & Carol, 1981). Until now (2015), the CO_2 percentage in the sparging gas is used as the primary condition for growth, especially, to substrate when sufficient CO_2 is supplied. This approach is straightforward, but it seriously oversimplifies nature of gas transfer and carbon species that microalgae can take up. I discuss this aspect in detail in Chapter 5, in which growth kinetics on C_i and growth pH are the main foci.

Studies on the effects of nitrogen species and alkalinity are presented in Goldman et al. (1972), Brewer and Goldman (1976) and Goldman et al. (1982c). The summary in Table 7 in Brewer and Goldman (1976) indicates that alkalinity changes in a way associated with biomass synthesis. While the authors presented the "fashion" of alkalinity correctly, they provided no quantitative estimate of the relationship of alkalinity to biomass synthesis. An attempt to quantify the C_i in relation to biomass grown was presented later by Novak and Brune (1985) and Goldman et al. (1982c), but the study did not produce any systematic and quantitative outcome.

According to the CCM, only dissolved CO_2, carbonic acid, and bicarbonate are usable by microalgae; I give the sum of these three species the symbol C_{ib}, for being the bioavailable form of inorganic C. Details of CCM are introduced in chapter 5. In this chapter, I quantify the relationships among uptake of nitrogen sources, the biomass produced, and changes in Dissolved Inorganic Carbon (DIC or C_i). I normally use C_i to represent DIC, which is expressed directly to measurement by the TOC analyzer. As I show later, computing C_{ib} from (measured) C_i is straightforward when the pH of bulk liquid is known.

While the source of C_i may not affect microalgae growth (Navid Reza Moheimani, 2013), the pH and C_i concentration can have profound effects. These relationships are explored in-depth in Chapter 5. In short, most microalgae grow best at modestly alkaline pH (J. Goldman, Azov, et al., 1982; A. Mayo, 1997), and very low concentrations of C_i can limit growth of microalgae (J. C. Goldman, Oswald, Jenkins, & Oswald, 1974; Novak & Brune, 1985; Tittel, Bissinger, Gaedke, & Kamjunke, 2005). Despite these generally well-established facts, trends of how C_i controls biomass growth have not been systematically quantified. Having a quantitative foundation for how C_i affects microalgal growth kinetics would be of high value for the management of microalgae production systems.

The choice of growth medium and nutrient components can influence the C_i concentration that occurs for a given pH. Typical growth media, such as BG-11 and f/2 (UTEX, 2009, 2014), contain sodium nitrate as the nitrogen source. Although a few microalgae can fix nitrogen gas (Fay, Stewart, Walsby, & Fogg, 1968), ammonium is the only widely relevant alternative to nitrate as the nitrogen source. Utilizing an ammonium-rich waste stream, such as in many wastewaters, to grow microalgae appears to be win-win situation: simultaneously removing nutrient pollution and producing useful biomass (Park, Craggs, & Shilton, 2011; Sialve, Bernet, & Bernard, 2009).

Here, I systematically evaluate how the nitrogen source affects the C_i concentration during the growth of cyanobacteria with pH fixed by at a constant level by means of automated CO_2 supply. First, I apply the Proton Condition (PC), a special mass balance for acid and base equivalents, to track the change in proton-deficient and excess species when using different nitrogen sources: nitrate alone, ammonium alone, and a

mixture of nitrate and ammonium. My analysis indicates that the trends of C_i concentration systematically depend on the nitrogen source. Second, I evaluate the PC-based predictions by carrying out experiments with the wild-type cyanobacterium *Synechocystis*. The experimental results with a fixed pH confirm that nitrate increases the C_i proportionally to biomass synthesis, ammonium reduces C_i in proportion to biomass synthesis, and ammonium nitrate holds the C_i in a narrow range.

4.2 pH-Stat PBR

The inherent connection of growth pH to carbonate speciation in the medium makes impossible to independently control pH and C_i by the use of a simple experimental apparatus, such as with flask and a constant atmospheric aeration. Previous studies employed high concentration of pH buffering to retain pH in a desired range to create a pH-stabilized environment (see Azov, 1982; Azov and Goldman, 1982; Badger et al., 199 4; Miller et al., 1984). Sheng (2011) tested different concentration of buffers to control pH, and some of them led to a *Synechocystis* culture crash, and while the growth was irregular in most cases. The use of high-concentration chemical buffers for pH control is not economical in large-scale application. Several researchers stated that pH-Static control via sparing CO_2 to the microalgae culture is the most convenient and desirable method (Navid R Moheimani & Borowitzka, 2011; Navid Reza Moheimani, 2013), and it is used in large-scale practice. This approach provides pH control while supplying inorganic carbon for photosynthesis (Grobbelaar, 2004).

The need for pH-Static controller encouraged me to search different hardware options, such as the CO_2 Gas/pH controller (Harvard Apparatus, MA) and MC122 pH

controller (Milwaukee Instruments, NC). These designs are marketed for pH control, but I found that they are inflexible to configure and lack continuous data recording and monitoring. My third attempt to control pH involved my own design featuring a central control unit connected with a power replay (Neptune Systems, CA) and a solenoid valve connected to a compress tank that feeds CO_2 gas to the reactor. **Figure 4.1** presents a simplified schematic diagram of pH-Stat PBR that I built. More functions were later added to the system, including temperature control using air cooling, light control with a timer. I added a DO probe (**Figure 4.2**) to monitor oxygen concentration of photoperiod experiments in Chapter 6.

The pH-Stat measures the pH of the microalgae culture through a pH electro-chemical probe submerged in the culture. When the pH reading exceeds a set point, the pH controller opens the solenoid valve and feeds pure CO_2 gas to the reactor in order to reduce pH. The valve is closed when the pH reading is below the set point. The pH of culture oscillates around the set point, and I can adjust the CO_2 gas flow rate to achieve a low degree of pH fluctuation. The desired pH could be set through the software in the range of 3.99 to 9.99. The software allows online monitoring with up to 7-day data logging, as well as remote control via Internet connection.

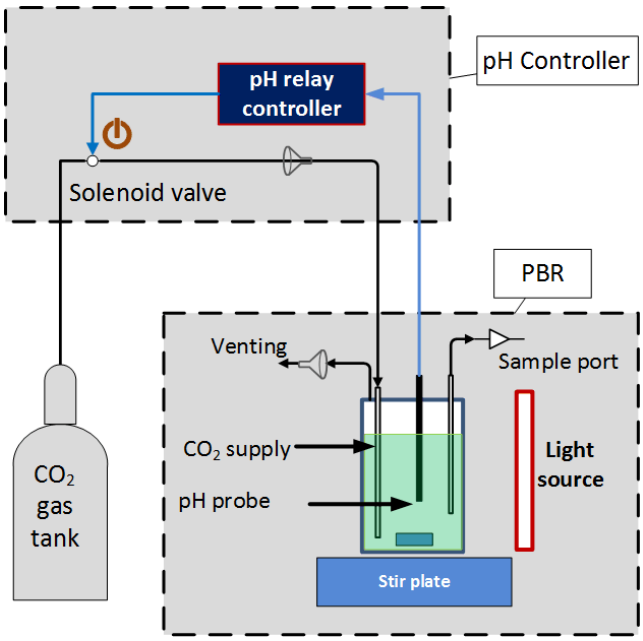

Figure 4.1: Schematic Diagram of the PBR Equipped with a pH-Stat

The PBR that housed the culture and pH probe was a ~1.8-L glass jar with 1.5-L working volume. A gas-flow meter with a stop valve connected to a compressed tank delivered CO_2 gas to the bulk liquid by a ¼-inch plastic tube inserting through the reactor's lid. To increase gas transfer, the tube was connected to a 1/16 -inch tip that was situated right above the stir bar. Influent and exit gas were filtered through 1-µm Bacterial Filter (Pall Life Sciences) to prevent contamination to and from the culture. Biomass was mixed by one 5-cm magnetic stir bar at a constant rate of 200 rpm. Samples were taken twice a day through a silicon tube inserted through the reactor's lid.

During experiments, the culture temperature was maintained at 30°C by automated air-cooling. The incident LI was 324 µE/m^2-s from T5 fluorescent bulbs (Hydrofarm, U.S.). The target pH was set by a web-based interface before each run and maintained at ± 0.05 pH units.

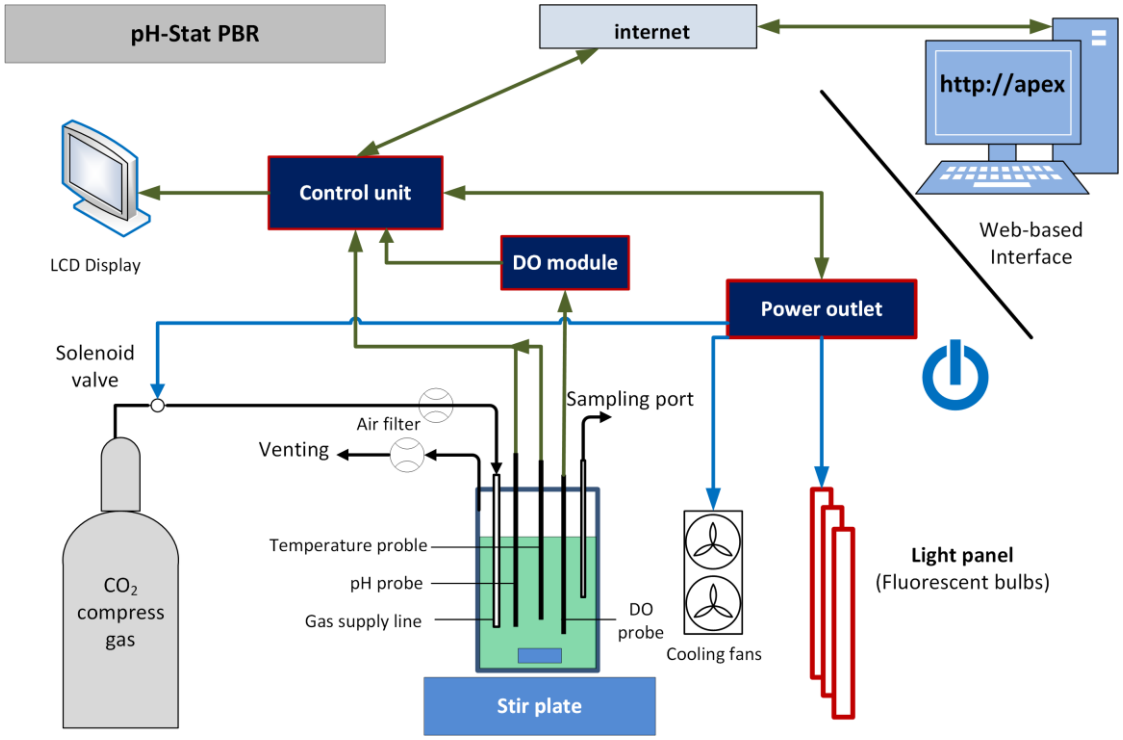

Figure 4.2: Schematic Diagram of the Full Version of the pH-Stat PBR

4.3 Using the Proton Condition to Model Dissolved Inorganic Carbon Trends

To relate the effects of the N source to the alkalinity and C_i concentration, I employed the proton condition (PC), a special mass balance that tracks proton-deficient and proton-excess species (Morel & Morgan, 1972; VanBriesen & Rittmann, 1999). Unlike an electro-neutrality condition, the PC specifically tracks the change in proton status of all components that participate in acid-base reactions by using the change in total base (or alkalinity) in the system. Thus, the PC focuses only on species relevant to acid-base reactions, and it also eliminates problems of rounding errors when changes in acid-base status are small compared to the concentrations of all cations and anions. One

example of PC balance is total alkalinity (ALK, mole/L; regular unit: mg eq/L $CaCO_3$) for the carbonate system:

$$\text{Total ALK} + [H^+] = [OH^-]+[HCO_3^-]+2[CO_3^{2-}]$$

or

$$\text{Total ALK} = [OH^-]+[HCO_3^-]+2[CO_3^{2-}]-[H^+] \quad (4.1)$$

In the top version, the left-hand side in eqn. (4.1) presents the total concentration of proton-excess species, and the right hand side presents the total concentration of proton-deficient species. The bottom version shows how total ALK is the sum of the other species.

BG-11 growth medium contains sodium bicarbonate ($NaHCO_3$, 0.189 mM), sodium nitrate ($NaNO_3$, 17.6 mM), potassium hydrogen phosphate (K_2HPO_4, 0.175 mM), and minor nutrients and trace minerals. To simplify this system for pH analysis, I include only $NaHCO_3$ and K_2HPO_4 for below analyses.

To apply the PC, equilibrium speciation (e.g., from alpha factors), and the total concentrations of each reference species are calculated based on the pH and the speciation at equilibrium. I often assume that {activity of species A} = [concentration of species A], although it is easy to use activity coefficients if the ionic strength can be estimated and is large. Alpha factors for the carbonate and the phosphate systems are:

$$\alpha_{0,C} = \frac{[H_2CO_3^*]}{DIC} = \frac{[H^+]^2}{[H^+]^2 + K_{a,1}[H^+] + K_{a,1}K_{a,2}}$$

$$\alpha_{1,C} = \frac{[HCO_3^-]}{DIC} = \frac{K_{a,1}[H^+]}{[H^+]^2 + K_{a,1}[H^+] + K_{a,1}K_{a,2}} \quad (4.2)$$

$$\alpha_{2,C} = \frac{[CO_3^{2-}]}{DIC} = \frac{K_{a,1}K_{a,2}}{[H^+]^2 + K_{a,1}[H^+] + K_{a,1}K_{a,2}}$$

and

$$\alpha_{0,P} = \frac{[H_3PO_4]}{[\text{Total P}]} = \frac{[H^+]^3}{[H^+]^3 + K_{a1}[H^+]^2 + K_{a1}K_{a2}[H^+] + K_{a1}K_{a2}K_{a3}}$$

$$\alpha_{1,P} = \frac{[H_2PO_4^-]}{[\text{Total P}]} = \frac{K_{a1}[H^+]^2}{[H^+]^3 + K_{a1}[H^+]^2 + K_{a1}K_{a2}[H^+] + K_{a1}K_{a2}K_{a3}} \quad (4.3)$$

$$\alpha_{2,P} = \frac{[HPO_4^{2-}]}{[\text{Total P}]} = \frac{K_{a1}K_{a2}[H^+]}{[H^+]^3 + K_{a1}[H^+]^2 + K_{a1}K_{a2}[H^+] + K_{a1}K_{a2}K_{a3}}$$

$$\alpha_{3,P} = \frac{[PO_4^{2-}]}{[\text{Total P}]} = \frac{K_{a1}K_{a2}K_{a3}}{[H^+]^3 + K_{a1}[H^+]^2 + K_{a1}K_{a2}[H^+] + K_{a1}K_{a2}K_{a3}}$$

in which [Total P] is total concentration of dissolved phosphorous (M), $K_{a1}=10^{-2.15}$; $K_{a2}=10^{-7.20}$; $K_{a3}=10^{-12.38}$ are equilibrium constants. For water, $\{H^+\}\times\{OH^-\} = 10^{-14}$ (i.e., K_w).

To use the PC, I first selected reference species: in this case, water (H_2O), carbonic acid (H_2CO_3), and phosphoric acid (H_3PO_4). The PC contains all other species that have more or fewer protons than the reference level. Also included in the PC is the total amount of base or alkalinity that is added to the system from any source; I designate this value as b (eq/L). The PC for a general case is:

$$[H^+] + b = [OH^-] + (\alpha_{1,C} + 2\alpha_{2,C})C_C + (\alpha_{1,P} + 2\alpha_{2,P} + 3\alpha_{3,P})C_P \quad (4.4)$$

where $[H^+]$ and $[OH^-]$ are the concentrations of hydrogen and hydroxyl ions in bulk liquid [mole/L); C_C and C_P are the concentrations of C_i and total soluble phosphate in bulk liquid [mole/L]; $\alpha_{1,C}$ and $\alpha_{2,C}$ are the ionization fractions of bicarbonate (HCO_3^-) and carbonate (CO_3^{2-}); $\alpha_{1,P}$, $\alpha_{2,P,}$ and $\alpha_{3,P}$ are the ionization fractions of dihydrogen phosphate ($H_2PO_4^-$), hydrogen phosphate (HPO_4^{2-}), and phosphate (PO_4^{3-}); and b is the total alkalinity (eq/L).

Photoautotrophic synthesis fixes C from C_i, N from the N source, and P from phosphoric acid into biomass, represented as $C_5H_7NO_2P_{0.05}$ based on Kim et al. (2010); and Rittmann and McCarty (2001), in which N comprises 13.2% and P comprises 1.3% of the dry weight. The N source makes a major difference in how photosynthesis affects the alkalinity, or b. I first present the reaction for biomass synthesis like eqn. (4.5) when the N source is NO_3^-, as in BG-11.

$$5\,CO_2 + NO_3^- + 0.05\,H_3PO_4 + 3.925\,H_2O \rightarrow C_5H_7O_2NP_{0.05} + 7.0625\,O_2 + OH^- \quad (4.5)$$

When one mole of new biomass is generated according to eqn. (4.5), one mole of alkalinity (OH^-) is generated. Hence, the total alkalinity in the system is $b = b_0 + \Delta b$, where b_0 = the starting alkalinity (eq/L) and Δb = the increase in alkalinity, which also equals the increase in the molar concentration of biomass (Eqn. (4.6)). The concentration of phosphate declines due to uptake for biomass synthesis, making $C_{P,\Delta b} = C_{P,0} - 0.013\Delta b$, where $0.013\Delta b$ accounts for phosphorus taken up into biomass based on $C_5H_7O_2NP_{0.05}$. Then, the PC becomes:

$$[H^+]_{\Delta b} + b = [OH^-]_{\Delta b} + (\alpha_{1,C,\Delta b} + 2\alpha_{2,C,\Delta b})C_{C,\Delta b} + (\alpha_{1,P,\Delta b} + 2\alpha_{2,P,\Delta b} + 3\alpha_{3,P,\Delta b})C_{P,\Delta b} \quad (4.6)$$

where b was defined above, and subscript Δb indicates after growth of Δb moles of biomass.

The initial alkalinity of the cell-free medium (b_0) can be adapted from (4.1) for the initial conditions:

$$b_0 = [OH^-]_0 + (\alpha_{1,C,0} + 2\alpha_{2,C,0})C_{C,0} + (\alpha_{1,P,0} + 2\alpha_{2,P,0} + 3\alpha_{3,P,0})C_{P,0} - [H^+]_0 \quad (4.7)$$

where the subscript 0 reflects the condition before photosynthesis begins.

Rearranging (4.7) to solves for the concentration of inorganic C based on biomass synthesis with NO_3^- as the N source:

$$C_{C,s} = \frac{[H^+]_{\Delta b} + b_0 + \Delta b - (\alpha_{1,P,\Delta b} + 2\alpha_{2,P,\Delta b} + 3\alpha_{3,P,\Delta b})C_{P,\Delta b} - [OH^-]_{\Delta b}}{\alpha_{1,C,\Delta b} + 2,_{2,C,\Delta b}} \quad (4.8)$$

When the growth pH is fixed, the ionization fractions for each component, $[H^+]$, and $[OH^-]$ are known and constant, e.g., $\alpha_{1,C,0} = \alpha_{1,C,\Delta b}$. Substituting b_0 given in (4.7) into (4.8) and cancelling terms lead to:

$$C_{C,\Delta b} = C_{C,0} + \frac{\Delta b(1 + 0.013(\alpha_{1,P} + 2\alpha_{2,P} + 3\alpha_{3,P}))}{\alpha_{1,C} + 2,_{2,C}} \quad (4.9)$$

Eqn.(4.9) indicates that the concentration of C_i increases with biomass growth and alkalinity generation (i.e., Δb), and the proportionality is set by the pH, which determines the ionization factors.

When ammonium (NH_4^+) is the N source, the stoichiometric reaction is:

$$5CO_2 + NH_4^+ + 0.05\ H_3PO_4 + 1.925\ H_2O \rightarrow$$
$$\rightarrow\ C_5H_7O_2NP_{0.05} + 5.0625\ O_2 + H^+ \tag{4.10}$$

The PC with NH_4^+ remains (4.7), but the total alkalinity is $b = b_0 - \Delta b$ due to the mole of hydrogen ion produced with each mole of biomass synthesized (4.10). Following the same steps as with NO_3^-, the PC can be solved for $C_{C,\Delta b}$ for NH_4^+:

$$C_{C,\Delta b} = C_{C,0} - \frac{\Delta b(1 - 0.013(\alpha_{1,P} + 2\alpha_{2,P} + 3\alpha_{3,P}))}{\alpha_{1,C} + 2,_{2,C}} \tag{4.11}$$

The trends of C_i and alkalinity in (4.11) are opposite to those in (4.9). As biomass grows, alkalinity and C_i decline.

Eqns. (4.9) and (4.11) illustrate why it is impossible to keep pH and C_i constant when either nitrate or ammonium is the nitrogen source and the biomass concentration is increasing. In principle, this situation can be alleviated if ammonium nitrate (NH_4NO_3) is the N source. The following reaction occurs if NO_3^- and NH_4^+ are utilized equally for synthesis:

$$5\ CO_2 + \frac{1}{2}NO_3^- + \frac{1}{2}NH_4^+ + 0.05\ H_3PO_4 + 2.425\ H_2O \rightarrow$$
$$\rightarrow C_5H_7O_2NP_{0.05} + 6.0625\ O_2 \tag{4.12}$$

The PC remains (4.6), and substitution yields:

$$C_{C,\Delta b} = C_{C,0} + \frac{0.013\Delta b(\alpha_{1,P} + 2\alpha_{2,P} + 3\alpha_{3,P})}{\alpha_{1,C} + 2,_{2,C}} \tag{4.13}$$

The alkalinity and C_i depend mainly on the starting alkalinity for a fixed pH. The consumption of phosphate as the P source leads to only a small increase in C_i. This

means that it ought to be possible to maintain nearly constant pH and C_i as biomass grows photoautotrophically. This outcome is particularly valuable for studying how C_i and pH independently affect growth kinetics of photoautotrophic microalgae.

4.4 Materials and Methods

4.4.1 Inoculum preparation

I obtained and prepared inoculum of wild-type *Synechocystis* sp. PCC 6803 and described in Chapter 2. I centrifuged the inoculum twice (3,220*g* for 5 minutes), and then I washed and suspended the pellet in a modified BG-11 medium prepared for the incoming experiment.

4.4.2 Modified BG-11 growth medium

To evaluate different source of nitrogen, I modified standard BG-11 by substituting other nitrogen sources for sodium nitrate, but keeping all other constituents the same. I prepared separate stocks of ammonium nitrate and ammonium chloride (0.5 N) and added to the culture during experiment. The medium was steam sterilized with a liquid cycle (121^{o}C and 15 minutes) in a Tabletop Sterilizer (SterileMax, Thermo Scientific, IA).

4.4.3 Experimental setup

I used the pH-Stat PBR to evaluate the PC-based modeling of C_i with different source. Samples were taken twice a day through a silicon tube inserted through the

reactor's lid. Roughly 25 ml of liquid was pulled out using a syringe and contained in 50-mL polypropylene centrifuge tube (VWR). Aliquots were assayed for biomass density by spectrometry.

During experiments, the incident LI was 324 $\mu E/m^2$-s and the culture temperature was maintained at 30°C by automated air-cooling. The target pH was set by a web-based interface before each run and maintained at ± 0.05 pH units. The software could record and store the pH and temperature for up to 7 days. In each set of experiments, I replicated selected runs to evaluate the reproducibility of the results. The bars on each data points represent analytical standard deviations of at least triplicate measures.

I tested effects of pH and nitrogen sources in several ways. For standard BG-11, I experimented with fixed pH values of 6.5, 7.5, 8.5, 9.5, and 10.0. To evaluate effect of starting alkalinity, I augmented additional 1.5, 3.5, or 5.0 mM bicarbonate with pH of 8.5 and with only 5.0 mM bicarbonate added for pH values of 7.5 and 9.5. With ammonium chloride as N source, I augmented the modified BG-11 with different starting alkalinity by adding bicarbonate at 3.0, 4.8, or 6.0 mM, all runs with a fixed pH of 8.5. Finally, I used ammonium nitrate as N source and augmented starting alkalinity at 0.2, 2.0, 2.6, or 5.0 mM of bicarbonate and a fixed pH of 8.5.

4.4.4 Analysis

Optical Density (OD) was measured by a UV-Vis BioSpec-mini spectrometer at 730 nm (Shimadzu Corp., Japan). The OD reading was converted to biomass dry weight using an empirical conversion factor of 254 mg dry weight biomass/L per of unit of OD

(Kim et al., 2013). A mole-per-liter concentration of biomass was calculated from dry weight using an empirical biomass formula of $C_5H_7O_2NP_{0.05}$.

C_i (also called DIC) was analyzed using a TOC-V_{CPH} analyzer with an auto-sampling tray (Shimadzu Corp., Japan). Culture samples were filtered through a 0.20-μm polyvinylidene fluoride (PVDF) syringe filter (Whatman GPX), and the filtrate was collected into glass Falcon tubes and immediately sealed by parafilm to prevent any carbon or water loss. To analyze DIC, a 50-μL aliquot was injected into the Inorganic Carbon chamber, which contained 25% H_3PO_4 by weight (IC reagent, pH~ 0.3) so that all inorganic carbonic species were converted to CO_2. The CO_2 was purged, using ultra-pure air, to a non-dispersive infrared (NDIR) gas analyzer. The DIC concentration then was determined by a calibration using a 50/50 molar ratio of sodium hydrogen carbonate/ sodium carbonate standards (Nacalai Tesque, Inc., Japan). This instrument can inject each sample up to 20 times. I used from 5 to 10 injections. Vials with acidified deionized water (18.2 MΩ, pH=2.5) were included at beginning, at the end, and between every 4 to 6 samples.

4.5 Results and Discussion

To validate the PC-based predictions, I carried out a series of batch runs in standard and modified BG-11.

The left panel in **Figure 4.3** presents growth curves of wild-type culture of *Synechocystis* with growth pH of 6.5, 7.5, 8.5, 9.5 and 10.0 in standard BG-11 medium (NO_3^- is the N source). All culture grew normally and exhibited a healthy green color. The accumulation of C_i during growth of the cyanobacteria in standard BG-11 (with NO_3^-

as the N source) is shown in left panel of **Figure 4.4**. The experimental results (symbols) confirm the trends predicted by eqn. (4.9) (lines): As biomass grew, the C_i increased proportionally when nitrate was the sole N source with a fixed growth pH. Furthermore, the pH affected the accumulation rate of C_i in ways that conform to the changes in the fraction ionization factors in eqn. (4.9): The increase was greatest for the lowest pH value, which had the smallest values of $\alpha_1 + 2\alpha_2$ for the carbonate system. The experimental data fit the PC-based modeling well, except for the run with pH = 6.5, which had lower C_i concentration than predicted. A possible cause is that slow CO_2 gas transfer at this relatively low pH prevented equilibrium of gas-phase CO_2 with liquid-phase CO_2. Another possibility is the hydroxyl generated from photosynthesis is consumed by functional groups in microalgal culture such as simple carboxylic (pK_a=4-6) (Deo, Songkasiri, Rittmann, & Reed, 2010). Those possibilities needed to be investigated further.

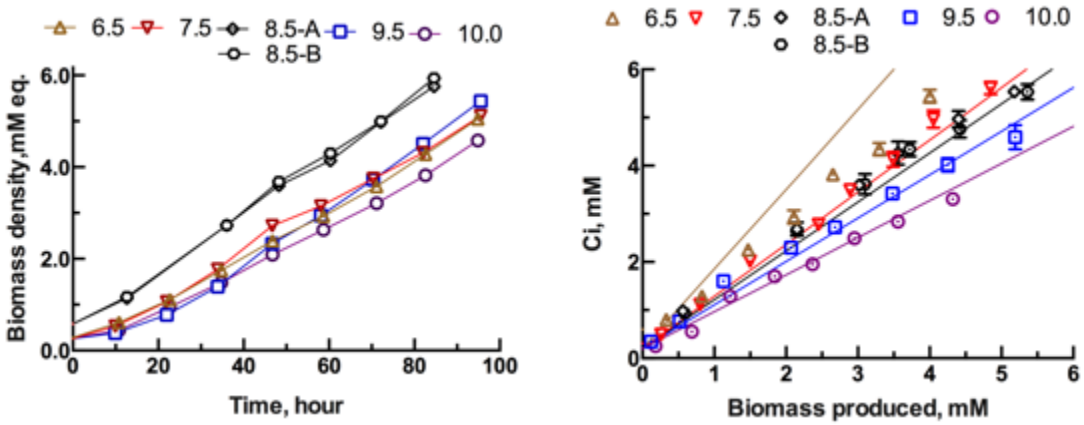

Figure 4.3: Left Panel: Growth Curves of *Synechocystis* in the Standard BG-11 Medium with Different Growth pHs, Shown on the Top Row. Right Panel: C_i Concentration as S*ynechocystis* Grew in Standard BG-11 (Containing only NO_3^-), Starting with ~0.2 mM Carbonate

The lines are the predictions based on eqn. (4.9), and the symbols are the experimental data. The bars present two standard deviation of C_i measurement, or the 95% confidence level. Runs ending with (-A) and (-B) are duplicates

Figure 4.4 presents similar data similar for experiments in BG-11, but with addition of more bicarbonate to augment the starting alkalinity. The right panel shows the growth curves, and the right panel shows the experimental and modeling trends with the addition of 5.0 mM bicarbonate at the beginning of the experiments with a fixed pH of 7.5, 8.5, and 9.5. For the fixed pH of 8.5, two runs with additional 1.5 and 3.5 mM bicarbonate are presented as well. From eqn. (4.9), the higher starting alkalinity should result in a higher C_i concentration for the same pH. Comparing panels, the slope of each line is unchanged for the same pH, but the curve is offset exactly by the increase in b_0 as predicted by eqn. (4.9).

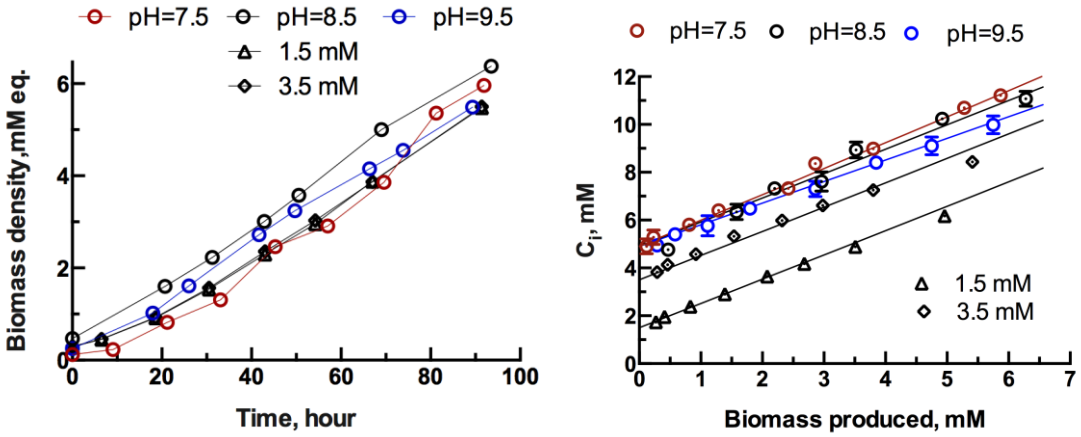

Figure 4.4: Left Panel: Growth Curves of *Synechocystis* in a Modified BG-11 Medium and Right Panel: C_i Trends as *Synechocystis* Grew in the Standard BG-11 Augmented with 5 mM of Bicarbonate (i.e., Making the Starting Alkalinity 5.4 meq/L (pH = 8.5), Circles with Growth pH = 7.5, 8.5 and 9.5) and BG-11 Contained 1.5 and 3.5 mM of C with Growth pH = 8.5

The lines are the predictions based on eqn. (4.9), and the symbols are the experimental data

The right panel of **Figure 4.5** present growth curves of the wild-type *Synechocystis* in a modified BG-11 growth medium using ammonium as the sole N source. All culture grew regularly and exhibited healthy green color. The left panel of **Figure 4.5** shows the changes in C_i when ammonium was the sole N source. As predicted by eqn. (4.11), using ammonium reduced alkalinity and C_i as biomass grew when the pH was controlled by CO_2 addition. The decline with biomass growth was the same for all initial C_i concentrations (3.0 to 6.0 mM C of added bicarbonate), which made b_0 be 3.4 to 6.4 meq/L of alkalinity. Therefore, the starting alkalinity was especially important to maintain sufficient C_i for photosynthesis when ammonium was the N source, because using ammonium as the N source can deplete C_i and halt photosynthesis. I also carried experiments in Chapter 6 exploiting this means to deplete C_i.

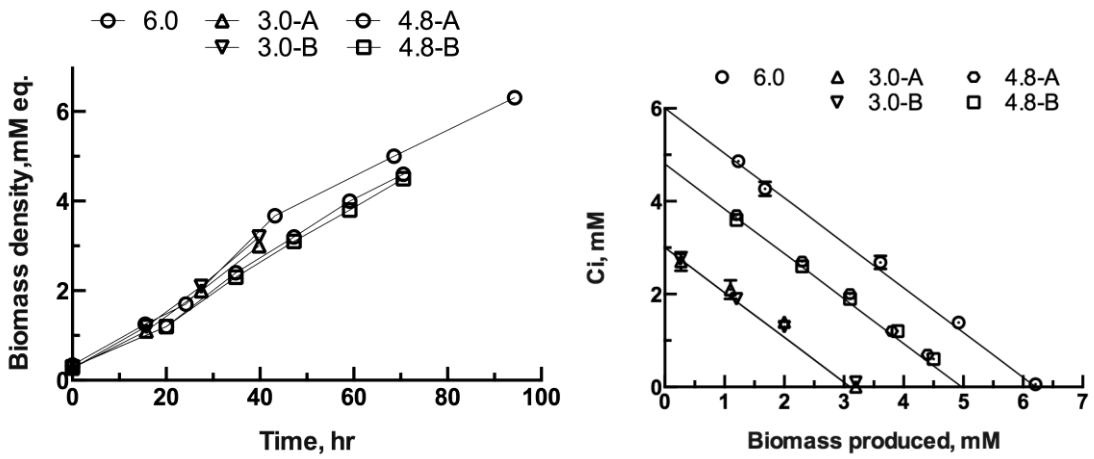

Figure 4.5: Left Panel, the Growth Curves of *Synechocystis* and Right panel, C_i Trends as *Synechocystis* Grew in BG-11 Modified by Substituted Sodium Nitrate with Ammonium Nitrate

The pH was fixed at 8.5. The lines are predictions from eqns. (4.11) for the right panel, and the symbols are the experimental data

Finally, I grew *Synechocystis* wild-type using ammonium nitrate as the N source to validate the prediction of eqn. (4.13) the C_i can be fixed if ammonium and nitrate are taken up equally. The left panel of **Figure 4.6** presents growth curves in BG-11 modified with NH_4NO_3 as the N source and with different starting amounts of alkalinity. All cultures grew normally and with a typical growth rate, except the run started with 0.2 mM DIC, the same concentration as in standard BG-11. The slower growth rate with this run resulted from C_i limitation, because C_i never increased. I investigated the growth kinetic of *Synechocystis* based C_i in Chapter 5. The right panel of **Figure 4.6** shows the C_i trends with ammonium nitrate as the N source. As expected from eqn. (4.13), the C_i changed only slightly from the starting level. The small increases in C_i were due to the uptake of phosphate P for synthesis; the alkalinity originally in phosphate species was

redistributed to carbonate species, which required a slightly higher C_i concentration for the fixed pH.

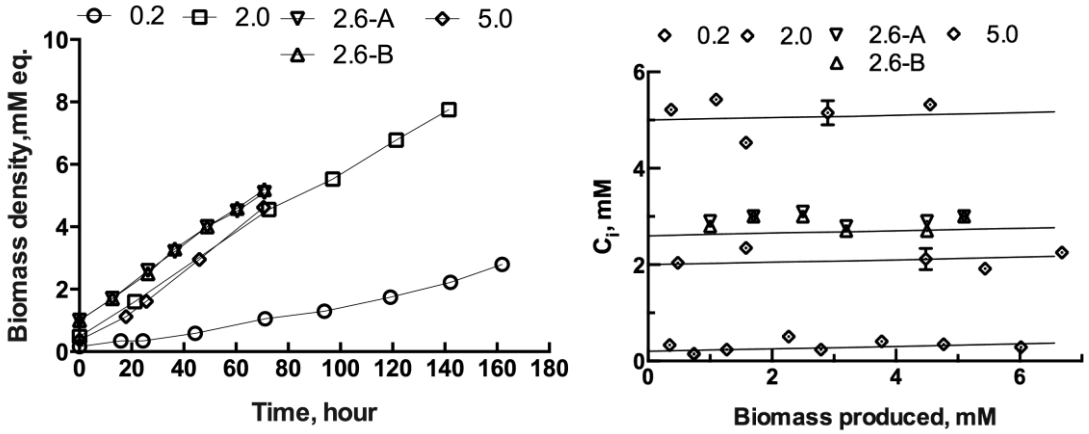

Figure 4.6: Left Panel: Growth Curves and Right Panel: C_i Trends as *Synechocystis* Grew in BG-11 Modified by Substituted Sodium Nitrate with Ammonium Nitrate For both panels, the pH was 8.5. The lines are predictions from eqn.(4.13) for the right panel, and the symbols are the experimental data.

The results in **Figure 4.4** to **Figure 4.6** confirm the value of using PC-based eqns. (4.9), (4.11), and (4.13) to explain and quantify the effects of the N source on alkalinity and DIC. The equations directly link the changes in C_i and alkalinity to the amount of biomass generated, the pH, and the starting concentration of alkalinity. Key to using the PC-based equations is knowing the starting concentration of alkalinity (b_0), which is the sum of all sources of alkalinity, including carbonate and phosphate salts, hydroxide salts, and any other added bases. Also critical for correct use is that the pH at the beginning of the experiment is the same as the pH value held constant by addition of CO_2 and the stoichiometric formula for biomass is known.

Perhaps the most important finding is that the choice of N source has a very strong impact on the alkalinity and C_i concentration when the pH is held constant. Using

nitrate causes the C_i to rise in proportion to the amount of biomass synthesized, while using ammonium causes both concentrations to decline. The former can have profound impacts on the precipitation of carbonate minerals, such as $CaCO_3$. The latter can lead to severe C_i limitation of the photoautotroph's growth rate.

4.6 Synthesis and Application

Assembling and successfully operating a pH-Stat system, I used the PC to predict and experimentally validated C_i trends for microalgae grown in a fixed pH and with different N sources. Using nitrate increased alkalinity and C_i, while ammonium reduced alkalinity and C_i; in both cases, the changes were proportional to new biomass synthesized. Because pH and C_i can have separate impacts on photoautotrophic growth kinetics, it is valuable to have a system in which C_i and pH can be controlled independently. My results show that using ammonium nitrate at the N source makes it possible to control the C_i independently of the pH. Achieving this goal was a primary motivation that led us to develop the PC-based analysis, and I am exploiting it to carry out experiments to quantify how pH and C_i control the growth kinetics of *Synechocystis*.

The effects of nitrate and ammonium uptake on the alkalinity have been discussed briefly in several previous studies (Brewer & Goldman, 1976; Novak & Brune, 1985). However, none provided a systematic and quantitative tool to understand how the N sources affect C_i. My work contributes to fundamental understanding and to managing microalgae mass culturing. Another direct outcome of this chapter is that it enabled my follow-up research on growth kinetics – in which the C_i in the growth culture could be stabilized using combined ammonium and nitrate. Using this strategy, I could independently control pH and C_i and study growth kinetics as a function pH and as a function of C_i.

5 INDEPENDENT EFFECTS OF PH AND INORGANIC CARBON ON GROWTH KINETICS OF *SYNECHOCYSTIS*[*]

5.1 Introduction

Inorganic carbon (C_i) is essential to microalgae that grow autotrophically, because C makes up ~50% mass of the biomass dry weight and contains about 70% electrons generated by photosystem II (Ducat et al., 2011; Kim et al., 2010). Effects of C_i concentration on growth kinetics have been studied extensively at the cellular and molecular levels (M. Badger & Gallagher, 1987; M. R. Badger, 2003; Price, Badger, Woodger, & Long, 2008) and in mass-culture contexts (Azov, 1982; J. C. Goldman et al., 1974; Navid Reza Moheimani, 2013; Mari Shibata, Ohkawa, Katoh, Shimoyama, & Ogawa, 2002). The CO_2-concentrating mechanism (CCM) enables microalgae to accumulate the intracellular HCO_3^- up to1000-fold over the HCO_3^- concentration in the growth medium (Price, 2011). That accumulation elevates dissolved CO_2 in the carboxysome, making carbon fixation by Rubisco more efficient (M. Badger & Gallagher, 1987).

Techno-economics indicates that the cultivation contributes a big portion of production costs, in the same order of magnitude as separation (Davis et al., 2011; Harun et al., 2011). To reduce expense associated with cultivation, improving biomass productivity is the key and most advantageous characteristics of cyanobacterium

[*] Results in this chapter were submitted to *Algal Research* as Nguyen, B.T. and Rittmann, B.E. (2015). Effects of inorganic carbon and pH on growth kinetics of *Synechocystis* sp. PCC 6803**.**

Synechocystis. Construction costs of closed systems. i.e., PBRs, was reported as major capital cost; therefore, reducing PBR volume and growing biomass faster directly benefit all financial metrics (Davis et al., 2011).

Growing microalgae in wastewater adds another positive effects, simultaneously removing nutrients (Mallick, 2002; L. A. Wang et al., 2010; Woertz, Feffer, Lundquist, & Nelson, 2009). However, the use ammonium as the nitrogen source depletes the alkalinity of culture and can lead to C_i limitation as demonstrated in Chapter 4. On the other hand, high-productivity PBRs can consume C_i so rapidly that the pH becomes very high, which converts most of C_i to carbonate, an unusable species for uptake (Giordano, Beardall, & Raven, 2005; Kim et al., 2010; Long, Rae, Badger, & Price, 2011; Price et al., 2008).

Investigating how the C_i concentration and the growth pH control the growth rate of microalgae is essential for large-scale microalgae cultivation that is economically viable. My first step to study effect of C_i and pH on growth of *Synechocystis* was to evaluate the relationship of carbon speciation to the pH of the bulk liquid.

5.1.1 Carbon speciation

Henry's law (Eqn. (5.1)) and gas-liquid mass-transfer kinetics govern the transfer between gaseous and dissolved CO_2:

$$C_{CO2(aq)} = P_{CO2(gas)} \times K_H \tag{5.1}$$

where: C_{CO2} is concentration of dissolved CO_2 in water (mole/L), $P_{CO2(gas)}$ is partial pressure of CO_2 in gas phase, $P_{CO2(gas)}$ =1.0 (bar) with pure CO_2 in open atmosphere, and K_H is Henry's constant for CO_2, which is 3.0×10^{-2} (mole/L-bar) at 30°C.

$CO_{2(aq)}$ is hydrated to carbonic acid (H_2CO_3), and the two species normally are grouped together as $H_2CO_3^*$ (Eqns. (5.2) and (5.3)) (Snoeyink & Jenkins, 1980):

$$CO_{2(aq)} + H_2O \leftrightarrow H_2CO_3 \tag{5.2}$$

$$[H_2CO_3^*] = [H_2CO_3] + [CO_{2(aq)}] \tag{5.3}$$

$H_2CO_3^*$ dissociates to two more basic species – bicarbonate (HCO_3^-) and carbonate (CO_3^{2-}) – that are in equilibrium with H_2CO_3* according to two well-known acid-base reactions and their acid-dissociation constants ($K_{a,1}$ and $K_{a,2}$, value extrapolated for 30°C) ((Snoeyink & Jenkins, 1980)).

$$H_2CO_3^* \leftrightarrow H^+ + HCO_3^-, K_{a,1} = 10^{-6.3} \tag{5.4}$$

$$HCO_3^- \leftrightarrow H^+ + CO_3^{2-}, K_{a,2} = 10^{-10.3} \tag{5.5}$$

C_i is the sum of the three species: $C_i = [H_2CO_3^*] + [HCO_3^-] + [CO_3^{2-}]$, while $C_{ib} = [H_2CO_3^*] + [HCO_3^-]$. If C_i and pH are known, concentrations of H_2CO^*, HCO_3^-, and CO_3^{2-} can be computed by Eqns. (5.6), (5.7) and (5.8) (Snoeyink & Jenkins, 1980):

$$[H_2CO_3^*] = C_i \frac{[H^+]^2}{[H^+]^2 + K_{a,1}[H^+] + K_{a,1}K_{a,2}} \tag{5.6}$$

$$[HCO_3^-] = C_i \frac{K_{a,1}[H^+]}{[H^+]^2 + K_{a,1}[H^+] + K_{a,1}K_{a,2}} \tag{5.7}$$

$$[CO_3^{2-}] = C_i \frac{K_{a,1}K_{a,2}}{[H^+]^2 + K_{a,1}[H^+] + K_{a,1}K_{a,2}} \tag{5.8}$$

Figure 5.1 illustrates the pH-dependent partitioning of the carbonate system. pH can be measured by an electro-chemical probe, and DIC, a term quantitatively equivalent to C_i, is analyzed by TOC analyzer or by thermo-chemical digestion with colorimetry. Those measurements provide fast and convenient parameters to calculate each (inorganic) carbon species.

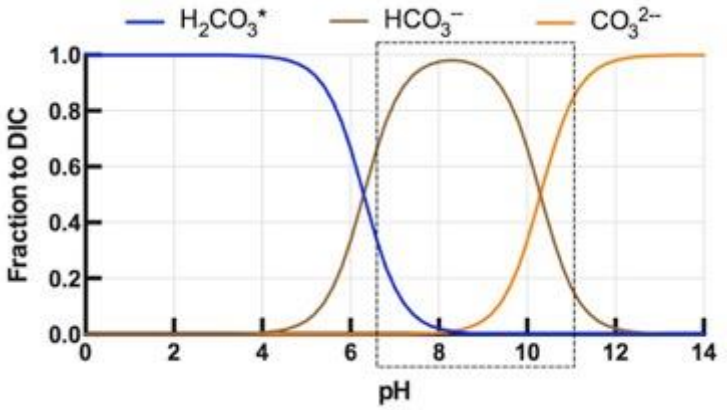

Figure 5.1: Distribution of Carbon Species from Total DIC with pH
Dashed area shows a typical growth range of pH (6.5-11) for cyanobacteria

5.1.2 CO_2-concetrating mechanism

Cyanobacteria are famous for their capability to elevate their intracellular concentration of C_i up to a level sufficient to compensate for the fact that the RubisCO enzyme has poor affinity for CO_2 (K_{CO2} = 150 μM). C_i elevation occurs via the CO_2-Concentrating Mechanisms (CCM), in which cyanobacteria deploy suitable C_i transporters to collect C_i in environment and elevate the internal concentration of C_i for the Calvin-Benson-Bassham (CBB) cycle of C fixation. Through CCM, cyanobacteria can accumulate internally up to 40 mM C_i, about 1000-fold higher than the concentration in natural water.

Cyanobacteria can take up dissolved CO_2 or HCO_3^- (M. Badger & Gallagher, 1987; Price et al., 2008; Price, 2011). When taking up CO_2, cyanobacteria can either use a transporter with low CO_2 affinity and a high flux or a transporter with high CO_2 affinity and low flux, depending on the exogenous C_i concentration. A similar strategy is available for HCO_3^-: a combination of transporters of low flux-high affinity and high flux-low affinity to HCO_3- (Price et al., 2008). Using such complementary transporters allows C_i uptake for a wide range of C_i concentrations: 1 µM to 170 µM (Price et al., 2008).

After being imported across the cytoplasmic membrane, CO_2 and HCO_3^- are stored in the cytoplasm as HCO_3^- because of the weakly alkaline environment in the stroma, a space inside chloroplast (in eukaryotic microalgae) or thylakoid membrane (in prokaryotic cyanobacteria) that houses chlorophylls, light harvesting complex, and reaction centers (Moroney & Ynalvez, 2007). Bicarbonate is then converted to CO_2 and pumped into special organelles called pyrenoid (eukaryotic microalgae) or carboxysome (prokaryotic cyanobacteria) that elevate the C_i concentration still further. In a carboxysome, C_i is becomes available to RubisCO as CO_2 and enters inorganic carbon fixation process or CBB cycle.

Synechocystis sp. PCC 6803, in particular, is fully equipped with all C_i transporters known to exist in cyanobacteria. The C_i transporter system has three known transporters for HCO_3^- and two for CO_2. *BCT1* has a high affinity for HCO_3^- (K_m=15 µM) and supports a medium flux (Omata at el., 2002). Another HCO_3^- transporter is *SbtA*, which is Na^+-dependent, requiring 1 mM Na^+ for half maximal C_i uptake, but it has good C_i affinity, or K_{ci} around 16 µM. The most-recently discovered HCO_3^- transporter,

BicA, also is Na^+-dependent, has poorer affinity for C_i (around 29 μM), and reaches saturation of C_i transport with 20 mM Na^+. The two CO_2 transporters, namely NDH-I_3 and NDH-I_4, are recently discovered. Interestingly, those CO_2 transporters are linked to NADPH dehydrogenase that is part of dark respiration and cyclic electron transport (McGinn & Price, 2003; Ogawa & Kaplan, 2003).

Work done to define the kinetics of the different C_i transporter has been archived by constructing modified strains that inhibit the complementary transporters (McGinn & Price, 2003; Omata et al., 2002). This approach yields essential information on functional molecules that take part in C_i uptake. Based on those works, BG-11 medium was composed to have 190 μM C_i, which should satisfy the maximum uptake rate of HCO_3^- transporter BCT1 and the HCO_3^- sodium-dependent transporter BicA, which also needs 18 mM Na^+. However, the growth kinetics of modified strains was not compared to kinetics of the wild-type strain. Therefore, evaluating growth kinetics for C_i for *Synechocystis* strains to be used in large scale remains to be accomplished.

Together, these five C_i transporters – three for bicarbonate (HCO_3^-) and two for dissolved CO_2 – are located in the outer and thylakoid membranes, respectively (Price et al., 2008; Price, 2011; M Shibata, Ohkawa, & Katoh, 2002). The C_i transporters work in concert. Which transporters take the dominant role depends on the medium's C_i concentration and pH, which controls the C_i speciation among the bioavailable species -- $CO_{2(aq)}$, H_2CO_3, HCO_3^- -- and non-bioavailable carbonate (CO_3^{2-}). For typical growth pHs of 7.5 to 9.5, HCO_3^- is the dominant species. However, intense photosynthesis and insufficient supply of C_i can lead to a higher pH, which partitions the C_i to CO_3^{2-} is not be taken up by C_i transporters. Operation of C_i transporters supports C_i fixation that is

active and energy demanding. The first aspect means that cyanobacteria actively accumulate C_i to satisfy the rate of carbon fixation. The latter aspect means that ATP, NADPH, and/or reduced ferredoxin are consumed as a part of uptake.

5.1.3 Effects of pH on growth kinetics

In addition to controlling C_i speciation, medium pH is well known to affect the functioning of proteins and the cell membrane (Fourest & Volesky, 1996; Matheickal, Yu, & Woodburn, 1999), ATP/ADP pools (Robt Emerson, 1958; Padan & Schuldiner, 1978), microalgal species selection (J. Goldman, Riley, & Dennett, 1982), and growth kinetics (J. Goldman, Azov, et al., 1982; A. Mayo, 1997). Likewise, pH has a universal control over the speciation of certain nutrients, particularly phosphate, iron, and ammonium (Azov & Goldman, 1982).

Bown (1985) experimented with microalgae grown in equilibrium with CO_2-enriched air (> 5% CO_2) and found that the intracellular pH was lower when the cells were grown in equilibrium with atmospheric CO_2. For eukaryotic algae, pH is typically about 8 in stroma and 4-5 in the lumen space (Moroney & Ynalvez, 2007). Exogenous pH affects transport in the plasma membrane and the pH of cytoplasm, and the latter changes the pH gradient across the thylakoid membrane, which sets up the proton motive force for ATP generation (Poole, 1978; Zimmermann, Büchner, & Benz, 1982).

In an interesting pH study with the alga *Chorella vulgaris*, Mayo (1997) fed glucose and illuminate 200 $\mu E/m^2$-s PAR light to the culture, finding that the pH optimum was 6.3 to 6.8 for the maximum growth rate. Mayo (1997) also applied the "substrate self – inhibition" model for pH and temperature based empirical data of *C.*

vulgaris. According to results of this model, *C. vulgaris* grew optimally (maximum specific growth rate of 0.5/day) over a large range of pH (from 5.0 to 9.0). Having a large pH range benefits mass culturing, because the system requires less pH control; however, the pH predictions for *C. vulgaris* were not tested in a practical setting. In addition, growing the culture in a heterotrophic mode reduced the study's application to autotrophic growth, in which pH and C_i speciation are well connected.

Another problem with improper pH is a partitioning of certain nutrients that are toxic to microalgae and cyanobacteria. For example, cyanobacteria are very sensitive to unionized ammonia (NH_3). For example, 1.2 mM NH_3 led to 50% reduction in photo-assimilation of two chlorophyta and one diatom (Azov & Goldman, 1982) for pH = 8.0 – 9.5. NH_3 is a base, and the pK_a value for its conjugate acid NH_4^+ is about 9.3 (Snoeyink & Jenkins, 1980). Higher pH partitions more total ammonium to toxic NH_3.

In addition, when a modified strain produces a fatty acid, the solubility of the fatty acid and its salt form depends on pH. For example, lauric acid has a pK_a of 5.3 (PubChem, 2014). The dissociated form can be harvested with an anion-exchange resin, but also can precipitate with Ca^{2+}. The undissociated form may be extractable into an organic solvent.

In a nutshell, maintaining a proper pH for *Synechocystis* clearly is important in order to optimize the following factors:

- Each species has its optimal range of pH, in which it minimizes the energy it needs to spend to transport nutrients.

- pH controls the speciation of inorganic carbon. The relative availabilities of carbonic acid, bicarbonate, and carbonate strongly affect the growth rate. More information on inorganic carbon is presented below.
- pH controls the thermodynamic activity of functional groups on the cell membrane.
- pH affects the solubility of nutrients, trace minerals, and excreted products.

Separating the effects of C_i and pH is challenging, because pH governs carbon speciation in growth medium and can induce changes in membrane functions that affect C_i uptake.

5.1.4 Effects of C_i to growth kinetics

Early studies with a more "engineering approach" indicated that significantly larger C_i concentration -- 1 – 2 mM -- may be required to prevent C_i limitation (Clark & Flynn, 2000; J. C. Goldman et al., 1974; Miller et al., 1984). More recent studies, like one done by Moheimani, (2013b) with plastic hanging-plastic-bag reactors that grow two microalgae -- *Tetraselmis suecica* CS-187 and *Chlorella* sp -- and are maintained at pH = 7.0 to 7.5, reported daily biomass production of 320 mg/L and 407 mg/L for *T. suecica* and *Chlorella*, respectively. C_i was maintained between 1 to 4 mM, but no kinetic parameters were reported. Interestingly, Moheimani, (2013b) also evaluated different sources of C_i (pure CO_2, sodium bicarbonate, and untreated flue gas). Biomass production of the two algal species was not different as long as the pH was set at the optimum. No drop of biomass production rate when using flue gas is promising for mass algae, because toxicity from components of the flue gas has been a concern. Despite the

promising results of (Navid Reza Moheimani, 2013), that work gave no quantitative relationship for how pH or C_i affected the growth rate.

It is well recognized that C_i uptake during photosynthesis causes the pH to rise, since the medium's alkalinity is distributed into a smaller C_i concentration (J. Goldman, Azov, et al., 1982). Nguyen and Rittmann (2015) recognized that using either NO_3^- or NH_4^+ as the sole N source causes systematic changes in alkalinity: uptake of NO_3^- systematically increases the alkalinity, while uptake of NH_4^+ decreases the alkalinity. These systematic changes in alkalinity complicate the control of pH and C_i, since pH, C_i, and alkalinity are intrinsically linked (Nguyen & Rittmann, 2015; Snoeyink & Jenkins, 1980).

I presented different strategies to manage alkalinity of a photosynthetic culture with a pH-Stat PBR in Chapter 4. The alkalinity of the BG-11 growth medium is mainly composed of hydroxyl, carbonates, and a negligible amount of phosphates. The pH-Stat maintains a constant level of pH and hydroxyl ion, and the alkalinity then directly regulates total C_i. I evaluated different approaches to control pH and C_i. The first approach is simply augmenting the starting alkalinity by bicarbonate to the standard BG-11. Later, I designed a novel approach to achieve simultaneously fixed, but independent values of pH and C_i. The pH was fixed by adding CO_2 gas automatically using a pH-Stat based on insights. The alkalinity and C_i concentrations were held constant by combining ammonium and nitrate as the N source so that the alkalinity and C_i did not change with photosynthetic growth (Nguyen and Rittmann, 2015).

In this chapter, I systematically investigate the independent effects of the pH and the concentration of bioavailable carbon (C_{ib}, which is the sum of dissolved CO_2, H_2CO_3,

and HCO_3^-) and on the growth kinetics of cyanobacterium *Synechocystis* sp. PCC 6803. I first screened pH preference of *Synechocystis* from 6.5 to 10.0 in the standard BG-11 and then attempted to augment bicarbonate to the standard BG-11 for different C_i concentration. Later, I successfully controlled pH and C_i independently by using the combined N source with the pH-Stat. This offered a basis to systematically teste pH values of 7.5, 8.5, and 9.5 and C_i concentration between 0.05 mM and 3.3 mM with the wild-type and laurate-excreting *Synechocystis*. Therefore, I was able to separate the effects of growth pH and C_i on the growth kinetics of *Synechocystis*. I applied Monod kinetics to interpret the results through the maximum specific growth rate (μ_{max}) and the half-maximum-rate concentration for C_{ib} ($K(C_{ib})$), as well as to identify which C_i species best represented the rate of C_i uptake. The preference was consistent between two approaches: pH = 8.5 supported the best growth.

5.2 Methods and Materials

5.2.1 Experiment setup

Fresh plates of *Synechocystis* wild-type and laurate-excreting strains on agar were provided by the Dr. Vermaas Laboratory, and inocula and growth medium (BG-11) were presented in the previous chapters 2 and 5.

5.2.2 Growth media

Based on the ingredients of the standard BG-11 medium (Rippka et al., 1979), I modified the components to suit the experiment objectives. For the first approach, I

augmented the standard BG-11 by adding a known amount of bicarbonate (0.4 M) to obtain the final C_i concentration. The medium pH was adjusted one time, before the start of the experiment, by adding NaOH (0.5 M) or CO_2 gas to obtain the desired value.

For the second approach, I prepared growth medium with a fixed C_i concentration by modifying the standard BG-11 medium (Rippka et al., 1979) through doubling K_2HPO_4 from the standard BG-11 medium and eliminating $NaNO_3$ as the N source. The medium was steam-sterilized by a liquid cycle (121^oC and 15 minutes) in a Tabletop Sterilizer (SterileMax, Thermo Scientific, IA). Each liter of modified BG-11 contained 0.46 mM K_2HPO_4, 0.30 mM $MgSO_4$, 0.24 mM $CaCl_2$, 0.01 mM citric acid, 0.021 mM ferric ammonium citrate, 0.0027 mM Na_2EDTA, trace metals and with inorganic carbon and nitrogen were added as described below.

Two steps established independent values of the C_i concentration and pH. First, $NaNO_3$ was replaced by ammonium nitrate (NH_4NO_3) supplied from a separate stock (0.5 N NH_4NO_3). NH_4NO_3 stock was titrated with NaOH to obtain the pH for sets of experiment at pH 7.5, 8.5, or 9.5. I added at the beginning of each experiment 2.0 mM $NaNO_3$, and then I added NH_4NO_3 stepwise from its stock after each sampling event. Adding NH_4NO_3 stepwise eliminated any effects from the possible preferential uptake of NH_4^+ over NO_3^-. Second, I augmented the initial alkalinity of the modified BG-11 by adding a combination of 0.4 N $NaHCO_3$ and 0.5 N NaOH to achieve the desired values of pH and C_i at the beginning of each experiment.

5.2.3 Experimental setup

I used a 1.5-L photobioreactor equipped with a pH-Stat as described in Chapter 4. In brief, the pH-Stat automatically maintained a set pH value by adding pure CO_2 gas when the pH reading exceeded the set points. The PBR was continually mixed by stir bar at 200 rpm (VWR, U.S), and the culture temperature was maintained at 30^{o}C by 3×12-W air fans (Minebea-Matsushita Motor Corp., Japan). The total incident light intensity was 324 μE/m^2-s, provided by two T5 florescent bulbs (Hydrofarm, U.S.). **Figure 5.2** below shows the layout of the PBR and light source. Key differences between two approaches were summarized in **Table 5.1**.

Table 5.1: Summary of Key Difference Between Two Approaches to Study Growth Kinetics by C_i and pH

	First approach	Second approach
Tested pH	6.5, 7.5, 8.5, 9.5, 10.0	7.5, 8.5, 9.5
Control pH	Automatic CO_2 delivery via pH-Stat	
Medium used	Augment the standard BG-11 by bicarbonate	Displace nitrate by ammonium nitrate, double P, C_i augmented by bicarbonate
N source	Nitrate only	Nitrate and ammonium combined
Outcomes	Evaluate pH preference Determine range of C_i concentration for growth kinetics	Independently evaluate pH and C_i concentration on growth kinetics

Each batch experiment (with a set pH of 7.5, 8.5, or 9.5) lasted from 24 hours to 5 days, and samples were taken at 4-h to 12-h intervals. For sampling, I withdrew 24 mL of liquid using a syringe inserted through a tube that reached midway into the culture.

Optical density (OD) was measured immediately by a spectrometer (described in chapter 2), and the remainder of the sample was placed in a 50-ml conical plastic tube (VWR) and stored at 4^{o}C refrigerator until assayed for dissolved inorganic carbon, i.e., C_i.

To ensure that N and P were sufficient for biomass synthesis, I doubled the P content of the standard BG-11 medium and added 2 mM of N. Using stoichiometry, P comprises about 1.3% of dry weight (Kim et al., 2010). After production of biomass to 0.5 OD (~130 mg), P in medium was about 8.0 mg/L. For N, I also measured the medium's N content periodically and always found at least 28 mgN/L.

5.2.4 Analyses

OD, C_i, and pH were measured using the same protocols as discussed in Chapters 2, 3, and 4.

5.2.5 Average Internal Light Intensity

The incident LI was measured by a U1252 micro-ammeter (Agilent, US) equipped with a LI-190 PAR sensor (LI-COR, US). I took measurements at 32 points inside the PBR. I then applied the Beer-Lambert law (Kim et al., 2010; Suh & Lee, 2003) to calculate the average internal LI (AILI) inside the PBR. Details of the LI measurements and calculation of AILI are provided in **Table 5.2**.

To compute AILI, I used the Beer-Lambert law (Kim et al., 2010; Suh & Lee, 2003), which is based on isotropic absorption of monochromatic light (Fernández et al., 1997). For a given depth [distance from the light-entering surface] and biomass

concentration, a local light intensity (LI, μE/m^2-s) can be calculated based on incident LI at surface (LI_0, μE/m^2-s) by:

$$LI = LI_0 . \exp[-\varepsilon . d . X] \quad (5.9)$$

where

d: distance from light source [length]

ε: absorptivity coefficient [$length^3$/mass.length]

X: biomass concentration [mass/$length^3$].

I assumed the absorptivity coefficient for all wavelengths within the PAR region and used an value used for Synechocystis biomass (Kim et al., 2010).

The plan view of the PBR is shown in **Figure 5.2**. Two cubes (plan-view areas shown by the squares) were used to simplify the dimensions of the tubular reactor to a flat-panel reactor. The plan view also shows locations of LI measuring: Four positions each for the large and small squares. In the vertical direction, I measured four locations: top, mid-top, mid-bottom, and bottom. The PAR sensor (LI-190, LI-COR, atmosphere only) was placed on the inside glass surface to measure the actual LI_0 entering the PBR listed in **Table 5.2**. I averaged the light intensity of the four vertical locations for each measurement point in the plan view. Then, I averaged the LI_0 of each side and then summed the average LI_0 to yield the average incident LI_0 (the large cube). I used the same averaging technique for the internal LI for the location of the small cube.

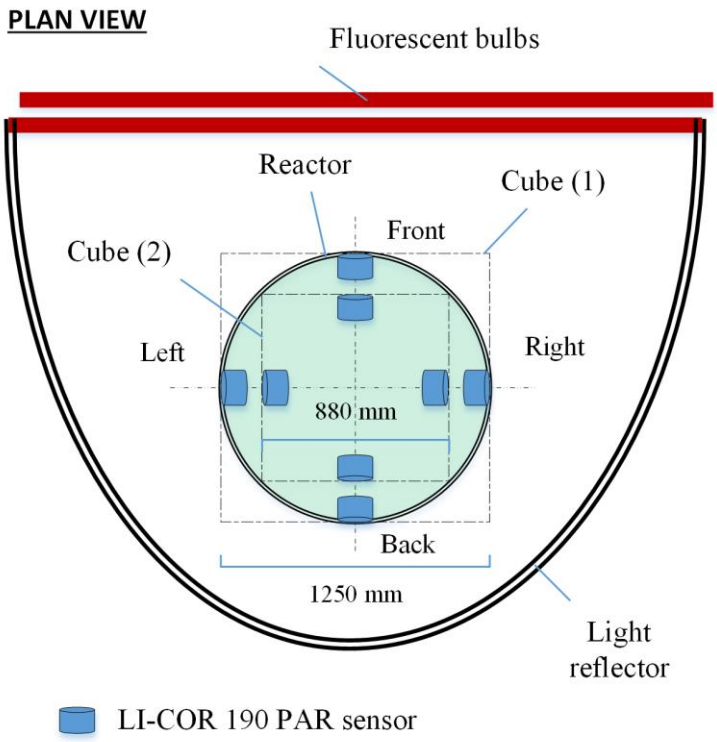

Figure 5.2: Plan View of PBR Includes the Main Reactor (Circle, Center), Two Squares, Light Reflector, and Fluorescent Bulbs

Table 5.2: Incident LI Each Location by PAR Sensor

		Location				
		Front	Right	Left	Back	Total
		$\mu E/m^2$-s				
Large cube	Top	167	53	54	35	
	Mid-top	175	62	63	39	
	Mid-bottom	176	63	63	40	
	Bottom	170	55	55	37	
	Average	172	58.25	58.75	37.75	327
Small cube	Top	157	53	61	39	
	Mid-top	163	55	63	40	
	Mid-bottom	168	58	61	40	
	Bottom	165	56	68	37	
	Average	163.25	55.5	63.25	39	321

Calculating AILI based Beer-Lambert law was presented briefly in Analyses section, chapter 2. The incident LI (LI_0) and absorptivity coefficient (ε) shown in **Table 5.3** while X is the biomass concentration (g/m^3) and dw is integral variant (m) as shown in eqn. (2.3).

Table 5.3: Summary of Inputs for the Beer-Lambert Law

	Maximal depth, m	Incident Light Intensity, LI_0, $\mu E/m^2$-s	Absorptivity coefficient (Beer-Lambert constant), m^3/g-m (Kim et al., 2010; Suh & Lee, 2003)
Large cube	0.1250	327	0.255
Small cube	0.088	321	0.255

I validated independently the absorptivity coefficient (ε) using the value of 0.255 m^3/g-m for the *Synechocystis* sp. PCC 6803 culture via an underwater PAR sensor (LI-192, LI-COR). The result in **Figure 5.3** confirmed ε value I used is appropriate. The data also show that measurements and modeling values based the Beer-Lambert law are consistent with LI > 50 μE/m^2-s. In this study, I experimented with the biomass concentration about 38 g/m^3 that yields an corresponding AILI of 202 ± 13 μE/m^2-s.

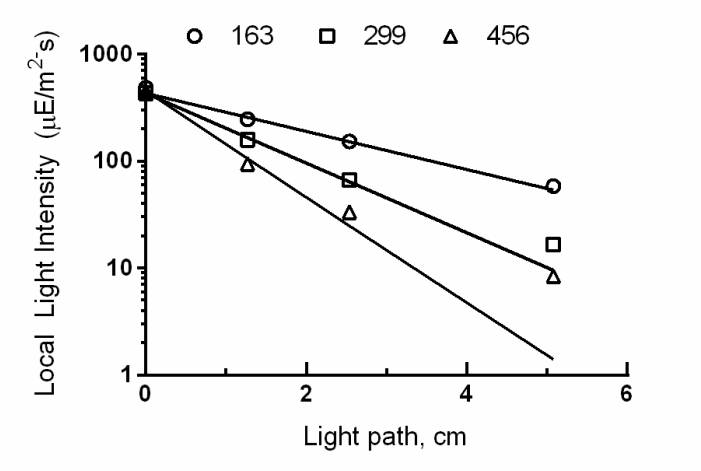

Figure 5.3: Local Light Intensity (Open Symbols) and Predicting Values by Beer-Lambert Law for *Synechocystis* Culture
The numbers on top gives biomass concentration (g/m^3) converted from optical density at 730 nm

5.2.6 Kinetic modeling

I used Monod (1949) kinetics to represent the effect of a C_i species on the specific growth rate:

$$\mu = \mu_{max} \frac{C_x}{K_{Cx} + C_x} \tag{5.10}$$

where: μ is the experimental specific growth rate (1/day); μ_{max} is the maximum specific growth rate (1/day); C_x is the mM concentration of either the concentration of C_{ib} (the sum of H_2CO_3* and HCO_3^-), H_2CO_3*, HCO_3^-, or CO_3^{2-}; and K_C is the C_x concentration giving one-half the maximum specific growth rate (mM). I calculated the experimental μ in two ways (Rittmann and McCarty, 2001):

$$\mu = \frac{1}{OD}\frac{dOD}{dt} = \frac{\ln(\frac{OD_{t2}}{OD_{t1}})}{t_2 - t_1} \approx \frac{OD_{t2} - OD_{t1}}{\frac{1}{2}(OD_{t1} + OD_{t1})}\frac{1}{t_2 - t_1} \tag{5.11}$$

where: OD_{t2} and OD_{t1} are the optical biomass densities at times t_2 and t_1 (day). The right-hand expression in eqn. (5.11) is the linear expression for μ. When the (t_2 - t_1) increment is small, linear and natural-logarithm approximations give the same μ value. The μ values I computed with the logarithmic and linear approaches were almost the same, and I present μ values computed with the logarithmic expression.

5.3 Results and Discussion

5.3.1 Growth kinetics in pHs and nutrient-sufficient medium

I carried out experiments to evaluate growth of *Synechocystis* on pH through several steps. In the first step, I manually controlled pH by adjusting the supply rate and composition of air and CO_2 gas periodically. These preliminary results revealed some key information, summarized in **Figure 5.4**. The specific growth rate for *Synechocystis* wild type in the left panel indicates that pH of ~9.5 supported the faster biomass growth rate, more than pH > 10.5 or oscillating pH between 8 to 11.

The right panel of **Figure 5.4** compares the specific growth rates of the wild type and the modified strains in the first set of experiments. The wild type grew faster than the modified strains with the same pH, light intensity, and growth medium. For example, with OD < 0.5, specific growth rates of the modified strain clearly were smaller than for the wild-type, sometimes less than one-half. In addition, lag periods were apparent with the modified strain, suggesting that the modified strain required more time to adapt to new growth conditions.

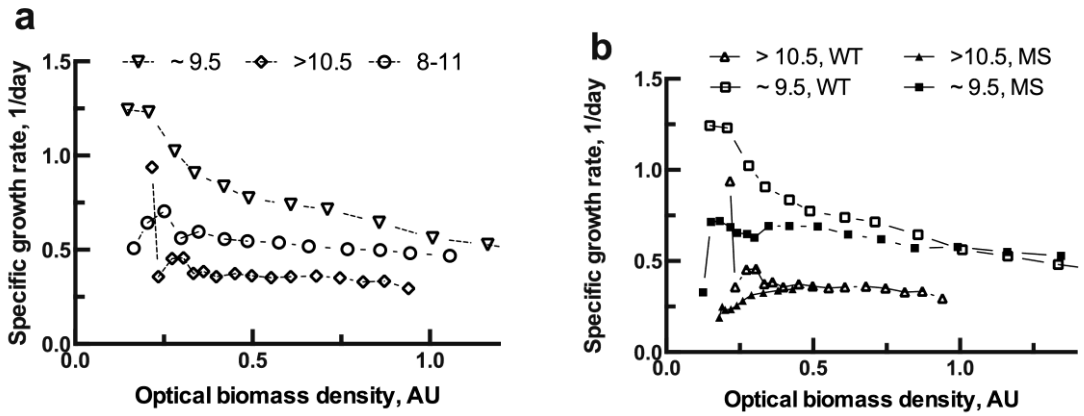

Figure 5.4: Specific Growth Rates of *Synechocystis* Wild-Type (WT, Panel a) and a Comparison of the Wild-Type and the Modified Strains (MS) in BG – 11 Growth Medium (Panel b)
The pH was managed by manually adjusting the carbon dioxide supply rate

Slower growth with pH > 10.5 suggests that C_i or pH could be a limiting factor. With pH > 10.3, at least a half of C_i is carbonate, which is not usable by *Synechocystis* (Badger, 2003; Price et al., 2008). In addition, very high pH may be toxic on its own. For example, Sheng (2011) used 25 mM TAPS (N-Tris(hydroxymethyl-3-aminoproponesulfonic acid) as a pH buffer and concluded that pH = 11 was toxic to *Synechocystis* and caused a culture crash. My results indicate that growing *Synechocystis* with pH >10.5 hampered growth. I also found that manually adjusting gas flow and its composition provided only approximate control of the pH. To overcome this limitation, I developed the pH-Stat PBR in Chapter 4. I used the pH-Stat PBR for all following experiments in Chapter 5 and photoperiods with the wild-type strain in Chapter 6.

Figure 5.5 presents growth of *Synechocystis* wild type with pH from 6.5 to 10.0 using the pH-Stat in the standard BG-11 using nitrate as N source. Cultures grew significantly faster with pH = 7.5 to 9.5, and pH = 8.5 showed the best growth among all

experimental pH values. With a low pH (6.5), the culture grew normally at first, but later slowed; cells aggregated and settled out. Higher pH (10.0) gave a lag period for the first day; however, the culture adapted to its new conditions and grew with a rate similar to the rate for pH = 7.5 to 9.5.

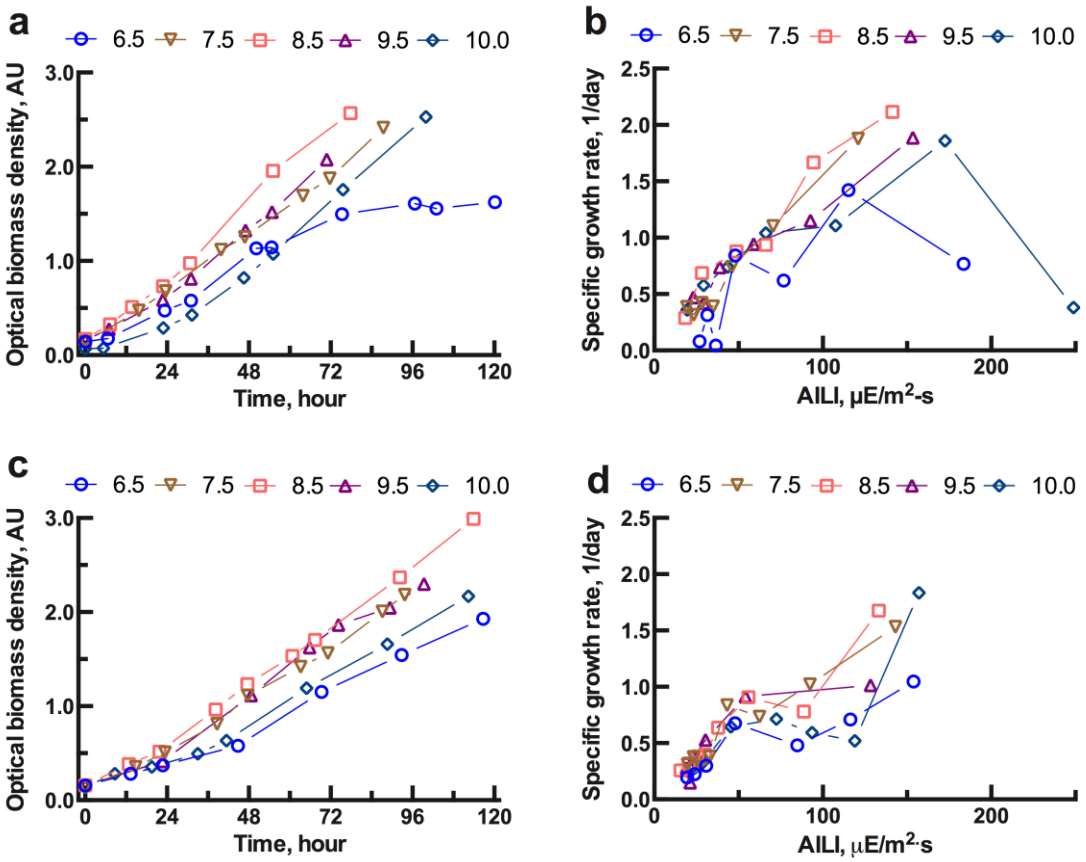

Figure 5.5: Biomass Growth of *Synechocystis* Wild-Type Strain (Panel a and b) and of the Modified Strain (Panel c and d) in Standard BG-11 with pH = 6.5 to 10.0.
pH = 7.5-9.5 supported the fastest growth. pH = 10.0 gave a lag period, and pH = 6.5 slowed growth by 3 days and led to flocculation

Panel b of **Figure 5.5** relates the specific biomass density to the AILI, as well as to pH. Cultures with pH = 7.5 to 9.5 exhibited higher growth rates at higher AILI, as expected from the results with the wild-type strain. The culture grown with pH = 10.0 showed a lag period, but the specific growth rates were systematically lower with pH = 6.5.

Similarly, panels c and d of **Figure 5.5** present biomass densities and specific growth rates of the modified strain for the different pH values. pH from 7.5 to 9.5 allowed the modified strain to grow better than did the lower or higher pHs in the experimental range; pH 8.5 gave the best growth of the modified strain. That a pH as low as 6.5 or as high as 10.0 slowed growth of the modified strain is consistent with trends of *Synechocystis* wild type. The specific growth rates for the modified strain were about 75% of those for the wild-type strain for the same pH and AILI.

Later, I replicated the experiments with the wild type in standard BG-11 medium with a fixed growth pH from 6.5 to 10.0 (**Figure 5.7**). Recorded pH data demonstrated our success to maintain at testing level (**Figure 5.6**). Growth pattern and pH preference were identical to the previous experiments (Panel a and b, **Figure 5.5**). *Synechocystis* had normal linear growth for pH values of 7.5, 8.5, and 9.5, and growth was fastest with a pH of 8.5. The lowest pH (6.5) gave normal growth of *Synechocystis* at first, but later growth slowed, with the cells aggregating and settling out; these phenomena are consistent with another study on *Synechococcus* (Robt Emerson, 1958). The highest pH (10.0) gave a lag period for the first day; however, the culture adapted to its new conditions and grew with a rate similar to the rate for pH = 7.5 to 9.5.

In this section, I learnt that wild-type and modified *Synechocystis* in the standard BG-11 grew fastest from 7.5 to 9.5 and showed the best growth at pH=8.5. Higher growth rates were clearer at the beginning of the experiments, which corresponded to a higher AILI (Figure 5.5, panels b, d and Figure 5.6b). This suggests that, with a denser biomass (and a lower corresponding AILI), the effects of pH on growth are smaller than the effects of the availability of light energy. In the next experiment, I selected a lower OD and 3 values of pH -- 7.5, 8.5, and 9.5 -- for in-depth growth kinetic study of these two strains on C_i.

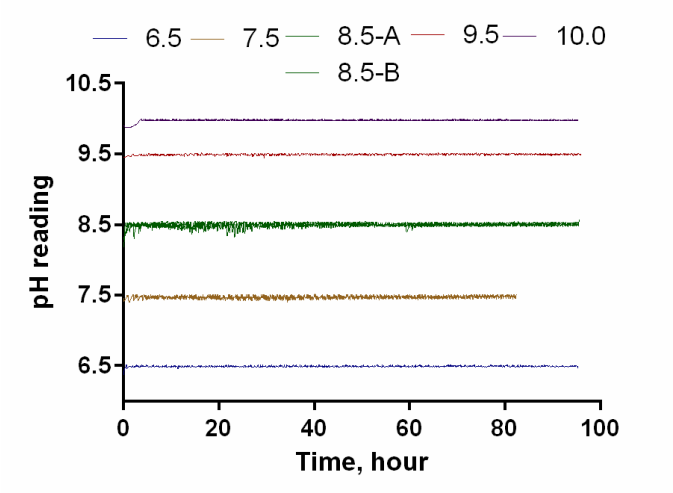

Figure 5.6: pH Readings of Screening Experiments
The numbers on top gives the value of pH, two runs ended with (-A) and (-B) are the replicate

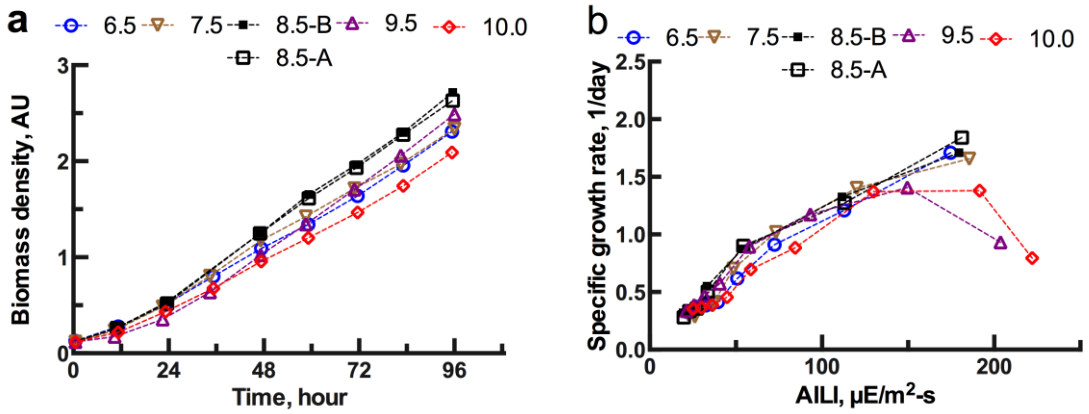

Figure 5.7: Biomass Concentration (Panel a) During Growth of *Synechocystis* Wild-Type Strain in Standard BG-11 with pH = 6.5 to 10.0.
Runs 8.5-A and 8.5-B are replicates. pH = 8.5 supported the fastest growth, while pH = 10.0 and 6.5 had the slowest growth. Panel b presents relationship of specific growth rate and AILI calculated from biomass concentration in the experiments of panel a

5.3.2 Growth kinetics of *Synechocystis* based on inorganic carbon

5.3.2.1 Augmenting C_i by adding bicarbonate to BG-11

My first attempt to control alkalinity was to add different amounts of bicarbonate salt to the standard BG-11 medium. I assumed that, by adding bicarbonate salt, I could manage the alkalinity and, thus, the C_i concentration to study the growth kinetics of *Synechocystis* on C_i. This assumption turned out to be incorrect.

Figure 5.8 presents growth curves (panel a) and specific growth rates (panel b) of wild-type *Synechocystis* in standard BG-11 augmented with 5 mM bicarbonate. Adding inorganic carbon to the standard BG-11 improved growth rates, but only slightly (panel b in **Figure 5.7** and **Figure 5.8**).

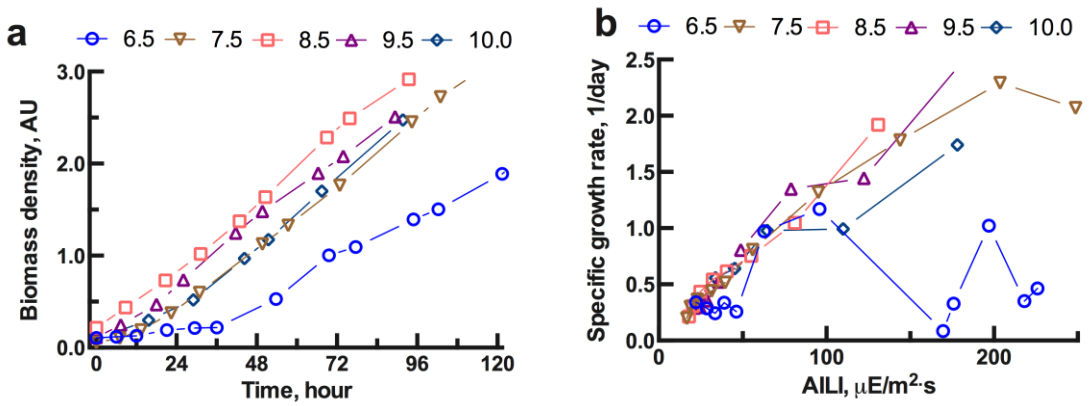

Figure 5.8: Biomass Growth of *Synechocystis* Wild-Type in in the BG-11 with Additional 5 mM Bicarbonate (Panel a) and Specific Growth Rate with Corresponding AILI in Different Growth pH Given by the Top Row (μE/m^2-s).

The improvement also was evidenced at low OD and ~200μE/m^2-s, which suggests that the light energy was sufficient to support culture growth. Insignificant difference of the growth rates in lower AILI (<100 μE/m^2-s) in 5-mM C + BG-11 agrees with the growth rates of *Synechocystis* grown in the standard BG-11 (starting with 0.2 mM C_i). With a denser biomass, the C_i concentration of culture grown in standard BG-11 or with additional bicarbonate becomes less different. In Chapter 4, I demonstrated that using NO_3^- as N source increases the alkalinity and C_i, which saturates C_i demand for growth.

The distinct improvement of growth rate of BG-11 augmented with 5 mM C_i is intriguing. I hypothesized that, between 0.2 and 5.0 mM of Ci, an effect of C_i on growth kinetics is likely; therefore, I designed several experiments to explore concentration in between to determine what concentration of C_i would make a difference in growth rates of *Synechocystis*. The identical pattern of growth rate and AILI indicates light energy is the prominent factor that drives photosynthesis rate and biomass productivity.

Comparing **Figure 5.7** and **Figure 5.8**, the grow rates of culture with 5 mM bicarbonate and the culture grown in the standard BG-11 growth medium (which has 0.2 mM bicarbonate) are similar. With constant incident LI of 324 $\mu E/m^2$-s, pH = 7.5 and 9.5 led to the fastest growth of *Synechocystis* wild type, compared to pH = 6.5 or 10.0. This trend is similar to previous runs with the standard BG-11. Adding alkalinity with bicarbonate gave a modest improvement in the specific growth rate, evidenced by a short burst at low OD. These trends were the basis to search for a fundamental understanding of interaction of pH, N source and alkalinity that was presented in Chapter 4.

Although adding more bicarbonate to the growth medium yielded some insights, this approach did not give conclusive results for a correlation of C_i to growth rate because of accumulating alkalinity and C_i as biomass grew.

5.3.2.2 Controlling C_i and pH independently

5.3.2.2.1 Monod-kinetics for C_{ib}

Using NH_4NO_3 as the N source, I carried out experiments with C_i concentrations from 0.05 to 3.3 mM and pH values of 7.5, 8.5, and 9.5 for the wild-type (**Figure 5.9**, **Figure 5.10**, and **Figure 5.11**) and for the laurate-excreting *Synechocystis* (**Figure 5.12**, **Figure 5.13**, and **Figure 5.14**). In all case, the AILI was 202 $\mu E/m^2$-s. This value was sufficient to avoid photo-limitation (**Figure 5.6** to **Figure 5.8**), and the culture exhibited clear preferences by pH.

Each panel presents the biomass concentrations for each fixed pH. In all experiments, *Synechocystis* wild type and laurate-excreting strain grew well with the

stable C_i values shown in the legends. The cultures also exhibited a healthy green color throughout all experiments.

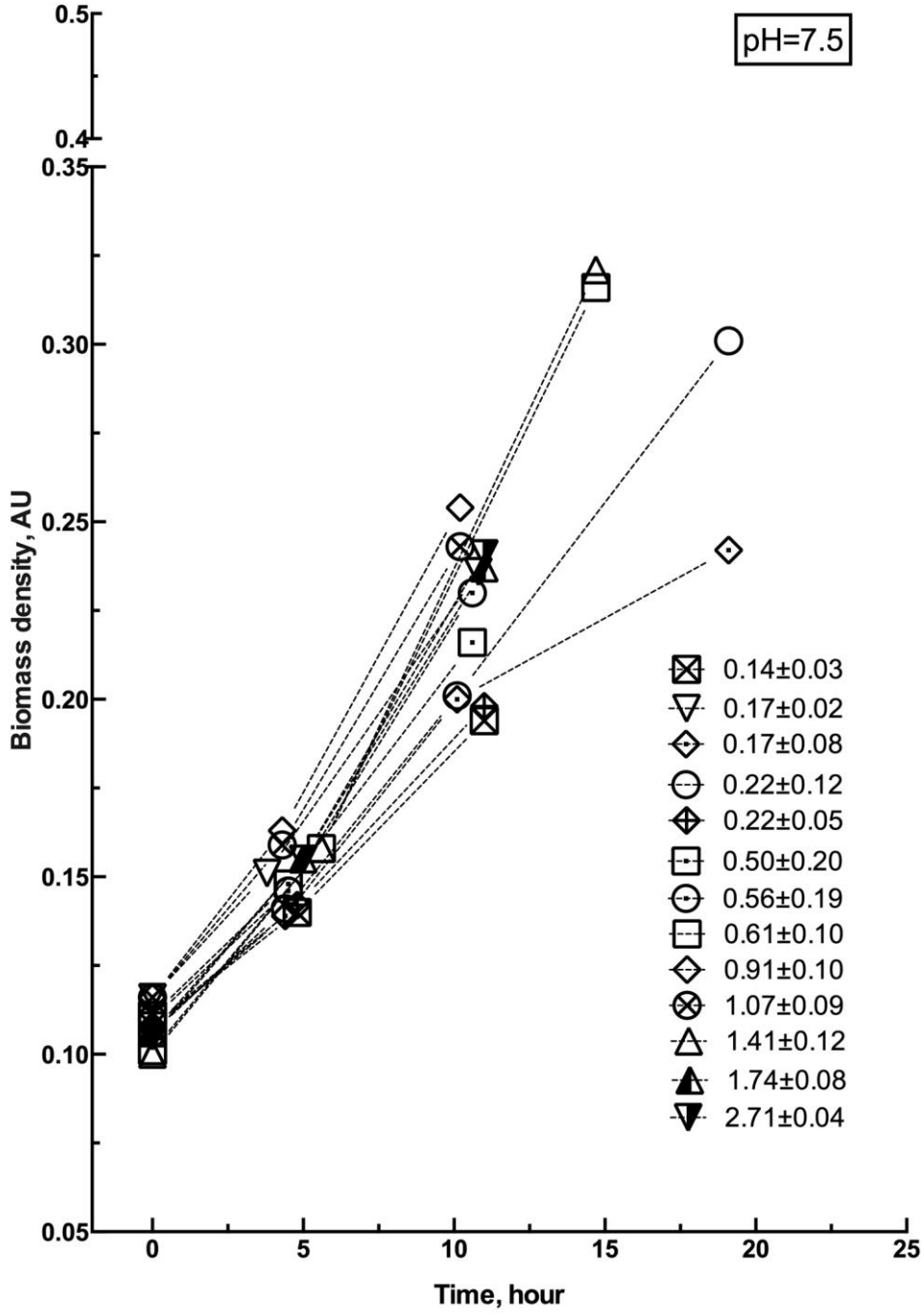

Figure 5.9: Biomass Growth for Wild-Type *Synechocystis* Grown at a Fixed pH of 7.5 NH_4NO_3 is the N source and the average C_i concentrations are shown in the legends (averages with the 95% confidence levels)

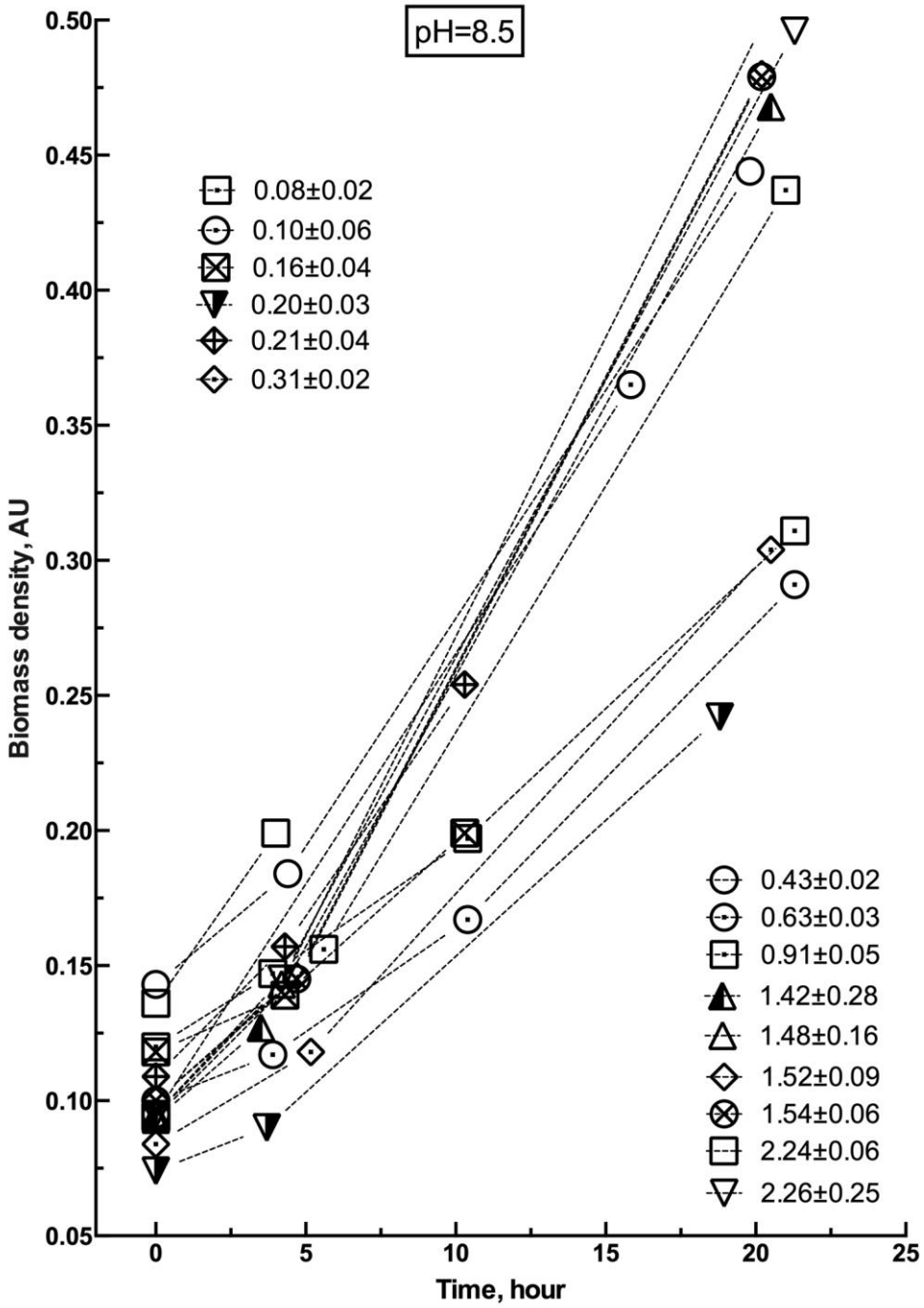

Figure 5.10: Biomass Growth for Wild-Type *Synechocystis* Grown at a Fixed pH of 8.5 NH_4NO_3 is the N source and the average C_i concentrations are shown in the legends (averages with the 95% confidence levels)

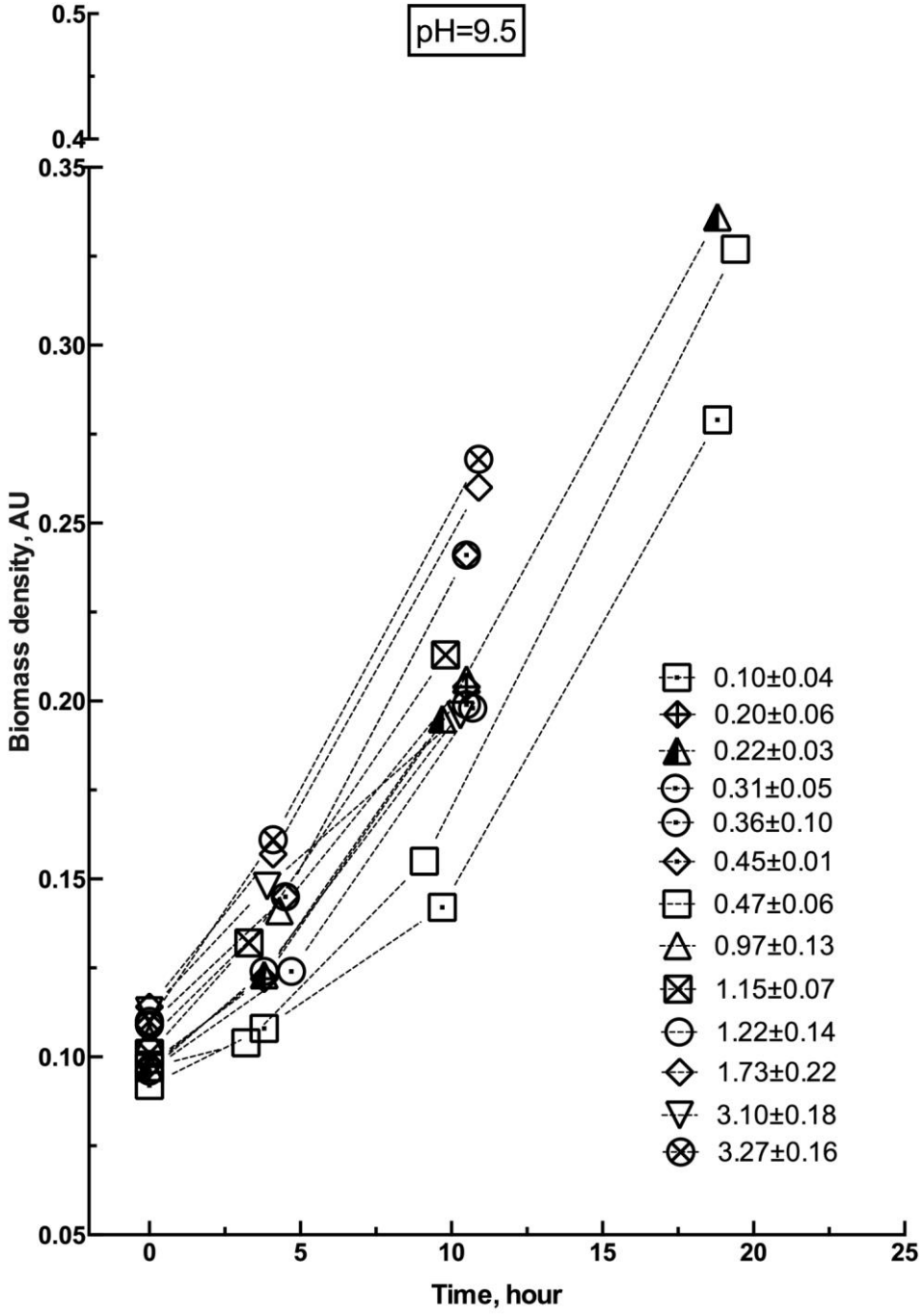

Figure 5.11: Biomass Growth for Wild-Type *Synechocystis* Grown at a Fixed pH of 9.5 NH_4NO_3 is the N source and the average C_i concentrations are shown in the legends (averages with the 95% confidence levels)

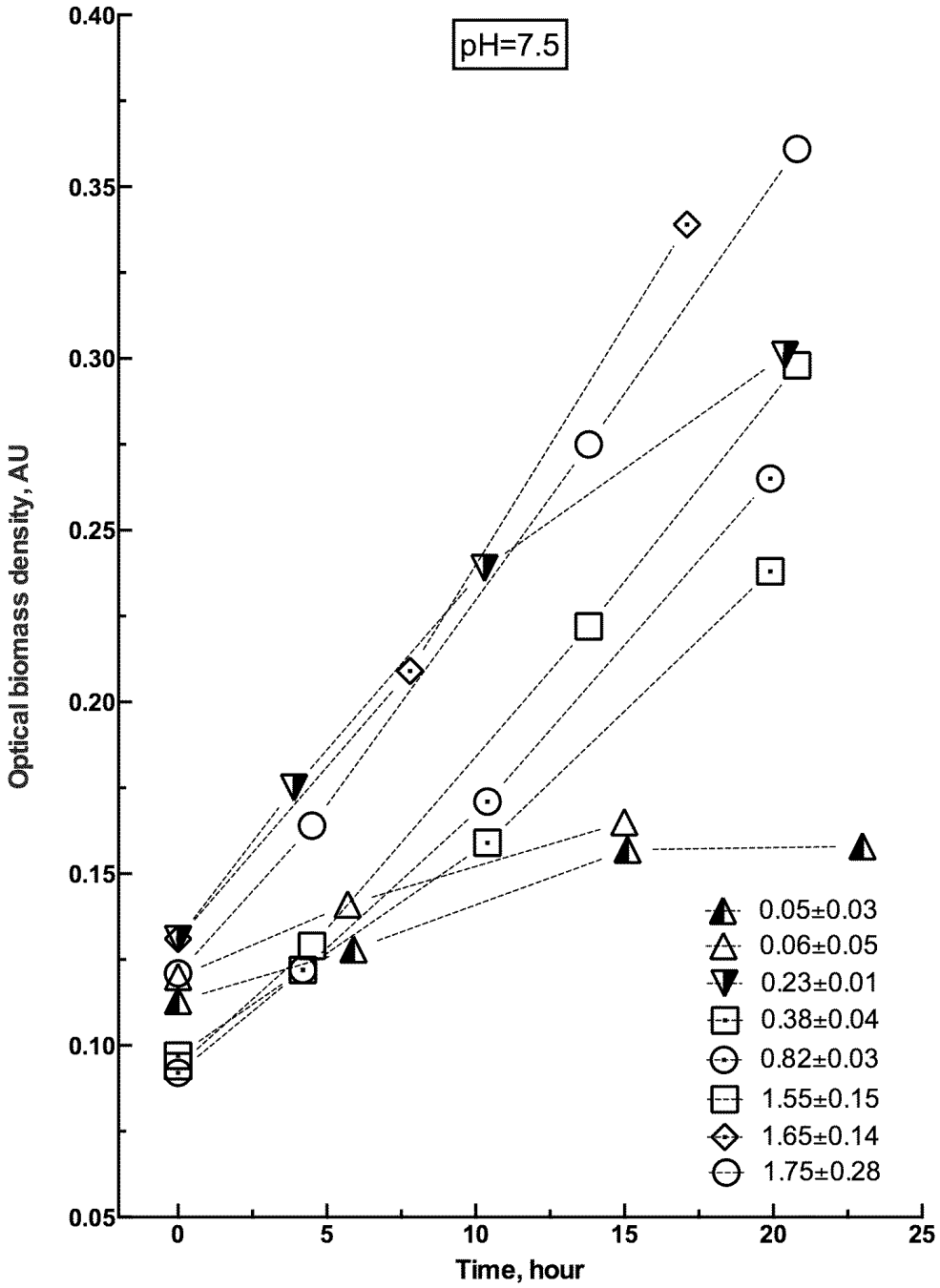

Figure 5.12: Biomass Growth for Laurate-Excreting *Synechocystis* Grown at a Fixed pH of 7.5

NH_4NO_3 is the N source and the average C_i concentrations are shown in the legends (averages with the 95% confidence levels)

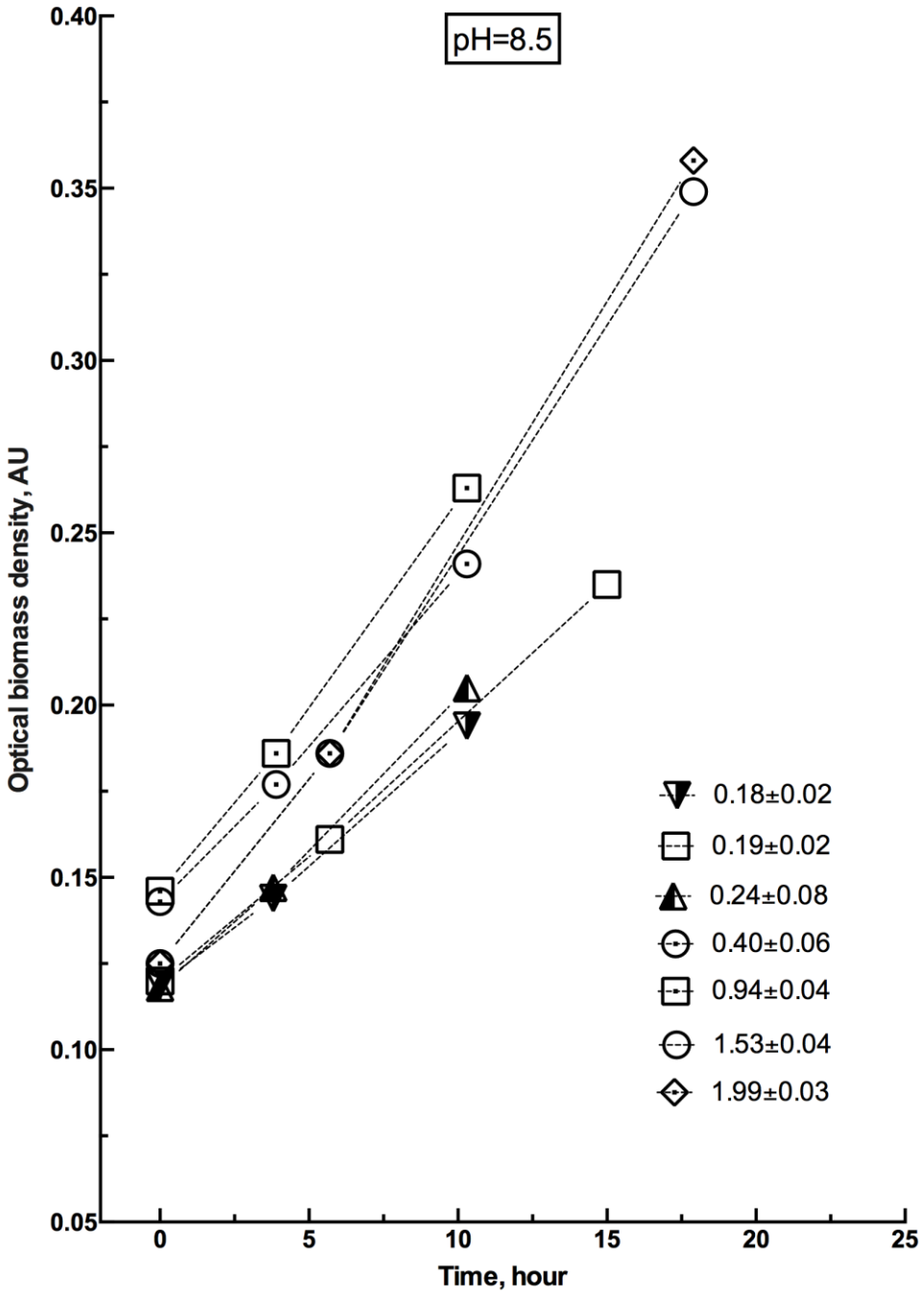

Figure 5.13: Biomass Growth for Laurate-Excreting *Synechocystis* Grown at a Fixed pH of 8.5

NH_4NO_3 is the N source and the average C_i concentrations are shown in the legends (averages with the 95% confidence levels)

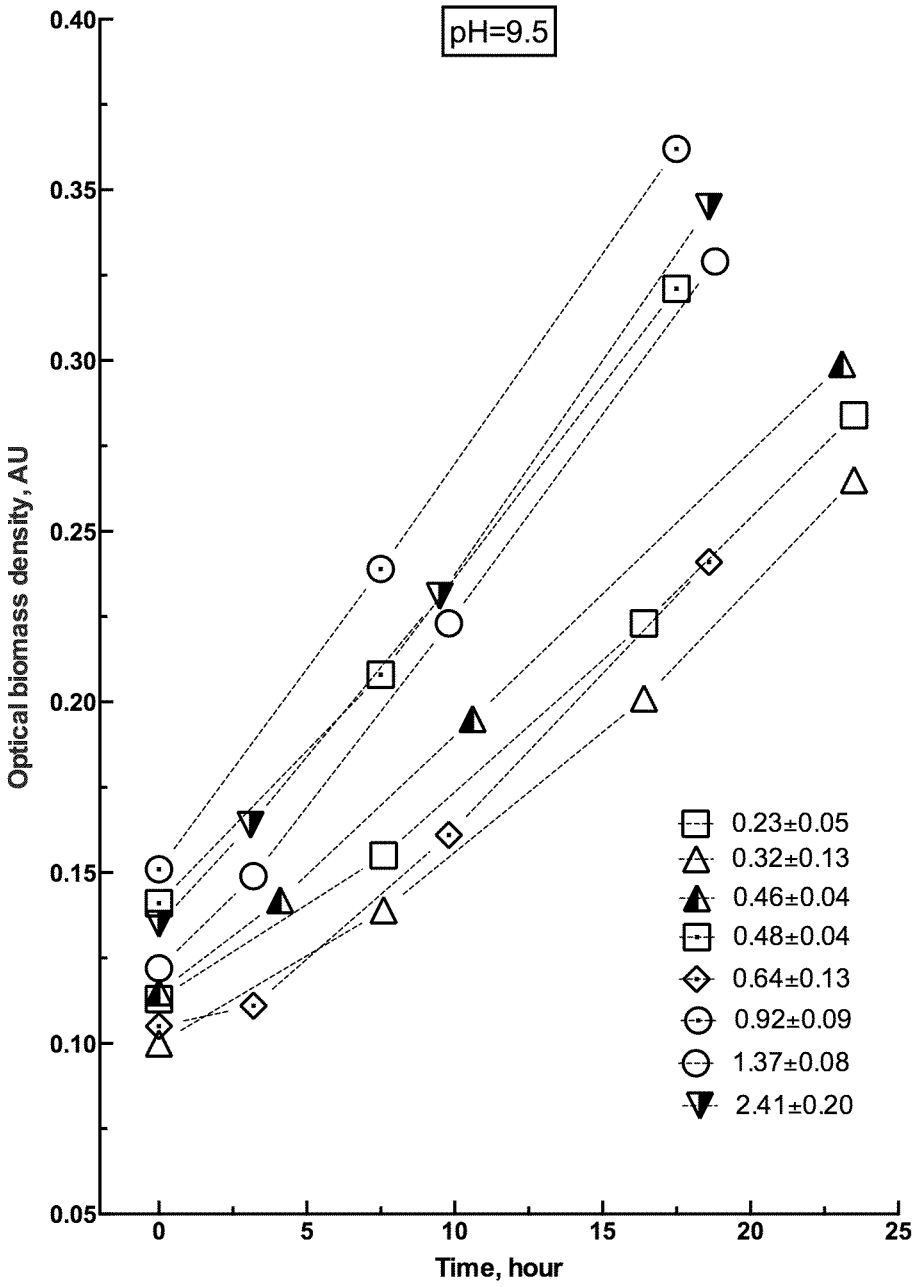

Figure 5.14: Biomass Growth for Laurate-Excreting *Synechocystis* Grown at a Fixed pH of 9.5

NH_4NO_3 is the N source and the average C_i concentrations are shown in the legends (averages with the 95% confidence levels)

I applied eqns. (5.6) to (5.8) to obtain the concentration of each C_i species and eqn. (5.11) to compute μ for each strain. I fit the Monod model, eqn. (5.10), to obtain estimates for μ_{max} and K_C when C_{ib}, $H_2CO_3^*$, HCO_3^-, or CO_3^{2-} was the rate-limiting C_i species. **Figure 5.15** presents the measured μ of *Synechocystis* (symbols) and the curves for the Monod-model fitting using C_{ib} as the modeled rate-limiting species of the wild type in the top row and the laurate-excreting strain the bottom room. The top rows of **Table 5.4** summarize the best-fit Monod parameters when C_{ib} was the rate-limiting species of the wild-type *Synechocystis*. The wild-type strain had the fastest growth rate at pH 8.5: μ_{max} was 2.4/day for pH 8.5, compared to ~2.0/day for pH 7.5 and 9.5. The K_C for total C_{ib} had a small range, from 72 to 96 μM, with the lowest value at pH 9.5 and highest for 7.5.

Similarly, the top rows of **Table 5.5** summarize fitting parameters for Monod model with C_{ib} as the rate-limiting C_i species. The modified strain grew at faster at pH 8.5 with μ_{max} was 1.68/day, compared to 1.61 at pH 7.5 and 1.60 at pH 9.5. K(C_{ib}) ranges from 82 μM to 130 μM.

The modified strain had smaller μ_{max} values than the wild type's were expected and consistent with previous observation (see **Figure 2.11** and **Figure 5.5**). Diverting fixed electrons to laurate and higher products of other soluble organics reduces the energy for growth of the modified strain. The obtaind K_{Cib} values are similar to those of Badger and Andrews (1982), who estimated the photosynthesis rate of the cyanobacterium *Synechococcus* sp. using buffers to control pH and measuring the kinetics of oxygen evolution.

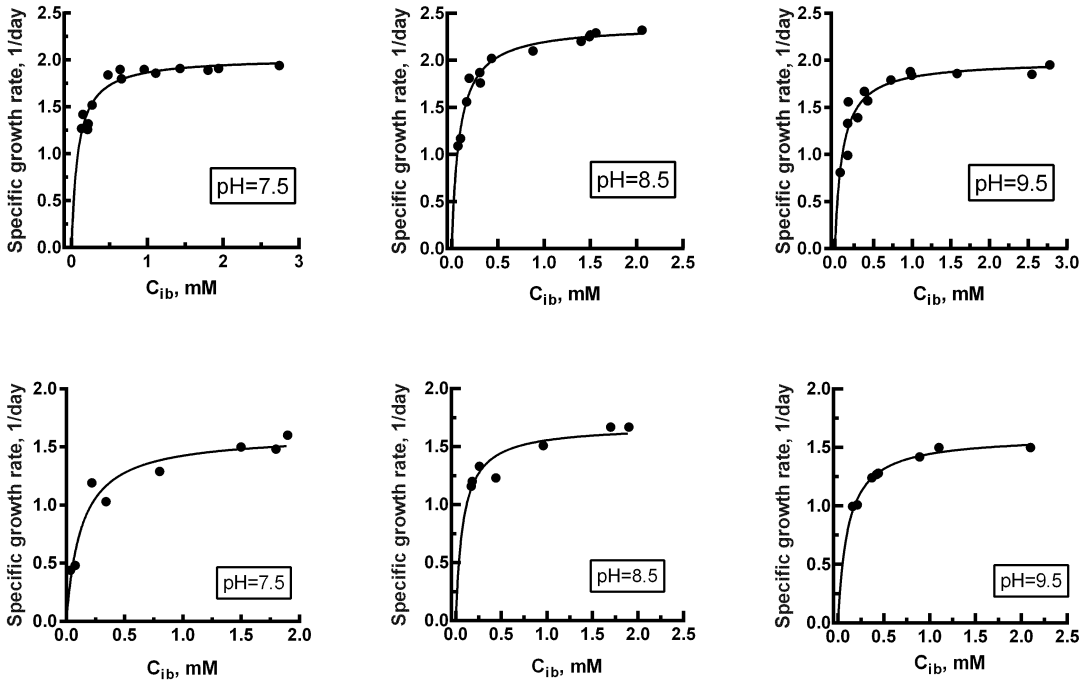

Figure 5.15: Measured Specific Growth Rate (Symbols) and Monod Best-Fit Curves Using C_{ib} (the Sum of H_2CO_3* and HCO_3^-) for the Fixed pH of 7.5, 8.5, and 9.5
The best-fit values of μ_{max} and K_{Cib}, along with R^2 values, are given in the top rows of **Table 5.4**

Table 5.4: Best-Fit Monod Parameters for Wild-Type *Synechocystis* sp. PCC 6803 With Three pH Values and a Common AILI of 202 $\mu E/m^2$-s

Monod-parameter value	Growth pH		
	7.5	8.5	9.5
μ_{max}, day^{-1}	2.03±0.05	2.37±0.04	2.00±0.07
$K(C_{ib})$, mM	$8.6\times10^{-2}\pm1\times10^{-2}$	$8.5\times10^{-2}\pm7\times10^{-3}$	$9.6\times10^{-2}\pm2\times10^{-2}$
$R^2(C_{ib})$	0.891	0.971	0.878
$K(H_2CO_3^*)$, mM	$5.1\times10^{-3}\pm7\times10^{-4}$	$5.2\times10^{-4}\pm4\times10^{-5}$	$6.0\times10^{-5}\pm1\times10^{-5}$
R^2 $(H_2CO_3^*)$	0.892	0.972	0.878
$K(HCO_3^-)$, mM	$8.1\times10^{-2}\pm1\times10^{-2}$	$8.3\times10^{-2}\pm7\times10^{-3}$	$9.6\times10^{-2}\pm2\times10^{-2}$
$R^2(HCO_3^-)$	0.891	0.971	0.878
$K(CO_3^{2-})$, mM	$1.3\times10^{-4}\pm2\times10^{-5}$	$1.3\times10^{-3}\pm1\times10^{-4}$	$1.5\times10^{-2}\pm3\times10^{-3}$
$R^2(CO_3^{2-})$	0.891	0.971	0.877

Figure 5.16 compiles the measured μ values for all pH values (7.5, 8.5, and 9.5) as a function of C_{ib} of the wild type (top panel) and the laurate-excreting strain (bottom panel). In both cases, the rapid increase of μ up to μ_{max} confirms that *Synechocystis* has a high affinity to C_{ib}: The wild type achieved more than 90% of its μ_{max} and the modified strain achieved 80% of its μ_{max} with $C_{ib} > 0.5$ mM (6 mgC/L) and approaches its maximum growth rate with $C_{ib} > 1.0$ mM (12 mgC/L). Natural waters typically contains C_{ib} from 0.6 to 4.3 mM (Assayag, Rivé, Ader, Jézéquel, & Agrinier, 2006), values that saturate the rate of the inorganic carbon uptake by *Synechocystis*. A *Synechocystis*-based PBR should be able to attain a high growth rate with a modest C_{ib} concentration (≥1.0

mM) with a pH in the range of 7.5 to 9.5. However, if a PBR with a high biomass-production rate has an inadequate CO_2-supply rate, intense photosynthesis can cause the pH to reach as high as 11, which shifts the speciation of C_i towards non-bioavailable CO_3^{2-} (Kim, Vannela, Zhou, & Rittmann, 2011). In such a high-pH situation, a high-productivity PBR would need to maintain a very high C_i concentration, achieved by using a very high alkalinity, to avoid C_{ib} limitation and to achieve a maximum production rate.

Table 5.5: Best-Fit Monod Parameters for the Laurate-Excreting *Synechocystis* sp. PCC 6803 with Three pH Values and a Common AILI of 202 $\mu E/m^2$-s.

Monod-parameter value	Growth pH		
	7.5	8.5	9.5
μ_{max}, day^{-1}	1.61±0.08	1.68±0.07	1.60±0.03
$K(C_{ib})$, mM	$1.3\times10^{-1}\pm3\times10^{-2}$	$8.2\times10^{-2}\pm2\times10^{-2}$	$1.1\times10^{-1}\pm9\times10^{-3}$
R^2 (C_{ib})	0.938	0.828	0.977
$K(H_2CO_3^*)$, mM	$7.6\times10^{-3}\pm2\times10^{-3}$	$5.1\times10^{-4}\pm1\times10^{-4}$	$6.7\times10^{-5}\pm6\times10^{-5}$
R^2 ($H_2CO_3^*$)	0.938	0.832	0.976
$K(HCO_3^-)$, mM	$1.2\times10^{-1}\pm3\times10^{-2}$	$8.1\times10^{-2}\pm2\times10^{-2}$	$1.1\times10^{-2}\pm1\times10^{-2}$
R^2 (HCO_3^-)	0.938	0.831	0.973
$K(CO_3^{2-})$, mM	$2.0\times10^{-4}\pm5\times10^{-5}$	$1.3\times10^{-3}\pm3\times10^{-4}$	$1.7\times10^{-2}\pm2\times10^{-3}$
R^2 (CO_3^{2-})	0.938	0.971	0.973

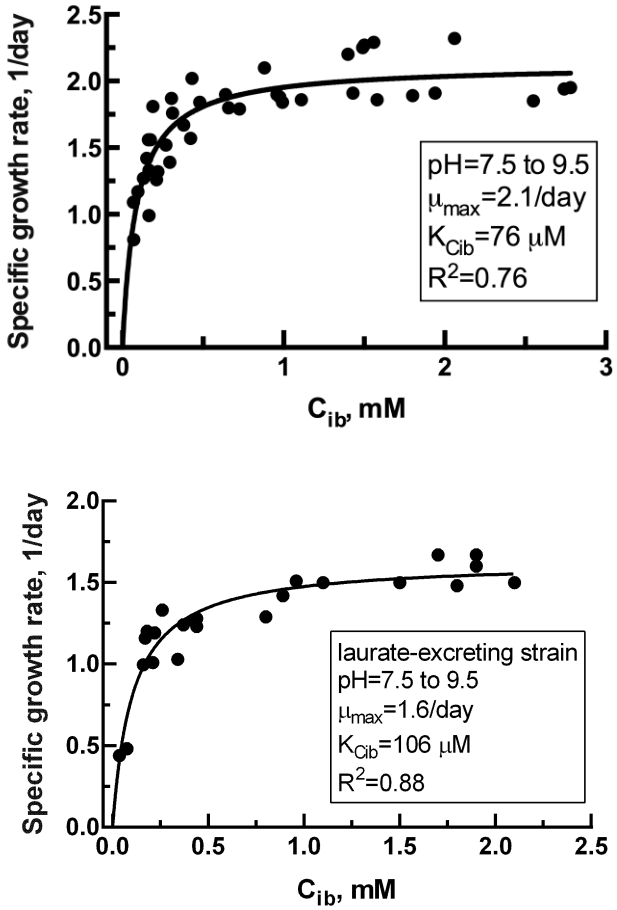

Figure 5.16: Measured Specific Growth Rate (Symbols) and Monod Best-Fit Curves Using Bioavailable Inorganic Carbon (C_{ib}) with pH= 7.5, 8.5, and 9.5
The parameter values for the Monod model were best fit to the composite data

5.3.2.2.2 Kinetics for H_2CO_3, HCO_3^-, and CO_3^{2-}*

I evaluated each C_i species for its ability to fit the measured specific growth rate to the Monod-kinetic model each strain. **Figure 5.17** shows the experimental data and model fits, and the best-fit values of μ_{max} and K_C are included in the bottom rows of **Table 5.4** for the wild type. The similar presentation for the modified strain is in **Figure 5.18** and **Figure 5.5**. Each species was able to give a good fit to the experimental value

of μ; this includes CO_3^{2-}, which is not available for uptake by *Synechocystis* (Giordano et al., 2005; Price et al., 2008). This pattern is identical in the wild type and modified strain.

While each C_i species could give a good fit to the experimental data, the K_C values had very different patterns that shed light on what species best represents C_i uptake. Using HCO_3^- as the modeled species (middle rows of **Figure 5.17** and **Figure 5.18**), K_C had a narrow range, from 81 μM to 96 μM of C by the wild type and 81 μM to 120 μM by the modified strain. In contrast, the K_C value for $H_2CO_3^*$ (second rows of **Figure 5.17** and **Figure 5.18**) varied by about two orders of magnitude, from 0.06 μM (pH 9.5) to 8 μM (pH 7.5). This change in K_C corresponds to the change in H_2CO_3* concentration with pH. CO_3^{2-} (bottom rows of **Figure 5.17** and **Figure 5.18**) had a similarly wide range of K_C, but with the opposite pattern, from 0.13 μM (pH 7.5) to 17 μM (pH 9.5). Similar to the trend with $H_2CO_3^*$, the K_C value for CO_3^{2-} correlated with it pH-dependent change in concentration in both strains.

Three pieces of information support that HCO_3^- best represented the rate of C_i uptake for our experiments: HCO_3^- was the dominant species, only K_C for HCO_3^- had little variability with pH, and CO_3^{2-} is not taken up by *Synechocystis*. HCO_3^- was the dominant inorganic-carbon species, comprising 86% (pH 9.5), 94% (pH=7.5), or 97% (pH 8.5) of C_i. The wide ranging and opposite trends for H_2CO_3* and CO_3^{2-} reflect that their concentrations, which were small compared to HCO_3^-, were tied to the HCO_3^- concentration via the pH, as shown in Eqns. (5.6), (5.7) and (5.8). That non-bioavailable CO_3^{2-} could give a good fit strongly reinforces that a K_C value that changes in proportion to pH is evidence that the C_i species was not rate controlling.

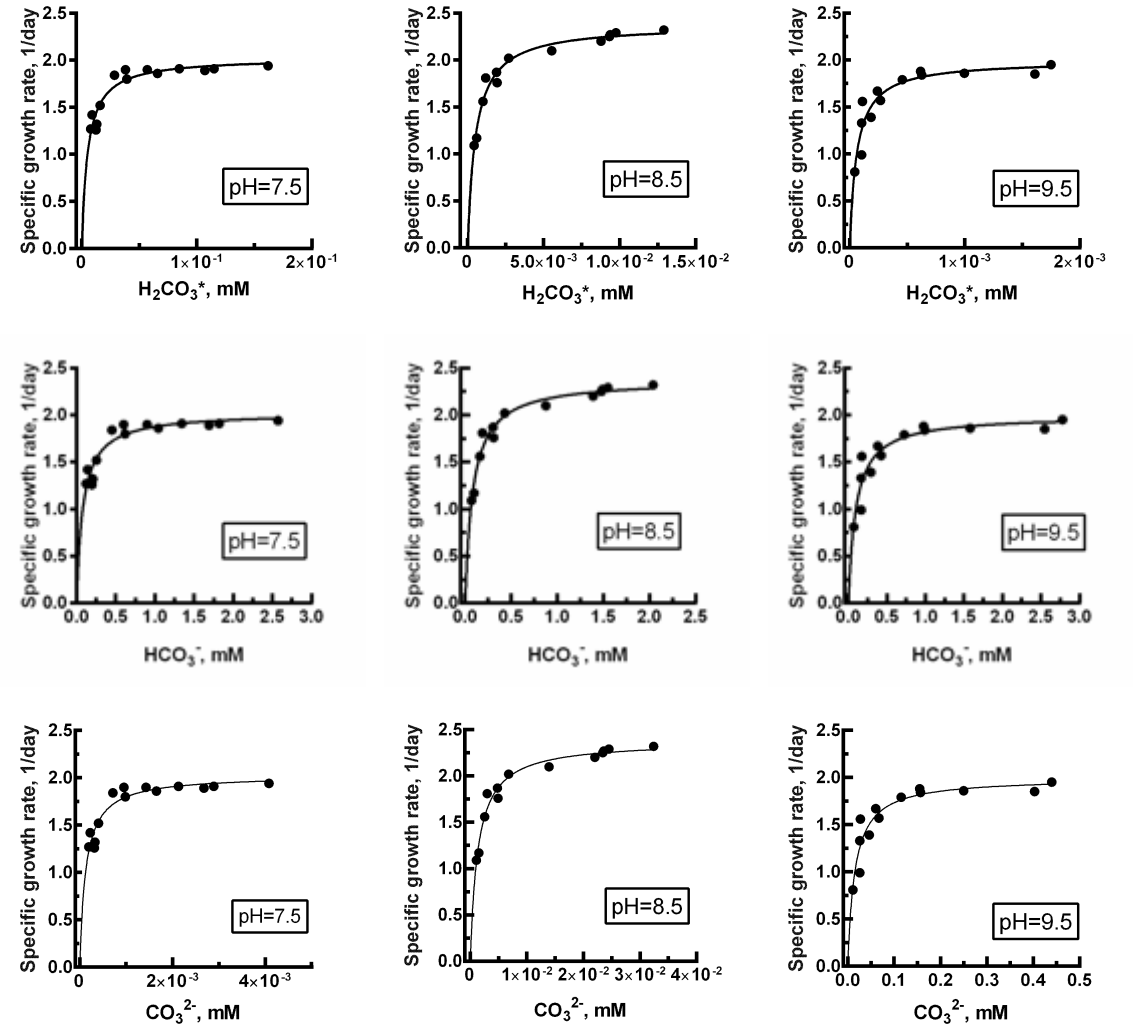

Figure 5.17: Measured Specific Growth Rate (Symbols) of Wild-Type *Synechocystis* and Monod Best-Fit Curves Using $H_2CO_3^*$ (Top Row), HCO_3^- (Middle Row), and CO_3^{2-} (Bottom Row) for the Fixed pH of 7.5, 8.5, and 9.5

The best-fit values of μ_{max} and K_C, along with R^2 values, are given in **Table 5.4**.

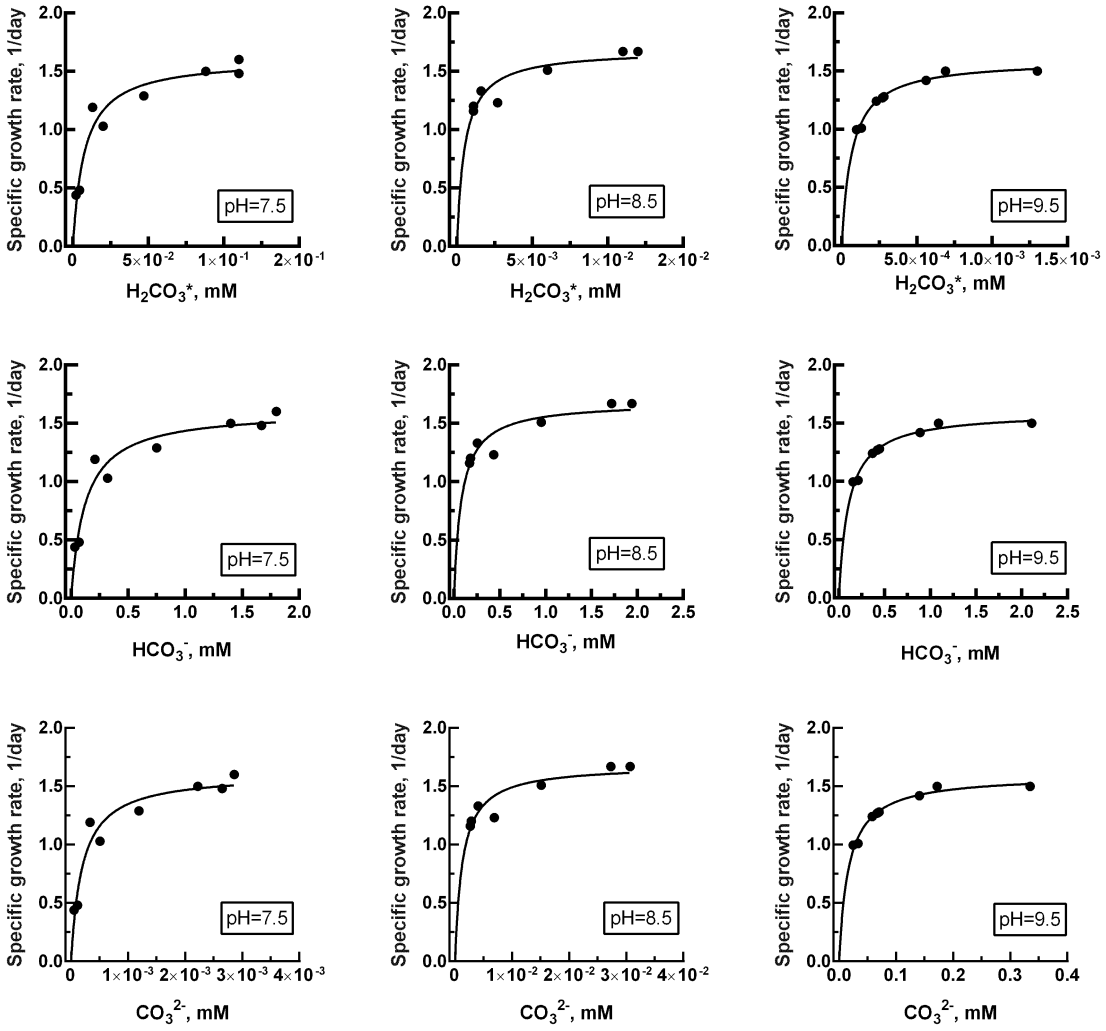

Figure 5.18: Measured Specific Growth Rate (Symbols) of the Laurate-Excreting *Synechocystis* and Monod Best-Fit Curves Using $H_2CO_3^*$ (Top Row), HCO_3^- (Middle Row), and CO_3^{2-} (Bottom Row) for the Fixed pH of 7.5, 8.5, and 9.5

The best-fit values of μ_{max} and K_C, along with R^2 values, are given in **Table 5.4**.

5.3.2.2.3 Improved research approach

Beyond quantifying the separate effects of C_{ib} and pH on the growth kinetics of *Synechocystis* sp. PCC 6803 wild type and laurate-excreting strain, my approach provides a general tool that overcomes the drawbacks of previous attempts to evaluate effects of

pH and C_i. Delivering CO_2 automatically based on a pH-Stat function offers a superior tool to control pH. Using a high buffer intensity to maintain pH is impractical at large scale and can introduce side effects from salts build up (Bérubé et al. 1999; Takagi and Yoshida 2006; Yeesang and Cheirsilp 2011). Buffers have limited pH working ranges that depend on acid-disassociation constant(s) (K_a) of each acid/base pair. A working pH must be close to the acid/base pair's pK_a if the buffer is to have strong buffering capability, but it is not feasible to find a biologically acceptable acid/base pair for all pH values of interest. This buffer-intensity limitation is overcomed by a CO_2-based pH-Stat, which directly controls the pH based on feedback from a pH probe. Because of its advantages, controlling pH by automated CO_2 addition is the most practical technique for large-scale PBRs (Moheimani and Borowitzka 2011; Moheimani 2013;).

The amount of base generated by photosynthesis with NO_3^- as the N source increases alkalinity and C_i, which means that pH and C_i cannot be controlled independently in typical situations (see Mayo et al. 1986; Clark and Flynn 2000; Wangwibulkit et al. 2008; Kezhen et al. 2014; Nguyen and Rittmann, 2015). Likewise, using NH_4^+ as the N source causes a systematic decline in alkalinity and C_i. I demonstrated that using NH_4NO_3 as the N source, when combined with a pH-Stat, stabilized the alkalinity of the growth medium so that I could study C_i-limited kinetics independently from the effects of pH. Exploiting this advantage, I were able to manipulate the C_i concentration independently of growth pH and identify which C_i species best represented inorganic carbon-uptake kinetics.

5.4 Synthesis and Application

Using my pH-Stat and combining nitrate and ammonium as the N source, I successfully controlled growth pH (at 6.5, 7.5, 8.5, 9.5 or 10.0) and C_i (ranging from 0.05 to 3.3 mM) independently. My results confirm that wild-type *Synechocystis* has an optimal pH of 8.5, where it achieved a μ_{max} of 2.4 per day at an average internal LI of 202 $\mu E/m^2$-s. The laurate-excreting strain attained its best μ_{max} of 1.7 per day, also at pH 8.5. Analyzing K_C values for each C_i species indicates that HCO_3^- was the most likely rate-limiting Ci species. K_C values for HCO_3^- values were consistent and in the range from 81 µM to 120 µM. Based on the results in this chapter, practical guidance for attaining a high biomass-production rate is to maintain C_i >1.0 mM and pH near 8.5.

6 EFFECT OF PHOTOPERIODS TO BIOMASS PRODUCTION, DARK AND LIGHT RESPIRATION*

6.1 Introduction

Microalgae offer a sustainable platform to convert sunlight into biofuels and fix that energy in carbon. They have higher quantum yield, faster growth, more versatility to growth conditions, and better ability to be genetically modified than do plants (Mata et al., 2010; W. Vermaas et al., 2011). Taking full advantage of microalgae requires understanding how the diurnal sunlight cycle affects their productivity. A particular concern is biomass decay that occurs during night periods (Q. Hu, Kurano, Kawachi, Iwasaki, & Miyachi, 1998; G. Torzillo, Sacchi, Materassi, & Richmond, 1991). While geography and season affect the length of day and night periods, a common factor is that the night period reduces biomass production, particularly if biomass loss is substantial in the dark.

The effects of photoperiods on mass algal culturing have been studied for a long time. One of the earliest and most extensive studies on photoperiods, more than 60 years ago, looked at the effect of a 12-h day: 12-h dark cycle on *Chlorella* (Tamiya, Shibata, Sasa, Iwamura, & Morimura, 1953). More recent studies have focused on biomass production in the day according to the duration of illumination, but have not investigated

* The results in this chapter will be organized into two journal manuscripts: one on the basic phenomena occurring during decay in the dark, and a second on methods to minimize the negative impacts of decay.

biomass loss at night. Those studies consistently agreed on the positive effect of a longer illuminating period on biomass production (Meseck, Alix, & Wikfors, 2005; Tang et al., 2011; Wahidin, Idris, & Shaleh, 2013). For example, Tang et al. (2011) studied *Chlorella* with photoperiods of 12:12; 15:9; 24:0 (hours of light: dark) and a constant light intensity (LI of 200 $\mu E/m^2$-s), and they found biomass productivities with light:dark cycling (12:12 and 15:9) were 69% and 82% of that with continuous LI; both increases were larger than the fraction of time of illumination. None of these studies addressed directly the role of biomass decay at night (see Tang et al., 2011; Wahidin et al., 2013).

The loss of light availability at night forces the microalgae to rely on endogenous respiration, which leads to biomass decay that undermines photosynthetic growth in the light. Past studies report a large range of specific decay rates, from 0.01 to 0.6 per day (Geider & Osborne, 1989). The larger biomass loss rates were observed in cultures having low biomass density (Q. Hu et al., 1998), an exponential growth rate in the light (Ogbonna & Tanaka, 1996), actively growing cells instead of starved cells (Kratz & Myers, 1955), or exposure to high LI during the day time (G. Torzillo et al., 1991).

Previous studies also documented changes to carbohydrate and protein fractions before and after dark periods (Ogbonna & Tanaka, 1996; G. Torzillo et al., 1991). Carbohydrate was reduced by 8%, while protein was increased proportionally for *Spirulina* grown in an outdoor tubular photobioreactor (PBR). Higher LI led to more carbohydrate in the microalgal biomass, and carbohydrate was the main internal product to be respired in dark periods (Geider & Osborne, 1989).

Another key effect of night period is the interaction of engineered microbial products (e.g. laurate) to biomass. The modified strain, laurate-excreting strain, has its genome engineered. Gene *slr 1609* was deleted to prevent re-uptake of laurate in the medium. Outdoor experiments such as those in 2000L Tube-In-Dessert PBR (Research Engineering Center, ASU) with the laurate-excreting strains repeatedly observed the laurate concentration disappeared after 1-2 days of inoculation. That reduction was more obvious with the sample taken in mornings. Obviously, laurate was not produced during the night and there is a question if deleting that gene has produced the expecting result. Therefore, I carried a several batch tests with only the laurate-excreting *Synechocystis* sp. PCC 6803 to investigate effect of photoperiods to laurate in the modified strain of *Synechocystis*.

In this study, I use the cyanobacterium *Synechocystis* sp. PCC 6803 laurate-excreting strain to evaluate fate of laurate in light/dark cycles. The batch test with modified strain confirmed that the gene modification prevent re-uptake of excreted laurate by the modified strain. I also experimented *Synechocystis* wild type in various photoperiods and focused on the specific decay rate (μ_{dec}) during dark periods for a wide range of illumination scenarios. I found that *Synechocystis* biomass decayed at a rate ranging from 0.05 to 1.0 per day in night periods and that the dark-period μ_{dec} correlated with the specific growth rate during the preceding light period. Lastly, I applied LI at ~10% the daylight LI in the night period (i.e., at 30 $\mu E/m^2$-s) and observed a pronounced decrease in μ_{dec} with low-density biomass.

6.2 Methods and Materials

6.2.1 Experiment setup

There are two separate sets of experiments with photoperiods. In Set #1, I evaluated laurate-excreting strain in one photoperiod: 12 h light: 12 dark. One control flask was illuminated continuously during the experiment time. Each treatment (with and without light acclimation) was in biological duplicate.

To acclimate the culture to full light of 225 $\mu E/m^2$-s, a 1-cm piece of aluminum foil was opened to expose the culture to a fraction of the total LI for 30 minutes. The 1-cm opening allowed about ~10% of the total incident LI into the flask. No light acclimation means the culture exposed to full incident LI and darkness immediately. I covered the flasks by two layers of aluminum foil and checked with light meter to assure the dark condition.

In Set # 2, I used two pH-stat PBRs and Dissolved Oxygen (DO) probe in one reactor to carry out different photoperiods (**Figure 4.2**). I described the operation and components of the pH-stat PBR in chapter 4 (pH-Stat PBR). In all experiments, the culture temperature was maintained at 30°C by automated air-cooling and a fixed pH at 8.5 when light cycle is on. The incident light intensity was 280$\mu E/m^2$-s to 324 $\mu E/m^2$-s by two-T5-fluorescent bulbs (Hydrofarm, US). Photoperiods were controlled by turning on and off the bulbs based on the setup time. During experiments, the culture temperature was maintained at 30°C by automated air-cooling, and the pH was fixed at 9.5 or 8.5 when the light was on; the pH was less than the set value when the light was off.

I expanded with more photoperiods allocated 24 hours in these patterns of (hours on: hours off): continuous illumination (24:0), long day (15:9), equal day and night (12:12), short day (9:15) and a very short night (21:3). The last cycle (21:3) was used to evaluate biomass loss at the beginning of the dark time and lowered the fixed pH to 8.5. This pH was identified to support a better biomass production. Growth media with pH 8.5 and 9.5 have drastic different in buffer intensity.

Besides the photoperiod experiments, I also designed and implemented an experiment to evaluate biomass loss when light was available, but C_i was depleted enough to become rate limiting. I achieved very low C_i by depleting the alkalinity of the culture by adding ammonium (0.4 M, pH~8) to the BG-11 medium as the N source instead of nitrate; uptake of ammonium for synthesis causes a systematic loss of alkalinity and C_i as described in Chapter 4. I later added bicarbonate (0.4 M) to restart photosynthesis after it has been arrested due to C_i depletion. I carried out a total four cycles of C_i depletion and re-supply. I measured DO, OD, pH, and C_i, and calculated the average LI and decay rate from the biomass's OD.

I set up an additional run with two duplicates with the pH fixed at 9.5 and the 12:12 light: dark cycle. I took 4 samples during the dark periods to evaluate correlation of DO, C_i, and biomass loss, as well as effect of buffer intensity on the rate of pH drop in the dark periods.

In an effort to reduce the decay rate at night, I illuminated the culture with a constant LI of 30 $\mu E/m^2$-s during the night periods. I covered the T5 bulbs with thick cardboard, cut a thin open line, and allowed only limited LI to shine onto the PBR. The third bulbs occupied the space between two light bulbs and reduced the incident LI in

daytime of two bulbs from 324 μE/m^2-s to 280 μE/m^2-s. I noted the difference of this change in the results and discussion section.

6.2.2 Medium and inoculum preparation

I obtained wild-type and laurate-excreting modified strains of *Synechocystis* were provided by the laboratory of Dr. Willem F.J. Vermaas and prepared innocula as described in Chapter 2 (with the modified strain) and Chapter 4 (with the wild type).

I used the standard BG-11 medium (Rippka et al., 1979) in experiments Set # 1. For Set # 2, I made several modifications. First, I reduced 50% nitrate and doubling phosphate. Extra nitrate does not improve biomass growth while wasting resource. Additional phosphate prevents possible P limitation because the standard BG-11 is unbalanced N:P ratio compared to elemental N:P found in biomass.

I used modified BG-11 medium in experiments for respiration with depleted C_i. In the modified BG-11, ammonium is used as N source instead of nitrate. During the run, I added ammonium chloride to deplete C_i. Detailed modification of BG-11 medium is also described in Chapter 5.

6.2.3 Sampling and assaying

In both sets, each experiment lasted approximately ~5 days and was carried out in biological duplicates.

I took samples right on the change of light/dark cycle. In Set #1, I took 10 mL of samples and then assayed for optical density (OD) and measured pH immediately. The

rest of samples were prepared for Light Microscopy (LM) imagining for bacteria representation and Gas Chromatography for laurate quantification.

For Set # 2, I took ~ 25 mL culture using a syringe and placed in a 50-mL polypropylene centrifuge tube (VWR). Biomass optical density (OD) and laurate were assayed as described in Chapters 2 and 3. One AU is equivalent to 90% attenuation of the incident light intensity by the spectrometer. Details of C_i (Dissolved Inorganic Carbon) assay were also presented in Chapter 4 where C_i is the focus of my investigation.

Growth pH was monitored continually. I measured the pH after samples taken in Set #1 and set up automated logging of the pH every 5 minutes in Set # 2.

The DO (Set # 2 only) acquired from *in-situ* probe monitored photosynthesis status and was useful during night periods and with the depleted C_i experiment. I calibrated DO probe regular in accordance with the manufacturer's recommendation (Neptune, CA) and checked with sodium sulfite (1M) for zero DO. I spiked 1X BG-11 and observed only minimal increment of DO.

6.2.4 Kinetic analysis

I calculated the observed specific growth rate during the day time (μ_{obs}) and the decay rate during the night time (μ_{dec}) using (Bruce E Rittmann & McCarty, 2001). The equation was presented previously in by eqn. (5.11).

6.2.5 Buffer intensity

I computed the buffer intensity (β, moles/L) of BG-11 growth medium (nitrate is the N source) using eqn. (6.1) (Snoeyink & Jenkins, 1980), and the buffer intensity with different amount of biomass produced is shown in **Figure 6.1**.

$$\beta = 2.3([H^+] + [OH^-] + C_i(\alpha_{0,C}\alpha_{1,C} + \alpha_{1,C}\alpha_{2,C}) + C_P(\alpha_{0,P}\alpha_{1,P} + \alpha_{1,P}\alpha_{2,P} + \alpha_{2,P}\alpha_{3,P}) \quad (6.1)$$

C_P is the total phosphate concentration, C_i is total dissolved inorganic carbon concentration, and □s are ionization factor of the carbonate system or of the phosphate system. In BG-11, carbonate is major buffering system, especially with more biomass is produced to increase C_i.

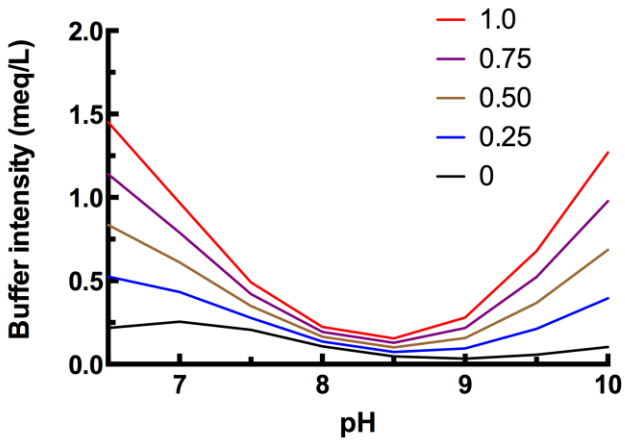

Figure 6.1: Buffer Intensity over Applicable pH Range for BG-11
Each lines gives the buffer intensity with the noted additional biomass produced in adsorption units (AU). One AU is approximately 254 mgDW/L.

6.3 Results and Discussion

6.3.1 Biomass and FFA production in uncontrolled pH

Figure 6.2 shows biomass and pH responses for the experiment with 12-h light: 12-h dark. After five cycles, the two flasks with light acclimation showed a regular pattern in pH: pH increased during light periods and decreased during dark periods. Flasks with no light acclimation had a regular pH reading at first-four cycles, but then the culture exhibited a pale color, lower biomass production, and an irregular pH pattern during the fifth cycle. The control flask (continuous light) grew fastest and maintained pH constant during the run. Flasks illuminated periodically showed 35-40% of the biomass production compared to the control did over the entire run.

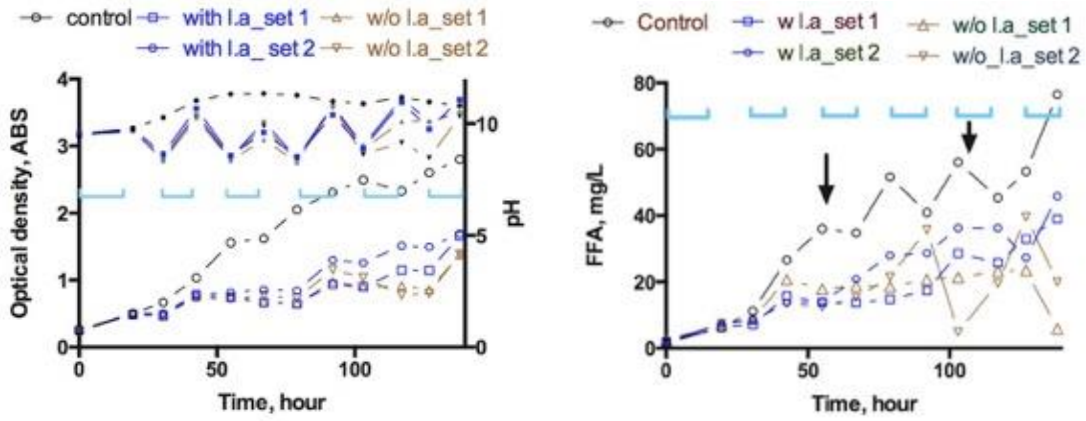

Figure 6.2: Effects of Photoperiods with Light Acclimation (l.a) and Without Light Acclimation (w/o l.a) by the Laurate-Excreting Strain; Biomass Density (Open Symbols); pH (Closed Symbols) on the Left Panel, and FFA, Mainly Laurate, over Time on the Right Panel
Lines in black are the control experiment (continuous illumination); lines in blue indicates treatment with light acclimation (12h light: 12 dark); lines in brown indicates treatment without light acclimation (12h light: 12 dark); set 1 and 2 are duplicates; blue bracket indicates when culture illuminated with intensity of 225 $\mu E/m^2$-s; black arrows indicates when fresh medium BG – 11 was added

Lower biomass productivity with photoperiod illumination could be explained by two mechanisms. The first is the cost of photo adaptation, in which cells have to switch from dark to light regime and *vice versa* when illumination pattern changed. The second is biomass loss due to respiration. Marra (1980) reported a change in chlorophyll concentration when LI was varied, indicating that the deployment of enzymes to switch the cell's state was energy expensive. I applied a constant incident LI, and the AILI decreased over time. The energy cost of switching from different LI is applicable if AILI is the better representation of LI. Nevertheless, I am inclined to favor the mechanism of respiratory loss. For one, the dark regime lasted much longer than the adaptation time. Lloyd, Canvin, & Culver (1977) used ^{14}C isotopes to track carbon exchange in 4 microalgae strains and found about 1.5 to 5 times higher rate of carbon evolution in the dark regime than in the light regime; this means that respiration loss of biomass is greater in dark periods. Cells also relied on internal energy to repair proteins and to maintain minimum operations in dark periods that leads to consumption of labile biomass.

Whether the modified strain can take up FFA from the medium is another important issue. *Synechocystis* wild type has this capacity to incorporate exogenous FFA into internal FFA pools (Qiang Hu et al., 2008; W. Vermaas, 1996). No uptake is expected for the mutant strain in these experiments, because deletion of *slr1609* should block the FFA uptake pathway in *Synechocystis* (Liu et al., 2011). The best approach to assess if laurate is taken up is to measure FFA before and after dark periods. The data in **Figure 6.2** suggest no significant laurate loss during the dark regime. Each flask had biomass and laurate concentrations that accumulated over time, confirming a trend in **Figure 6.2**: laurate is produced proportionally to biomass, about 15% of the COD of

particulate biomass. LM results by light microscopy indicated that all culture were free from heterotrophs up to the second-last sampling point. This is important to eliminate re-uptake by *Synechocystis* during diurnal cultivation as a cause of losing excreted laurate.

The initial data suggest that switching the culture between dark and light lowers culture productivity, but I need more in-depth information on photoperiods, such as for 9-hour light: 15-hour dark, 12-hour light: 12-hour dark, and 15-hour light: 9-hour dark. This will simulate the diurnal cycles with different latitudes and seasons.

6.3.2 Photoperiods with pH-Stat PBR

6.3.2.1 Biomass production and decay rates

Similar to the previous photoperiod experiment with the laurate-excreting culture in an uncontrolled pH environment, **Figure 6.3a** shows the increase in biomass for wild-type *Synechocystis* culture with 12-h light: 12-h dark and at pH 9.5 fixed by the pH-Stat. Biomass increased during the light and was lost during the dark period. Biomass loss during the dark time was significant, ranging from 13% to 40% of biomass synthesized in the previous light period. The higher loss rates were associated with lower biomass density. **Figure 6.3b** presents the growth or loss kinetics calculated based on eqn. (5.11) and observations in panel a. The biomass grown in 12:12 photoperiod showed two clear trends: (i) higher decay rate in the beginning of dark periods and (ii) higher decay rate with lower-density cultures, which were exposed to higher internal LI. Quantitatively, 42% of the decrease in OD occurred in the first 28% of the dark period. The specific decay rates averaged over entire dark periods were from 0.12/day to 0.49/day. The

higher decay rate with a lower biomass density with photoperiods is also consistent with previous studies (G. Torzillo et al., 1991) in which the loss of *Spirulina* biomass increased 56% in the culture having half of the biomass density with equal light and dark periods. Higher AILI that should have supported a higher μ_{obs} and more accumulation of labile materials (Foy & Smith, 1980; Q. Hu et al., 1998) that can be quickly consumed for cell maintenance during dark periods which in turns, lowers biomass density.

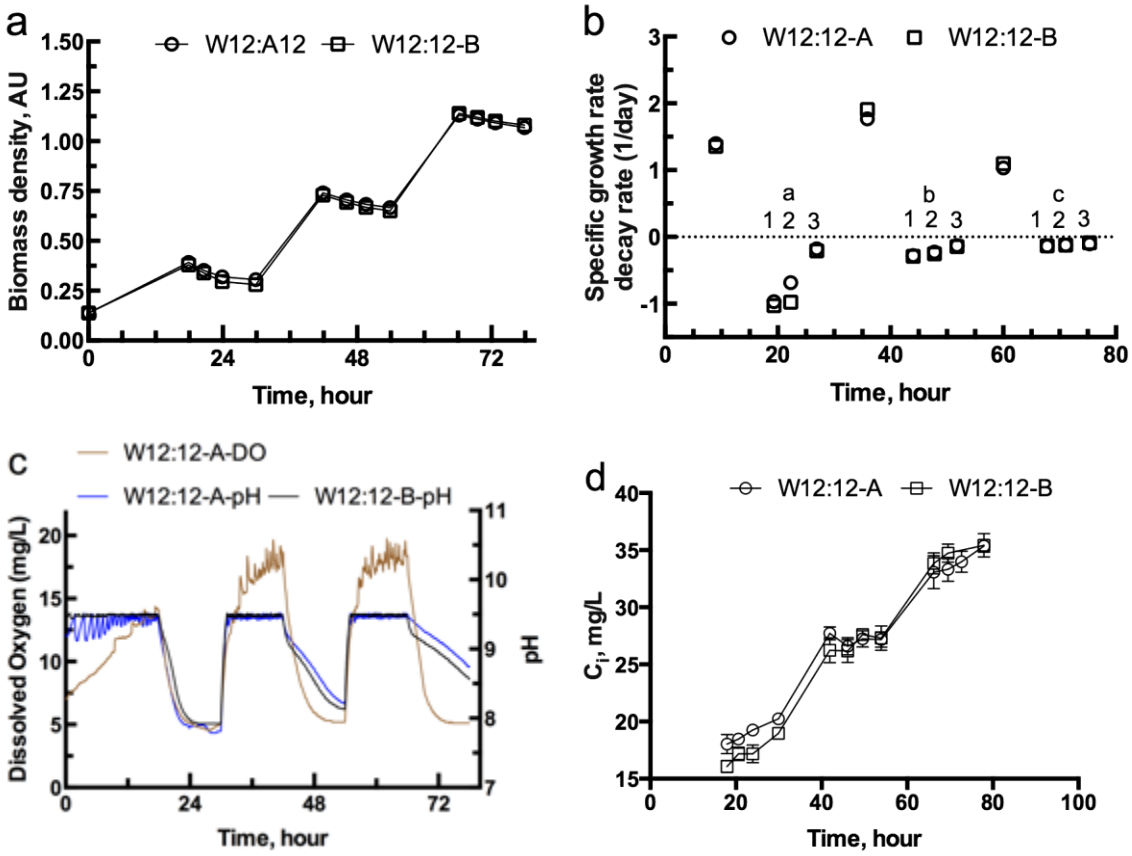

Figure 6.3: Panels a to d: Biomass Density, Specific Growth and Decay Rate, the Culture pH and Dissolved Oxygen, and Inorganic Carbon of Experiments with a Fixed pH of 9.5

Runs ending in (-A) and (-B) are replicates. On panel b: 1, 2, 3 represents for each fragment during each dark period (marked by a, b, c)

Panel c of **Figure 6.3** depicts clear patterns for pH and DO. The pH dropped faster for the early dark periods, particularly the first dark period. The buffer intensity of the culture for the different pHs and after biomass was produced influenced the pH-drop pattern. At pH of 9.5, the buffer intensity was at least 1.2 times higher than at 8.5, and the difference became much higher with denser biomass (**Figure 6.1**) when nitrate was the N source and increased the C_i centration with more biomas (**Figure 6.1**). Thus, the C_i accumulation after each light period (**Figure 6.3**d) substantially increasing the buffer intensity and damped t he pH-drop pattern. For comparison, the DO drop was not affected by the buffer intensity, and its pattern remained identical in each dark period.

Measuring DO is one approach to study dark respiration over a short duration (<1 h) (see Geider and Osborne, 1989). I collected DO concentrations in unit A over the entire experiments. During the light periods, *Synechocystis* carried out photosynthesis and produced oxygen. The uptake of C_i during photosynthesis activated the pH-Stat to maintain a fixed at 9.5. The DO concentration rose to ≥ 20 mg/L (the limit on the DO probe) with the light on, and it declined to ~7.3 at an average of 3.3 hour after the light was turned off. Faster drop of DO also was observed in microalgae grown outdoor. For example, DO in *Coelastrum* sp. culture reduced DO from 7 mg/L in 4mg/L in 3 hours and 4mg/L to 2.5 mg/L in next 12 hours (Grobbelaar & Soeder, 1985).

DO loss could result from the combined effects of endogenous respiration and off gassing of super-saturated DO. At the dark temperature of 28ºC and an elevation of 350 m (for our laboratory), the saturation concentration for DO is 7.3 mg/L (Reynolds, 1977). The lowest DO concentration was ~5.0 mg/L and no further reduction of DO was observed during last 3.0 hours in the dark periods. Thus, the loss of DO from

endogenous respiration was either balanced by DO gas transfer from the air or insignificant respiration occurred in later time because labile substrates were exhausted.

Endogenous respiration can be represent by eqn. (6.2). For simplicity, I assumed that internal compounds have the same biomass elemental ratio as the biomass, which is $C_5H_7O_2NP_{0.05}$. The respiration reaction can be written as:

$$C_5H_7O_2NP_{0.05} + 5.0625\ O_2 + 4.075\ H_2O \rightarrow 5\ H_2CO_3 + NH_4^+ + 0.05\ H_3PO_4 + OH^- \quad (6.2)$$

In eqn. (6.2), for every mole of biomass respired, the additional C_i released to the culture is 5 moles, and 5.0625 moles of oxygen are needed to oxidize biomass completely.

Without light energy, the biomass was forced to oxidize internal materials that are relatively labile. During that process, inorganic carbon (C_i) is released as a product. **Figure 6.3d** shows that 5 of 6 dark cycles resulted in a net C_i increase in the medium. However, the C_i increase only accounted about 20% of carbon in biomass loss based on stoichiometric ratios by eqn. (6.2).

One way to connect endogenous decay in the dark to photosynthesis is the light is to linearly correlate the specific decay rate at night with the preceding specific growth rate in the light (Geider & Osborne, 1989):

$$\mu_{dec} = \mu_{dec,0} + b\mu_{obs} \quad (6.3)$$

where: $\mu_{dec,0}$ is a dark minimum decay rate (at $\mu_{obs} = 0$), and b is a linear correlation factor. Data extracted from **Figure 6.3**b, while showing different decay rates in each dark period, do not exhibit an obvious trend according to eqn. (6.3). However, the unusually low specific growth in the first light period led to the poor correlation (**Figure**

6.3b). I normally observed with OD < 0.5, *Synechocystis* biomass can achieved μ_{obs} of 1.7 to 2.0/day, which is 20% to 43% faster than those with pH = 9.5. Inoculum aging could result lagging growth and a lower μ_{obs}. Thus, I continued to evaluate the model (eqn.(6.3)) in later experiments.

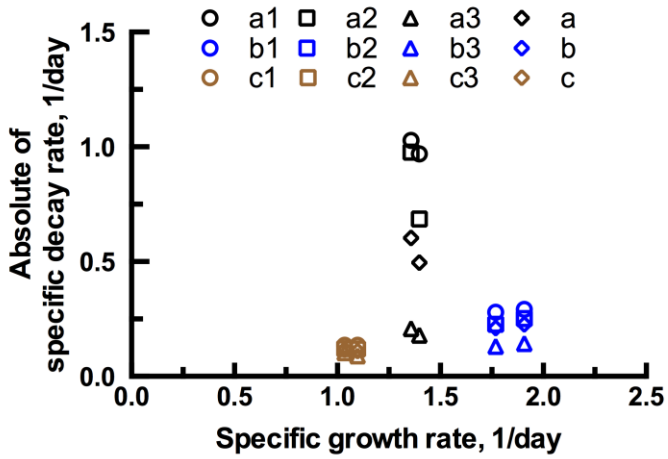

Figure 6.4: Correlation of Specific Growth Rate (μ_{obs}) with Absolute Value of Specific Decay Rate (μ_{dec})
Each legend gives μ_{obs} denoted in **Figure 6.3**b, e.g. a1, is the rates in first window in the dark period a while a alone is the average during that dark period

6.3.2.2 Effects of Different Photoperiod Cycles

Differences of decay rates during dark periods were evaluated further by experimenting with five photoperiods ranging from 9 and 24 hours of light per day and growth pH was fixed at 8.5 during light periods to obtain the highest productivity. The OD result in **Figure 6.5a** presents a clear effect of the duration of illumination for light periods of 9 to 24 hours for pH = 8.5. Continuous illumination produced the most biomass for the same experimental time, and longer night periods systematically lowered

the concentration of biomass. **Figure 6.5b** presents the same data, but with the horizontal axis including only the time of illumination. The biomass concentrations for all of the day-night cycles were similar, while continuous illumination (24:0) had more biomass production.

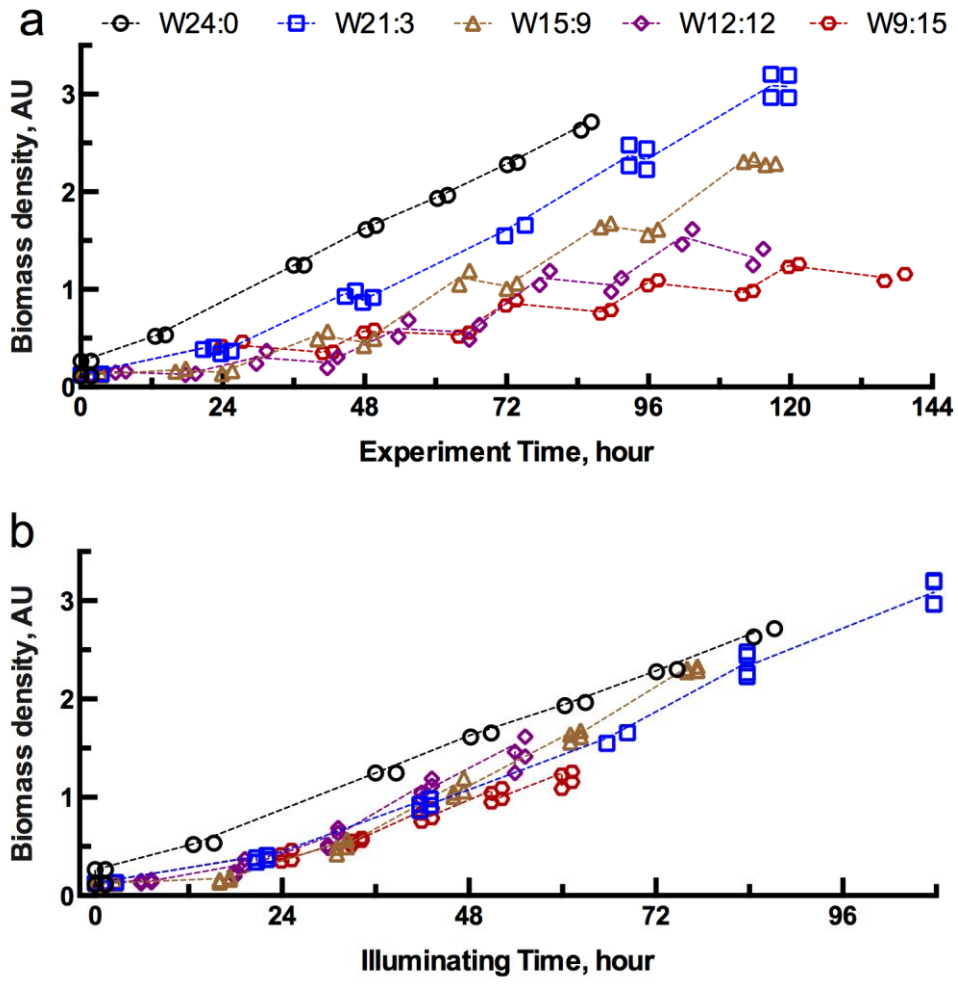

Figure 6.5: Biomass Production in Batch Experiments with Different Photoperiods at pH = 8.5 in the Light. Panel a: OD Values over all of the Entire Experimental Time. Panel b: OD Values Plotted for the Time of Illumination Only
Each photoperiod experiment was run in duplicate, and each symbol represents an individual measurement of OD.

Figure 6.6 presents μ_{obs} for day periods and μ_{dec} for dark periods. Most μ_{obs} values with light-dark cycling were higher than with continuous illumination, particularly for lower biomass density (OD < 1), which is consistent to one trend observed in **Figure 6.3**b.

The μ_{dec} values ranged from 0.05 to 1.0 per day. In general, the highest μ_{dec} values corresponded to the largest μ_{obs} value, both of which occurred at low OD and higher average internal LI. In addition, μ_{dec} value tended to be higher with photoperiods having shorter night duration for the same biomass density. For example, the highest μ_{dec} were observed with the shortest night period (W21:3), while the lowest μ_{dec} was observed with the longest night period (W9:15). This pattern confirmed the major biomass loss occurred at the beginning of dark periods observed in the previous experiment (**Figure 6.3**).

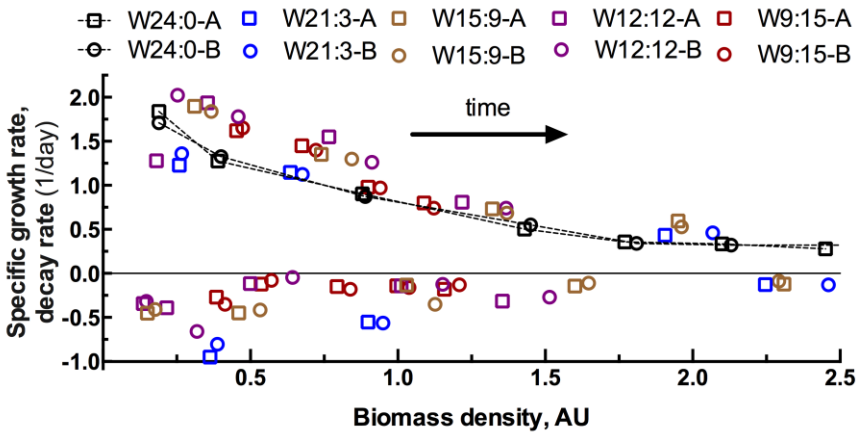

Figure 6.6: Specific Growth Rate (μ_{obs}, Positive Values for Light On) and Specific Decay Rate (μ_{dec}, Negative Values for Light Off) for *Synechocystis* Experiencing Different Photoperiods
Runs ending with (-A) and (-B) are replicates

I used the model by eqn.(6.3) for each μ_{obs} and μ_{decay} pair (**Figure 6.6**). The regression fittings show different trends for each photoperiod, and the correlations are better with shorter dark periods (**Figure 6.7**). Pooling all data give a linear correlation factor (b) of 0.016 and $\mu_{dec,0}$ of 0.21/day. When this approach was applied for bacteria, protozoans, and vascular plant (Geider and Osborne, 1989), b, ranged from 0.1 to 0.76, with $\mu_{dec,0}$ from 0.01 to 0.20/day. Positive correlation between higher decay rate during the dark and high growth rate of previous day time indicates that the decay rate depnds on the prior growth state. This set of data also fit the model better than the one at pH = 9.5. All μ_{obs} values (**Figure 6.6**) were typical and expected, which were faster with lower OD and obtained a rate of ~2.0/day. More importantly, a highest slope and good fit with 3-hour night support the consumption of internal products that lead to higher biomass loss.

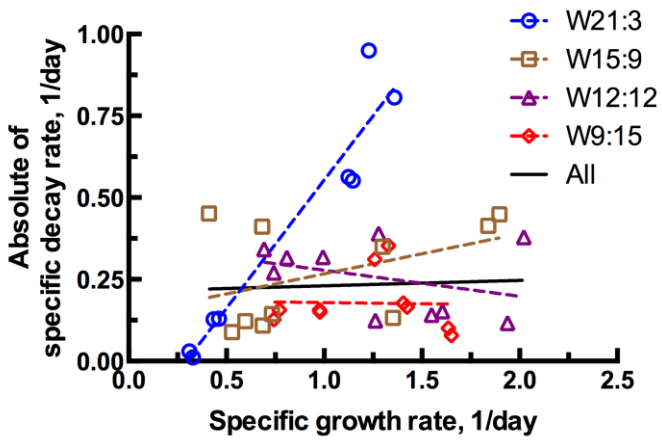

Figure 6.7: Correlation of Specific Decay Rate in Dark with the Preceding Specific Growth Rate in the Light

Symbols are for each μ_{dec} and μ_{obs} pair in **Figure 6.6**, and lines are the regression best fits by photoperiod (colored and dashed lines) and for all runs pooled (black solid line)

The OD and pH patterns remained mostly similar the experiments with pH 9.5 (**Figure 6.8**). When the light was turned off, the pH dropped to 7.5 within the first two hours and leveled off there. The shapes of pH dropping remained identical through the experiment. The buffer intensity at 7.5 is several times higher than at 8.5. Even with more biomass produced, the buffer intensity in pH 8.5 is minimal (**Figure 6.1**), making the rate of pH dropping pattern unaffected by different amount of biomass produced.

The DO pattern was similar to the experiments with pH 9.5. The maximum of DO concentration of 20 mg/L with the light on, but declined to ~10 mg/L within 120 minutes and to ~7.3 within 180 minutes after the light was turned off (**Figure 6.8**). In each dark period and with different photoperiod, the shape of DO drop was not changed and consistent to those in pH = 9.5.

Seeing a faster decay rate with a shorter dark period and a faster drop of pH and DO at the beginning of dark period are consistent with hypothesis that the availability of labile intracellular materials controlled the decay rate. The rate of pH and DO drops were faster at the beginning of dark periods, but remained nearly unchanged after two hours in the dark. The lowest DO concentration was ~4 mg/L, which means that DO was not limiting endogenous decay during the night. Therefore, a slower decay rate resulted from the depletion of labile internal materials. This finding is supported by the observation that carbohydrates were utilized to maintain cells during dark periods (Foy & Smith, 1980; Q. Hu et al., 1998; G. Torzillo et al., 1991). Higher decay rate because of the availability of internal materials is not favorable for high productivity systems, such as PBRs, in which the biomass is supplied with high light and achieved high growth rate.

This challenge is pronounced especially with starting up state. A low OD of inoculum resulted in a higher μ_{dec} at night that prolonged the time needed to accumulate biomass.

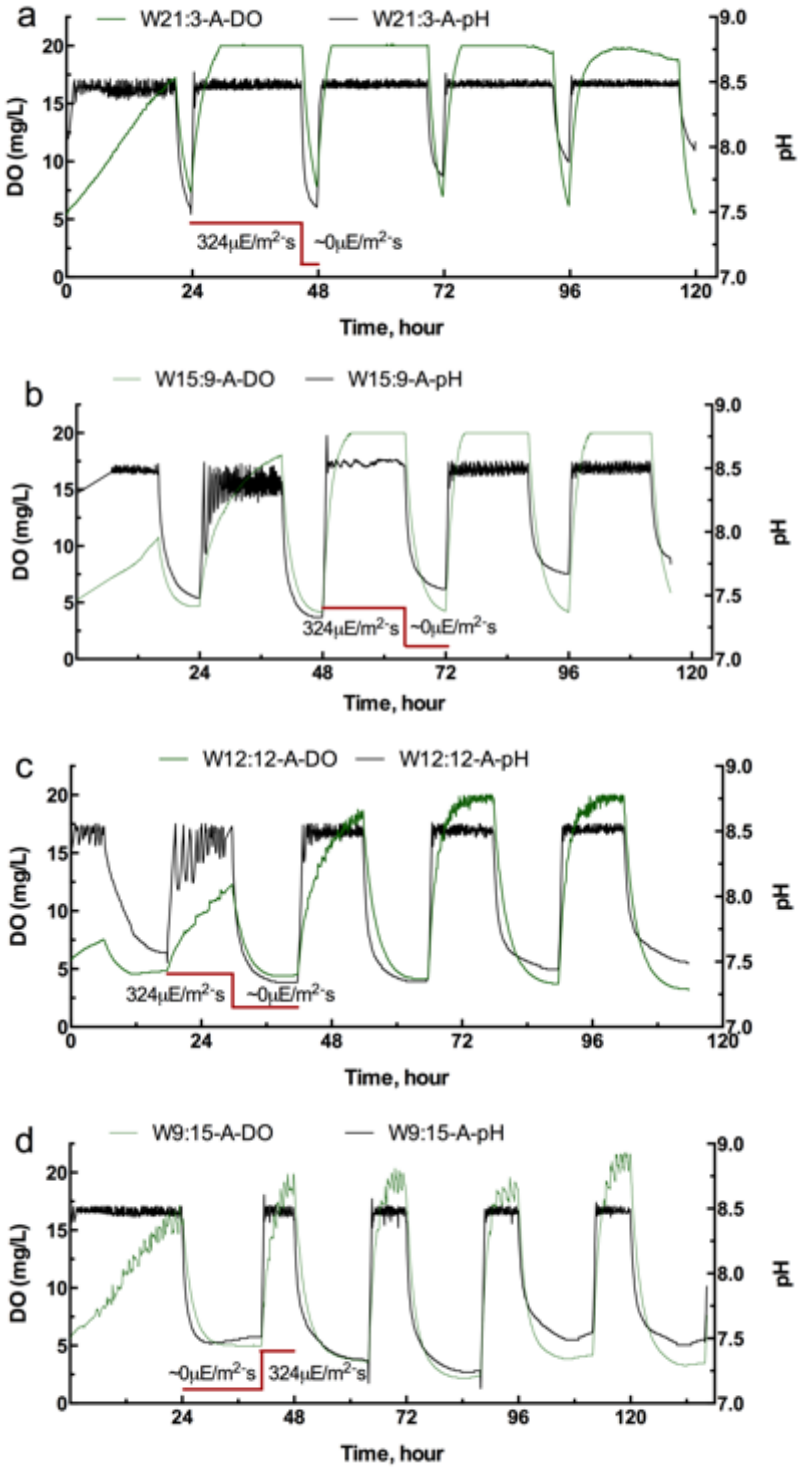

Figure 6.8: pH and DO Value for the *Synechocystis* Culture with Four Different Photoperiods Using the A-unit pH-Stat. The pH Patterns Were the Same with the B-unit.

6.3.2.3 Photosynthesis in depleted inorganic carbon

Since a large decay rate is not desirable, I assessed an approach to reduce μ_{dec}. One way is to evaluate decay in availability of light and depleted C_i by deploying NH_4^+ as the sole N source, which depleted alkalinity and C_i. **Figure 6.9a** presents the continuous readings of pH in which the period of C_i starvation period is marked by a dip in pH, between two arrows. A stabilized pH indicates net zero photosynthesis. The C_i data in panel b confirmed that C_i was in the range of 1.1-2.0 mg/L. The average LI was at least 25 $\mu E/m^2$-s at all times. This C_i concentration is higher than the half-maximum-rate concentration, K_C, (~ 85 µM) identified in Chapter 5 for the wild type that could be influenced by different AILI.

DO concentrations confirmed photosynthesis status (**Figure 6.9c)**. An upward increment indicates net photosynthesis, and downward trends indicate loss of oxygen consumed via off gassing or respiration. Stable DO at ~5 mg/L confirms that photosynthesis was arrested given that C_i was low but AILI was sufficient.

The μ_{dec} values with depleted C_i ranged from 0.03 to 0.40/ day (**Figure 6.9**d), much lower than those in dark periods with high C_i (**Figure 6.6**). The higher value was still with lower OD and a higher corresponding internal LI. A lower decay rate is promising because only a small biomass was loss with augmenting light energy.

More importantly, this experiment confirms that microalgae required energy to maintain themselves either by internal products or by light energy. C_i depletion did not destroy or intoxicate the microalgae; they were readily return to photosynthesize when light becomes available.

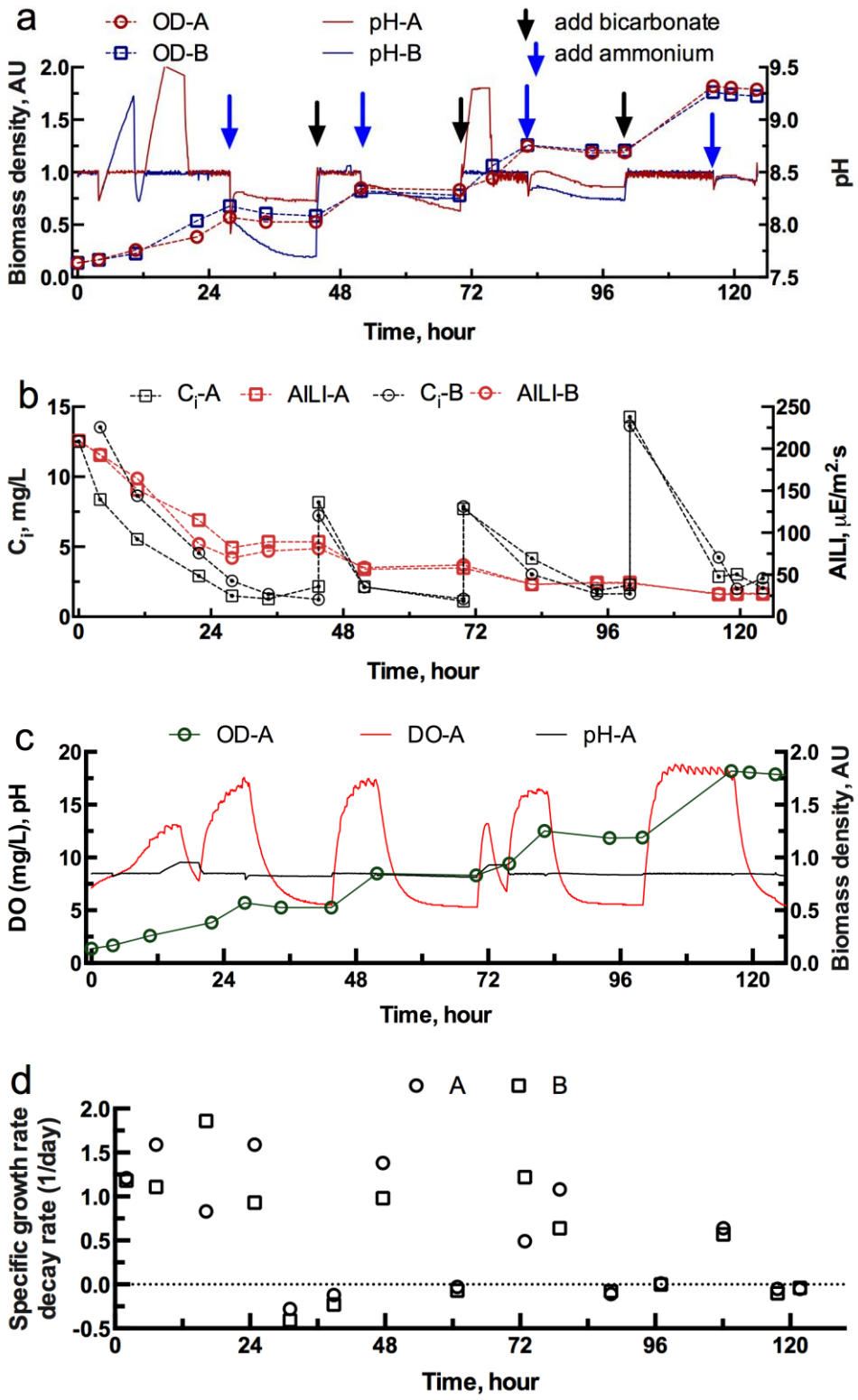

Figure 6.9: Photosynthesis of Culture with Depleted C_i and Sufficient Light Energy

6.3.2.4 Reduce decay rate by augmenting light in night

Panels a to d of **Figure 6.10** shows the specific growth and decay rates of four photoperiods in two cases: completed dark at night marked by open symbols and a constant 30 $\mu E/m^2$-s during the night that marked by filled symbols. μ_{dec} in **Figure 6.10** clearly supports that low light illumination in the night period lowers the decay rate, although the impacts varied among the light/dark cycles.. The impacts on μ_{dec} was greater in cultures with lower OD and a corresponding higher μ_{obs}, such as with W21:3 and W15:9 (panels a and b, **Figure 6.10**).

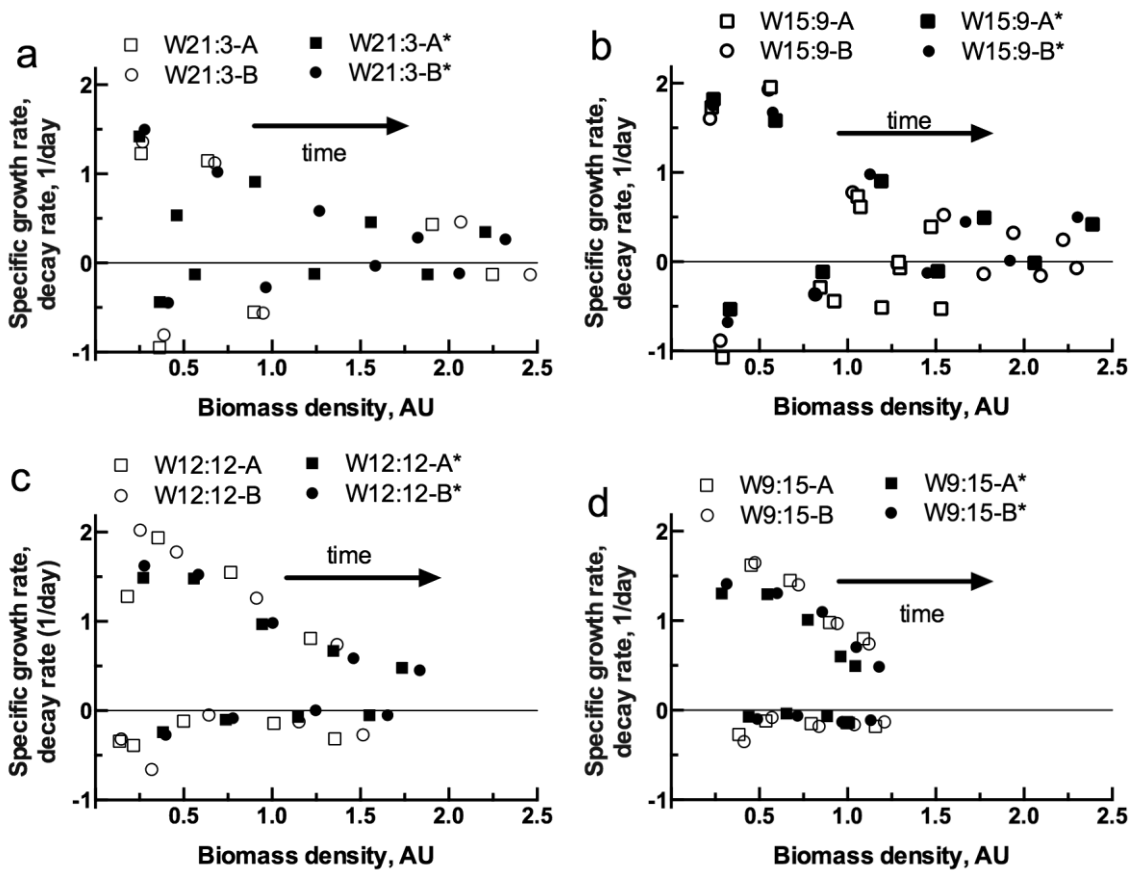

Figure 6.10: Comparison of Decay Rate During Dark Periods of Different Photoperiods with no Light (Open Symbols) and Illuminating Culture with 30 µE/m^2-s (Filled Symbols)

Adding a small bulb illuminating at nights blocks part of two bulbs, reduces the incident LI from 320 µE/m^2-s to 280 µE/m^2-s

Figure 6.11 presents the net specific growth rate in light and dark photoperiods with and without augmenting 30 µE/m^2-s at night. Each pair of the same photoperiod showed a comparable net value. Interference of additional light setup contributes to lower μ_{obs} during the day, results in less meaningful improvement when the net specific growth rate is considered.

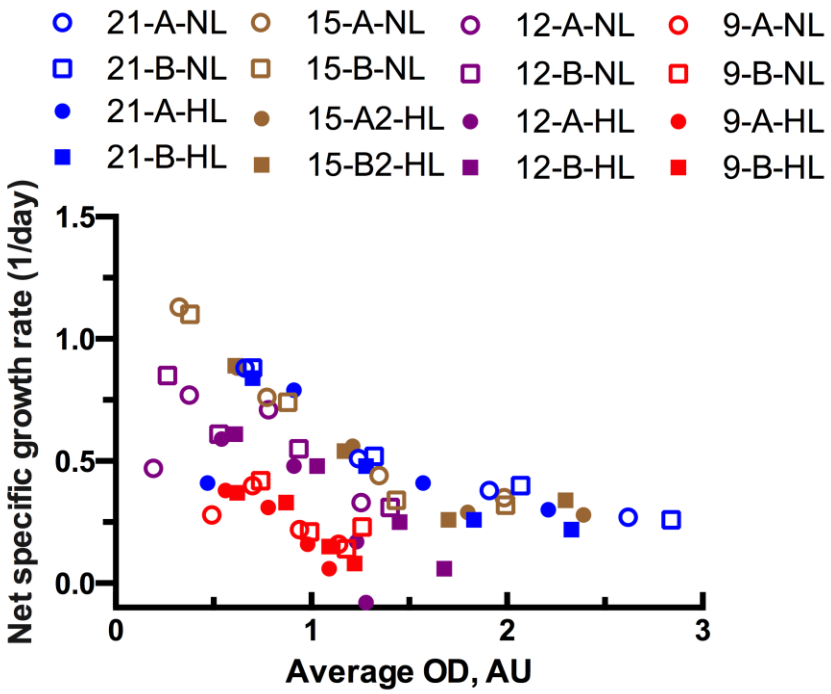

Figure 6.11: Net Specific Growth Rate over One Day Duration, Including Dark and Light Periods. The Open Symbols Gives Runs With Dark Periods (-NL) and the Filled Symbols Represents Runs Augmented with 30 µE/m^2-s at Night (-HL)
The numbers give the hour of light in each photoperiod

Figure 6.12 presents pH and DO data of unit A with a small light augmented at night. The patterns were identical to the experiments no light in night periods. Two differences were the drop of OD and pH during the nights were much less than the experiment without light augmentation.

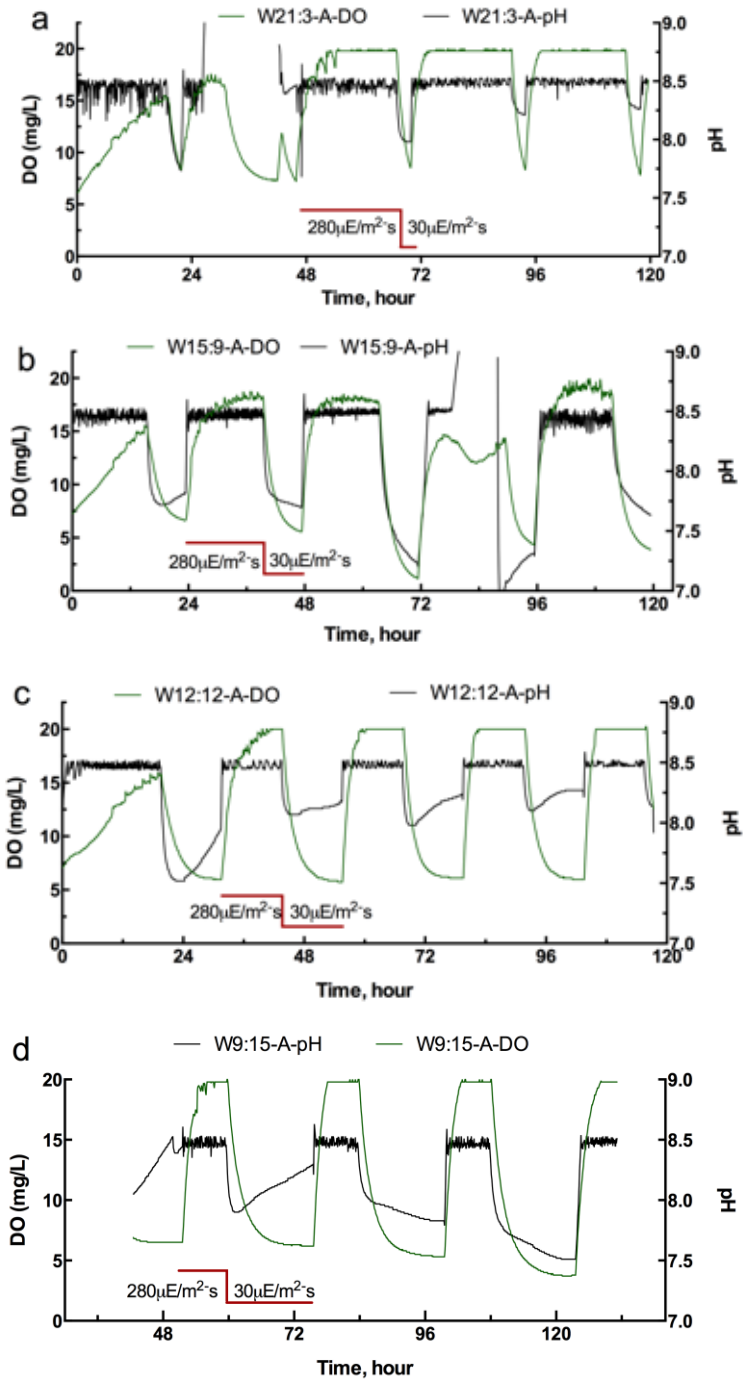

Figure 6.12: pH and DO with 30 µE/m^2-s Illuminated at Night

A lower incident LI (280 µE/m^2-s) resulted from the additional light bulbs inserted between the two T5 bulbs, reducing the surface of bulbs to emit photons during the day time

The small upward of pH during the nights indicates a net hydroxyl ion produced. This phenomenon was observed in beginning of each run and with all cycles of W12:12 (the third panel, **Figure 6.12**). A lower biomass density and a higher corresponding internal LI support a higher photosynthesis rate. However, that increment of pH was insufficient to increase DO or a net biomass production, which is also consistent with the C_i analysis. This highlights an advantage of pH probe as a monitoring tool. A 30 $\mu E/m^2$-s applied during the nights was minimal and aimed at reducing biomass loss as the mean to shorten for starting up PBR.

6.4 Synthesis and Application

In summary, batch-test experiments with laurate-excreting *Synechocystis* confirmed no significant loss of laurate during night periods. This outcome supports the gene modification to prevent re-uptake of fatty acid by this modified strain.

Experiments carried in pH-Stat PBRs revealed that biomass loss in the dark periods was significant, with specific decay rates ranging from 0.05 to 1.0/day. In some cases, the loss in the dark was as much as 40% of the gain in the preceding light period. The loss rate was higher with diluted biomass that also had higher growth rate; this correlation suggests that rapidly growing biomass has labile materials that are more rapidly oxidized for endogenous respiration. This interpretation is bolstered by the observation that the dissolved oxygen concentration and the pH dropped faster in the beginning of dark periods. The higher buffer intensity at pH 9.5, compared to pH 8.5, led to a more stable pH in the dark periods, particularly after significant biomass had grown and led to higher alkalinity and C_i.

Depleting the C_i concentration led to lower specific decay rates at night (0.03 – 0.40/day); this trend further supports the interpretation that rapid growth leads to readily oxidized organic materials.

Applying at night 10% of the daylight intensity reduced the dark-period loss rate significantly, even when the previous light-period growth rate was high. Thus, supplying a small amount of light at night has maximum benefits for low-density, fast-growing biomass, and this may be a good strategy for shortening the startup time and reducing the night loss of high productivity PBR.

7 SUMMARY, SIGNIFICANCE, AND FUTURE WORK

Techno-economic analyses make it clear that productivity of biomass and high-value products, i.e., laurate by the modified *Synechocystis*, improves economic feasibility and directly reduces per-unit production cost (Davis et al., 2011; Georgianna & Mayfield, 2012; Jones & Mayfield, 2012). Investigating growth conditions provides a framework to advance research and technology for photoautotrophic *Synechocystis* sp. PCC 6803. Starting from general understanding that this cyanobacterium strain has a versatile growth capability and employing different bench-scale experiments, my work systematically evaluates the conditions controlling autotrophic growth: light intensity, growth pH, and inorganic carbon concentration. Proper control of these factors can lead to maximum biomass productivity. In addition, this work evaluates electron partitioning in generic soluble biomass, particulate biomass, and lauric acid (by the modified strain).

The most important outcome of my work is my method to predict the Dissolved Inorganic Carbon (DIC) concentration as a function of the nitrogen source, growth pH, starting DIC, and biomass produced. On the one hand, this tool is essential for independently evaluating how growth pH and DIC affect the growth kinetics of microalgae grown in autotrophic mode. On the other hand, it provides a practical tool for manipulating these rate-controlling parameters to optimize the productivity and physiological condition of the microalgae.

The effects of Light Intensity (LI) can be divided to 3 régimes: photo-limitation, photo-saturation, and photo-inhibition. I started my research by evaluating these limits of photosynthesis and defining a working window of LI for *Synechocystis* (Chapter 2).

Using bench-scale batch experiments with continuous illumination, I found that photosynthesis of wild-type *Synechocystis* culture was photo-limited at an average internal LI ~5 $\mu E/m^2$-s and photo-inhibited at an incident LI of ~ 600 $\mu E/m^2$-s. A strain modified to excrete laurate has a similar incident LI for photo-limitation, but a smaller value (~ 350 $\mu E/m^2$-s) for photo-inhibition. This range defined LI windows for other experiments. Most of experiments I carried out later were with an average incident LI of 324 $\mu E/m^2$-s.

Photosynthesis uses light energy to fix electrons in organic compounds. Fixing the energy and electrons in the right type of organic material is of obvious importance for ensuring production of valuable outputs from photosynthesis. Photosynthesis by *Synechocystis* can generate particulate biomass, generic soluble organics, or specific organic products, such as laurate with the laurate-excreting strain. Of these, the general soluble microbial products have no known economic value; producing them is a waste of photosynthetically fixed energy and electrons. Generic soluble products also are food sources allowing invasive heterotrophs to proliferate.

I used the batch experiments with continuous illumination to evaluate the distribution of photosynthetically fixed electrons, assayed as Chemical Oxygen Demand (COD) (Chapter 3). Normalized to the total COD (TCOD), wild-type *Synechocystis* partitioned 75 to 84% of its TCOD into particulate biomass and 16 to 25% into generic Soluble Microbial Products (SMP). The laurate-excreting strain partitioned 6.6% to 10% of its TCOD into laurate, 21% to 30% in generic SMP, and 64% to 69% in particulate biomass. The greatest electron partitioning into SMP occurred with the highest LI tested,

which suggests that moderating the LI in the PBR is a promising mean to accentuate the production of valuable forms of photosynthetically fixed electrons.

Inorganic carbon is another key input that affects the rate of photosynthetic growth, since C comprises about 50% of the cell dry weight and 70% of the fixed electrons. pH and inorganic carbon are interconnected by the chemistry of the carbonate system; thus, the effect of inorganic carbon cannot be separated easily from the effects of pH. In Chapter 4, I predicted how biomass growth and pH controlled DIC using the proton condition (PC), a special mass to track acid-base equivalents. I experimentally validated the predictions using a pH-Stat PBR. I found that common nitrogen sources nitrate and ammonium affected C_i in drastically different ways. Nitrate uptake increased alkalinity and C_i, but ammonium uptake reduced alkalinity and C_i. This outcome led me to a novel approach to stabilize C_i by combining ammonium and nitrate as the N source. Equal uptake of ammonium and nitrate produced zero net change of alkalinity by the N source and stabilized the C_i concentration at a value I determined by addition of initial alkalinity.

The success of Chapter 4 made it possible for me to study the separate effects of pH and C_i on the growth of *Synechocystis*. pH was controlled by the pH-Stat, and the C_i was set by addition of alkalinity at the beginning the run. Carrying out growth experiments with wild-type and laurate-excreting strains at 30^{o}C and Average Internal LI (AILI) of 202 $\mu E/m^2$-s, I found that the two strains prefer pH = 8.5. A maximum specific growth rate of 2.4/day was attained with growth pH = 8.5 by the wild type, and it was 1.7/day for the modified strain. The lower μ_{max} of the laurate-excreting strain than the wild type is logical because the modification to excrete laurate that is diverted fixed

electrons to make laurate and more SMP. Using the sum of dissolved CO_2, carbonic acid, and bicarbonate to fit Monod kinetics, I found the half-maximum-rate concentrations (K_C) were 0.086 mM to 0.130 mM for the two strains. All K_C values are small, indicating that *Synechocystis* has a high affinity for inorganic carbon, and the specific growth rate approaches its maximum value by ~1 mM (12 mgC/L) for the wild type.

Continuing my investigation of light intensity, I studied the effects of light/dark photoperiods on biomass production (Chapter 6). Photoperiods simulated the diurnal cycles of outdoor settings, helping me to assess the impact of realistic variations of LI on microalgal production. I found that biomass production depended on the duration of illumination; different photoperiod-patterns did not have an impact of the production when it was normalized to the time of light exposure. I also focused on the respiration decay rate in night periods and found that the specific rate decay was significant, from 0.05 to 1.0 per day. Decay rates were higher in the culture having higher specific growth rate. DO and pH pattern during dark periods suggests high decay rate resulted from availability of internal products. As part of this study, I also was able to verify that deletion of the gene to prevent re-uptake laurate was effective, as laurate produced by the modified culture was maintained after four cycles of photoperiods.

Each microalgae strain brings its unique challenges for achieving its best growth conditions. While the quantitative details of my work are specific to *Synechocystis* sp. PCC 6803, my approach is applicable assessing growth characteristics of other photoautotrophs. It always is essential to understand the effects of light intensity, energy and electron partitioning, growth rate versus decay rate, and the effect of pH and

inorganic carbon. My work lays out the methods for doing the necessary characterizations.

I envision three especially promising areas for future research: (1) independently control C_i and mixing by using membrane carbonation, (2) expand automated control to biomass density, and (3) evaluate the effects of ammonium as the N source and an inhibitor at high pH. All three areas take advantage of the pH-Stat PBR that I established for independently controlling pH and C_i.

Area (1) is a continuation of work I carried out in Chapter 5 and 6. Conventional aeration keeps the biomass suspended and supplies C_i for photosynthesis by continuous injecting air into microalgae culture. Aeration by atmospheric air (at ~400 ppm CO_2) versus a concentrated source, such as flue gas from power plant (at ~ 100,000 to 150,000 ppm) could create very different fluid dynamics, turbulence, and shear forces. Higher turbulence and shear force with the more intense aeration using atmospheric air should promote mass transfer to the cell, and it may also lead to more detachment of Extracellular Polymeric Substances (EPS), with subsequent hydrolysis to SMP. The former effect may be desirable, but the latter is not desirable. Applying membrane carbonation (Kim, Marcus, Shin, & Rittmann, 2011) to supply C_i and submerged mixing to have independent control over each factor.

Relying on manual adjustment to achieve steady state biomass density is laborious and often ineffective. Deploying a turbidity sensor with multiple wavelengths provides an instant reading of corresponding biomass density and a basis to automatically adjust biomass density to a desired value (area (2)). Coupling such a Turbido-Stat to my

pH-Stat-offers more experimental control and may be practical and robust for outdoor setting.

Area (3) evaluates ammonium as the N source to grow biomass. For instance, utilizing ammonium in wastewater could be a win-win situation – providing nitrogen for microalgae biomass while removed N as a pollutant. However, ammonia, the conjugate base of ammonium, has been reported to be toxic to microalgae (Azov & Goldman, 1982). The acid-disassociation constant of ammonium/ammonia is ~9.3. This introduces a complexity when high growth pH is desired. Area (3) looks at the effect of ammonium as a potential "self-inhibitory" nutrient.

REFERENCES

Acién, F. G., Fernández, J. M., Magán, J. J., & Molina, E. (2012). Production cost of a real microalgae production plant and strategies to reduce it. *Biotechnology Advances*. Elsevier. doi:10.1016/j.biotechadv.2012.02.005

Adir, N., Zer, H., Shochat, S., & Ohad, I. (2003). Photoinhibition - a historical perspective. *Photosynthesis Research*, *76*(1-3), 343–70. doi:10.1023/A:1024969518145

Algenol. (2011). Direct to Ethanol | Algenol Biofuels. Retrieved October 5, 2014, from http://www.algenol.com/direct-to-ethanol/direct-to-ethanol

Amaro, H. M., Guedes, A. C., & Malcata, F. X. (2011). Advances and perspectives in using microalgae to produce biodiesel. *Applied Energy*, *88*(10), 3402–3410. doi:10.1016/j.apenergy.2010.12.014

Angermayr, S. A., Hellingwerf, K. J., Lindblad, P., & de Mattos, M. J. T. (2009). Energy biotechnology with cyanobacteria. *Current Opinion in Biotechnology*, *20*(3), 257–63. doi:10.1016/j.copbio.2009.05.011

Assayag, N., Rivé, K., Ader, M., Jézéquel, D., & Agrinier, P. (2006). Improved method for isotopic and quantitative analysis of dissolved inorganic carbon in natural water samples. *Rapid Communications in Mass Spectrometry : RCM*, *20*(15), 2243–2251. doi:10.1002/rcm.2585

Atchison, J. E., & Hettenhaus, J. R. (2004). *Innovative methods for corn stover collecting, handling, storing and transporting*. DTIC Document. Retrieved from http://www.dtic.mil/cgi-bin/GetTRDoc?Location=U2&doc=GetTRDoc.pdf&AD=ADA436531

Azov, Y. (1982). Effect of pH on inorganic carbon uptake in algal cultures. *Applied and Environmental Microbiology*, *43*(6), 1300–6. Retrieved from http://aem.asm.org/content/43/6/1300.short

Azov, Y., & Goldman, J. C. (1982). Free ammonia inhibition of algal photosynthesis in intensive cultures. *Applied and Environmental Microbiology*, *43*(4), 735–739. Retrieved from http://aem.asm.org/content/43/4/735.short

Badger, M., & Gallagher, A. (1987). Adaptation of Photosynthetic CO_2 and HCO_3^- Accumulation by the Cyanobacterium Synechococcus PCC6301 to Growth at Different Inorganic Carbon. *Functional Plant Biology*, 189–201. Retrieved from http://www.publish.csiro.au/?act=view_file&file_id=PP9870189.pdf

Badger, M. R. (2003). CO_2 concentrating mechanisms in cyanobacteria: molecular components, their diversity and evolution. *Journal of Experimental Botany*, *54*(383), 609–622. doi:10.1093/jxb/erg076

Badger, M. R., Palmqvist, K., & Yu, J.-W. (1994). Measurement of CO2 and HCO3- fluxes in cyanobacteria and microalgae during steady-state photosynthesis. *Physiologia Plantarum*, *90*(3), 529–536. doi:10.1111/j.1399-3054.1994.tb08811.x

Balat, M., & Balat, H. (2009). Recent trends in global production and utilization of bio-ethanol fuel. *Applied Energy*, *86*(11), 2273–2282. doi:10.1016/j.apenergy.2009.03.015

Balskus, E. P., & Walsh, C. T. (2010). The genetic and molecular basis for sunscreen biosynthesis in cyanobacteria. *Science (New York, N.Y.)*, *329*(5999), 1653–1656. doi:10.1126/science.1193637

Barbosa, M. J., & Wijffels, R. H. (2013). Biofuels from Microalgae. In *Handbook of Microalgal Culture: Applied Phycology and Biotechnology* (Vol. 24, pp. 566–577). doi:10.1002/9781118567166.ch29

Béchet, Q., Shilton, A., & Guieysse, B. (2013). Modeling the effects of light and temperature on algae growth: State of the art and critical assessment for productivity prediction during outdoor cultivation. *Biotechnology Advances*. doi:10.1016/j.biotechadv.2013.08.014

Belay, A. (1981). An Experimental Investigation of Inhibition of Phytoplankton Photosynthesis at Lake Surfaces. *New Phytologist*, *89*(1), 61–74. doi:10.1111/j.1469-8137.1981.tb04748.x

Belkin, S., & Boussiba, S. (1991). Resistance of *Spirulina platensis* to ammonia at high pH values. *Plant and Cell Physiology*, *32*(7), 953–958. Retrieved from http://pcp.oxfordjournals.org/content/32/7/953.abstract

Benemann, J., Woertz, I., & Lundquist, T. (2012). Life Cycle Assessment for Microalgae Oil Production. *Disruptive Science and Technology*, *1*(2), 68–78. doi:10.1089/dst.2012.0013

Bérubé, K. A., Dodge, J. D., & Ford, T. W. (1999). Effects of chronic salt stress on the ultrastructure of *Dunaliella bioculata* (Chlorophyta, Volvocales): mechanisms of response and recovery. *European Journal of Phycology*. Cambridge Univ Press. doi:10.1017/S0967026299002085

Blankenship, R. (2008). *Molecular mechanisms of photosynthesis*. Wiley. com. Retrieved from http://books.google.com/books?hl=en&lr=&id=jvQw22ykyeIC&oi=fnd&pg=PP8&dq=Molecular+mechanisms+of+photosynthesis&ots=6XBWIFjtSR&sig=sZctRVTa028anjWLcr971g-7cWE

Blankenship, R. E. (2010). Early evolution of photosynthesis. *Plant Physiology*, *154*(2), 434–8. doi:10.1104/pp.110.161687

Boddiger, D. (2007). Boosting biofuel crops could threaten food security. *Lancet*, *370*(9591), 923–924. doi:10.1016/S0140-6736(07)61427-5

Bouterfas, R., Bouterfas, R., Belkoura, M., Belkoura, M., Dauta, A., & Dauta, A. (2002). Light and temperature effects on the growth rate of three freshwater algae isolated from a eutrophic lake. *Hydrobiologia*, *25*(489), 207–217.

Bown, Al. W. (1985). CO2 and intracellular pH. *Plant, Cell and Environment*, *8*(6), 459–465. doi:10.1111/j.1365-3040.1985.tb01681.x

BP. (2013). BP Statistical Review of World Energy. Retrieved from http://www.bp.com/content/dam/bp/pdf/statistical-review/statistical_review_of_world_energy_2013.pdf

Brennan, L., & Owende, P. (2010). Biofuels from microalgae—A review of technologies for production, processing, and extractions of biofuels and co-products. *Renewable and Sustainable Energy Reviews*, *14*(2), 557–577. doi:10.1016/j.rser.2009.10.009

Brenner, M., Bildsten, L., Dyson, F., & Fortson, N. (2006). Engineering Microorganisms for Energy Production. DTIC Document. Retrieved from http://oai.dtic.mil/oai/oai?verb=getRecord&metadataPrefix=html&identifier=ADA457082

Brewer, P. G., & Goldman, J. C. (1976). Alkalinity changes generated by phytoplankton growth. *Limnology and Oceanography*, *21*(January), 108–117. doi:10.4319/lo.1976.21.1.0108

Brown, L. (2008). Why Ethanol Production Will Drive World Food Prices Even Higher in 2008. *Earth Policy Institute*. Retrieved from http://www.earth-policy.org/plan_b_updates/2008/update69

Burger, J., & Edwards, G. E. (1996). Photosynthetic Efficiency, and Photodamage by UV and Visible Radiation, in Red versus Green Leaf Coleus Varieties. *Plant and Cell Physiology*, *37*(3), 395–399. doi:10.1093/oxfordjournals.pcp.a028959

Campbell, P. K., Beer, T., & Batten, D. (2011). Life cycle assessment of biodiesel production from microalgae in ponds. *Bioresource Technology*, *102*(1), 50–56. doi:10.1016/j.biortech.2010.06.048

Cheng, Y.-C., & Fleming, G. R. (2009). Dynamics of light harvesting in photosynthesis. *Annual Review of Physical Chemistry*, *60*, 241–262. doi:10.1146/annurev.physchem.040808.090259

Chisti, Y. (2007). Biodiesel from microalgae. *Biotechnology Advances*, *25*(3), 294–306. doi:10.1016/j.biotechadv.2007.02.001

Chisti, Y. (2008). Biodiesel from microalgae beats bioethanol. *Trends in Biotechnology*, *26*(3), 126–31. doi:10.1016/j.tibtech.2007.12.002

Cho, H., & Cronan, J. E. (1995). Defective export of a periplasmic enzyme disrupts regulation of fatty acid synthesis. *Journal of Biological Chemistry*, *270*(9), 4216–4219. doi:10.1074/jbc.270.9.4216

Chynoweth, D. P., Owens, J. M., & Legrand, R. (2000). Renewable methane from anaerobic digestion of biomass. *Renewable Energy*, *22*(1-3), 1–8. doi:10.1016/S0960-1481(00)00019-7

Clark, D. R., & Flynn, K. J. (2000). The relationship between the dissolved inorganic carbon concentration and growth rate in marine phytoplankton. *Proceedings. Biological Sciences / The Royal Society*, *267*(1447), 953–9. doi:10.1098/rspb.2000.1096

Danielsen, F., Beukema, H., Burgess, N. D., Parish, F., Brühl, C. a, Donald, P. F., … Fitzherbert, E. B. (2009). Biofuel plantations on forested lands: double jeopardy for biodiversity and climate. *Conservation Biology : The Journal of the Society for Conservation Biology*, *23*(2), 348–58. doi:10.1111/j.1523-1739.2008.01096.x

Davis, R., Aden, A., & Pienkos, P. T. (2011). Techno-economic analysis of autotrophic microalgae for fuel production. *Applied Energy*, *88*(10), 3524–3531. doi:10.1016/j.apenergy.2011.04.018

Deo, R. P., Songkasiri, W., Rittmann, B. E., & Reed, D. T. (2010). Surface complexation of Neptunium(V) onto whole cells and cell components of *Shewanella* alga: modeling and experimental study. *Environmental Science & Technology*, *44*(13), 4930–5. doi:10.1021/es9035336

DiPardo, J. (2000). Outlook for biomass ethanol production and demand. US Energy Information Administration. Www. Eia. Doe. Gov/oiaf/analysis Paper/pdf/biomass. Pdf.

Donot, F., Fontana, a., Baccou, J. C., & Schorr-Galindo, S. (2012). Microbial exopolysaccharides: Main examples of synthesis, excretion, genetics and extraction. *Carbohydrate Polymers*, *87*(2), 951–962. doi:10.1016/j.carbpol.2011.08.083

Dubinsky, Z., & Berman-Frank, I. (2001). Uncoupling primary production from population growth in photosynthesizing organisms in aquatic ecosystems. *Aquatic Sciences*. Springer. doi:10.1007/PL00001343

Ducat, D. C., Way, J. C., & Silver, P. a. (2011). Engineering cyanobacteria to generate high-value products. *Trends in Biotechnology*, *29*(2), 95–103. doi:10.1016/j.tibtech.2010.12.003

Dunlap, W. C., & Shick, J. M. (1998). Ultraviolet Radiation-Absorbing Mycosporine-Like Amino Acids in Coral Reef Organisms: a Biochemical and Environmental Perspective. *Journal of Phycology*, *34*(3), 418–430. doi:10.1046/j.1529-8817.1998.340418.x

EIA, U. S. (2013). *Annual Energy Outlook 2013 with Projection 2040*. Retrieved from http://www.eia.gov/forecasts/aeo/pdf/0383(2013).pdf

Emerson, R. (1958). The Quantum Yield of Photosynthesis. *Annual Review of Plant Physiology*, *9*(1), 1–24. doi:10.1146/annurev.pp.09.060158.000245

Emerson, R., & Arnold, W. (1932). The photochemical reaction in photosyntheis. *The Journal of General Physiology*, *16*(2), 191–205. doi:10.1085/jgp.16.2.191

Emerson, R., & Green, L. (1938). Effect of hydrogen-ion concentration on *Chlorella* photosynthesis. *Plant Physiology*, *13*(1), 157–168. doi:10.1104/pp.13.1.157

Emerson, R., & Lewis, C. M. (1943). The Dependence of the Quantum Yield of *Chlorella* Photosynthesis on Wave Lenghth of Light. *American Journal of Botany*. JSTOR. doi:10.2307/2437236

Engineering ToolBox. (2015). Relative Permittivity - Dielectric Constant. Retrieved January 1, 2015, from http://www.engineeringtoolbox.com/relative-permittivity-d_1660.html

Escobar, J. C., Lora, E. S., Venturini, O. J., Yáñez, E. E., Castillo, E. F., & Almazan, O. (2009). Biofuels: Environment, technology and food security. *Renewable and Sustainable Energy Reviews*, *13*(6-7), 1275–1287. doi:10.1016/j.rser.2008.08.014

Evans, J. (1987). The Dependence of Quantum Yield on Wavelength and Growth Irradiance. *Australian Journal of Plant Physiology*. CSIRO. doi:10.1071/PP9870069

FAOSTAT. (2013). The FAO Statistical Programme of Work. Retrieved from http://faostat3.fao.org/faostat-gateway/go/to/browse/R/RL/E

Fargione, J., Hill, J., Tilman, D., Polasky, S., & Hawthorne, P. (2008). Land clearing and the biofuel carbon debt. *Science (New York, N.Y.)*, *319*(5867), 1235–8. doi:10.1126/science.1152747

Fay, P., Stewart, W. D., Walsby, A. E., & Fogg, G. E. (1968). Is the heterocyst the site of nitrogen fixation in blue-green algae? *Nature*, *220*(5169), 810–812. doi:10.1038/220810b0

Feher, G., Allen, J. P., Okamura, M. Y., & Rees, D. C. (1989). Structure and function of bacterial photosynthetic reaction centres. *Nature*. doi:10.1038/339111a0

Fernández, F. G., Camacho, F. G., Pérez, J. a, Sevilla, J. M., & Grima, E. M. (1997). A model for light distribution and average solar irradiance inside outdoor tubular photobioreactors for the microalgal mass culture. *Biotechnology and Bioengineering*, *55*(5), 701–14. doi:10.1002/(SICI)1097-0290(19970905)55:5<701::AID-BIT1>3.0.CO;2-F

Fernández, I., Acién, F. G., Fernández, J. M., Guzmán, J. L., Magán, J. J., & Berenguel, M. (2012). Dynamic model of microalgal production in tubular photobioreactors. *Bioresource Technology*, *126*, 172–81. doi:10.1016/j.biortech.2012.08.087

Fischer, G. (2009). *Biofuels and food security*. Retrieved from http://agris.fao.org/agris-search/search.do?recordID=US201300139900

Fourest, E., & Volesky, B. (1996). Contribution of sulfonate groups and alginate to heavy metal biosorption by the dry biomass of *Sargassum fluitans*. *Environmental Science and Technology*, *30*(1), 277–282. doi:10.1021/es950315s

Foy, R. H., & Smith, R. V. (1980). The role of carbohydrate accomulation in the growth of planktonic *Oscillatoria* species. *British Phycological Journal*. doi:10.1080/00071618000650161

Gao, Q., Wang, W., Zhao, H., & Lu, X. (2012). Effects of fatty acid activation on photosynthetic production of fatty acid-based biofuels in *Synechocystis* sp. PCC6803. *Biotechnology for Biofuels*. doi:10.1186/1754-6834-5-17

Garcia-Pichel, F., Wingard, C. E., & Castenholz, R. W. (1993). Evidence regarding the ultraviolett sunscreen role of the Mycosporin-like compounds in the cyanobacterium *Gloeocapsa* sp. *Applied and Environment Microbiology*, *59*(1), 170–176. Retrieved from http://aem.asm.org/content/59/1/170.short

Ge, H., Xia, L., Zhou, X., Zhang, D., & Hu, C. (2014). Effects of light intensity on components and topographical structures of extracellular polysaccharides from the cyanobacteria *Nostoc* sp. *Journal of Microbiology (Seoul, Korea)*, *52*(2), 179–83. doi:10.1007/s12275-014-2720-5

Ge, H., Zhang, J., Zhou, X., Xia, L., & Hu, C. (2014). Effects of light intensity on components and topographical structures of extracellular polymeric substances from *Microcoleus vaginatus* (Cyanophyceae). *Phycologia*, *53*(2), 167–173. doi:10.2216/13-163.1

Geesey, G. (1982). Microbial exopolymers: Ecological and economic considerations. *ASM American Society for Microbiology News*, *48*(1), 9–14.

Geider, R. J., & Osborne, B. A. (1989). Respiration and microalgal growth: a review of the quantitative relationship between dark respiration and growth. *New Phytologist*, *112*(3), 327–341. doi:10.1111/j.1469-8137.1989.tb00321.x

Georgianna, D. R., & Mayfield, S. P. (2012). Exploiting diversity and synthetic biology for the production of algal biofuels. *Nature*. doi:10.1038/nature11479

Giordano, M., Beardall, J., & Raven, J. a. (2005). CO_2 concentrating mechanisms in algae: mechanisms, environmental modulation, and evolution. *Annual Review of Plant Biology*, *56*, 99–131. doi:10.1146/annurev.arplant.56.032604.144052

Glassner, D., Hettenhaus, J., & Schechinger, T. (1998). Corn stover collection project. In *BioEnergy'98—Expanding Bioenergy Partnerships: Proceedings* (Vol. 2, pp. 1100–1110). Retrieved from http://lanshark.ctic.purdue.edu/Core4/bio98paper.pdf

Goldman, J., Azov, Y., Riley, C., & Dennett, M. (1982). The effect of pH in intensive microalgal cultures. I. Biomass regulation. *Journal of Experimental …*, *57*, 1–13. Retrieved from http://www.sciencedirect.com/science/article/pii/002209818290140X

Goldman, J. C., Dennett, M. R., & Carol, B. (1981). Inorganic Carbon Sources and Biomass Regulation in Intensive Microalgal Cultures. *Biotechnology and Bioengineering*, *23*(5), 995–1014. doi:10.1002/bit.260230508

Goldman, J. C., Dennett, M. R., & Riley, C. B. (1982). Effect of nitrogen-mediated changes in alkalinity on pH control and CO(2) supply in intensive microalgal cultures. *Biotechnology and Bioengineering*, *24*(3), 619–631. doi:10.1002/bit.260240308

Goldman, J. C. J. (1979a). Outdoor algal mass cultures—I. Applications. *Water Research*, *13*(1), 1–19. Retrieved from http://www.sciencedirect.com/science/article/pii/0043135479902495

Goldman, J. C. J. (1979b). Outdoor algal mass cultures—II. Photosynthetic yield limitations. *Water Research*, *13*(2), 119–136. Retrieved from http://www.annualreviews.org/doi/pdf/10.1146/annurev.pp.09.060158.000245

Goldman, J. C., Oswald, W. J., Jenkins, D., & Oswald, J. (1974). The kinetics of inorganic carbon limited algal growth. *Journal (Water Pollution Control Federation)*, *46*(3), 554–574. Retrieved from http://www.jstor.org/stable/25038157

Goldman, J. C., Porcella, D. B., Joe Middlebrooks, E., & Toerien, D. F. (1972). The effect of carbon on algal growth—Its relationship to eutrophication. *Water Research*, *6*(1960), 637–679. doi:10.1016/0043-1354(72)90182-0

Goldman, J., Riley, C., & Dennett, M. (1982). The effect of pH in intensive microalgal cultures. II. Species competition. *Journal of Experimental Marine …*, *57*, 15–24. Retrieved from http://www.sciencedirect.com/science/article/pii/0022098182901411

Grigorieva, Grigorieva, G., & Shestakov, S. (1981). Transformation in the cyanobacterium *Synechocystis* sp. PCC 6803. *FEMS Microbiology Letters*, *13*(4), 367–370. Retrieved from http://www.ncbi.nlm.nih.gov/pubmed/12040098

Grima, E., Sevilla, J., Pérez, J., & Camacho, F. (1996). A study on simultaneous photolimitation and photoinhibition in dense microalgal cultures taking into account incident and averaged irradiances. *Journal of Biotechnology*, *45*, 59–69. Retrieved from http://www.sciencedirect.com/science/article/pii/0168165695001441

Grobbelaar, J. U. (2004). Algal Nutrition - Mineral Nutrition. In *Handbook of Microalgal Culture* (pp. 95–115). Oxford, UK: Blackwell Publishing Ltd. doi:10.1002/9780470995280.ch6

Grobbelaar, J. U., & Soeder, C. J. (1985). Respiration losses in planktonic green algae cultivated in raceway ponds. *Journal of Plankton Research*, *7*(4), 497–506.

Hach. (2014). COD. Retrieved September 17, 2014, from http://www.hach.com/chemical-oxygen-demand-cod-reagent-tntplus-hr-25-tests/product-downloads?id=7640193976&callback=qs

Hall, D. O., Markov, S. A., Watanabe, Y., & Krishna Rao, K. (1995). The potential applications of cyanobacterial photosynthesis for clean technologies. *Photosynthesis Research*, *46*(1-2), 159–167. doi:10.1007/BF00020426

Hall, D. O., Rao, K., Biology, I. of, & of Biology, I. (1999). *Photosynthesis*. Cambridge University Press. Retrieved from http://books.google.com/books?id=6F7yuf1Sj30C

Harto, C., Meyers, R., & Williams, E. (2010). Life cycle water use of low-carbon transport fuels. *Energy Policy*, *38*(9), 4933–4944. doi:10.1016/j.enpol.2010.03.074

Harun, R., Davidson, M., Doyle, M., Gopiraj, R., Danquah, M., & Forde, G. (2011). Technoeconomic analysis of an integrated microalgae photobioreactor, biodiesel and biogas production facility. *Biomass and Bioenergy*, *35*(1), 741–747. doi:10.1016/j.biombioe.2010.10.007

Heaton, E. A., Dohleman, F. G., & Long, S. P. (2008). Meeting US biofuel goals with less land: The potential of *Miscanthus*. *Global Change Biology*, *14*(9), 2000–2014. doi:10.1111/j.1365-2486.2008.01662.x

Hill, J., Nelson, E., Tilman, D., Polasky, S., & Tiffany, D. (2006). Environmental, economic, and energetic costs and benefits of biodiesel and ethanol biofuels. *Proceedings of the National Academy of Sciences of the United States of America*, *103*(30), 11206–10. doi:10.1073/pnas.0604600103

Howard, T. P., Middelhaufe, S., Moore, K., Edner, C., Kolak, D. M., Taylor, G. N., … Love, J. (2013). Synthesis of customized petroleum-replica fuel molecules by targeted modification of free fatty acid pools in *Escherichia coli*. *Proceedings of the National Academy of Sciences of the United States of America*, *110*(19), 7636–41. doi:10.1073/pnas.1215966110/-/DCSupplemental.www.pnas.org/cgi/doi/10.1073/pnas.1215966110

Hu, Q., Kurano, N., Kawachi, M., Iwasaki, I., & Miyachi, S. (1998). Ultrahigh-cell-density culture of a marine green alga Chlorococcum littorale in a flat-plate photobioreactor. *Applied Microbiology and Biotechnology*, *49*(6), 655–662. doi:10.1007/s002530051228

Hu, Q., Sommerfeld, M., Jarvis, E., Ghirardi, M., Posewitz, M., Seibert, M., & Darzins, A. (2008). Microalgal triacylglycerols as feedstocks for biofuel production: perspectives and advances. *The Plant Journal : For Cell and Molecular Biology*, *54*(4), 621–39. doi:10.1111/j.1365-313X.2008.03492.x

Huner, N. P. A., Öquist, G., Hurry, V. M., Krol, M., Falk, S., & Griffith, M. (1993). Photosynthesis, photoinhibition and low temperature acclimation in cold tolerant plants. *Photosynthesis Research*. Springer. doi:10.1007/BF02185436

Huntley, M. E., & Redalje, D. G. (2006). CO_2 Mitigation and Renewable Oil from Photosynthetic Microbes: A New Appraisal. Mitigation and Adaptation Strategies for Global Change (Vol. 12). doi:10.1007/s11027-006-7304-1

Ikeuchi, M., & Tabata, S. (2001). *Synechocystis* sp. PCC 6803 - a useful tool in the study of the genetics of cyanobacteria. *Photosynthesis Research*, *70*(1), 73–83. doi:10.1023/A:1013887908680

Jensen, S., & Knutsen, G. (1993). Influence of light and temperature on photoinhibition of photosynthesis in *Spirulina platensis*. *Journal of Applied Phycology*. Springer. doi:10.1007/BF02182508

Jones, C. S., & Mayfield, S. P. (2012). Algae biofuels: Versatility for the future of bioenergy. *Current Opinion in Biotechnology*, *23*(3), 346–351. doi:10.1016/j.copbio.2011.10.013

Kaczmarzyk, D., & Fulda, M. (2010). Fatty acid activation in cyanobacteria mediated by acyl-acyl carrier protein synthetase enables fatty acid recycling. *Plant Physiology*, *152*(3), 1598–1610. doi:10.1104/pp.109.148007

Kaneko, T., Sato, S., Kotani, H., Tanaka, A., Asamizu, E., Nakamura, Y., … Tabata, S. (1996). Sequence analysis of the genome of the unicellular cyanobacterium *Synechocystis* sp. strain PCC6803. II. Sequence determination of the entire genome and assignment of potential protein-coding regions. *DNA Research : An International Journal for Rapid Publication of Reports on Genes and Genomes*, *3*(3), 109–136. doi:10.1093/dnares/3.3.109

Kazi, F. K., Fortman, J. A., Anex, R. P., Hsu, D. D., Aden, A., Dutta, A., & Kothandaraman, G. (2010). Techno-economic comparison of process technologies for biochemical ethanol production from corn stover. *Fuel*, *89*(SUPPL. 1), S20–S28. doi:10.1016/j.fuel.2010.01.001

Kezhen, Y., Gilmour, D., J., & Zimmerman, W., B. (2014). Effects of CO_2 and pH on Growth of the Microalga *Dunaliella salina*. *Journal of Microbial & Biochemical Technology*, *06*(03), 167–173. doi:10.4172/1948-5948.1000138

Khanna, M., Dhungana, B., & Clifton-Brown, J. (2008). Costs of producing *Miscanthus* and switchgrass for bioenergy in Illinois. *Biomass and Bioenergy*, *32*(6), 482–493. doi:10.1016/j.biombioe.2007.11.003

Kim, H. W., Marcus, A. K., Shin, J. H., & Rittmann, B. E. (2011). Advanced control for photoautotrophic growth and CO2-utilization efficiency using a membrane carbonation photobioreactor (MCPBR). *Environmental Science and Technology*, *45*(11), 5032–5038. doi:10.1021/es104235v

Kim, H. W., Vannela, R., & Rittmann, B. E. (2013). Responses of *Synechocystis* sp. PCC 6803 to total dissolved solids in long-term continuous operation of a photobioreactor. *Bioresource Technology*, *128*, 378–84. doi:10.1016/j.biortech.2012.10.046

Kim, H. W., Vannela, R., Zhou, C., Harto, C., & Rittmann, B. E. (2010). Photoautotrophic nutrient utilization and limitation during semi-continuous growth of *Synechocystis* sp. PCC6803. *Biotechnology and Bioengineering*, *106*(4), 553–63. doi:10.1002/bit.22724

Kim, H. W., Vannela, R., Zhou, C., & Rittmann, B. E. (2011). Nutrient acquisition and limitation for the photoautotrophic growth of *Synechocystis* sp. PCC6803 as a renewable biomass source. *Biotechnology and Bioengineering*, *108*(2), 277–85. doi:10.1002/bit.22928

Klock, J.-H., Wieland, A., Seifert, R., & Michaelis, W. (2007). Extracellular polymeric substances (EPS) from cyanobacterial mats: characterisation and isolation method optimisation. *Marine Biology*, *152*(5), 1077–1085. doi:10.1007/s00227-007-0754-5

Kok, B. (1956). On the inhibition of photosynthesis by intense light. *Biochimica et Biophysica Acta*, *21*(2), 234–244. doi:10.1016/0006-3002(56)90003-8

Kratz, W. A., & Myers, J. (1955). Photosynthesis and Respiration of Three Blue-Green Algae. *Plant Physiology*, *30*(3), 275. Retrieved from http://www.ncbi.nlm.nih.gov/pmc/articles/PMC540644/

Krause, G. H. (1988). Photoinhibition of photosynthesis. An evaluation of damaging and protective mechanisms. *Physiologia Plantarum*, *74*(3), 566–574. doi:doi: 10.1111/j.1399-3054.1988.tb02020.x

Krauss, R. W. (1953). Inorganic nutrition of algae. *Algal Culture from Laboratory to Pilot Plant. Carnegie Inst. Wash. Publ*, *600*, 85–102. Retrieved from http://publicationsonline.carnegiescience.edu/publications_online/algal_culture.pdf#page=96

Lamparter, T., Mittmann, F., Gärtner, W., Börner, T., Hartmann, E., & Hughes, J. (1997). Characterization of recombinant phytochrome from the cyanobacterium Synechocystis. *Proceedings of the National Academy of Sciences of the United States of America*, *94*(22), 11792–11797. doi:10.1073/pnas.94.22.11792

Lardon, L., Hélias, A., Sialve, B., Steyer, J.-P., Bernard, O., Hélias, A., … Steyer, J.-P. (2009). Life-cycle assessment of biodiesel production from microalgae. *Policy Analysis*, *43*(17), 6475–6481. doi:10.1021/es900705j

Larsen, T. A., Udert, K. M., & Lienert, J. (2013). *Source Separation and Decentralization for Wastewater Management*. *IWA Publishing*. Iwa Publishing. Retrieved from http://www.iwapublishing.com/books/9781843393481/source-separation-and-decentralization-wastewater-management

Larson, W. E., Holt, R. F., & Carlson, C. W. (1978). Residues for soil conservation. *Crop Residue Management Systems*, (cropresiduemana), 1–15. Retrieved from https://dl.sciencesocieties.org/publications/books/abstracts/asaspecialpubli/cropresiduemana/1

Laspidou, C. (2002). A unified theory for extracellular polymeric substances, soluble microbial products, and active and inert biomass. *Water Research*, *36*(11), 2711–2720. doi:10.1016/S0043-1354(01)00413-4

Lee, J.-Y., Yoo, C., Jun, S.-Y., Ahn, C.-Y., & Oh, H.-M. (2010). Comparison of several methods for effective lipid extraction from microalgae. *Bioresource Technology*, *101*(1), S75–S77. doi:10.1016/j.biortech.2009.03.058

Leuenberger, M., Siegenthaler, U., & Langway, C. (1992). Carbon isotope composition of atmospheric CO_2 during the last ice age from an Antarctic ice core. *Nature*. Nature Publishing Group. doi:10.1038/357488a0

Li, Z., Wakao, S., Fischer, B. B., & Niyogi, K. K. (2009). Sensing and responding to excess light. *Annual Review of Plant Biology*, *60*, 239–260. doi:10.1146/annurev.arplant.58.032806.103844

Lindstrom, M. J., Gupta, S. C., Onstad, C. A., Larson, W. E., & Holt, R. F. (1979). Tillage and crop residue effects on soil erosion in the Corn Belt [USA]. *Journal of Soil and Water Conservation*, *34*. Retrieved from http://agris.fao.org/agris-search/search.do?recordID=US7913771

Liu, X., Sheng, J., & Curtiss, R. (2011). Fatty acid production in genetically modified cyanobacteria. *Proceedings of the National Academy of Sciences of the United States of America*, *108*(17), 6899–904. doi:10.1073/pnas.1103014108

Lloyd, N. D. H. N., Canvin, D. D. T., & Culver, D. A. (1977). Photosynthesis and photorespiration in algae. *Plant Physiology*, *59*(5), 936–940. Retrieved from http://www.plantphysiol.org/content/59/5/936.short

Long, B. M., Rae, B. D., Badger, M. R., & Price, G. D. (2011). Over-expression of the β-carboxysomal CcmM protein in *Synechococcus* PCC7942 reveals a tight co-regulation of carboxysomal carbonic anhydrase (CcaA) and M58 content. *Photosynthesis Research*, *109*(1-3), 33–45. doi:10.1007/s11120-011-9659-8

Mallick, N. (2002). Biotechnological potential of immobilized algae for wastewater N, P and metal removal: A review. *BioMetals*, *15*(4), 377–390. doi:10.1023/A:1020238520948

Marra, J. (1980). Time course of light intensity adaptation in a marine diatom. *Mar. Biol. Lett*, *1*, 175–183. Retrieved from http://www.researchgate.net/publication/237050663_Time_course_of_light_intensity_adaptation_in_a_marine_diatom/file/72e7e51b0aee55f18f.pdf

Marsh & McLennan Companies, Swiss Re, Zurich Insurance Group, National University of Singapore, Oxford Martin School - University of Oxford, & Pennsylvania, W. R. M. and D. P. C.-U. of. (2014). *Global Risks 2014*. Retrieved from http://www3.weforum.org/docs/WEF_GlobalRisks_Report_2014.pdf

Mata, T. M., Martins, A. a., & Caetano, N. S. (2010). Microalgae for biodiesel production and other applications: A review. *Renewable and Sustainable Energy Reviews*, *14*(1), 217–232. doi:10.1016/j.rser.2009.07.020

Matheickal, J. T., Yu, Q., & Woodburn, G. M. (1999). Biosorption of cadmium(II) from aqueous solutions by pre-treated biomass of marine alga *Durvillaea potatorum*. *Water Research*, *33*(2), 335–342. doi:10.1016/S0043-1354(98)00237-1

Mayo, A. (1997). Effects of temperature and pH on the kinetic growth of unialga *Chlorella vulgaris* cultures containing bacteria. *Water Environment Research*, *69*(1), 64–72. Retrieved from http://www.ingentaconnect.com/content/wef/wer/1997/00000069/00000001/art00009

Mayo, W. P., Williams, T. G., Birch, D. G., & Turpin, D. H. (1986). Photosynthetic Adaptation by *Synechococcus leopoliensis* in Response to Exogenous Dissolved Inorganic Carbon. *Plant Physiology*, *80*(4), 1038–1040. doi:10.1104/pp.80.4.1038

McCree, K. J. (1972). Test of current definitions of photosynthetically active radiation against leaf photosynthesis data. *Agricultural Meteorology*, *10*, 443–453.

McGinn, P., & Price, G. (2003). Carbon limitation and light control the expression of transcripts related to the CO_2-concentrating mechanism in the cyanobacterium Synechocystis sp. strain PCC6803. *Plant Physiology*, *132*, 218–229. doi:10.1104/pp.102.019349.electron

Melis, A. (2009). Solar energy conversion efficiencies in photosynthesis: Minimizing the chlorophyll antennae to maximize efficiency. *Plant Science*, *177*(4), 272–280. doi:10.1016/j.plantsci.2009.06.005

Merkey, B. V, Rittmann, B. E., & Chopp, D. L. (2009). Modeling how soluble microbial products (SMP) support heterotrophic bacteria in autotroph-based biofilms. *Journal of Theoretical Biology*, *259*(4), 670–683. doi:10.1016/j.jtbi.2009.05.010

Meseck, S. L., Alix, J. H., & Wikfors, G. H. (2005). Photoperiod and light intensity effects on growth and utilization of nutrients by the aquaculture feed microalga, *Tetraselmis chui* (PLY429). *Aquaculture*, *246*(1-4), 393–404. doi:10.1016/j.aquaculture.2005.02.034

Miller, A., Turpin, D., & Canvin, D. (1984). Growth and photosynthesis of the cyanobacterium Synechococcus leopoliensis in HCO_3^--limited chemostats. *Plant Physiology*, *75*, 1064–1070. Retrieved from http://www.plantphysiol.org/content/75/4/1064.short

Mittler, R. (2002). Oxidative stress, antioxidants and stress tolerance. *Trends in Plant Science*, *7*(9), 405–410. doi:10.1016/S1360-1385(02)02312-9

Moheimani, N. R. (2013). Inorganic carbon and pH effect on growth and lipid productivity of *Tetraselmis suecica* and *Chlorella* sp (Chlorophyta) grown outdoors in bag photobioreactors. *Journal of Applied Phycology*, *25*(2), 387–398. doi:10.1007/s10811-012-9873-6

Moheimani, N. R., & Borowitzka, M. A. (2011). Increased CO2 and the effect of pH on growth and calcification of Pleurochrysis carterae and Emiliania huxleyi (Haptophyta) in semicontinuous cultures. *Applied Microbiology and Biotechnology*, *90*(4), 1399–1407. doi:10.1007/s00253-011-3174-x

Molina Grima, E., Belarbi, E.-H., Acién Fernández, F. . G., Robles Medina, A., & Chisti, Y. (2003). Recovery of microalgal biomass and metabolites: process options and economics. *Biotechnology Advances*, *20*(7-8), 491–515. doi:10.1016/S0734-9750(02)00050-2

Morel, F., & Morgan, J. (1972). A numerical method for computing equilibria in aqueous chemical systems. *Environmental Science & Technology*, *6*(1), 58–67. doi:10.1021/es60060a006

Moreno, J., Vargas, M. A., Olivares, H., Rivas, J., & Guerrero, M. G. (1998). Exopolysaccharide production by the cyanobacterium *Anabaena* sp. ATCC 33047 in batch and continuous culture. *Journal of Biotechnology*, *60*(3), 175–182. doi:10.1016/S0168-1656(98)00003-0

Moroney, J. V, & Ynalvez, R. A. (2007). Proposed carbon dioxide concentrating mechanism in *Chlamydomonas reinhardtii*. *Eukaryotic Cell*. Am Soc Microbiol. doi:10.1128/EC.00064-07

Nakamura, Y., Kaneko, T., Hirosawa, M., Miyajima, N., & Tabata, S. (1998). CyanoBase, a www database containing the complete nucleotide sequence of the genome of *Synechocystis* sp. strain PCC6803. *Nucleic Acids Research*, *26*(1), 63–67. doi:10.1093/nar/26.1.63

Namkung, E., & Rittmann, B. E. (1986). Soluble microbial products (SMP) formation kinetics by biofilms. *Water Research*. Elsevier. doi:10.1016/0043-1354(86)90106-5

NAP. (2008). Water Implications of Biofuels Production in the United States. Retrieved from http://www.nap.edu/openbook.php?record_id=12039&page=15

Nguyen, B. T., & Rittmann, B. E. (2015). Predicting Dissolved Inorganic Carbon in Photoautotrophic Microalgae Culture via the Nitrogen Source. *Environmental Science & Technology*, *49*(16), 9826–9831. doi:10.1021/acs.est.5b01727

Ni, B.-J., Xie, W.-M., Chen, Y.-P., Fang, F., Liu, S.-Y., Ren, T.-T., … Tian, Y.-C. (2011). Heterotrophs grown on the soluble microbial products (SMP) released by autotrophs are responsible for the nitrogen loss in nitrifying granular sludge. *Biotechnology and Bioengineering*, *108*(12), 2844–52. doi:10.1002/bit.23247

Nixon, P. J., Michoux, F., Yu, J., Boehm, M., & Komenda, J. (2010). Recent advances in understanding the assembly and repair of photosystem II. *Annals of Botany*, *106*(1), 1–16. doi:10.1093/aob/mcq059

NOAA. (2013). Recent Monthly mean CO_2 at Mauna Loa. Retrieved from http://www.esrl.noaa.gov/gmd/webdata/ccgg/trends/co2_trend_mlo.pdf

Novak, J. T., & Brune, D. E. (1985). Inorganic carbon limited growth kinetics of some freshwater algae. *Water Research*, *19*(2), 215–225. doi:10.1016/0043-1354(85)90203-9

NREL. (2010). NSRDB: Alphabetical List by State. Retrieved from http://rredc.nrel.gov/solar/old_data/nsrdb/1991-2010/targzs/targzs_by_state.html

Ogawa, T., & Kaplan, A. (2003). Inorganic carbon acquisition systems in cyanobacteria. *Photosynthesis Research*, *77*(2-3), 105–15. doi:10.1023/A:1025865500026

Ogbonna, J. C., & Tanaka, H. (1996). Night biomass loss and changes in biochemical composition of cells during light/dark cyclic culture of *Chlorella pyrenoidosa*. *Journal of Fermentation and Bioengineering*, *82*(6), 558–564. doi:10.1016/S0922-338X(97)81252-4

Olson, G. J., & Ingram, L. O. (1975). Effects of Temperature and Nutritional Changes on the Fatty Acids of Agmenellum quadruplicatum. *Journal of Bacteriology*, *124*(1), 373–379. Retrieved from http://jb.asm.org/content/124/1/373.short

Omata, T., Takahashi, Y., Yamaguchi, O., & Nishimura, T. (2002). Structure, function and regulation of the cyanobacterial high-affinity bicarbonate transporter, BCT1. *Functional Plant Biology*, *29*(3), 151–159. doi:Doi 10.1071/Pp01215

Otero, A., & Vincenzini, M. (2003). Extracellular polysaccharide synthesis by Nostoc strains as affected by N source and light intensity. *Journal of Biotechnology*, *102*(2), 143–152. doi:10.1016/S0168-1656(03)00022-1

Pachauri, R. K., & Reisinger, A. (2007). Climate Change 2007: Synthesis Report. Contribution of Working Groups I, II and III to the Fourth Assessment Report of the Intergovernmental Panel on Climate Change. *Intergovernmental Panel on Climate Change*, *1*.

Padan, E., & Schuldiner, S. (1978). Energy transduction in the photosynthetic membranes of the cyanobacterium (blue-green alga) *Plectonema boryanum*. *Journal of Biological Chemistry*, *253*, 3281–3286. Retrieved from http://www.jbc.org/content/253/9/3281.short

Park, J. B. K., Craggs, R. J., & Shilton, a N. (2011). Wastewater treatment high rate algal ponds for biofuel production. *Bioresource Technology*, *102*(1), 35–42. doi:10.1016/j.biortech.2010.06.158

Patterson, G. W. (1970). Effect of culture temperature on fatty acid composition of *Chlorella sorokiniana*. *Lipids*. Springer. doi:10.1007/BF02531336

Pech-Canul, A., Nogales, J., Miranda-Molina, A., Álvarez, L., Geiger, O., Soto, M. J., & López-Lara, I. M. (2011). FadD is required for utilization of endogenous fatty acids released from membrane lipids. *Journal of Bacteriology*, *193*(22), 6295–6304. doi:10.1128/JB.05450-11

Perlack, R. D., & Stokes, B. J. (2011). US Billion Ton Update: Biomass supply for a bioenergy and bioproducts industry (executive summary). *Industrial Biotechnology*. Oak Ridge National Laboratory. doi:10.1089/ind.2011.7.375

Philippis, R. De. (1992). Glycogen and poly-β-hydroxybutyrate synthesis in *Spirulina maxima*. *Journal of General …*, 1623–1628. Retrieved from http://mic.sgmjournals.org/content/138/8/1623.short

Pimentel, D. (2008). Biofuel Impacts on World Food Supply: Use of Fossil Fuel, Land and Water Resources. *Energies*. doi:10.3390/en1020041

Poole, R. J. (1978). Energy Coupling for Membrane Transport. *Annual Review of Plant Physiology*. Annual Reviews 4139 El Camino Way, PO Box 10139, Palo Alto, CA 94303-0139, USA. doi:10.1146/annurev.pp.29.060178.002253

Posten, C., & Schaub, G. (2009). Microalgae and terrestrial biomass as source for fuels-A process view. *Journal of Biotechnology*, *142*(1), 64–69. doi:10.1016/j.jbiotec.2009.03.015

Powles, S. (1984). Photoinhibition of photosynthesis induced by visible light. *Annual Review of Plant Physiology*, *35*(1), 15–44. doi:10.1146/annurev.pp.35.060184.000311

Price, G. D. (2011). Inorganic carbon transporters of the cyanobacterial CO_2 concentrating mechanism. *Photosynthesis Research*, *109*(1-3), 47–57. doi:10.1007/s11120-010-9608-y

Price, G. D., Badger, M. R., Woodger, F. J., & Long, B. M. (2008). Advances in understanding the cyanobacterial CO2-concentrating-mechanism (CCM): functional components, C^i transporters, diversity, genetic regulation and prospects for engineering into plants. *Journal of Experimental Botany*, *59*(7), 1441–61. doi:10.1093/jxb/erm112

Proteau, P. J., Gerwick, W. H., Garcia-Pichel, F., & Castenholz, R. (1993). The structure of scytonemin, an ultraviolet sunscreen pigment from the sheaths of cyanobacteria. *Experientia*, *49*(9), 825–829. doi:10.1007/BF01923559

PubChem. (2014). lauric acid. Retrieved April 2, 2014, from http://pubchem.ncbi.nlm.nih.gov/summary/summary.cgi?cid=3893

Radakovits, R., Jinkerson, R. E., Darzins, A., & Posewitz, M. C. (2010). Genetic engineering of algae for enhanced biofuel production. *Eukaryotic Cell*, *9*(4), 486–501. doi:10.1128/EC.00364-09

Radmer, R., & Kok, B. (1977). Photosynthesis: Limited Yields, Unlimited Dreams. *BioScience*. Oxford University Press. doi:10.2307/1297655

Raven, J. A., & Giordano, M. (2014). Algae. *Current Biology*, *24*(13), R590–R595. doi:10.1016/j.cub.2014.05.039

Reynolds, T. D. (1977). Unit operations and processes in environmental engineering. Brooks.

Richmond, A. (2000). Microalgal biotechnology at the turn of the millennium: a personal view. *Journal of Applied Phycology*, *1*, 441–451. doi:10.1146/annurev.pp.09.060158.000245

Richmond, A. E., & Soeder, C. J. (1986). Microalgaculture. *Critical Reviews in Biotechnology*, *4*(4), 369–438. Retrieved from http://informahealthcare.com/doi/pdf/10.3109/07388558609150801

Rippka, R., Deruelles, J., Waterbury, J. B., Herdman, M., & Stanier, R. Y. (1979). Generic Assignments, Strain Histories and Properties of Pure Cultures of Cyanobacteria. *Journal of General Microbiology*. doi:10.1099/00221287-111-1-1

Rittmann, B. E. (2008). Opportunities for renewable bioenergy using microorganisms. *Biotechnology and Bioengineering*, *100*(2), 203–12. doi:10.1002/bit.21875

Rittmann, B. E., Bae, W., Namkung, E., & Lu, C. J. (1987). A critical evaluation of microbial product formation in biological processes. *Water Science & Technology*, *19*(3-4), 517–528.

Rittmann, B. E., & McCarty, P. L. (2001). *Environmental biotechnology: principles and applications*. Tata McGraw-Hill Education.

Rittmann, B. E., Torres, C. I., & Marcus, A. K. (2008). Understanding the distinguishing features of a microbial fuel cell as a biomass-based renewable energy technology. In *Emerging Environmental Technologies* (pp. 1–28). Springer. doi:10.1007/978-1-4020-8786-8_1

Rodolfi, L., Chini Zittelli, G., Bassi, N., Padovani, G., Biondi, N., Bonini, G., & Tredici, M. R. (2009). Microalgae for oil: strain selection, induction of lipid synthesis and outdoor mass cultivation in a low-cost photobioreactor. *Biotechnology and Bioengineering*, *102*(1), 100–12. doi:10.1002/bit.22033

Roessler, P. G., Chen, Y., Liu, B., & Dodge, C. N. (2008, December 11). Secretion of fatty acids by photosynthetic microorganisms. Google Patents. Retrieved from https://www.google.com/patents/US20090298143

Rosillo-Calle, F., & Cortez, L. A. B. (1998). Towards proalcool II-A review of the Brazilian bioethanol programme. *Biomass and Bioenergy*, *14*(2), 115–124. doi:10.1016/S0961-9534(97)10020-4

Rotman, D. (2009). Natural Gas Changes the Energy Map | MIT Technology Review. Retrieved from http://www.technologyreview.com/featuredstory/415725/natural-gas-changes-the-energy-map/

Saha, S. K., Uma, L., & Subramanian, G. (2003). Nitrogen stress induced changes in the marine cyanobacterium *Oscillatoria willei* BDU 130511. *FEMS Microbiology Ecology*, *45*(3), 263–272. doi:10.1016/S0168-6496(03)00162-4

Samuelsson, G., Lönneborg, A., Gustafsson, P., & Oquist, G. (1987). The Susceptibility of Photosynthesis to Photoinhibition and the Capacity of Recovery in High and Low Light Grown Cyanobacteria, Anacystis nidulans. *Plant Physiology*, *83*(2), 438–41. Retrieved from http://www.plantphysiol.org/content/83/2/438.short

Sander, K., & Murthy, G. S. (2010). Life cycle analysis of algae biodiesel. *The International Journal of Life Cycle Assessment*, *15*(7), 704–714. doi:10.1007/s11367-010-0194-1

Schopf, J. W., & Walter, M. R. (1982). Origin and early evolution of cyanobacteria: the geological evidence. In *The biology of cyanobacteria* (Vol. 19, pp. 543–564).

Schwarz, R., & Grossman, a R. (1998). A response regulator of cyanobacteria integrates diverse environmental signals and is critical for survival under extreme conditions. *Proceedings of the National Academy of Sciences of the United States of America*, *95*(18), 11008–13. Retrieved from http://www.pnas.org/content/95/18/11008.short

ScienceDaily. (2013). Algal bloom. Retrieved from http://www.sciencedaily.com/articles/a/algal_bloom.htm

Scott, S. a, Davey, M. P., Dennis, J. S., Horst, I., Howe, C. J., Lea-Smith, D. J., & Smith, A. G. (2010). Biodiesel from algae: challenges and prospects. *Current Opinion in Biotechnology*, *21*(3), 277–86. doi:10.1016/j.copbio.2010.03.005

Scragg, A. H., Illman, A. M., Carden, A., & Shales, S. W. (2002). Growth of microalgae with increased calorific values in a tubular bioreactor. *Biomass and Bioenergy*, *23*(1), 67–73. doi:10.1016/S0961-9534(02)00028-4

Searchinger, T., Heimlich, R., Houghton, R. a, Dong, F., Elobeid, A., Fabiosa, J., … Yu, T.-H. (2008). Use of U.S. croplands for biofuels increases greenhouse gases through emissions from land-use change. *Science (New York, N.Y.)*, *319*(5867), 1238–40. doi:10.1126/science.1151861

Sheehan, J., Dunahay, T., Benemann, J., & Roessler, P. (1998). Look Back at the U.S. Department of Energy's Aquatic Species Program: Biodiesel from Algae; Close-Out Report. doi:10.2172/15003040

Sheng, J. (2011). *Downstream Processing of* Synechocystis *for Biofuel Production*. Retrieved from http://search.proquest.com/docview/926211293/abstract/F5D0A2DF3E44411EPQ/1?accountid=4485

Sheng, J., Kim, H. W., Badalamenti, J. P., Zhou, C., Sridharakrishnan, S., Krajmalnik-Brown, R., … Vannela, R. (2011). Effects of temperature shifts on growth rate and lipid characteristics of *Synechocystis* sp. PCC6803 in a bench-top photobioreactor. *Bioresource Technology*, *102*(24), 11218–25. doi:10.1016/j.biortech.2011.09.083

Sheng, J., Vannela, R., & Rittmann, B. E. (2011). Evaluation of methods to extract and quantify lipids from *Synechocystis* PCC 6803. *Bioresource Technology*, *102*(2), 1697–703. doi:10.1016/j.biortech.2010.08.007

Shibata, M., Ohkawa, H., & Katoh, H. (2002). Two CO2 uptake systems in cyanobacteria: four systems for inorganic carbon acquisition in *Synechocystis* sp. strain PCC6803. *Functional Plant …*, *29*. Retrieved from http://www.publish.csiro.au/?paper=PP01188

Shibata, M., Ohkawa, H., Katoh, H., Shimoyama, M., & Ogawa, T. (2002). Two CO_2 uptake systems in cyanobacteria: four systems for inorganic carbon acquisition in <i>Synechocystis </I> sp strain PCC6803. *Functional Plant Biology*, *29*(2-3), 123–129. doi:Doi 10.1071/Pp01188

Sialve, B., Bernet, N., & Bernard, O. (2009). Anaerobic digestion of microalgae as a necessary step to make microalgal biodiesel sustainable. *Biotechnology Advances*, *27*(4), 409–16. doi:10.1016/j.biotechadv.2009.03.001

Siegenthaler, U., & Sarmiento, J. L. (1993). Atmospheric carbon dioxide and the ocean. *Nature (London)*, *365*(6442), 119–125. Retrieved from http://www.nature.com/nature/index.html

Silva, P., Thompson, E., & Bailey, S. (2003). FtsH is involved in the early stages of repair of photosystem II in *Synechocystis* sp PCC 6803. *The Plant Cell …*, *15*(September), 2152–2164. doi:10.1105/tpc.012609.tivity

Snoeyink, V. L. V. V. L., & Jenkins, D. (1980). *Water chemistry*. John Wiley. Retrieved from http://www.wiley.com/WileyCDA/WileyTitle/productCd-0471051969.html

Spoehr, H. A., & Milner, H. W. (1949). The chemical composition of *Chlorella*; effect of environmental conditions. *Plant Physiology*, *24*(1), 120. Retrieved from http://www.ncbi.nlm.nih.gov/pmc/articles/PMC437916/

Suh, I. S., & Lee, S. B. (2003). A light distribution model for an internally radiating photobioreactor. *Biotechnology and Bioengineering*, *82*(2), 180–9. doi:10.1002/bit.10558

Sun, Y., & Cheng, J. (2002). Hydrolysis of lignocellulosic materials for ethanol production: a review. *Bioresource Technology*, *83*(1), 1–11. doi:10.1016/S0960-8524(01)00212-7

Takagi, M., Karseno, & Yoshida, T. (2006). Effect of salt concentration on intracellular accumulation of lipids and triacylglyceride in marine microalgae *Dunaliella* cells. *Journal of Bioscience and Bioengineering*, *101*(3), 223–226. doi:10.1263/jbb.101.223

Tamiya, H., Shibata, K., Sasa, T., Iwamura, T., & Morimura, Y. (1953). Effect of diurnally intermittent illumination on the growth and some cellular characteristics of *Chlorella*. *Algal Culture: From Laboratory to Pilot Plant. Carnegie Institution of Washington Publication*, *600*, 76–84. Retrieved from http://shelf2.library.cmu.edu/Tech/01847533.pdf#page=87

Tang, H., Chen, M., Garcia, M. E. D., Abunasser, N., Ng, K. Y. S., & Salley, S. O. (2011). Culture of microalgae *Chlorella minutissima* for biodiesel feedstock production. *Biotechnology and Bioengineering*, *108*(10), 2280–2287. doi:10.1002/bit.23160

Tennessen, D. D. J., Bula, R. R. J., & Sharkey, T. T. D. (1995). Efficiency of photosynthesis in continuous and pulsed light emitting diode irradiation. *Photosynthesis Research*, *44*(3), 261–269. Retrieved from http://link.springer.com/article/10.1007/BF00048599

Timilsina, G. R., & Shrestha, A. (2011). How much hope should we have for biofuels? *Energy*, *36*(4), 2055–2069. doi:10.1016/j.energy.2010.08.023

Tittel, J., Bissinger, V., Gaedke, U., & Kamjunke, N. (2005). Inorganic carbon limitation and mixotrophic growth in *Chlamydomonas* from an acidic mining lake. *Protist*, *156*(1), 63–75. doi:10.1016/j.protis.2004.09.001

Tokgoz, S., & Elobeid, A. (2006). An Analysis of the Link between Ethanol , Energy , and Crop Markets. *Director*, (November). Retrieved from http://www.card.iastate.edu/publications/DBS/PDFFiles/06wp435.pdf

Torzillo, G. (2004). Photosynthesis in Microalgae. *Handbook of Microalgal Culture: Biotechnology and Applied Phycology*, 20–39. Retrieved from http://www.wiley.com/WileyCDA/WileyTitle/productCd-0632059532.html

Torzillo, G., Sacchi, A., Materassi, R., & Richmond, A. (1991). Effect of temperature on yield and night biomass loss in *Spirulina platensis* grown outdoors in tubular photobioreactors. *Journal of Applied Phycology*, *3*(2), 103–109. doi:10.1007/BF00003691

Tredici, M. R., & Zlttelli, G. C. (1998). Efficiency of sunlight utilization: Tubular versus flat photobioreactors. *Biotechnology and Bioengineering*, *57*(2), 187–197. doi:10.1002/(SICI)1097-0290(19980120)57:2<187::AID-BIT7>3.0.CO;2-J

US EPA, C. C. D. (2013). Carbon Dioxide Emissions. Retrieved November 8, 2013, from http://www.epa.gov/climatechange/ghgemissions/gases/co2.html

USDA. (2013). USDA Economic Research Service - Background. Retrieved from http://www.ers.usda.gov/topics/crops/corn/background.aspx#.Un0iPHAqjTp

UTEX. (2009). BG-11 Medium. Retrieved June 26, 2014, from http://web.biosci.utexas.edu/utex/mediaDetail.aspx?mediaID=26

UTEX. (2014). F/2 Medium. Retrieved October 8, 2014, from http://web.biosci.utexas.edu/utex/mediaDetail.aspx?mediaID=44

VanBriesen, J. M., & Rittmann, B. E. (1999). Modeling speciation effects on biodegradation in mixed metal/chelate systems. *Biodegradation*, *10*(5), 315–330. doi:10.1023/A:1008375722721

Vermaas, W. (1996). Molecular genetics of the cyanobacterium *Synechocystis* sp. PCC 6803: Principles and possible biotechnology applications. *Journal of Applied Phycology*, *8*(4-5), 263–273. doi:10.1007/BF02178569

Vermaas, W. (2013). Solar-Powered Production of Biofuels and Other Petroleum Substitutes by Cyanobacteria: Stoichiometries of Reducing Equivalents and Chemical Energy, and Energy Conversion Efficiency. In *Photosynthesis Research for Food, Fuel and the Future* (pp. 353–357). doi:10.1007/978-3-642-32034-7_74

Vermaas, W., Cheney, S., Krajmalnik-Brown, R., Lamb, H., Nielsen, D., Rittmann, B., … Thompson, D. (2011). Cyanobacteria as solar-powered biocatalysts for production of biofuels. *J. Phycol*, *47*, S1–S98. Retrieved from http://swenergyforum.com/pdfs/Wim Vermaas 200pm.pdf

Vermaas, W. F. J. (2014, June 17). Modified cyanobacteria. Google Patents. Retrieved from https://www.google.com/patents/US8753840

Wahidin, S., Idris, A., & Shaleh, S. R. M. (2013). The influence of light intensity and photoperiod on the growth and lipid content of microalgae *Nannochloropsis* sp. *Bioresource Technology*, *129*, 7–11. doi:10.1016/j.biortech.2012.11.032

Waley, S. G. (1964). A note on the kinetics of multi-enzyme systems. *The Biochemical Journal*, *91*(3), 514–517. Retrieved from http://www.ncbi.nlm.nih.gov/pmc/articles/PMC1259181/

Walker, D. A. (2009). Biofuels, facts, fantasy, and feasibility. *Journal of Applied Phycology*, *21*(5), 509–517. doi:10.1007/s10811-009-9446-5

Walsh, B. (2013). NOAA Estimate of Gulf of Mexico Dead Zone Is Shockingly Large | TIME.com. Retrieved from http://science.time.com/2013/06/19/this-years-gulf-of-mexico-dead-zone-could-be-the-biggest-on-record/

Walter, W. G. (1999). Standard Methods for the Examination of Water and Wastewater (20th ed.). *American Journal of Public Health and the Nations Health*. doi:10.2105/AJPH.51.6.940-a

Wang, C. Y., Fu, C. C., & Liu, Y. C. (2007). Effects of using light-emitting diodes on the cultivation of *Spirulina platensis*. *Biochemical Engineering Journal*, *37*(1), 21–25. doi:10.1016/j.bej.2007.03.004

Wang, L. A., Min, M., Li, Y. C., Chen, P., Chen, Y. F., Liu, Y. H., … Ruan, R. (2010). Cultivation of green a *Chlorella* sp in different wastewaters from municipal wastewater treatment plant. *Applied Biochemistry and Biotechnology*, *162*(4), 1174–1186. doi:10.1007/s12010-009-8866-7

Wangwibulkit, S., Limsuwan, C., & Chuchird, N. (2008). *Effects of salinity and pH on the growth of blue-green algae*, Oscillatoria *sp. and* Microcystis *sp., isolated from pacific white shrimp (*Litopenaeus vannamei*)*. Retrieved from http://www.fish.ku.ac.th/pdf/Fishery Bulletin no 32-1-1.pdf

Wingender, J., Neu, T., & Flemming, H.-C. (1999). What are Bacterial Extracellular Polymeric Substances? In *Microbial Extracellular Polymeric Substances SE - 1* (pp. 1–19). Springer. doi:10.1007/978-3-642-60147-7_1

Woertz, I., Feffer, A., Lundquist, T., & Nelson, Y. (2009). Algae Grown on Dairy and Municipal Wastewater for Simultaneous Nutrient Removal and Lipid Production for Biofuel Feedstock. *Journal of Environmental Engineering*. American Society of Civil Engineers. doi:10.1061/(ASCE)EE.1943-7870.0000129

Wolfstein, K., & Stal, L. J. (2002). Production of extracellular polymeric substances (EPS) by benthic diatoms: Effect of irradiance and temperature. *Marine Ecology Progress Series*, *236*, 13–22. doi:10.3354/meps236013

Woods, R. P., Legere, E., Moll, B., Unamunzaga, C., & Mantecon, E. (2010, March 23). Closed photobioreactor system for continued daily in situ production, separation, collection, and removal of ethanol from genetically enhanced photosynthetic organisms. Washington, DC: U.S. Patent and Trademark Office. Retrieved from https://www.google.com/patents/US7682821

World Energy Council. (2013). World Energy Resources: 2013 Survey. Retrieved from http://www.worldenergy.org/publications/2013/world-energy-resources-2013-survey

Wu, G. F., Shen, Z. Y., & Wu, Q. Y. (2002). Modification of carbon partitioning to enhance PHB production in *Synechocystis* sp. PCC6803. In *Enzyme and Microbial Technology* (Vol. 30, pp. 710–715). doi:10.1016/S0141-0229(02)00044-3

Xu, D. D.-Q., & Shen, Y. Y.-K. (1999). Light stress: photoinhibition of photosynthesis in plants under natural conditions. *Hand Book of Plant and Crop Stress. 2nd. Marcel*

Dekker, Inc. New York. Basel, 483–497. Retrieved from http://www.annualreviews.org/doi/pdf/10.1146/annurev.pp.09.060158.000245

Yeesang, C., & Cheirsilp, B. (2011). Effect of nitrogen, salt, and iron content in the growth medium and light intensity on lipid production by microalgae isolated from freshwater sources in Thailand. *Bioresource Technology*, *102*(3), 3034–3040. doi:10.1016/j.biortech.2010.10.013

Yun, Y. S., & Park, J. M. (2003). Kinetic modeling of the light-dependent photosynthetic activity of the green microalga *Chlorella vulgaris*. *Biotechnology and Bioengineering*, *83*(3), 303–311. doi:10.1002/bit.10669

Zavřel, T., Sinetova, M. a., Búzová, D., Literáková, P., & Červený, J. (2015). Characterization of a model cyanobacterium *Synechocystis* sp. PCC 6803 autotrophic growth in a flat-panel photobioreactor. *Engineering in Life Sciences*, *15*, 122–132. doi:10.1002/elsc.201300165

Zhang, L., Gase, K., & Baldwin, I. T. (2010). Enhanced fluorescence imaging in chlorophyll- suppressed tobacco tissues using virus-induced gene silencing of the phytoene desaturase gene. *Biotechniques*, *31*(2), 125–129. doi:10.2144/000113345

Zimmermann, U., Büchner, K. K.-H., & Benz, R. (1982). Transport properties of mobile charges in algal membranes: Influence of pH and turgor pressure. *The Journal of Membrane Biology*, *67*(1), 183–197. Retrieved from http://link.springer.com/article/10.1007/BF01868660